93

Fischer-Tropsch Synthesis over SiO_2, ZnO and MnO Supported Cobalt Catalysts

By

Richard Walsh – B.Sc. (Chem. Eng.)

Submitted to the University of Cape Town in fulfillment of the requirements for the degree of

Master of Engineering

Department of Chemical Engineering
University of Cape Town
Rondebosch
Cape Town
South Africa

2 December, 1998

Acknowledgements

"The most important thing is not so much where we stand as the direction in which we are going". (Margaret Fishback Powers)

I would like to thank Dr Eric van Steen for the support and encouragement that he has given me throughout the course of this work, for helping me to keep moving when I felt like doing some standing.

I would like to add Sasol, FRD and the Catalysis Research Unit to my thanks for the postgraduate funding received, and trust that this work may serve as a suitable reward for their investment.

Also thanks to my personal support base, especially Christy Wheeler for her support, help and the use of her desk for several months.

Thank you to my parents, Rod and Jenny, for the opportunities that they have given me that have brought me to this point in my ongoing education about life, the universe and everything.

Viva Chemical Engineering!!!

Synopsis

Silica is well known as a support for cobalt supported Fischer-Tropsch catalysts. Silica has a high surface area with an amorphous structure that promotes dispersion of the active cobalt phase over the support surface. This dispersion is vital in terms of catalyst performance and derives from the strength of interaction between the cobalt and the support. However, the stronger the metal support interaction, the greater is the loss of active cobalt through formation of cobalt support species that are hard to reduce.

Consequently ZnO and MnO were evaluated in comparison to SiO_2 as supports for cobalt supported Fischer-Tropsch catalysts. The aim of the study was to characterise the interaction between cobalt and the three supports (SiO_2, ZnO and MnO) in terms of the cobalt reducibility as visualised using TPR, exposed cobalt surface area and cobalt dispersion as evaluated using hydrogen chemisorption, and catalytic performance under Fischer-Tropsch synthesis conditions.

Cobalt nitrate impregnated onto SiO_2, ZnO and MnO served as base catalysts with which to evaluate the changes in physical and performance properties associated with the following alterations in the preparation conditions:

- a change in precursor from cobalt nitrate to cobalt acetate,
- a change in impregnation solution from water to monoethylenediamine in water,
- a change in the pH of the impregnation solution, and
- a change in the contact time between the impregnation solution and the support.

The three supports showed significantly different behaviours in terms of both their metal support interaction and their resulting performance under Fischer-Tropsch conditions. These differences were largely a consequence of the physical characteristics of each support. The degree of crystallinity of the support material was seen to play the greatest role in determining the strength of metal support interaction. It was found that a high degree of crystallinity resulted in lower metal support interaction. This was most apparent with the ZnO support. The lower metal support interaction increased the ease of reducibility of the

supported cobalt, a favourable result, but lowered the cobalt dispersion decreasing the activity of the catalyst through agglomeration of the active cobalt phase.

Cobalt nitrate on SiO_2 was found to be the most active catalyst as a result of high cobalt reducibility while maintaining a sufficient metal support interaction to induce a high cobalt dispersion.

Table of Contents

Page

List of Figures

Page

List of Tables

Page

CHAPTER 1

INTRODUCTION

1. Introduction

Fischer-Tropsch synthesis involves the production of hydrocarbons from CO hydrogenation over transition metals from synthesis gas. This process is perhaps the most promising source of chemicals and fuels from non-petroleum based supply such as coal and natural gas [Adesina, 1996].

A great deal of work has been carried out in order to obtain the "optimal catalyst" for this process. Research has covered:

- The type of active metal - ruthenium [e.g. Regaini et al., 1996], iron [e.g. Donnelly and Satterfield, 1989, Bukur et al., 1995], cobalt [e.g. Kuipers et al., 1996, and Iglesia et al., 1992], and combinations of these [e.g. Kogelbauer et al., 1996],
- the choice of support – various inorganic oxides including silica [e.g. Coulter and Sault, 1995], alumina [e.g. Hilmen et al., 1996] as well as titania, magnesia and zirconia,
- the preparation procedure – including impregnation techniques such as incipient wetness and chemical vapour deposition,
- and the activation procedure [e.g. Bukur et al., 1995].

In order to optimise the production of the desired product in any catalytic process, we require a catalyst that is active and selective to that desired product. In order to achieve this optimisation, a thorough understanding of the functioning of the catalyst and the reaction pathway is needed. The specific functioning of the catalyst is affected and altered by a number of variables throughout the processes of preparation and activation. Variables such as pH of the impregnation solution, and the calcination temperature have a significant influence on the final activity and selectivity of the catalyst.

1.1 Commercial Fischer Tropsch Process

Currently South Africa is in the lead in terms of commercial Fischer Tropsch application. Sasol operates three plants with a combined production capacity of roughly 4 million tonnes per year. Other companies operating this process are Shell in Malaysia, and Mossgas in South

Africa. In order to make the FT process competitive with crude oil processes, innovative work is being carried out in the field of FT reactor technology and catalyst development.

1.1.1 History of Catalysts for Fischer Tropsch Synthesis

In 1902, Sabatier and Senderens [1902] formed methane over cobalt and nickel catalysts using a feed consisting of various ratios of H_2 and CO. In 1913, BASF produced a range of liquid products over cobalt at high pressure [BASF, 1913]. Fischer and Tropsch followed this work in 1923 with a liquid product formed at high pressure (~150 bar) over a fused iron catalyst. The liquid was rich in oxygenates. Further work focussed on cobalt and nickel as iron deactivated quickly under the reaction conditions employed, however interest in nickel waned for two reasons: firstly, the methane selectivity was high, and secondly, nickel was expelled from the reactors in the form of nickel carbonyl, resulting in loss of activity as the nickel mass dropped. Cobalt with ThO_2/MgO and Kieselguhr was the main catalyst used in the first commercial Fischer Tropsch operations in Germany in 1936. In 1936, Pichler [1952] discovered that lower reaction pressures extended the lifetime of the iron catalyst, introducing iron as a competitive alternative to cobalt. In 1955, Sasol went online commercially, making use of a precipitated iron catalyst [Dry, 1981]. Considerable research has been carried out on the iron catalyst, and currently a precipitated iron catalyst is used at Sasol that is promoted with copper, potassium and other oxides.

1.1.2 Reactor Technology Development

The type of reactor used and the operating conditions employed are governing factors with respect to FT product distribution. Temperature becomes a major factor because the FT process is highly exothermic (about 145 kJ per mole of carbon incorporated into a growing chain) requiring the efficient removal of large amounts of heat. Increased temperatures result in higher methane yields, carbon deposition and particle fragmentation, consequently the reactor design needs an effective heat removal system.

The first reactors used were glass tube fixed bed types and were laboratory scale with an ID of about 5mm. However as the Fischer-Tropsch process was upgraded and attempts were

made to commercialise it, more attention needed to be paid to the reactor design. The three major reactor configurations resulting were the fixed bed, the slurry bed and the fluidised bed reactor types.

For the fixed bed reactor, the bulk of the work focussed on the removal of heat from the system. Various designs have been employed to achieve this. In the original German reactors, catalyst was packed between parallel metal plates. Metal tubes carrying cooling water ran horizontally through the plates [Frohning et al., 1997]. Heat removal was poor as a result of low linear gas velocities through the bed. A recycle ratio was employed to increase the fresh feed velocity through the bed into the turbulent regime. At these conditions heat transfer between the catalyst and the reactor walls was vastly improved. The current commercial fixed bed system uses a multi-tubular design, with a typical reactor for industrial applications using between 1500 and 2200 tubes in order to combat the high exothermicity of reaction. The fixed bed configuration makes use of the cheapest catalyst available, namely alkalised fused iron, producing mainly linear waxes, which can be hydrocracked to diesel. A number of disadvantages arise with this reactor type. A high pressure drop across the bed results in increased gas compression costs, while higher temperatures leads to carbon deposition with particle expansion, disintegration and bed plugging.

The slurry bed reactor was first investigated by Fischer, and bears several advantages over the fixed bed type. In the slurry reactor, gas is bubbled through a suspension of fine catalyst particles. Heat is removed by circulating the slurry through external heat exchangers, or by heat exchangers immersed in the slurry bed, thus heat exchanger design is easier than in the fixed bed case. Higher temperatures than those used in fixed beds can be operated in slurry reactors as carbon deposition on the catalyst does not adversely affect the performance of the catalyst [Dry, 1981].

Interest in fluidised bed reactors for the Fischer Tropsch synthesis resulted from their successful employment as catalytic cracking units in the petroleum industry. Two types of reactors are available, (1) the fixed fluidised bed (FXFBR), and (2) the circulating fluidised bed (CFB). In the fixed fluidised bed, the catalyst remains "stationary", while catalyst is entrained in the gas stream in the circulating option. Problems associated with these configurations include achieving uniform fluidisation of the entire bed without gas bypass.

Sasol II and III plants use circulating fluidised beds (CFB) as the benefits of this configuration outweigh the negatives. Benefits include improved heat transfer characteristics and higher gas throughputs than fixed beds, while lower pressure drops reduce gas compression costs. Downtime is minimal as the reactor offers the option to add fresh catalyst online.

There is a great deal of interest in the fixed fluidised bed reactor (FXFBR) and the bubble column slurry reactor (BCSR). The FXFBR improves conversion and reduces installation and compression costs compared to the CFB. In the BCSR, catalyst attrition and erosion is minimised, while increased dispersion of the catalyst in the liquid suspension results in uniform temperature and allows higher catalyst loading.

1.2 Fischer Tropsch Synthesis

Interest in the Fischer Tropsch process has fluctuated with the troughs and crests of the petrochemical industry. For example the discovery of large oil deposits in the Middle East resulted in decreased interest in the FT process. However, since the Middle east oil crisis of 1973, interest in Fischer Tropsch has resurfaced strongly as a source of chemicals and fuels from non-petroleum based supplies such as coal and natural gas [Adesina, 1996]. The majority of interest has manifested itself in the search for promising catalysts, as well as the optimisation of reactor configurations and an understanding of the effect of reaction parameters.

1.2.1 Reaction Mechanisms and Kinetics

The following section serves to introduce how the Fischer Tropsch reaction takes place (i.e. what is happening to achieve the products from the reactants), as well as to evaluate certain parameters that determine the rate at which this reaction can be achieved and the factors inhibiting this.

1.2.1.1 Fischer-Tropsch Reaction Mechanisms

CO hydrogenation via the Fischer-Tropsch process involves a complex system of series parallel reaction steps and secondary reactions. Fischer-Tropsch synthesis is a polymerisation type reaction that uses CH_x monomers derived from synthesis gas to form higher molecular weight hydrocarbons on the catalyst surface. The reaction proceeds via the following steps:

1. H_2 and CO adsorption
2. Chain initiation
3. Chain growth
4. Chain termination
5. Product desorption
6. Readsorption and further reaction.

The simplified FT reaction can be written as follows:

$$(2n + 1)H_2 + nCO \rightarrow C_nH_{2n+2} + nH_2O$$

$$2nH_2 + nCO \rightarrow C_nH_{2n} + nH_2O$$

These reactions can be accompanied by the water-gas shift reaction illustrated as follows:

$$H_2O + CO \rightarrow CO_2 + H_2$$

A number of mechanisms have been proposed around this general picture of FTS. Wojciechowski [1988] has presented a more detailed formulation of the necessary components of each FTS mechanism as follows:

1. H_2 and CO adsorb onto the active sites at the catalyst surface to form dissociated H atoms and adsorbed C and O atoms. These adsorbed species interact leading to the formation of CH_x, OH, etc.
2. The monomeric species for chain growth can be visualised to be CH_2 adsorbed on the surface which is formed from adsorbed C and H species.

3. Chain growth takes place via monomers formed near the growing chain, which migrate towards the growing chain through surface diffusion.
4. 1-2 shift attachments may occur during chain growth resulting in branched hydrocarbon formation, however as yet there is no conclusive evidence.
5. The termination stage and the resulting product type is determined by the type of species adsorbed on the site adjacent to the growing chain. For example, when H atoms predominate around the growing chain, termination as an *n*-paraffin via α-hydrogenation becomes more likely.
6. The system pressure and temperature, and the H_2/CO ratio are governing factors that affect both kinetics as well as the product distribution of FTS.
7. Product spectrums tend to follow Anderson-Schulz-Flory chain length distributions. (See Chapter 1.2.1.1.1)

The main products of the FTS reaction are saturated and unsaturated aliphatic hydrocarbons, with minor amounts of alcohols, aldehydes and ketones formed as by-products. The growing linear alkyl chains are chemically bound to the surface of the catalyst at the terminal carbon. Termination of the chain occurs either by β-abstraction yielding an α-olefin, or by α-hydrogenation yielding an *n*-paraffin.

1.2.1.1.1 Anderson-Schulz-Flory Product Distributions

Because Fischer Tropsch synthesis is a chain growth reaction, its total product yield, on a molar basis, decreases exponentially with increasing chain length. This chain growth mechanism yields a molar distribution called the Anderson-Schulz-Flory distribution, which describes the probability of an alkyl group being inserted in an adsorbed chain. The probability α_n is defined as follows:

$$\alpha_n = \frac{\text{molar yield of chains with carbon number } n+1}{\text{molar yield of chains with carbon number } n}$$

The Anderson-Schulz-Flory (ASF) distribution is obtained from the following mathematical relationship:

$$\text{Log } M_{Cn} \quad = \quad \log((1-\alpha)/\alpha) \; + \; N \log(\alpha)$$

where N is the carbon number and M_n is the molar fraction of that carbon number. A plot of log M_n versus C_n yields a straight line with a slope of log α. The maximum achievable value of α would be 1. This is to all intents and purposes unachievable as a certain amount of chain termination takes place at every carbon number. A number of factors influence the chain growth probability. The probability varies according to the active metal used (i.e. iron, cobalt or ruthenium) and the synthesis conditions (i.e. the temperature, partial pressures of reactants, and molar feed ratio of H_2/CO). Further change in the growth probability derives from the addition of different promoters as well as differing amounts of the same promoter. These variations deal with the slope of the straight line. A number of authors [e.g. Wojciechowski and Sarup, 1988; Kuipers et al, 1995] have noted deviations from this straight-line prediction as a result of secondary reactions.

1.2.1.1.2 Secondary Reactions

Secondary reactions strongly influence the FT product spectrum and can even be used to optimise the selectivity to some desired product range. The secondary reactions that take place are reinsertion, hydrogenation, and hydrogenolysis. Reactive products such as olefins are able to be inserted in new growing chains via secondary reactions, or may act as chain initiation species themselves.

Kuipers et al [1996] produced product distributions that varied significantly from straight line ASF behaviour as shown in Figure 1.1.They attributed this deviation to reinsertion and/or hydrogenolysis reactions. These secondary reactions were found to be chain-length dependent resulting in high selectivities to middle distillates (C_{10} to C_{13}). The effect of these reactions in this carbon number region was so dominant that they observed chain growth probabilities (α) above 1. This is not possible, even though reinsertion of α-olefins reverses the termination reaction that takes place via β-dehydrogenation. This chain length dependence is explainable in terms of the exponential increase in physisorbed olefin concentration with increasing carbon number due to preferential adsorption of longer hydrocarbons at the catalyst surface.

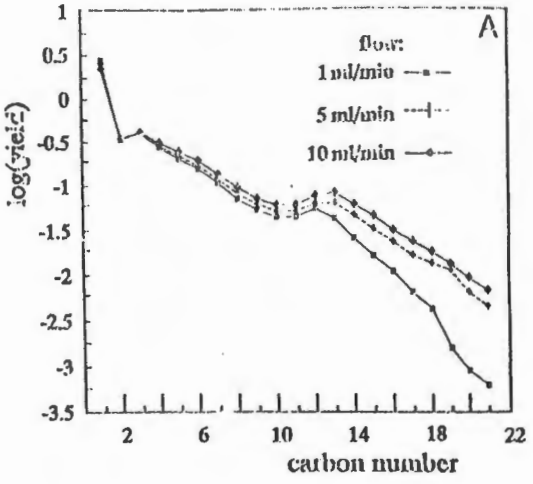

Figure 1.1. Total product yield (pmol/cm^2.s) as a function of carbon number obtained for a 50-nm Co particles on a flat SiO_2 wafer (reduced at 573 K for 5 min) for three different flows, T = 493 K, $H_2/CO = 2$, P = 1 bar. [Kuipers et al., 1996]

Other deviations in ASF behaviour have been noted by Satterfield and Huff [1984], Egiebor and Cooper [1985], Konig and Gaube [1983], Rosch [1980] and Anderson [1956]. Satterfield and Huff [1984] explained the phenomenon as a superimposition of two independent partial distributions. The two distributions were thought to be formed on different catalyst sites, with different chain propagation probabilities as illustrated in Figure 1.2.

The presence of secondary hydrogenation reactions was observed by Pichler *et al.* [1967] who showed that, as the contact time with the catalyst increased, the paraffin to olefin ratio increased. A number of other workers [Madon et al. 1991; Kuipers et al. 1995; Komaya and Bell, 1994; Dictor and Bell, 1986; Gaube and Hochstadt, 1978; Iglesia et al. 1991] have noted the same effect.

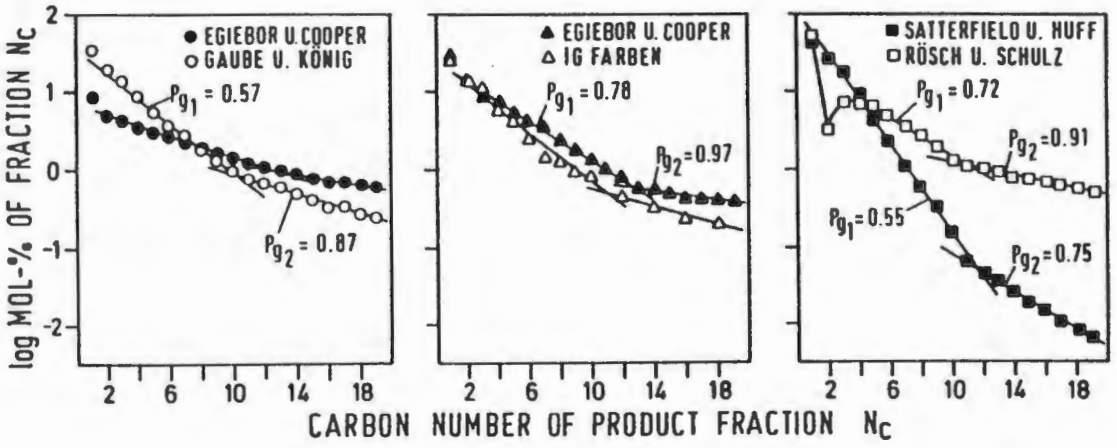

Figure 1.2. Experimental R. B. Anderson plots of FT-product distributions showing the change in chain growth rate constant in the range $C_{11} - C_{14}$.

- • 100 Fe – 5.2 CuO – 8 K_2O, 300°C, 7.1 bar, $H_2/CO = 1$ [Egiebor and Cooper, 1985]
- O Fe (2% K_2CO_3), 240°C, 10 bar, $H_2/CO = 1.1$ [Konig and Gaube, 1983]
- ▲ 100 Fe – 110 Mn, 300°C, 7.1 bar, $H_2/CO = 1$ [Egiebor and Cooper, 1985]
- △ 100 Fe – 1 K_2CO_3 – 2 Al_2O_3/CaO, 220°C, 10 bar, $H_2/CO = 1.25$ [Anderson, 1951]
- ■ 100 Fe – 716 Mn, 283°C, 12.4 bar, $H_2/CO = 1.19$ [Huff and Satterfield, 1984]
- □ 100 Co – 9 ThO_2 – 9 Mg – 100 Aerosil, 175°C, 9 bar, $H_2/CO = 1.9$ [Rosch, 1980]

Kuipers *et al* [1996] studied Fischer-Tropsch synthesis over Co/SiO_2 catalysts. By cofeeding hexene and hexadecane over a thin catalyst foil under conditions that excluded transport restrictions, they determined the extent of secondary reactions. Their findings showed that no measurable fraction of hexene was either reinserted or underwent hydrogenolysis. However, hydrogenation took place to the same extent as for the primary formed olefin. For hexadecane, hydrogenolysis was evident, but to a small extent. The presence of CO [Jordan and Bell, 1987; Jordan and Bell, 1987] and H_2O [Iglesia et al., 1991; Iglesia et al., 1993] is known to inhibit the rate of hydrogenation.

1.2.1.2 Reaction Kinetics

The temperature at which reaction takes place is a good indication of a catalyst's activity. The lower the temperature needed generally, the higher the catalyst activity. On this basis, activity declines in the order Fe < Ni < Co [Vannice, 1975]. For Fischer Tropsch catalysts, the activity is determined by the nature of CO and H_2 adsorption.

Carbon monoxide is strongly adsorbed on the catalyst and is known to poison hydrogenation reactions. Initial bonding of CO takes place in the carbon down position with its molecular axis perpendicular to the surface [Blyholder, 1964]. Carbon monoxide may be activated by a strong interaction of the C and/or O atom with the catalyst surface. The result is to weaken the C-O bond enabling reaction with hydrogen. It has been shown that surfaces which facilitate electron donation into the $2\pi^*$ antibonding orbital of the CO molecule exhibit higher probabilities of C-O bond rupture and hence dissociative adsorption of CO. The C-O bond severage at the surface speeds up reaction initiation and consequently the activity of the catalyst. The H_2 chemisorption plays a subservient role on the catalyst surface. The presence of CO adsorbed on the surface inhibits H_2 adsorption, while CO adsorption is uninhibited by the presence of H_2 on the surface. Consequently CO is a stronger competitor for surface adsorption sites than H_2. For Fischer Tropsch, since H_2 chemisorption is needed for reaction, CO chemisorption must not be too strong so as to allow H_2 access to the catalyst surface. This CO inhibition of reaction is illustrated in many of the proposed kinetic expressions to describe Fischer Tropsch synthesis. Table 1.1 shows several kinetic equations [Dry, 1981], the major feature being the power to which the partial pressure of CO and H_2 are raised.

Table 1.1. Kinetic equations for CO hydrogenation over different metals.

Metal	Kinetic Equation	Reference
Nickel	$r = k\, p_{H2}^{0.9}\, p_{CO}^{-0.2}$	Luytens and Jurgens [1945]
Cobalt	$r = k\, p_{H2}^{2} / p_{CO}$	Brötz [1949]
Iron	$r = k\, p_{H2} / (1 + a\, p_{H2O} / p_{CO})$	Anderson [1956]
Ruthenium	$r = k\, p_{H2}^{1.5}\, p_{CO}^{-0.6}$	Ekerdt and Bell [1979]

For CO the power is negative for nickel, cobalt and ruthenium revealing that increased presence of carbon monoxide at the catalyst surface inhibits the rate. The rate increases with increasing partial pressure of H_2. It is of interest to note that the kinetic expression for iron catalysts shows a dependence upon the partial pressure of water. This could be attributable to the ease with which iron oxidises relative to the other FT metals.

Thermodynamics dictates that methane should be the most favoured product for a significant range of Fischer Tropsch reaction conditions. In the Fischer Tropsch system, methane is not readily released from the surface, but undergoes numerous chain elongation steps. It has been shown that the favoured product of chemi-desorption is the α-olefin. Schulz et al. [1988] found that the rate of paraffin chemi-desorption from an iron manganese catalyst was approximately four times slower than the α-olefin chemi-desorption rate. Thus, the extended periods of intermediate adsorption results in methane inhibition and heightened surface polymerisation probabilities. The inhibition of chemi-desorption can be attributed to carbon monoxide.

1.2.2 Effect of Reaction Parameters

The choice of reaction parameters is key to product optimisation for any catalytic process. The reactor configuration to which these parameters are applied determines the range of applicable conditions due to physical constraints associated with that configuration. For example, fixed bed reactors have significant limitations with regard to heat removal.

1.2.2.1 Effect of Temperature

The temperature of reaction for Fischer Tropsch synthesis plays a major role in determining the rate of reaction as well as the product selectivity. The influence of temperature remains consistent for all Fischer Tropsch catalysts. Increased temperatures shift product selectivity to lighter molecular mass hydrocarbons. For example, at low temperatures (<190°C), nickel catalysts yield a product with a high wax fraction. The same catalyst operating at high temperatures (>300°C) produced mainly methane. Gall et al. [1952] found that the standard $Co/ThO_2/MgO/SiO_2$ catalyst gave a 1% yield of oxygenated product at temperatures in the

range of 180 to 200°C. As the temperature was lowered to between 160 and 175°C, the oxygenated fraction was seen to increase, yielding a liquid organic product with 40% alcohols. Anderson [1956] made a similar observation over a potassium promoted fused iron catalyst. In this particular case, the oxygenated fraction was found to decrease significantly as the temperature increased from 190°C to 220°C. Work done at Sasol over two iron catalysts showed that a lower temperature favoured the formation of straight chain products, while increased temperatures increased the branched product fraction [Dry, 1981]. Increased temperature (~325°C) was also found to increase the aromaticity of the product.

1.2.2.2 Effect of Total Pressure

Increased total pressure for Fischer Tropsch synthesis has been shown to shift the hydrocarbon selectivity to a higher molecular weight product. This observation has been noted for both cobalt [Martin, 1939] and fused iron catalysts [Friedman and Schlesinger, 1964]. No trend has been noted with regards olefinicity as pressure is increased, however several authors have observed increased oxygenate fractions with increasing pressure [Anderson et al., 1952; Friedman and Schlesinger, 1964].

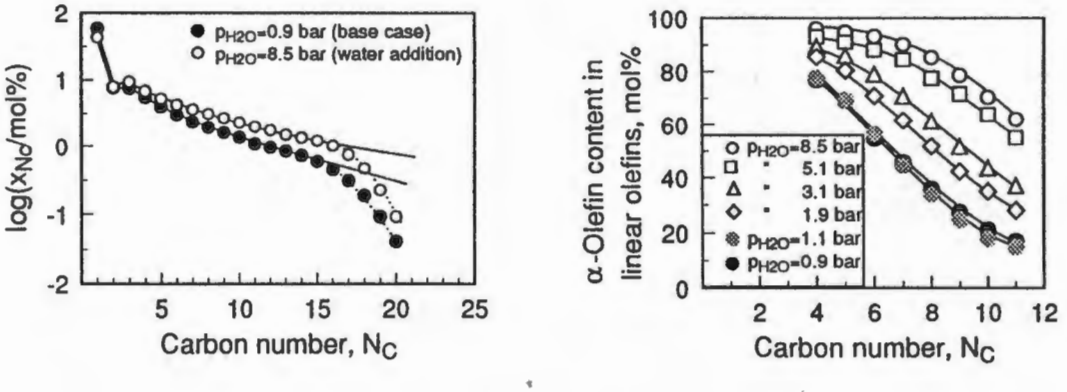

Figure 1.3. (A) ASF plots for 100 Co/15 ZrO_2/100 Aerosil/0.66 Ru, T = 190°C, P_{H2} = 6 bar, P_{CO} = 3 bar. (B) Molar α-olefin content in the fraction of linear olefins with the same carbon number as a function of carbon number. [Claeys et al., 1997]

Changes in product spectrums with increased pressure can be attributed to increased partial pressures of reactants and products. Claeys et al [1997] showed that increased partial pressures of water over a slurry phase cobalt catalyst lead to significant changes in product composition, including suppressed methane formation, enhanced chain growth, and the inhibition of secondary olefin formation. Figure 1.3 (A) illustrates the effect of water partial pressure on the chain growth probability while Figure 1.3 (B) shows the α-olefin variance.

1.2.2.3 Influence of H_2/CO Ratio

Work carried out on evaluating the effect of the H_2/CO ratio indicate that a decrease in the H_2/CO ratio results in a higher average molecular weight hydrocarbon product and higher olefinicity. Aromaticity was also found to increase over iron catalysts as the H_2/CO ratio decreased [Dry, 1981]. Anderson [1956] showed similar findings for a Co/Ni/ThO_2/Mn/Kieselguhr catalyst. A lower H_2/CO ratio resulted in a lower methane selectivity and a higher olefin content. These results are understandable in that a catalyst surface preferentially covered with hydrogen favours chain termination. Thus the desired product selectivity is largely determined by the fractional surface coverage of CO, H_2, CO_2 and H_2O.

1.3 Supported Metal Catalysts for Fischer-Tropsch Synthesis

Transition metals are being widely used as active catalysts in a variety of industrial processes including oil refining and reductive amination. The supported metal catalysts hold a number of significant advantages over their bulk metal counterparts. They are cheaper as the activity per weight of active metal is increased due to high dispersions on high surface area carriers that maximise active metal usage. They also show enhanced thermal stability due to interaction between the active metal and support which leads to a decrease in catalyst sintering and a prolonged lifespan, and they provide increased efficiency due to high metal dispersions supported on high surface area carriers. Transition metals are generally regarded as good hydrogenation catalysts. All Group VIII metals show certain amounts of FT activity, however not all are commercially viable [Vannice, 1975; Vannice, 1977; Vannice and

Garten, 1980; Dry, 1981]. The different metals show differing activities and product distributions, require different operating conditions, show different deactivation behaviours, and vary greatly in cost.

A Fischer-Tropsch catalyst usually consists of four components: an active metal, a small amount of a second metal (usually noble), oxide promoters (alkali, rare earth, and/or a transition metal oxide such as ZrO_2), and a support (silica, alumina or titania). Various combinations have been studied and documented in literature. The following section serves to elaborate more on the benefits and drawbacks of each component chosen.

1.3.1 Active Metal

The choice of active metal used is significant both in terms of the cost of the catalyst and the benefits that it brings in terms of activity and selectivity. The nature of carbon monoxide and hydrogen adsorption and the interaction with the metal that results greatly influences the effectiveness of that metal for Fischer-Tropsch synthesis. Commercially, cobalt and iron are the dominant active metal components, while nickel is largely used as a methanation catalyst. Nickel bears another disadvantage, namely that at CO partial pressures higher than about 0.5 bar, nickel carbonyl forms and is expelled from the reactor, lowering the catalyst activity as the mass of catalyst reduces. Ruthenium also commands a large amount of research both as an active metal specie and as a promoter. Other Group VIII metals such as Rh, Ir, Re, Os Pd and Pt all show FT activity, however in most cases the product spectrum consists mainly of oxygenates as CO does not chemisorb dissociatively on these metals [Somorjai, 1981; Janardaranao, 1990].

1.3.1.1 Iron

Iron has been used commercially in fixed bed and entrained fluidised bed reactors by Sasol South Africa for synthesis gas conversion to fuels via Fischer Tropsch synthesis. The commercial catalyst is prepared using a precipitation technique, and is promoted with copper and potassium and other oxides. In the case of the Ruhrchemie catalyst, silica is added as a structural promoter keeping up the pore structure. A large amount of research has been

carried out on the iron catalyst. It shows very high activity to Fischer Tropsch synthesis, second only to ruthenium [Vannice, 1975], but requires higher operating pressures (~15 bar). The formation of carbides, nitrides, oxides and carbonitrides takes place easily on the iron catalyst, however these compounds all show Fischer-Tropsch activity [Anderson, 1984]. Metallic iron is formed during the hydrogen reduction phase, but exposure to synthesis gas results in rapid metal carbide formation [Dry, 1981; Amelse et al., 1978; Raupp and Delgass, 1979; Jung and Thomson, 1992]. During synthesis, specifically at high conversions, the reaction mixture becomes more oxidising and magnetite is also formed [Dry, 1981; Anderson, 1956; Satterfield et al., 1986]. This easy movement between metal phases proves somewhat detrimental in that Fe has a stronger tendency to form elemental carbon than Co or Ni, leading to catalyst deactivation as carbonaceous deposits block the active sites.

1.3.1.2 Ruthenium

Ruthenium has been shown to have the highest specific activity for FT synthesis of all the Group VIII metals [Vannice, 1975], and may be active at temperatures as low as 373K. High molecular weight species can be produced at lower temperatures than those required for Fe and Co, while remaining carbide free under Fischer-Tropsch conditions. The three major products formed on the ruthenium catalyst are *n*-paraffins, α-olefins and β-olefins.

1.3.1.3 Cobalt

Cobalt catalysts have a number of significant advantages over iron based catalysts. Cobalt catalysts appear to provide the best compromise between performance and cost for the Fischer-Tropsch synthesis. Operating pressures for cobalt are milder (~5-15 atm) than for iron (~15 atm). The formation of carbides on cobalt is thermodynamically unfavourable, consequently there is a lower tendency for the build-up of carbonaceous material which deactivates the catalyst. Cobalt catalysts produce mainly straight chain (linear) hydrocarbons [Goodwin, 1991], with minimal alcohol formation and low water-gas shift activity [Newsome, 1980; Goodwin, 1991].

1.3.2 Metal and Oxide Promoters

The addition of an inactive species that serves to enhance selectivity/activity or stability of a metal-supported catalyst has long been used in the preparation of Fischer-Tropsch Synthesis catalysts. Alkali carbonates and alumina have been used to double promote iron catalysts, while alkalis such as ThO_2 have been used to promote supported cobalt catalysts. The promoter can show several significant effects in the case of Fischer-Tropsch synthesis:

1. They enhance the dissociation of CO on the surface of the catalyst which results in a shift in selectivity to higher hydrocarbons;
2. They increase the overall rate of synthesis;
3. They favour the formation of unsaturated products;
4. They determine the extent to which other reactions take place in conjunction with the hydrocarbon synthesis.

The fourth point largely refers to the formation of alcohols, as the C-O bond strength is weakened by the presence of a promoter such as vanadium, and hydrogenated to the alcohol.

Many studies have been carried out on catalyst promotion. Kogelbauer et al. [1996] promoted an alumina supported cobalt catalyst with ruthenium. They noted that the presence of ruthenium increased the reducibility of the catalyst and showed increased CO hydrogenation activity. This increased activity paralleled the increased number of exposed metal atoms on the surface following ruthenium addition as observed using H_2 chemisorption. Hilmen et al. [1996] noted that promotion of alumina supported cobalt catalysts with rhenium also resulted in higher reducibilities of cobalt. Increased catalyst activities were also observed following zirconia promotion of silica supported cobalt catalysts [Ali et al., 1995], and La promotion of alumina supported cobalt catalysts [Vada et al., 1995]. In both cases it was observed that there was an optimum promotion amount.

1.3.3 Choice of Support

The choice of support is of great importance in the design of a suitable supported metal catalyst. Parameters such as basicity, dispersion effect, surface area, thermal and chemical stability, mechanical strength, electronic modifications and strong metal-support interaction have a significant effect on the preparation and functioning of the catalyst [Foger, 1985].

Support materials can be classified into

1. Inert supports; like SiO_2 supplying high surface area for dispersion of the active component.
2. Catalytically active supports; like aluminas, silica-aluminas and zeolites currently the dominant support in industrial catalytic applications.
3. Supports influencing the active component as a result of strong metal support interactions, as in the case of TiO_2 and V_2O_5.
4. Structural supports such as the monoliths used in motor vehicle exhaust gas purification.

The most popular supports for Fischer-Tropsch catalysts are inorganic oxides such as silica, alumina, titania, magnesia and zirconia.

1.4 Catalyst Preparation

The goal of catalyst preparation is to make a catalyst with a highly dispersed metal phase to achieve a large surface area of active component. It is desirable to synthesise catalysts with high volumetric productivity. This can be achieved for supported cobalt catalysts by:

1. The synthesis of small metal crystallites at high local surface densities on the support surface, and
2. Using supports that increase the rate per surface cobalt atom (turnover rate). [Iglesia, 1997]

The ultimate performance of the prepared catalyst, as determined by its activity and

selectivity, is strongly dependent upon the interaction of numerous chemical processes taking place during its preparation. The preparation phase can be subdivided into 3 distinct categories, namely (a) the chemical synthesis (b) calcining and (c) activation. These steps become particularly important for Fischer-Tropsch synthesis where bulk phase changes in catalyst composition may lead to different activities and product distributions.

1.4.1 Catalyst Synthesis

Fischer Tropsch catalysts are usually synthesised via precipitation, impregnation, ion exchange or vapour phase deposition techniques. Commercial iron and cobalt catalyst have largely been prepared using precipitation techniques, while vapour phase deposition techniques are promising in that high metal dispersions are achievable without deactivation through strong metal support interactions.

Impregnation involves the deposition of a metal precursor on a support. The support acts as a mere physical surface, consequently the interaction between the metal and support is weak, and requires a calcination step to provide a stronger chemical interaction. For this reason the preparation procedure does not include a washing step so as not to eliminate the weakly bound metal salt [Che, 1993].

1.4.1.1 Interfacial Coordination Chemistry

Whenever a cation (specifically a transition metal ion- TMI) is placed in solution, anionic or neutral groups called ligands immediately surround the cation, and the chemistry associated with the way these ligands and the cation interact is called coordination chemistry. The chemistry involves an understanding of the properties of TMI complexes including the nature of the different chemical bonds that they can form and the optical and magnetic transformations associated with their interaction with other compounds. The preparation of supported catalysts through the deposition of transition metal complexes on metal oxides is an example of coordination chemistry at a liquid solid interface. In aqueous solution, TMIs are complexed by water and/or other ligands present. As an example of this, Smith and Jacobson [1956] noted the ability of silica to adsorb Co^{2+} complexed with ammonia and

ethylenediamine. Burwell et al. [1965] gave evidence to suggest that this adsorption occurred through substitution of the anionic ligand by a surface SiO^- group. Thus the preparation of the catalyst is strongly affected by the choice of metal precursor compound, the solution used for impregnation which determines the nature of the ligands surrounding the cation, the nature of the support surface, and the pH at which impregnation is done.

1.4.1.1.1 Influence of Precursor Compound

The choice of precursor compound has a strong effect on the performance of the finished catalyst. For the case of cobalt deposition, the anion of the cobalt salt used leads to variances in the strength with which the cobalt cation attaches to the support surface. This can be attributed to the effect that the anion has on the pH of the impregnation solution, where a lower pH results in a smaller interaction between cation and support. The purity of both the precursor compound and support is of great importance to the final catalyst performance as well. The presence of impurities such as chloride and sulphate ions, even in trace amounts has been shown to decrease catalyst performance.

1.4.1.1.2 Influence of Support Type

When inorganic oxides are contacted with water, a liquid solid interface arises yielding a perturbation in the first two layers of water surrounding the oxide. These layers are strongly immobilised resulting in a drastic decrease in the dielectric constant of water as the associated dipoles in the first water layer align themselves on the oxide surface [Antoniu, 1964]. The surface of inorganic oxides offers various sites with which the metal precursor can interact including oxygen atoms and hydroxyl groups. The oxide surface is able to enter the outer sphere of solvation of transition metal complexes (TMIs) through it's OH groups in the same way that the solvent can [Che, 1993], as illustrated in model I of Figure 1.4. Thus the oxide surface can act as a solid solvent shown in Figure 1.4 model II.

Oxygen atoms, different types of hydroxyl groups, and exposed metal atoms all affect the charge localisation on the support surface as each of these species has different chemical properties. Oxygen atoms behave as Lewis bases, metal cations as Lewis acids, while hydroxyl groups can be classified as acidic, neutral or basic depending upon there attachment

on the surface. Single bonded hydroxyl groups have a basic character, while bridged hydroxyl groups are more acidic. These functional groups have two major roles in supported metal catalysis. Firstly, they act as anchoring sites for the metal precursor during impregnation, and secondly, they supply active sites in multifunctional catalysis [Foger, 1985].

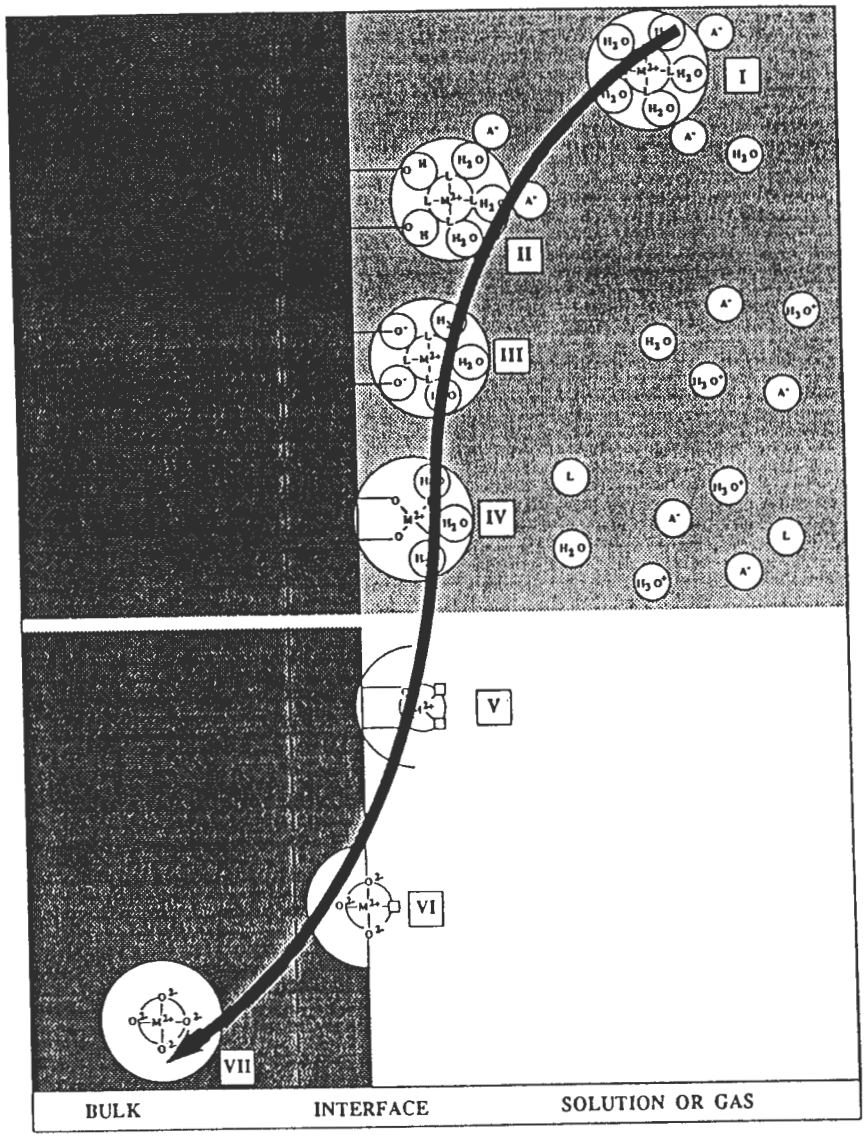

Figure 1.4. Representation of the outer sphere of solvation and coordination sphere of transition metal ions at various positions relative to the oxide-fluid interface. The left hand side represents the solid oxide. The shaded part on the right hand side represents the solution while the lower white part on the same side represents the gas. [Che, 1993]

In the case of Fischer Tropsch synthesis, their role as an anchorage point for the precursor greatly influences the final physical characteristics and performance of the catalyst. Parks et al. [1985] have studied one specific example of this anchorage. They investigated surface precipitation phenomena in the $Co(II)/Al_2O_3$ sorption system using $Co(NO_3)_2.6H_2O$ as precursor. When high concentrations of cations are sorbed onto oxide surfaces there is no observed limit on sorption due to occupation of vacant sites. In these under-saturated conditions, they showed that the presence of a sorbent material induces precipitation under certain pH and concentration levels, and that this precipitation results in a phase similar to $Co(OH)_2$, consisting of ternary or double hydroxides of Co and Al. This phase was seen to be hydrous and disordered with high concentrations of Co vacancies. These findings are significant for several reasons. The first is that formation of a disordered precipitate of the cation may happen easily, leading to non-uniform metal dispersions across the oxide surface. Furthermore, during activation treatments, there is a strong possibility that large quantities of cobalt will end up in forms other than the active phase. Consequently it is important to understand factors that induce surface precipitation. These factors include the concentration of metal ions in solution, the preparation temperature and the pH at which preparation takes place.

1.4.1.1.3 Influence of pH on surface charge in solution

When an oxide is brought into contact with an aqueous solution, for example in the case of an impregnation step, the surface hydroxyl groups enter into the following equilibria:

$$M\text{-}OH + H^+ \Leftrightarrow [M\text{-}OH_2]^+, \quad \text{or} \quad M\text{-}OH + H_2O \Leftrightarrow [M\text{-}OH_2]^+ + OH^- \qquad .....(1)$$

$$M\text{-}OH + OH^- \Leftrightarrow M\text{-}O^{(-)} + H_2O \qquad .....(2)$$

Equation one results from involvement of basic oxides, while equation two results from acidic oxides. This equilibration is a surface polarisation associated with the dissociation of surface hydroxyl species and the readsorption of hydroxo complexes that are formed via the partial dissolution of the oxide particle [Parks and DeBruyn, 1962]. The extent to which the surface charging takes place is dependent upon the pH of the solution with which the surface is in contact, as a result of the involvement of both H^+ and OH^- ions. At a specific pH, the net surface charge is zero. This is called the point of zero charge (PZC) or the isoelectric point

(IEP). Above the PZC, the surface of an oxide bears a net negative charge (δ-O^-) and will attract and adsorb cations, while below the PZC, anionic species will adsorb onto the positively charged (δ-OH_2^+) surface. The primary role of the pH in terms of what happens at the solid surface is to act as a surface charge selection switch [Che and Bonnevoit, 1988]. Consequently the PZC can be used to predict molecular structures of surface metal oxide species on oxide supports [Brunelle, 1978; Deo and Wachs, 1991].

The PZC becomes important when selecting the type of metal precursor and the pH at which impregnation is carried out due to metal support interactions that result from charge differences between the support surface and the metal precursor.

1.4.1.1.4 Metal Support Interactions

The term "strong metal support interactions" (SMSI) was introduced by Tauster et al. [1977] to explain the lower values for H_2 and CO chemisorption obtained on titania-supported platinum group metals that were reduced above 700K. A metal support interaction can be defined as a direct influence of the support on the chemisorption and catalytic properties of the metal phase either by stabilising unusual metal particle structures, by changing the electronic properties due to electron transfer processes between the metal particles and the support, or chemical bonding between the metal and support [Foger, 1985]. Consequently, support materials can be grouped according to their surface charge in solution within the pH range of 1-14 as [Foger 1985]:

1. Cation adsorbers (support surface showing a net negative charge in solution) for example silica, silica-aluminas and zeolites.
2. Anion adsorbers (surface showing a net positive charge in solution) for example magnesia.
3. Amphoteric supports (adsorb anions in acid, and cations in alkaline solutions) for example alumina, titania and zirconia.

The surface polarisation of the support oxide results in a net positive or negative charge that results in equilibria for anion and cation adsorption represented by the following equations [Foger 1985]:

$$S\text{-}OH + C^{+} \Leftrightarrow S\text{-}O^{-}C^{+} + H^{+} \quad \ldots.(1)$$

$$S\text{-}OH + A^{-} + H_2O \Leftrightarrow S\text{-}OH_2^{+}A^{-} + OH^{-} \quad \ldots.(2)$$

The strength of the interaction between metal and support is principally controlled by:

1. the type of support and nature of the surface (number of functional groups) and,
2. the impregnation solution; where pH, type and concentration of metal compound, and the presence of competing ions play an important role.

From the above equilibrium equations it is clear that cation uptake decreases with increasing acid strength as the presence of H^{+} ions in solution drives the equilibrium in equation (1) to the left. Cation exchange affinity is a function of charge and cation radius, i.e. $M^{4+} > M^{1+}$, while anion exchange affinity increases with the polarisability of the anions and the anionic charge, e.g. $I^{-} > Br^{-} > Cl^{-}$, and $SO_4^{2-} > Cl^{-}$ [Foger, 1985].

SMSI during impregnation result in a metal precursor concentration gradient from the pore mouth through to the centre of the support yielding an egg shell distribution. In order to minimise this gradient, care must be taken to:

1. Ensure that enough precursor is present to saturate every adsorption site;
2. And allow long contact times between the support and impregnating solution.

These factors are significant and an understanding of their influence is useful in selecting optimal impregnation solution conditions.

1.4.1.1.5 Influence of Impregnation Solution

The impregnation solution comprises molecules that can complex with the cation altering the bonds that form between cation and the support surface. In aqueous solution, transition metal ions are complexed by water and other ligands, forming an inner or coordination sphere surrounding the metal ion, with the ligands arranging themselves in an octahedral configuration around the cation. Ligands differ in the strength of the crystal field that they exert when complexed with the cation. As the field strength increases, the transition metal ion

becomes increasingly protected limiting the attachment options at the surface of the support. This is the case for transition metal ions complexed with ethylenediamine. In this case, the oxide surface acts as a monodentate ligand at the fluid-solid interface leading to trans-octahedral complexes. This contrasts to the water ammonia system as a solution. A substitution of water for ammonia in the nickel hexaamine complex results in a weakened coordination sphere. This weakening allows the oxide surface to act as a bidentate ligand forming a neutral cis-octahedral complex at the oxide surface [Burwell et al., 1965]. Thus in terms of ligand strength the order can be illustrated as follows:

H_2O < NH_3 < ethylenediamine

1.4.2 Catalyst Activation

Drying, calcination and reduction activate the catalyst. Each of these processes results in changes in the physical structure of the catalyst. In the case of supported metal catalysts, this change pertains particularly to the phase of the supported metal, it's dispersion, and the strength of interaction with the support.

1.4.2.1 Drying

Drying of the catalyst removes the solvent used in the precursor deposition. Because the solvent is usually water, this treatment often takes place between 80 and 220°C. During liquid-phase impregnation, the catalytically active species is transported to the interior of the support through capillary forces and diffusional effects. An equilibrium between the adsorbed phase and the solute phase results as determined by the adsorption isotherm. Most preparations aim at achieving a catalyst that has the active metal phase distributed uniformly throughout the support. This distribution, although affected during the reduction step, is largely determined by the concentration profile through the support during impregnation and drying. The strength of interaction between the metal and support strongly affects the spatial arrangement of the metal on the support following the drying phase. The stronger the interaction between precursor and support, the less likely it is that redistribution will take place during the drying phase.

Consequently, the presence of SMSI will result in a catalyst that shows a high dispersion of the metal phase. Dispersion is defined as the fraction of the exposed active metal atoms relative to the total number of metal atoms. From this definition it is clear that as the dispersion increases, the size groupings of active metal species on the surface will decrease so as to leave a greater fraction exposed. The reverse is also true. Weak interaction between metal and support leads to a uniform distribution initially, however the drying phase results in redistribution, as well as the formation of larger metal groupings on the surface. During drying, evaporation of the solvent takes place at the pore mouths while solution flows from the interior of the particles towards them. This has the effect of concentrating impregnation solution at the pore mouths giving an egg-shell distribution.

The transport of precursor to the outer shell of the support particle can be inhibited by

1. using very high heating rates [Fenelov et al., 1979]; or
2. increasing the solution viscosity which inhibits redistribution [Kotter and Riekert, 1979].

Both of these conditions increase the rate at which water is removed relative to the rate of liquid capillary flow.

1.4.2.2 Calcination

Calcination is a medium to high temperature treatment that is often performed in an oxidising atmosphere. The aim of calcination is three-fold [Foger, 1985]:

1. Calcination decomposes the precursor compound forming an oxide species. This takes place with $Co(NO_3)_2$, where the nitrate decomposes to Co_3O_4 releasing NO_2 gas;
2. Calcination results in a dehydroxylation reaction between the precursor oxide and the support that leads to chemical bonding that is absent during impregnation;
3. Calcination leads to sintering of the metal oxide, at the expense of metal dispersion on the support.

Two parameters play an important role during calcination. These are the final temperature at which the catalyst is calcined, as well as the rate at which that temperature is reached [Iglesia,

1997]. Higher temperature treatments often lead to extremely strong bonds between the metal oxide and the support. This effect has been noted for both cobalt and nickel on alumina [Arnouldy and Moulijn, 1985]. The mobility of the cobalt ions increases as the calcination temperature increases causing them to migrate into the lattice framework of the support. When this occurs, excessively high reduction temperatures are needed to yield the active metallic phase. This is not to say that any form of interaction between metal oxide and support is undesirable. On the contrary, interaction keeps the metal oxide well dispersed on the support. Consequently, the calcination step should be avoided if it results in the formation of large metal oxide clusters. Iglesia [1997] showed that cobalt dispersion on silica almost doubled on elimination of the calcination step.

The rate at which the temperature is increased to its final value has a significant effect on the final dispersion of the catalyst. This effect was well illustrated by Iglesia [1997]. His work showed that lowering the heating rate could increase the cobalt dispersion on a silica support significantly.
Where the cobalt nitrate precursor is used, the exothermicity of decomposition leads to increased local temperatures on the support surface resulting in larger Co agglomerates.

1.4.2.3 Reduction

Reduction is the final stage of catalyst activation. The metal oxide undergoes a transformation to the metallic state, leaving metal atoms and small metal clusters on the support surface. This reduction frequently takes place in hydrogen, although strong reducing agents such as CO are also employed. The transformation of the metal precursor (Metal nitrate in this case) is illustrated in the following equations:

$$M(NO_3)_2 \rightarrow MO + NO_2 \quad \text{.....(1) Decomposition of precursor}$$

$$MO + H_2 \rightarrow M + H_2O \quad \text{.....(2) Reduction of metal}$$

The possibility of reduction of the metal oxide is bound by thermodynamic constraints. The possibility arises if the change in Gibbs Free Energy (ΔG) becomes negative. The standard free energy for the reduction of oxides can be evaluated from equation (3)

$$\Delta G = \Delta G^\circ + RT \ln[P_{H2O} / P_{H2}] \quad .....(3)$$

From equation (3) it is clear that reduction becomes favourable for large negative values of ΔG°, or where the partial pressure of water is small. For the case of cobalt on silica, water has been shown to induce the formation of cobalt silicates where the thermodynamics do not favour reduction. These cobalt silicates are highly undesirable, as reduction temperatures between 800 and 1000°C are needed to achieve activation. These temperatures are not practical or feasible.

A possible solution to the effect of water partial pressure is to increase the flow of hydrogen over the catalyst while using slow temperature ramping protocols. The increased hydrogen flow results in a flushing of water vapour, and increases the hydrogen partial pressure. A slower temperature ramp reduces the rate at which reduction takes place, and in so doing, decreases the amount of water vapour present. Iglesia [1997] investigated both of the above effects for the reduction step. He noted that dispersion increased as H_2 flow increased, and the temperature ramping rate was slowed.

1.5 Catalyst Characterisation

Catalyst characterisation plays an integral role in catalyst design as it provides an evaluation of the physico-chemical properties of the catalyst on both a quantitative and qualitative level. These properties (mechanical strength, distribution of the metal phase, surface area, metal-support interaction etc.) influence the activity, selectivity and lifetime of the catalyst, as well as heat and mass transfer, which determine active site accessibility. The characterisation serves to link the catalyst performance under reaction with the structural and electronic properties of the catalyst, allowing changes in performance and properties to be correlated.

Many techniques are available for this purpose including X-ray methods (X-ray diffractometry (XRD), and Extended X-ray Absorption Fine Structure Spectroscopy (EXAFS)), electron microscopy (TEM or SEM), electron spectroscopy (XPS) and infrared spectroscopy (IR). The major limitation associated with these methods is that they are not applicable to catalysts under working conditions. Other techniques of importance to

supported metal catalyst characterisation are temperature programmed reduction and hydrogen chemisorption.

1.5.1 Temperature Programmed Reduction

Temperature programmed reduction (TPR) is one of a class of temperature programmed techniques including temperature programmed oxidation (TPO), desorption (TPD) and sulphidisation (TPS).

The basic format of all of these involves the monitoring of a chemical reaction while the temperature is increased linearly with time. In the case of TPR, a reducing gas (usually H_2) is passed over a fixed amount of solid catalyst. The temperature is ramped between two fixed temperatures at a linear rate. The progress of reaction is monitored using a thermal conductivity detector that picks up changes in hydrogen concentration in the exit due to consumption over the catalyst.

The reactor containing the catalyst is situated in a furnace that has a temperature programmable controller. The reactor effluent passes through a molsieve that traps the water, followed by a TCD to detect hydrogen consumption.

Other methods for monitoring the progress of reduction include measuring the change in pressure/concentration of the product gas, and observing the change in catalyst mass during reduction. Temperature programmed reduction is particularly useful for the characterisation of metal oxide catalysts. The results obtained are both quantitative and qualitative in nature. The amount of hydrogen consumed during reduction gives information on the fraction of metal oxide reduced, while the temperature and shape of the peaks give a qualitative assessment on the ease of reduction and knowledge of the particular metal or metal oxide species present.

1.5.1.1 Application of TPR to metal oxides

In TPR oxidic species are reduced according to the following general reduction pathway:

$$MO + H_2 \rightarrow M + H_2O \quad \ldots(1)$$

The thermodynamics of the reaction (1) as measured by the change in Gibbs Free Energy is :

$$\Delta G = \Delta G^\circ + RT \ln[P_{H2O} / P_{H2}] \quad \ldots(2)$$

During reduction, the constantly increasing temperatures as well as the gas flow rates over the catalyst keep the partial pressure of water low. Under these conditions, reduction of the metal oxide remains thermodynamically feasible.

1.5.2 Hydrogen Chemisorption

Chemisorption is the technique used to calculate the number of exposed metal atoms on the surface, and to obtain metal surface areas and average metal particle sizes. Other techniques such as TEM (Transition electron microscopy) and XRD-line broadening are also used to calculate metal particle sizes and metal surface areas.

During chemisorption, a selected gas (usually H_2) is adsorbed onto the supported metal such that under specified conditions such that a chemisorbed monolayer of gas is formed on the metal without a significant contribution from the support. The monolayer coverage is measured either by volumetric, gravimetric, chromatographic techniques or titration [Foger, 1985]. If the surface contribution is negligible, then the adsorbed gas is chemisorbed to the exposed metal atoms, allowing calculation of the metal surface area, the average particle size and the number of surface atoms exposed.

1.5.3 Zeta Potential Measurement

When particles are suspended in a liquid solution, they are observed to migrate in one direction when an electronic field is applied. As the particle-liquid system is as a whole electronically neutral, the existence of an electrical double layer is proposed to explain this movement. The velocity of the particle can be measured microscopically using lasers applied to dilute solutions in an analyser called a zetasizer. The effective surface charge of suspended particles is measured by applying a constant electrical current across the suspension. This current induces a movement of the particles into or out of a cell called electrophoresis and is brought about by a timed exposure to the electrical potential. Weighing the cell allows establishment of the excess or deficiency of particles in the cell. From this weight measurement the zeta potential is calculated. [Webb and Orr, 1997]

1.6 Catalyst Deactivation

Catalyst deactivation refers to a decline in the activity of a catalyst as a result of factors such as pore blockage and active site coverage that arise from the deposition of carbonaceous material (coke formation). Most catalysts undergo some degree of deactivation during reaction. The rate at which this happens is of extreme importance in industry, and can be the defining feature that makes or breaks the economic feasibility of a proposed venture. Other forms of catalyst deactivation that take place during Fischer Tropsch synthesis include [Royo et al., 1996]:

- catalyst sintering, a process where the metal crystallites on the catalyst surface agglomerate resulting in a decrease in active metal surface area,
- the conversion of the active metal phase to inert oxides, and
- the chemical poisoning of the surface resulting from the presence of poisons such as sulphur in the feed.

1.6.1 Catalyst Stability

The stability of the catalyst (i.e. resistance to deactivation) becomes more significant as the active metal used becomes more expensive. The high cost of cobalt relative to iron demands that cobalt catalysts show higher stabilities in order to ensure extended run times. Van Berge and Everson [1997] investigated the time on stream behaviour of a cobalt based catalyst. Figure 1.5 shows this behaviour over a 25 day period. They concluded that the deactivation of the catalyst involves two phases A and B. The first phase (A) results from the build-up of high molecular weight hydrocarbons in the catalyst pores, and is a reversible deactivation. Phase B was attributed to the irreversible poisoning of the catalyst and the rate of this poisoning was found to be directly proportional to the syngas space velocity. The deactivation was attributed to low level sulphur poisoning originating from the sulphur present in the coal-based syngas feedstock. Phase B is of critical importance to the commercial viability of the catalyst.

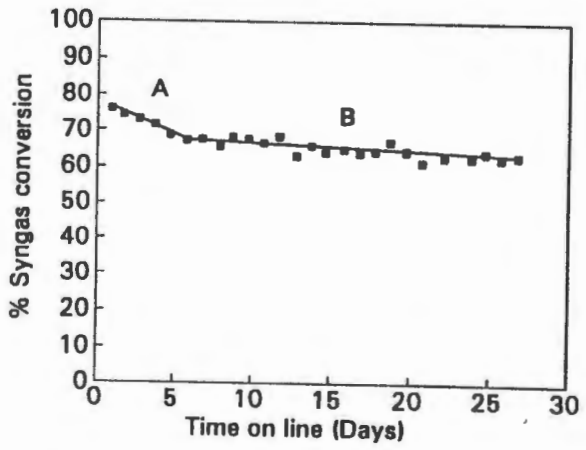

Figure 1.5. Stability run for a Sasol produced cobalt catalyst, T = 220°C, P = 20 bar, H_2/ CO = 2. [Van Berge and Everson, 1997]

1.6.2 Coke Formation

Coke formation and deposition is a common cause of catalyst deactivation in the chemical and petrochemical industries. Coke deposition decreases the number of active sites available for reaction in two ways; firstly by direct covering of the active sites, and secondly through indirect means where the active sites are unaffected, but access of reactant to these sites is limited through pore mouth blockage. Unlike sintering, which is an irreversible process, coke formation can often be reversed under mild thermal treatments. The removal of coke deposits is often carried out in a stream of either air, hydrogen, steam, carbon monoxide or a combination of these. This regeneration results in the combustion of coke from the surface, and is often accompanied by significant temperature increases due to its exothermic nature [Royo et al., 1996]. The maximum temperature needs to be limited to prevent irreversible sintering of the catalyst, and can be achieved by controlling the gas feed rate.

1.7 Problems with Supported Cobalt Catalysts for FT-synthesis

The use of cobalt as a Fischer-Tropsch catalyst provides certain beneficial features over other choices of active metal. These features include low water-gas shift activity, as well as high selectivity to high molecular weight straight-chain waxes that are valuable products or can be hydrocracked to products in the middle distillate range. These advantages gained with cobalt often come at a price, as activity can be reduced due to low reducibility of supported cobalt catalysts and deactivation via cobalt metal re-oxidation for small cobalt particles.

1.7.1 Low Reducibility of Supported Cobalt Catalysts

A great deal of work carried out to develop silica and alumina supported cobalt catalysts that maintain a high degree of dispersion has focussed on ways of increasing the reducibility of the cobalt oxide on the support. Both the silica and alumina supports often induce strong interactions with the metal. Reuel and Bartholomew [1984] studied the effect of support and preparation method on the behaviour of the cobalt catalyst. They concluded that low cobalt

reducibility derived from the formation of surface spinels through strong interaction between cobalt and the support. These species were seen to reduce at temperatures greater than 550°C. However reduction at these temperatures would induce rapid sintering of the metal, lowering instead of enhancing activity [Kogelbauer et al., 1995; Puskas et al., 1992].

Mehanjiev and Dimitrova [1981] and Mehanjiev et al. [1984] observed behaviour on alumina similar to that observed on silica. They identified two cobalt species prior to reduction. The first specie was an easily reducible Co_3O_4 phase, observed only for cobalt loadings greater than 2 wt%. The second phase was composed of Co^{2+} ions which had diffused into the alumina lattice. The Co^{2+} ions occupy tetrahedral and octahedral positions in the alumina framework forming a surface spinel of $CoAl_2O_4$ [Chin and Hercules, 1982]. The activity of the catalyst was largely determined by the percentage of cobalt present as the Co_3O_4 phase. The calcination temperature [Sewell et al., 1995], the pH of impregnation [Bonnevoit et al., 1989; Ming and Baker, 1995], the cobalt precursor [Rosynek and Polansky, 1991], the concentration of NO_x gas at the surface [Coulter and Sault, 1995] and the presence of water vapour over the SiO_2 supported cobalt catalyst [Kogelbauer et al., 1995] affect the percentage of each phase.

1.7.2 Deactivation Through Cobalt Re-oxidation

The reducibility of metal oxides increases in the order Fe, Co, Ni and Ru. The possibility of re-oxidation in an H_2/H_2O atmosphere decreases in the same order [Dry, 1981; Anderson, 1956]. Under Fischer-Tropsch synthesis conditions bulk oxidation of cobalt is not thermodynamically favoured, however, surface layers may oxidise more readily than the bulk oxides as metal dispersed on a support surface may have different properties to the bulk metal [Huffman et al., 1995; Iglesia et al., 1993]. Hilmen et al. [1997] studied the re-oxidation of alumina supported cobalt catalysts. Their study showed that promotion of the catalyst with Re aided both the initial reduction as well as the re-oxidation of the cobalt during exposure to H_2O/H_2 and H_2O/He feeds. The presence of H_2O resulted in the formation of aluminates with high reduction temperatures deactivating the catalyst. Van Schalkwyk [1998] noted a similar deactivation following water treatment using silica as a support.

1.7.3 Alternative Supports for Fischer Tropsch Cobalt Catalysts

Catalyst preparation focuses on manufacturing a catalyst that achieves the necessary production capability (activity) as well as being selective to some desired product or products. With this in mind, the specific preparation route with regard to metal supported catalysts should result in a catalyst that has high metal dispersion, minimal loss of activity due to interaction with the support, and stability that prevents deactivation. The extent of metal dispersion is largely a function of the strength of interaction with the support material. These two properties are counterproductive, as increased interaction between metal and support yields higher dispersions, but decreasing the metal reducibility. Consequently the choice of support is significant, the aim being to find a support material that enhances dispersion, while maintaining metal reducibility.

CHAPTER 2

EXPERIMENTAL

2. Experimental Procedures

A number of experimental procedures were carried out in order to evaluate the physical and chemical properties of the catalyst, including H_2 chemisorption, AA analysis, TPR, TPO and TEM. The performance of the catalyst was tested under reaction conditions. The following section documents these procedures and experimental set-ups.

2.1 Catalyst Synthesis

Three materials were used as supports for the cobalt catalysts, namely SiO_2, ZnO and MnO. Table 2.1 shows the physical data of SiO_2, ZnO and MnO. The supports were obtained from commercial suppliers and used as delivered. SiO_2 is a commonly used support material and has a high surface area. The surface area of the MnO is only 4% of that of SiO_2. ZnO has an even smaller surface area (only 1% of that of SiO_2). The average pore diameters of the materials were calculated using the following expression:

$$\text{Pore diameter} = 4 \times \text{Pore volume} / \text{Surface area}$$

The crystallinity of the three supports was determined by XRD and can be found in section 3.1.3.

The catalysts were prepared to yield each catalyst with a 9wt% loading of reduced cobalt metal. The catalysts were prepared using the following technique:

- The correct amount of cobalt nitrate $[Co(NO_3)_2.6H_2O]$ or cobalt acetate $[(CH_3COO)_2Co.4H_2O]$ was weighed out and placed in 50 ml of deionised water. The cobalt crystals were dissolved in the water. The resultant solution was added to 5 grams of support.
- As a result of the charge difference between the cobalt salt solution and the support used, the mixtures were allowed to stand for two days to allow charge equilibration.

- In order to study the effect of the pH of impregnation, nitric acid was added to vary the pH of the cobalt nitrate precursor, while glacial acetic acid was used to adjust the pH of the acetate precursor solution.
- Monoethylenediamine was used to raise the pH above neutral in order to study the effect of an alkaline precursor solution.
- The supernatant was removed under 50mmHg vacuum in a condenser system as illustrated in Figure 2.1. The oil bath temperature was set at 110°C, and the system yielded drying times of between 1.5 and 2.5 hours.
- The catalyst was reduced on the TPR rig using a gas mixture of 5% H_2 in N_2. The reduction was carried out by ramping the temperature at 1°C/min from room temperature to 400°C. The temperature was held at 400°C for 16 hours. It has been shown that the smaller the ramp temperature, the smaller is the cobalt cluster size on the surface, hence the slow ramp should yield higher dispersions [Iglesia, 1997].

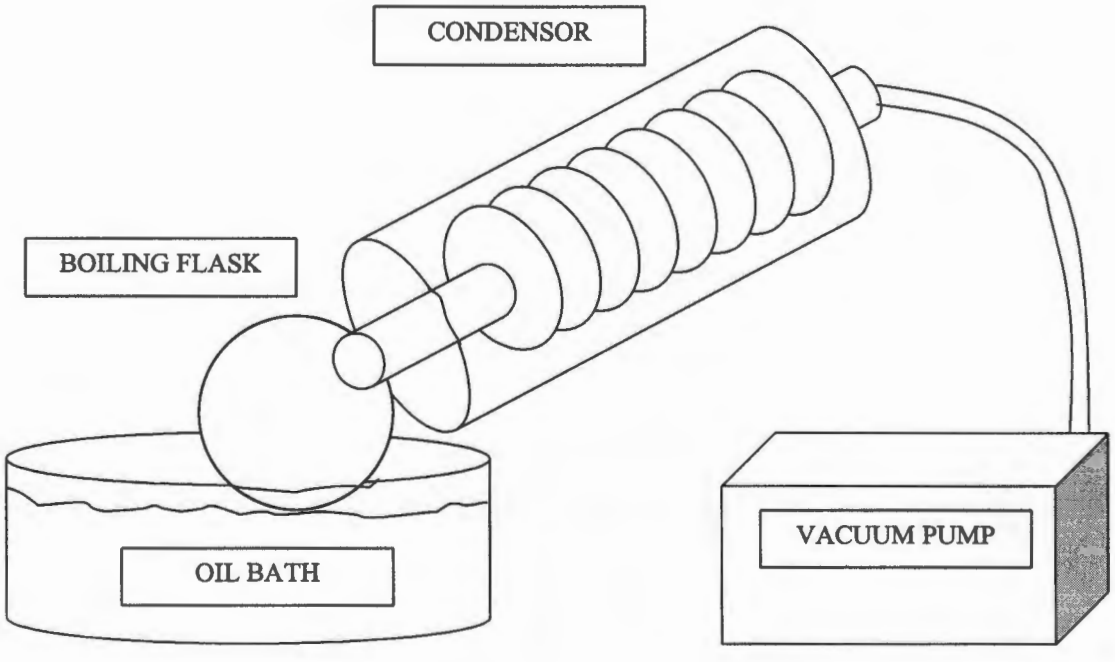

Figure 2.1 Experimental apparatus for catalyst drying procedure.

Table 2.2 shows the names given to each catalyst which where derived according to the

differences in preparation procedures.

Table 2.1 Physical characteristics of the three supports used.

Support	Surface Area (m^2/g)	Pore Volume (cm^3/g)	Pore Diameter (Å)	Supplier
SiO_2	300	1.15	153	Aldrich
ZnO	3	0.007	93	Saarchem
MnO	12	0.034	113	Aldrich

Table 2.2 Composition and nomenclature of catalysts

Catalyst Name	Precursor	Solvent	Final pH	Ageing Time	Support
Co/SiO_2	$Co(NO_3)_2$	Water	5.8	2 days	SiO_2
Co/ZnO	$Co(NO_3)_2$	Water	5.9	2 days	ZnO
Co/MnO	$Co(NO_3)_2$	Water	6.2	2 days	MnO
$Co(A)/SiO_2$	$Co(CH_3CO_2)_2$	Water	6.5	2 days	SiO_2
Co(A)/ZnO	$Co(CH_3CO_2)_2$	Water	6.7	2 days	ZnO
Co(A)/MnO	$Co(CH_3CO_2)_2$	Water	7.1	2 days	MnO
$Co/1/SiO_2$	$Co(NO_3)_2$	Water	1.0	2 days	SiO_2
$Co(A)/4/SiO_2$	$Co(CH_3CO_2)_2$	Water	4.0	2 days	SiO_2
Co/4/MnO	$Co(NO_3)_2$	Water	4.0	2 days	MnO
$Co(MED)/SiO_2$	$Co(NO_3)_2$	MED added	8.1	0 days	SiO_2
Co(MED)/ZnO	$Co(NO_3)_2$	MED added	8.3	0 days	ZnO
Co(MED)/MnO	$Co(NO_3)_2$	MED added	9.5	0 days	MnO
$Co/0/SiO_2$	$Co(NO_3)_2$	Water	4.9	0 days	SiO_2

2.2 Catalyst Characterisation

The various techniques outlined in the following section all play an important role in examining the physical properties that largely determine the success or failure of that catalyst. Characterisation provides valuable information about the structural, electronic and chemical properties of the active catalyst component, knowledge that provides the wherewithal to explain catalyst performance in detail. Characterisation techniques used in this work were zeta potential measurements, temperature programmed reduction (TPR), temperature programmed oxidation (TPO), transition electron microscopy (TEM), hydrogen chemisorption, and atomic absorption spectroscopy (AAS).

2.2.1 Zeta Potential Measurements

A Zetasizer was used to obtain zeta potential measurements of the three supports studied, namely SiO_2, ZnO and MnO. Zeta potential is a measure of the net charge on the surface of a substance (inorganic oxides in this case) when the substance is placed in solution. The equilibrium that develops between the positive and negative ions on the surface and in solution determines whether the surface charge has a net negative or positive value. Changes in the pH of the solution affect the equilibrium and alter the net surface charge. The surface charge is important in understanding the interaction that takes place between the support and the Co^{2+} ions that are loaded during impregnation.

Consequently plots of zeta potential versus pH were prepared for each support as follows:

- A small mass of support (~0.1 gram) was finely ground so that it would exist as a suspension in a solution.
- The support was placed in 50 ml of 0.05 M solution of KCl and shaken. KCl was chosen as both K^+ and Cl^- ions would behave as spectator ions and not avoid the surface-solution equilibrium.

- The pH of the solution was adjusted in the acid range using HCl, and in the alkaline range using KOH in order to add H^+ ions and OH^- respectively, while introducing only spectator ions as the conjugate ions.
- For each pH adjustment, an injection was done in the zetasizer. The zetasizer was set to take three measurements per injection and give an average zeta reading and error at that specific pH.
- Zeta results were stored on computer for further analysis.

2.2.2 Temperature Programmed Reduction

Temperature programmed reduction (TPR) was used to evaluate the reduction behaviours of the catalysts synthesised during this work. The theory behind TPR is discussed in section 1.5.1, this section will serve to outline the equipment used and the procedure followed.

2.2.2.1 TPR Equipment

Figure 2.2 is a schematic of the TPR equipment. The TPR rig consisted of a quartz cell housed in a furnace capable of achieving temperatures in excess of 1000°C. The quartz cell contained a thermowell which held a thermocouple in close proximity to the catalyst bed in order to maintain accurate control of the temperature.

A mixture of 5% H_2 in N_2 was used as the reducing gas, while N_2 gas was used as a reference gas. The flow of each of these gases was controlled using Brooks 9650 Series mass flow controllers. Bubble meters were used to calibrate the mass flow controller settings. A thermal conductivity detector was used to monitor the extent of consumption of hydrogen over the catalyst by logging changes in thermal conductivity of the reducing gas relative to the nitrogen reference stream of constant thermal conductivity. A 3 Å molecular sieve was situated downstream of the catalyst in order to trap water vapour formed during metal oxide reduction.

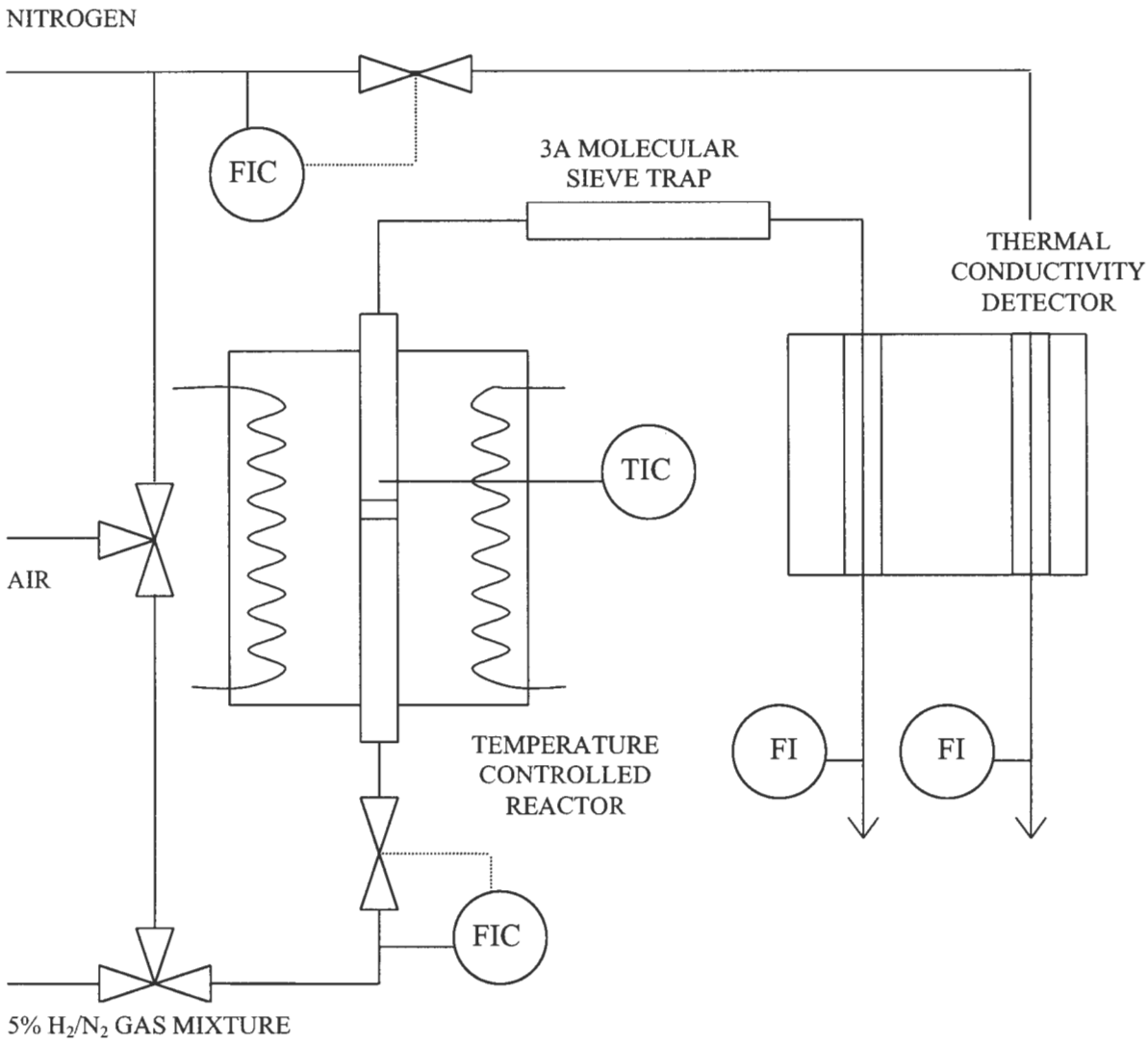

Figure 2.2. Diagram of the temperature programmed reduction apparatus

2.2.2.2 TPR Procedure

A mass of catalyst (typically 0.15 gram) was loaded into the quartz cell, resting upon a porous quartz frit. The quartz cell was secured inside the furnace through attachment at either end to stainless steel tubing. The reference and sample gas flows were adjusted to 60(NTP)ml/min using the mass flow controllers, the bubble columns and a stopwatch. A temperature programme for the run was chosen by logging the heating rate and final

temperature on a computer software program. The temperature program for the is shown in Figure 2.3.

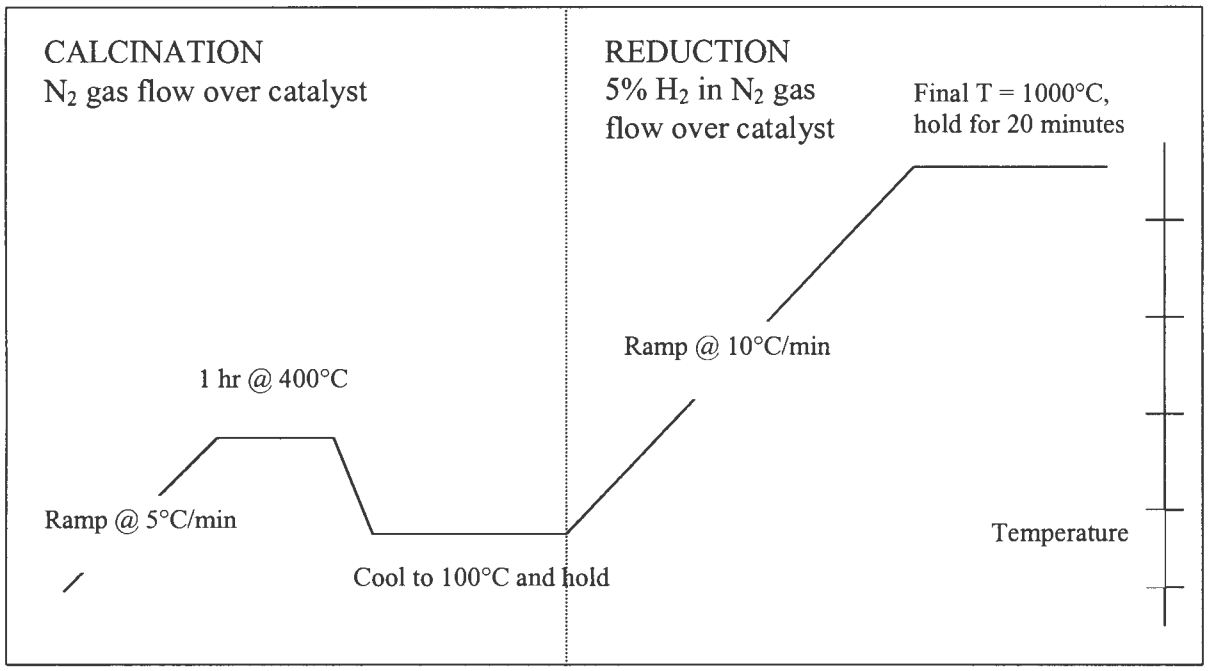

Figure 2.3. Temperature programme used for TPR runs for characterisation of the catalyst precursor.

Initially the catalyst underwent pretreatment in a nitrogen stream. The temperature was ramped at 1°C/min from room temperature to 400°C to decompose the nitrate or acetate still present after drying. The system was allowed to cool down to 100°C and the TCD was switched on and left to stabilise for at least 2 hours. The baseline TCD reading for nitrogen was logged to computer, then the hydrogen gas was switched to pass over the catalyst and the hydrogen baseline reading was logged to computer. The temperature was raised linearly at 10°C/min from 100°C to 1000°C and maintained at 1000°C for 20 minutes to ensure complete reduction of the cobalt to metal form. The data was logged to microcomputer and stored for further analysis. The H_2 in N_2 gas was calibrated using CuO. The calibration can be found in Appendix I. The program used for the TPR runs performed to determine the degree of reduction of the catalysts was as follows. A mass of catalyst at 400°C for 16 hours was placed in the TPR cell. The temperature was ramped at 5°c/min to 100°C. The baseline

nitrogen TCD reading and 5% H_2 in N_2 TCD readings were measured after which the temperature was ramped at 10°C/min from 100°C to 1000°C in the 5% H_2 in N_2 mixture.

2.2.3 X-Ray Diffractometry

Physical characterisation of the catalyst was done using x-ray diffractometry. The catalyst particle is an ordered structure consisting repeated planes of the same kind of atom. When x-rays are reflected from these planes, a diffraction pattern is generated and recorded. Analysis of these results allows for the assessment of the degree of crystallinity of the catalyst material, as well as information enabling determination of the positions of individual atoms in the particle structure.

A Phillips X-ray diffractometer was used to obtain x-ray diffraction spectra using Cu-Kα radiation. The diffractometer operated under the following settings:

- voltage 40kV
- current 25mA
- 2θ range 20 – 70°
- 2θ step size 0.1°
- step duration 1 second

2.2.4 Transmission Electron Microscopy

Transmission electron microscope pictures were taken using a JEOL JEM-200CX microscope. Prior to photography, the catalyst samples were prepared according to the following procedure. Catalyst samples were reduced at 400°C for 16 hours in 5% H_2 in N_2. Each sample was crushed using a mortar and pestle in order to obtain smaller aggregates. The finer catalyst particles were dispersed in methanol and placed on carbon coated copper grids. The samples were left to stand in order to dry. Samples were viewed at 200kV in the electron microscope.

2.2.5 Hydrogen Chemisorption

Hydrogen chemisorption was used to measure the metal surface area of cobalt on the different supports. Measurements were done using a Micrometrics ASAP 2000C apparatus. Hydrogen has been shown to yield monolayer coverage under certain conditions for supported cobalt catalysts [Reuel and Bartholomew, 1984].

The catalyst was first reduced on the TPR rig using a gas mixture of 5% H_2 in N_2. The reduction was carried out by ramping the temperature at 1°C/min from room temperature to 400°C. The temperature was held at 400°C for 16 hours. It has been shown that the smaller the ramp temperature, the smaller is the cobalt cluster size on the surface, hence the slow ramp should yield higher dispersions [Iglesia, 1997].

Following reduction, approximately 0.5g of catalyst was placed in the chemisorption apparatus and re-reduced in situ at 400°C in a H_2 gas stream. The sample was then evacuated for 1 hour to remove any residual hydrogen or water that was present during activation. The sample was then cooled to 100°C under vacuum and the hydrogen adsorption isotherms were measured between 100 and 450 mmHG. The reversibility of the hydrogen adsorption was measured by evacuating the sample at 100°C for 15 minutes and remeasuring the adsorption isotherm. The reversibility of hydrogen adsorption is defined as the amount of hydrogen not removed by evacuation relative to the total hydrogen adsorbed on the catalyst, and is calculated from the following expression :

$$\text{Reversibility} = V_{irr} / V_{total} \times 100\%$$

where V_{irr} represents the amount of hydrogen not able to be removed during 15 minutes of evacuation, and V_{total} represents the total hydrogen uptake of the catalyst. A sample calculation illustrating the procedure for determination of metal surface area, dispersion, average crystallite diameter and reversibility of adsorption can be seen in Appendix II.

2.3 Fischer Tropsch Synthesis

The following section discusses the experimental apparatus and procedures used to evaluate the catalysts' performance under Fischer Tropsch conditions.

2.3.1 Experimental Apparatus

The experimental system used for determining Fischer Tropsch catalyst performance is shown in Figure 2.6. A glass reactor with an ID of 16mm was used. The reactor was a fixed bed type using a frit to position the catalyst in the furnace. A thermowell ran vertically through the length of the reactor. The thermowell housed a thermocouple for accurate measurement of the temperature within the catalyst bed. The thermocouple could be moved vertically allowing measurement of the temperature profile of the bed. The axial temperature profile can be seen in Figure 2.4. The furnace created an isothermal region 3 cm long in which the catalyst was placed. The glass reactor was housed in stainless steel casing with two entrance lines and one exit line. The two entrance lines were separated using a rubber seal. This system allowed one entrance line to flow over the catalyst, while the other line ran as a bypass line down the outside of the reactor. Argon flowed in the one entrance line and served to pressurise the reactor to reaction pressure, while the syngas ($H_2/CO = 2$) flowed in the second entrance line. A schematic of the reactor configuration used for Fischer-Tropsch synthesis can be seen in Figure 2.5.

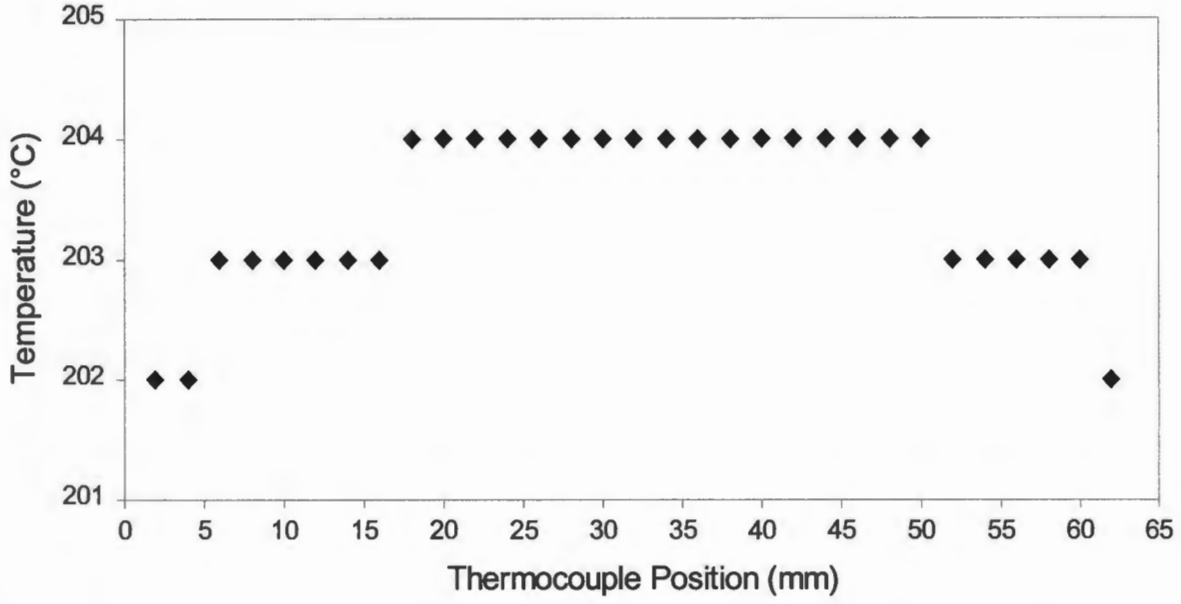

Figure 2.4. Axial bed temperature profile of the reactor in the furnace at approximately 200°C.

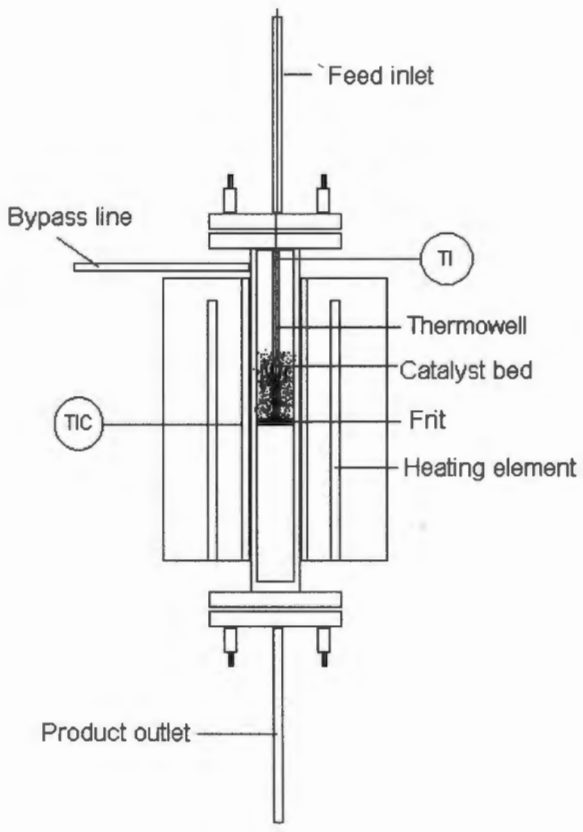

Figure 2.5. Schematic of reactor configuration used for FT synthesis

A four-way valve was used to switch between bypass and reaction, hence controlling which gas flow over the catalyst. The gas flow rates of hydrogen and carbon monoxide were controlled using Brooks Series 9650 mass flow controllers. The argon was controlled from the gas bottle with a pressure regulator to give the necessary reaction pressure. A wax trap was situated at the exit line of the reactor to trap the higher molecular weight hydrocarbons.

The wax trap consisted of a quarter inch stainless steel tube housed within an aluminium block. The temperature of the wax trap was controlled with heating tape and a thermocouple located within the aluminium block. The downstream line was heated to prevent product condensation in the lines, and carried the product stream to a ampoule breaker system for product sampling. A needle valve was situated on the line in order to control the pressure in the reactor and maintain it at 5 bar.

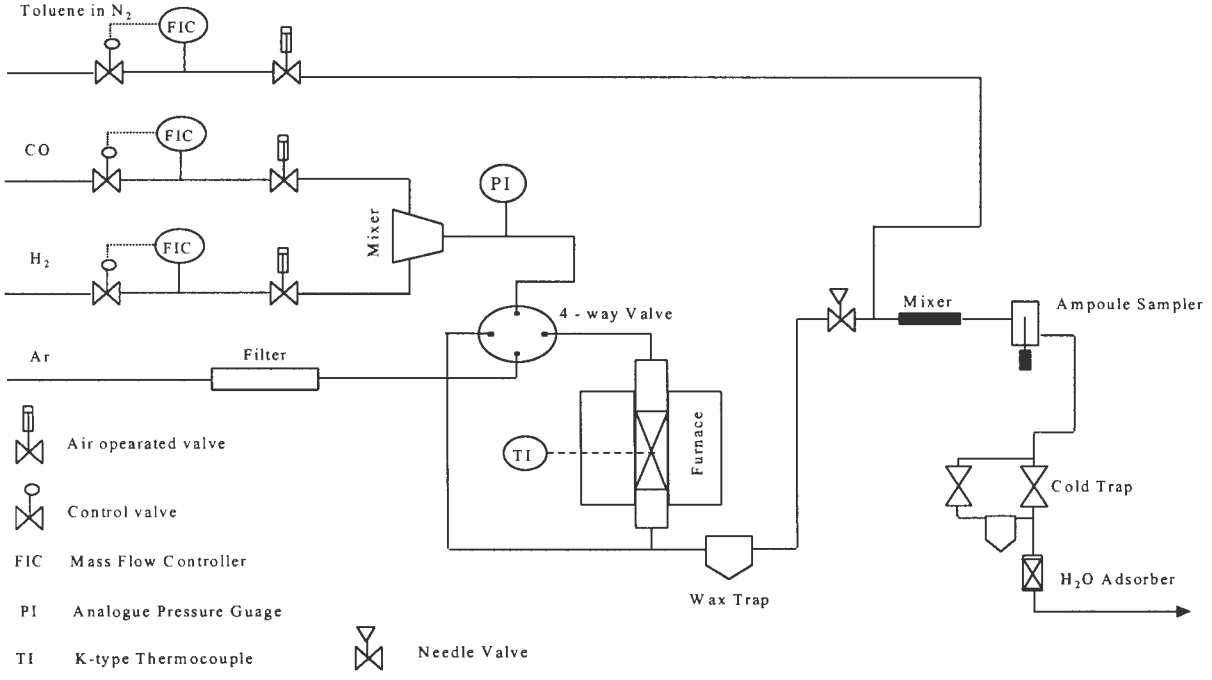

Figure 2.6. Schematic of experimental apparatus for Fischer-Tropsch synthesis reaction work.

A cold trap was used to trap the remaining heavier hydrocarbons and water produced, the exit line of which was vented to the atmosphere.

2.3.2 Experimental Procedure

The reduced catalyst was transferred to the glass reactor and placed in the furnace. Due to weight loss associated with reduction, a mass of approximately 1.4 grams of catalyst was reduced in order to obtain 1 gram of reduced catalyst. No care was taken to transfer the catalyst from reduction to the reactor in a reducing environment. The reduction and reaction conditions can be seen in Table 2.3. Van Steen et al. [1997] showed that surface oxidation was completely reversed after 4 hours with zirconia-containing Co/SiO_2 catalysts. Due to the fact that the CO/H_2 environment of syngas is strongly reducing, it was assumed that a few hours in this environment at reaction conditions would achieve any reversal of surface oxidation that may take place during transfer. In most cases, the catalyst was re-reduced for 4 hours at 200°C in 60 ml(NTP)/min of hydrogen.

Table 2.3. Re-reduction and reaction conditions for Fischer-Tropsch synthesis.

$m_{catalyst}$ (g)	1.0		
Reduction			
$T_{re\text{-}reduction}$ (°C)	200	$F_{Hydrogen}$ (ml (NTP)/min)	60
$t_{re\text{-}reduction}$ (hr)	4		
Reaction Conditions			
$F_{Hydrogen}$ (ml (NTP)/min)	10	$T_{reaction}$ (°C)	200
F_{CO} (ml (NTP)/min)	5	$T_{Wax\ trap}$ (°C)	180
$F_{Toluene\ in\ N2}$ (ml(NTP)/min)	10	$T_{Exit\ lines}$ (°C)	220

On completion of the re-reduction, the four-way valve was switched to allow argon to flow over the catalyst. The wax trap was heated to 180°C and the product lines were heated to 220°C during reduction in order to clean the lines of residual hydrocarbons from previous

runs. The reactor was pressurised to 5 bar with the argon. The H_2, CO and N_2 flows were switched on and adjusted to the desired flow rates. The same flow rates were used for all runs. They were 10 (NTP)ml/min H_2, 5 (NTP)ml/min CO and 10 (NTP)ml/min N_2. The flow rate of the exit line was controlled using the needle valve and a bubble metre connected to the cold trap. The exit flow line was set between 30 and 40 (NTP)ml/min, in order to maintain a low percentage of argon and avoid excessive product dilution.

2.3.3 Product Analysis

Product analysis was carried out in two gas chromatographs. Conversion measurements were obtained through permanent gas analysis on a Varian 3300 Series GC using a thermal conductivity detector (TCD) and a 80/100 Carbosieve II column. The organic product spectrum was analysed in a Varian 3400 gas chromatograph (GC) with a flame ionisation detector (FID) detector and cryogenics installed. The cryogenic system installed on the FID GC made use of CO_2 enabling GC oven temperatures of –70°C. The product separation was achieved using a 38 metre OV-1 type column with 0.25 μm film thickness and 0.25 mm ID. Several runs do not contain information on methane, C_2 and C_3 selectivities as the column in the FID GC broke with the net effect of reducing the column length from 50 m to 38 m upsetting lower hydrocarbon separation.

Prior to reaction, the composition of the bypass stream was analysed by injecting samples with a Hamilton 0.5 ml syringe into the injector port of the TCD GC. When the bypass flows were stable, the four way valve was switched to the reaction position. A Hamilton 5 ml syringe was used for direct injection into the FID GC while ampoule samples were taken for later analysis.

A mixture of 0.1% toluene in N_2 was used as a standard gas for both the TCD and FID analysis, and was fed to the product line after the needle valve. As nitrogen was constant throughout the reaction, and toluene is not a Fischer Tropsch product, this mixture was suitable as a standard.

Conversion and yield calculations are outlined in Appendix III.

CHAPTER 3

RESULTS

3. Results

The three supports used in this study were SiO_2, ZnO and MnO. Much work has been done investigating the performance of cobalt catalysts using SiO_2 as a support [Kuipers et al., 1996; Kogelbauer et al., 1995; Coulter and Sault, 1995]. Consequently SiO_2 is a good base to work from in order to compare the performance of ZnO and MnO as supports for Fischer Tropsch catalysts. The performance of the catalyst has been shown to depend significantly upon the nature of the support used [Bartholomew and Reuel, 1991] as well as upon factors such as the choice of precursor compound, the pH of impregnation and the impregnation solvent employed [Sewell, 1996]. The pH of impregnation affects the interaction between Co^{2+} ions and the support as determined by the zeta potential of the support. These factors affect the extent of reducibility of the active metal on the support which is vital in determining the catalyst activity. It is expected that the strength of interaction is the defining criterion for cobalt reducibility on the catalyst surface.

3.1 Catalyst Characterisation

The surface charge as a function of pH was obtained using a zetasizer. The point of zero charge (PZC) as defined in section 1.4.1.1.3 occurred at a different pH for each of the three supports. The catalyst reducibility of cobalt nitrate and acetate on SiO_2, ZnO and MnO under differing preparation conditions was evaluated using TPR, while metal surface area measurements were determined using hydrogen chemisorption. Base TPR runs were carried out on the supports and the bulk cobalt oxide in order to evaluate the reducibility of the support and metal separately, allowing more accurate interpretation of TPR data.

3.1.1 Zeta Potential Measurements

The charge equilibrium between the surface of an inorganic oxide and the solution in which it is placed is determined by the different functional groups (such as OH^-) that exist on the

support surface, as well as the ratio of OH^- to H^+ ions in solution. The equilibrium can be illustrated as follows:

$$M\text{-}OH + H^+ \Leftrightarrow [M\text{-}OH_2]^+, \quad \text{or} \quad M\text{-}OH + H_2O \Leftrightarrow [M\text{-}OH_2]^+ + OH^-$$

$$M\text{-}OH + OH^- \Leftrightarrow M\text{-}O^{(-)} + H_2O$$

Surface charging takes place to differing extents depending upon the acidity/alkalinity of the solution. An increase in pH will increase the H^+ concentration of the solution, shifting the charge equilibrium of the surface such that more H^+ are adsorbed. The net effect of this is that a decreased pH yields a more positively charged support surface. For each support there is a specific concentration of H^+ ions in solution that results in a net surface charge of zero. This point is called the point of zero charge (PZC). Figure 3.1 illustrates the change in zeta potential with pH for SiO_2, ZnO and MnO showing the pH at which the PZC occurs for each support.

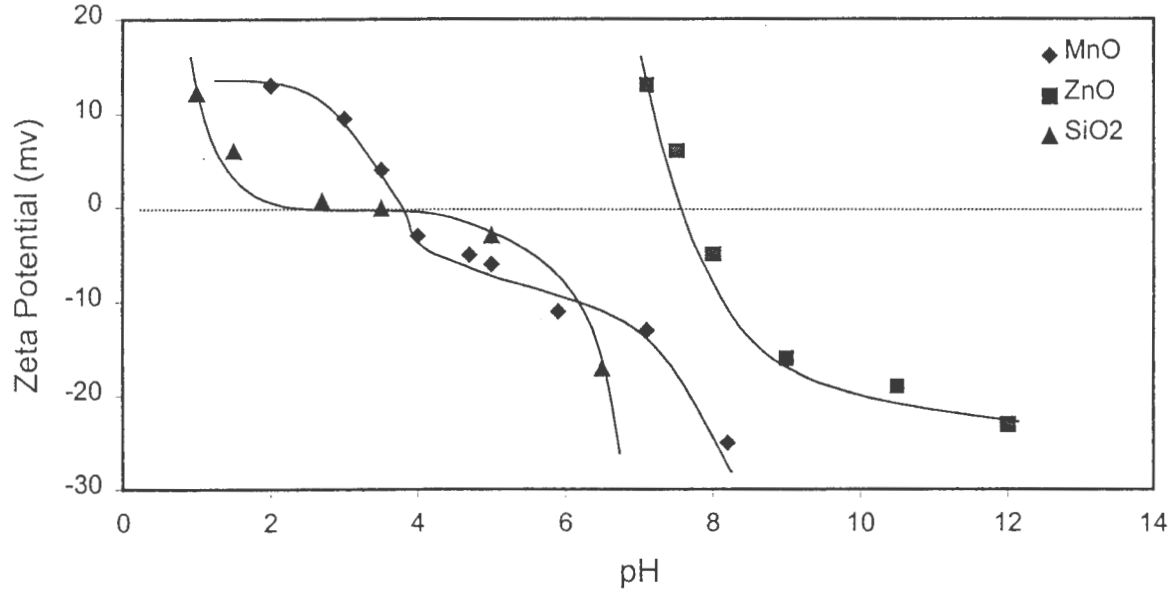

Figure 3.1. Zeta Potential vs. pH for SiO_2, ZnO and MnO.
(0.1g Support in 50ml 0.1 M KCl Solution)

The zeta potential of silica as a function of pH follows a similar trend to that observed by Che and Bonneviot [1988]. At a pH below 2.5, the zeta potential is positive and decreases rapidly

with increasing pH. In this pH range the surface of the silica is on average positively charged. Between a pH of 2.5 and 5, the zeta potential is approximately zero, although there exists a slight surplus of negative charge on the surface. At any pH larger than 5 the surface becomes rapidly more negatively charged.

The point of zero charge (PZC) for MnO is at a pH of approximately 4. At pH values lower than 4, the MnO surface is positively charged. For pH values larger than 4, the MnO surface bears a net negative charge. The zeta potential varies steadily with pH, unlike the ZnO curve which changes dramatically over a small pH range.

ZnO has a PZC at a significantly higher pH than either SiO_2 or MnO. The PZC for ZnO is at a pH of approximately 7.8. At a pH lower than 7.8, the ZnO surface experiences a net positive charge, while at pH values higher than 7.8 the ZnO surface has a net negative charge.

As the pH is lowered, the solubility of each support increases. The ZnO support dissolves completely at a pH of between 5 and 6. The MnO and SiO_2 supports are more resilient, however partial dissolution in strong acidic media does take place with MnO, and to a far lesser extent with SiO_2.

3.1.2 Equilibration of Impregnation pH

It is well known that when an inorganic oxide is placed in a solution of containing H^+ and OH^- ions, an equilibrium reaction begins in order to balance charge between the surface and the solution. This equilibration process may vary in speed depending upon the nature of the support and the concentration of ions in solution. Due to the porous nature of many supports, this equilibration may take days and even months. Consequently, when cobalt was loaded onto SiO_2, ZnO and MnO, the initial pH of solution, as determined by the strong acidic nature of $Co(NO_3)_2.6H_2O$ and the weak acidic nature of $Co(CH_3COO)_2.4H_2O$, was seen to change as a consequence of this equilibration. Table 3.1 shows the initial pH and the final pH after two days of equilibration.

Table 3.1. Impregnation pH equilibration for cobalt nitrate and cobalt acetate on SiO_2, ZnO and MnO.

Precursor	Support	Initial pH	Final pH
Cobalt Nitrate	SiO_2	4.9	5.8
	ZnO	4.9	5.9
	MnO	4.8	6.2
Cobalt Acetate	SiO_2	6.5	6.5
	ZnO	6.9	6.7
	MnO	7.0	7.1

Using cobalt nitrate, the initial pH of the solution is more strongly acidic than the acetate precursor solution. This can be ascribed to the ionic dissociation of $Co(NO_3)_2.6H_2O$ as described by the following equations;

$$Co(NO_3)_2.6H_2O \leftrightarrow Co(H_2O)_6^{2+} + 2NO_3^{2-} \quad \ldots(1)$$

$$Co(H_2O)_6^{2+} \leftrightarrow Co(H_2O)_5OH^{+} + H^{+} \quad \ldots(2)$$

$$H^{+} + NO_3^{-} \leftrightarrow HNO_3 \quad \ldots(3)$$

Equation (1) refers to the dissociation of the cobalt nitrate in solution into Co^{2+} ions and NO_3^- ions. The octahedral hydrated Co^{2+} ions dissociate further as shown in equation (2) in the aqueous solution resulting in the formation of H^+ ions that account for the increase in acidity associated with cobalt nitrate dissolution. Equation (3) illustrates the equilibrium between hydronium ions and nitrate ions. The presence of HNO_3 in water results in almost complete dissociation of the nitric acid. Consequently the equilibrium position of equation (3) lies far to the left, resulting in a high concentration of H^+ ions and a lower pH. The opposite effect is noted with acetate ions. The equilibrium of equation (3) when involving acetate ions lies far to the right as acetic acid remains almost completely undissociated in aqueous solution. Thus the pH of the cobalt acetate solution shows slight acidity but remains close to neutral.

The increase in pH of the cobalt nitrate solution results from the charge equilibration between support surface and impregnation solution.

3.1.3 X-Ray Diffractometry

The X-ray diffraction patterns for the three supports are illustrated in Figure 3.2. The plots show the peak intensity as the diffraction angle is varied. The intensity generated at different

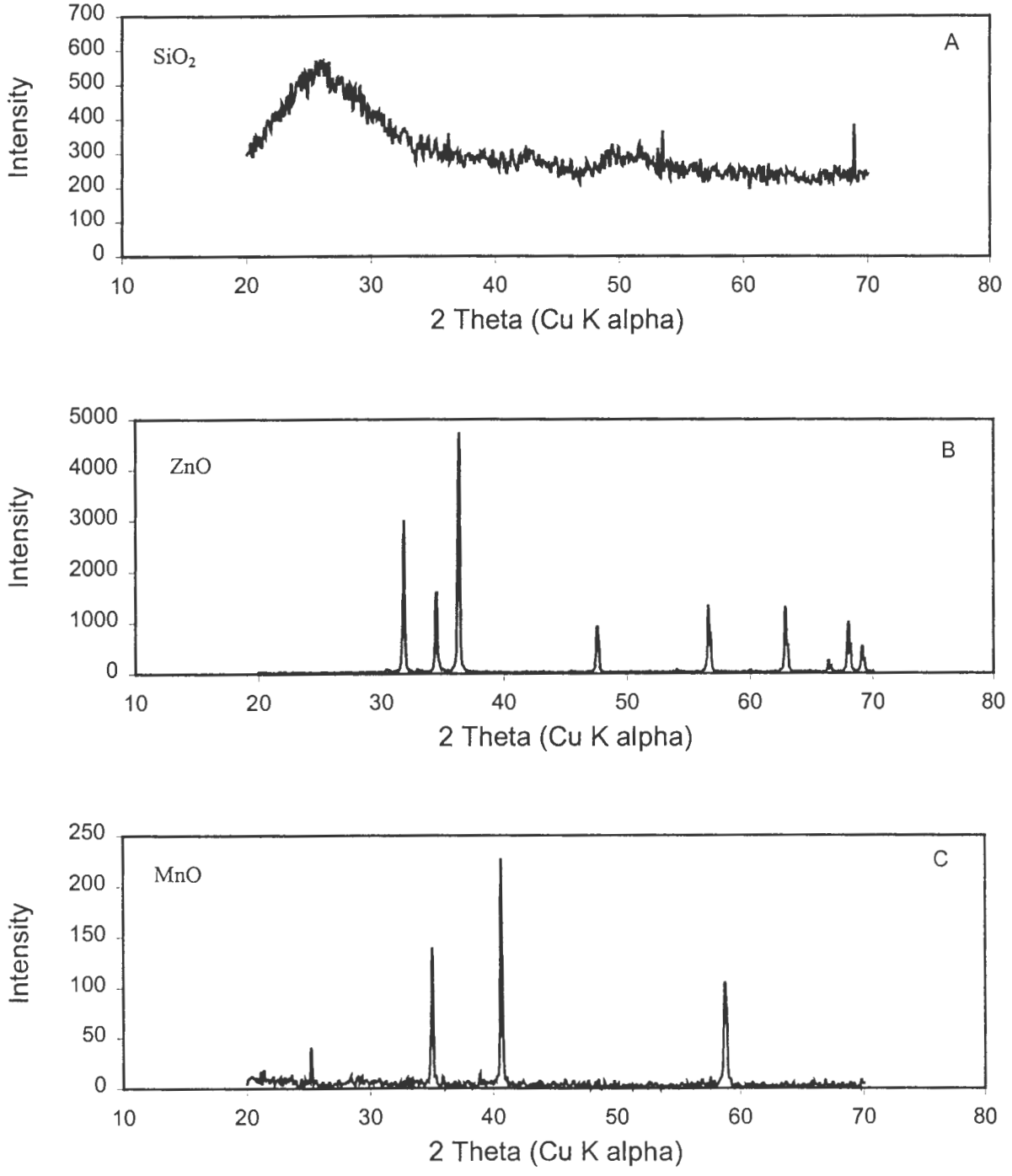

Figure 3.2. XRD patterns for (A) SiO_2, (B) ZnO and (C) MnO.

angles is a measure the degree of crystallinity of the bulk material. The degree of crystallinity can be observed from XRD patterns from the intensity of peaks associated with the relevant material, as well as the extent of peak broadening. The wider the peaks, and the lower the intensity, the more amorphous the material is. From Figure 3.2 (A) it is clear that the bulk structure of the SiO_2 support is amorphous. In other words the support does not exist as a highly structured framework. However the intensity of the characteristic peaks of the ZnO support ZRD pattern indicate a very high degree of crystallinity (Figure 3.2(B)). The XRD pattern of the MnO support (Figure 3.2 (C)) shows a higher degree of crystallinity than the SiO_2 support, but is less crystalline than the ZnO support.

These findings have implications with respect to the way in which cobalt interacts during impregnation, drying and activation. The less structured framework of the amorphous SiO_2 support will show more surface defects than both MnO and ZnO. As these defects serve as anchors for cobalt during impregnation, the SiO_2 will show a higher degree of metal support interaction than the other two supports. The ZnO support will show very little metal support interaction due to a surface poor in functional groups.

3.1.4 Temperature Programmed Reduction

The same procedure was used for all TPR runs. The catalyst was calcined in nitrogen gas for 1 hour at 400°C prior to reduction. The reduction was carried out using 60 ml(NTP)/min of 5% H_2 in N_2 gas. The temperature was ramped from 100°C to 1000°C at 10°C/min and held at 1000°C for 20 minutes to ensure complete reduction of the metal. The only alteration to this program occurred during runs involving the ZnO support. For these runs, a maximum temperature of 650°C was used to avoid interaction between the ZnO and the quartz cell, where the ZnO had previously been seen to diffuse into the quartz leading to disintegration of the quartz cell. Calibration of the TPR apparatus was performed using CuO. The calculation and spectrum can be found in Appendix I.

Reduction of the bulk metal oxide Co_3O_4 is illustrated in Figure 3.3. The bulk oxide Co_3O_4 was reduced under the same conditions as the prepared catalysts in order to compare the reducibility of cobalt on the studied supports. The reduction of the bulk cobalt oxide takes

place as two reduction steps. The first step corresponds to the reduction of Co_3O_4 to CoO, and the second step results from the reduction of CoO to zerovalent cobalt metal. These steps are not clearly evident in Figure 3.3 as a result of high hydrogen consumption and possible oxidation of the Co_3O_4 to Co_2O_3, although the main reduction section comprises a shoulder and a main peak. The stoichiometries of these two steps are illustrated below:

$$Co_3O_4 + H_2 \rightarrow 3CoO + H_2O \qquad H_2/Co = 0.33$$

$$CoO + H_2 \rightarrow Co + H_2O \qquad H_2/Co = 1$$

The experimental hydrogen to cobalt ratio obtained for the total hydrogen to cobalt molar ratio was 1.58. This value was higher than the expected ratio of 1.33, possibly a result of further oxidation of the sample to Co_2O_3 prior to use. Reduction of the cobalt oxide sample was complete by 490°C.

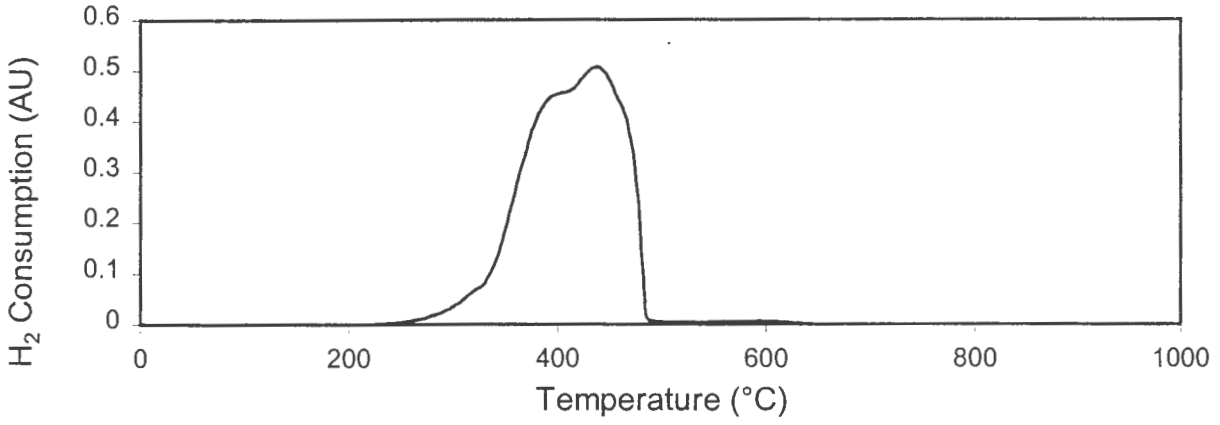

Figure 3.3. Temperature programmed reduction profile of Co_3O_4.
(mass cat ~ 0.05g, heating rate = 10°C/min, Reducing gas = 60ml(NTP)/min 5% H_2 in N_2)

Temperature programmed reduction runs were done on the base MnO support, as well as on MnO that was placed in a nitric acid solution and dried. Figure 3.4 illustrates the TPR profiles obtained. The TPR profile for unaltered MnO showed a very small reduction peak at 400°C, probably a result of small impurities or slight surface oxidation of the MnO support to Mn_2O_3 or MnO_2. The profiles with HNO_3 added were prepared in the same way as the catalysts. MnO was placed in 50ml deionised solution and HNO_3 was added, followed by drying in a

rotavap dryer under vacuum. This was to investigate the high hydrogen to cobalt molar ratios that were attained during TPR for the MnO supported catalysts (see chapter 3.2.1.1 and chapter 3.2.4.1). It was thought that the presence of the nitrate precursor and nitric acid may have resulted in oxidation of the MnO support. This was thought to account for the high ratios observed. This is indeed the case. HNO_3 was placed in solution over the MnO support and dried. One TPR run was carried out on the dried MnO, while a second TPR was performed following calcination of the dried MnO. The calcination step was performed to see if the presence of nitric acid oxidised the support, or whether oxidation took place during the nitrate decomposition.

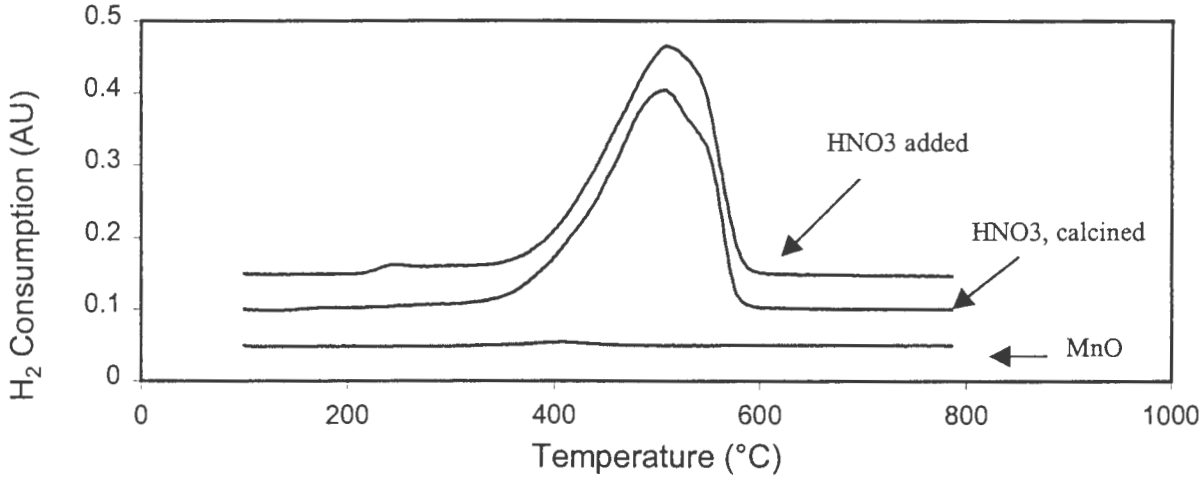

Figure 3.4. TPR profiles for MnO in bought form, with HNO_3 added, and with HNO_3 added and calcined.
(mass cat ~ 0.15g, heating rate = 10°C/min, Reducing gas = 60ml(NTP)/min 5% H_2 in N_2)

The TPR spectra for both cases illustrate significant enhancement of support reducibility relative to the unaltered MnO TPR run. This indicates that MnO can alter oxidation states quite easily. No precursor decomposition was seen for the uncalcined MnO spectrum indicating that the HNO_3 resulted in oxidation while in solution. Table 3.2 shows the hydrogen to manganese molar ratios associated with the spectra in Figure 3.4. The hydrogen to MnO molar ratios were almost unaffected by calcination, indicating that oxidation of the support was complete during the solution and drying phases. The slightly high hydrogen to manganese ratio for the calcined catalyst indicates that calcination may oxidise a fraction of

the MnO. Oxidation of the support was not observed with SiO_2 and ZnO. This can be ascribed to the reluctance of these materials to oxidise.

Table 3.2. TPR hydrogen consumption data for MnO with and without nitric acid addition.

Catalyst	H_2/Mn_{Total} (mol/mol)
HNO_3 on MnO (calcined)	0.325
HNO_3 on MnO	0.319
MnO	~0

3.2 Influence of Catalyst Preparation Procedure

During this investigation, the preparation procedure was varied in order to evaluate the effect of support type, precursor compound impregnation pH, impregnation solvent, and impregnation contact time. The effects were characterised using TPR, hydrogen chemisorption, and TEM, as well as an evaluation of these changes under reaction conditions in terms of catalyst activity and selectivity.

3.2.1 Base Case for SiO_2, ZnO and MnO

A base case catalyst was prepared for each support in order to create a basis with which to evaluate changes in catalyst precursor, impregnation pH, impregnation solution and impregnation contact time. The basis chosen was as follows:

The cobalt source was hydrous cobalt nitrate ($Co(NO_3)_2.6H_2O$). A mass of cobalt nitrate weighed out and dissolved in 50 ml deionised water in order to attain 9 wt% cobalt on the reduced catalyst. This solution was poured onto 5 g of each support. The mixture was shaken for several minutes and left for two days to stand. The pH was taken at the initial

impregnation, and once again just prior to drying 2 days later. Table 3.1 shows the changes in pH for the 3 supports. The supernatant was removed using a rotavap drier as described in chapter 2.1. This procedure yielded 3 cobalt-supported catalysts formed on different supports under the same conditions. The physico-chemical characteristics of the SiO_2, ZnO and MnO supported cobalt catalysts were evaluated using TPR, hydrogen chemisorption and TEM. The catalytic activity and selectivity of each catalyst was obtained under Fischer-Tropsch reaction conditions.

3.2.1.1 Temperature Programmed Reduction

The TPR spectra of the base case SiO_2, ZnO and MnO supported cobalt catalyst precursor prior to reduction can be seen in Figure 3.5. During the preliminary calcination step, the nitrate precursor decomposes releasing NO_2 gas. Nitrate decomposition takes place at approximately 240°C for SiO_2 supported cobalt catalysts [Sewell, 1996]. For this reason no decomposition peak is evident in the spectra. The slower heating rate of 5°C/min and the high gas flow rate over the bed both served to decrease the rate of decomposition and the partial pressure of NO_2 gas at the support surface. NO_2 gas can act as an oxidising agent for Co^{2+}, and consequently plays a role in determining the final state of supported cobalt. Control of the NO_2 concentration at the support surface may enhance metal dispersion on the support surface [Iglesia, 1997]. When the cobalt nitrate precursor is decomposed, the exothermicity of decomposition leads to increased local temperatures on the support surface resulting in larger Co agglomerates. Higher linear gas velocities result in efficient heat removal, minimising hotspots on the surface.

Table 3.3 gives the hydrogen to cobalt molar ratios for the total spectrum as well as below 400°C. Complete reduction of Co_3O_4 would result in a hydrogen to cobalt molar ratio of 1.33, while complete reduction of divalent cobalt (CoO) would result in a hydrogen to cobalt molar ratio of 1. Ratios obtained between 1 and 1.33 result from cobalt supported in a combination of Co_3O_4 and CoO forms on the support surface. The hydrogen to cobalt molar ratios obtained during TPR increase in the order $Co/ZnO < Co/SiO_2 < Co/MnO$.

Table 3.3. TPR hydrogen consumption data for the base case catalysts Co/SiO_2, Co/ZnO and Co/MnO

Catalyst	H_2/Co_{Total} (mol/mol)	$H_2/Co_{<400°C}$ (mol/mol)
Co/SiO_2	1.346	0.457
Co/ZnO	1.041	0.607
Co/MnO	3.361	1.968

Figure 3.5 illustrates that the hydrogen consumption as a function of temperature varies significantly for the three supports. This observation is evidence of the differences in interaction that take place between the cobalt and the support as well as the influence of the support reducibility. In the previous section it was shown that bulk cobalt oxide (Co_3O_4) underwent two distinct reduction phases during the oxide transition to the zerovalent state as defined in chapter 3.1.4. The reduction behaviour of the supported cobalt showed significant variation from the bulk cobalt oxide reduction.

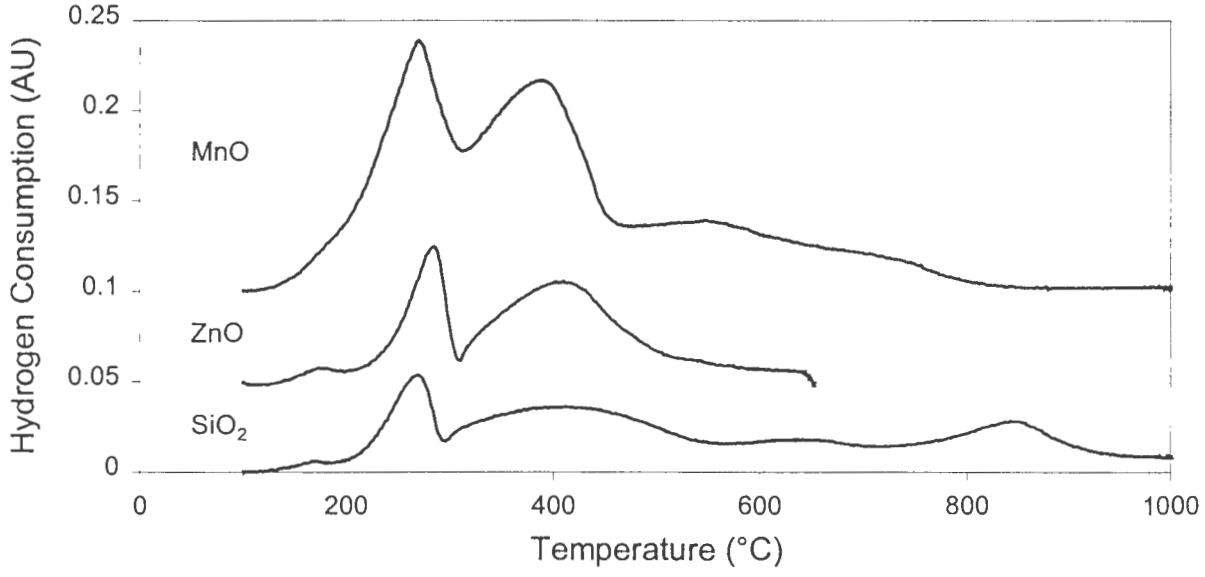

Figure 3.5. TPR spectra for base case catalysts Co/SiO_2, Co/ZnO and Co/MnO. Cobalt nitrate loaded SiO_2, ZnO and MnO.
(mass cat ~ 0.15g, heating rate = 10°C/min, Reducing gas = 60ml(STP)/min 5% H_2 in N_2)

In the case of Co/SiO_2, four regions were noted during reduction of the catalyst up to 1000°C. The first two temperature regions of reduction, with the peak maxima at 270°C and 410°C respectively result from the reduction of Co_3O_4 species to zerovalent metal [Sewell, 1996]. The third and fourth regions are characterised by broad flat reduction peaks. The reduction of bulk cobalt oxide was seen to be complete by 490 °C, consequently the appearance of reducible species at higher temperatures may indicate a resistance to reduction imposed through interaction between cobalt and the SiO_2 support. The third region may be associated with the formation of hydrosilicates, while the fourth peak, ranging from 750°C to 930°C, is probably caused by the reduction of cobalt silicates [Ming and Baker, 1995].

The Co/ZnO catalyst showed two distinct reduction steps, with peak maxima at 280°C and 410°C. These two stages of reduction are due to the reduction of supported Co_3O_4. The peak maxima are at temperatures lower than observed for the bulk Co_3O_4 seen in Figure 3.3. This indicates that interaction between the ZnO surface and the supported cobalt is minimal or that the interaction may aid reduction of the supported cobalt. Even though the spectrum only shows reduction up to 650°C, previous TPR runs with ZnO have shown that cobalt reduction is complete by this temperature as illustrated in Appendix I.

The Co/MnO spectrum seems to combine features from the Co/SiO_2 and Co/ZnO spectra. Like the Co/ZnO catalyst, there are two distinct peaks with maxima at 260°C and 400°C, as well as a broad shoulder above 450°C arising from interaction between cobalt and manganese oxide. The initial two peaks seem to result from the two-step reduction of Co_3O_4 to metal cobalt, however this is unlikely in lieu of the high hydrogen to cobalt ratio observed for the two reduction region. Two explanations are possible for these two reduction steps. The first is that the two peaks may be superimposed on a broad flat reduction peak resulting from support reduction. This would explain the apparently high hydrogen to cobalt molar ratios observed. The second explanation is that the first peak may result from divalent cobalt reduction followed by a second peak attributed to support reduction. Figure 3.4 shows the reduction profile of MnO treated in HNO_3. The peak maximum of the MnO reduction peak occurred at a temperature of 500°C. As Figure 3.5 does not contain the same peak, it is clear that the presence of cobalt has altered the support reducibility. The cobalt may enhance the dissociation of hydrogen on the catalyst surface. In this way, support reduction would take

place at a lower temperature through promotion of hydrogen dissociation that can migrate to the oxidised MnO sites.

The broad higher temperature peak may result from interaction between cobalt and support. The hydrogen consumption peaks were significantly larger for Co/MnO than for Co/SiO_2 or Co/ZnO. This increase in hydrogen consumption resulted from reduction of the MnO support material that had been oxidised during the impregnation or calcination stage. This support reduction seems to take place at the same time as the reduction of the cobalt oxide, as there is no specific peak that can be attributed to the support reduction alone. This observation may intimate that the cobalt combines easily with the MnO support integrating into the MnO framework during either the impregnation, drying or calcination phase. It is most likely that this incorporation results during the decomposition of the nitrate precursor. The high exothermicity of this decomposition may enhance the cobalt mobility as well as loosening the MnO structure for cobalt incorporation. As the hydrogen consumption was so high, it may be that the entire surface of the MnO alters oxidation state, leading to variations in interaction between cobalt and support.

The TPR results obtained for the three supports can be explained in terms of zeta potential at the impregnation pH of each support.

The Co/SiO_2 catalyst showed the largest temperature range of reduction during TPR. The zeta potential measured for SiO_2 in Figure 3.1 shows that there is a pH range (pH ~ 2-5) where the zeta potential is approximately zero. At pH's greater than 5, the zeta potential becomes strongly negative. This indicates that the net charge on the surface of the SiO_2 has moved from neutral to strongly negative. At this stage the ratio of positive to negative surface species has decreased. The more abundant negative charge on the surface results in a strong electronic attraction of the Co^{2+} ions in solution. The electronic attraction initiates bonding of the cobalt ions at the SiO_2 surface enhancing the probability of the formation of cobalt silicates which may appear as high temperature peaks (>550°C) during TPR. Table 3.3 shows that the overall hydrogen to cobalt ratio during TPR for Co/SiO_2 was 1.346, indicating that on silica Co^{3+} and Co^{2+} are in equivalent ratios, as present in the Co_3O_4 form. Cobalt was loaded

in Co^{2+} form, consequently oxidation of the cobalt took place during calcination Below 400°C, 34% of the total hydrogen consumption had already taken place.

The Co/ZnO base catalyst had a final impregnation pH of 5.9. At this pH, Figure 3.1 shows that the ZnO surface still has a net positively charged surface. The implications of this are that the Co^{2+} ion sees an electronic repulsion from the ZnO surface resulting in weak interaction between the cobalt and the support. ZnO readily dissolves in strong acidic mediums, even in pH's as high as 5-6. Consequently the strong acidity of the nitrate precursor is thought to partially dissolve the ZnO support at the initial impregnation pH of 4.9. As equilibration takes place over two days, the pH rises from 4.9 to 5.9 (Table 3.1). As the pH rises, the ZnO may precipitate out of solution covering cobalt that had already attached to the ZnO and will remain built into the support structure. For this reason the hydrogen to cobalt molar ratio for the Co/ZnO TPR is 1.041 (Table 3.3) as opposed to the expected value of 1.33 for complete reduction of Co_3O_4.

An alternate explanation for this discrepancy may be that cobalt was lost during loading and drying where some of the support was not recoverable due to attachment to the boiling flask. This could lead to irregularities in cobalt concentration on the recoverable catalyst and give an inaccurate cobalt loading. Below 400°C, 58% of the hydrogen consumption had already taken place indicating a higher ease of reducibility than the SiO_2 supported cobalt. The absence of high temperature reduction regions illustrates that zinc oxide does not show a propensity to form stable spinel type structures ($A_2^{3+}B^{2+}O_4$) as observed with the SiO_2 support. Zinc oxide cannot form spinel structures unless cobalt was in trivalent form, as zinc will not shift to the trivalent form. A possible reason for this could be the fact that the zinc oxide had a significantly more structured crystal framework than the largely amorphous SiO_2. The less ordered nature of SiO_2 results in a surface that is significantly more defective. It is these defects that provide numerous functional groups that are possible attachment sites for cobalt. The ZnO surface is less defective providing fewer attachment points. The net result is that zinc oxide repels any interaction with the cobalt that might upset the regimented structure. Thus when cobalt is loaded, the calcination step will result in complete oxidation of divalent cobalt to Co_3O_4. This is confirmed by the presence of two peaks during reduction in Figure 3.5, as well as the absence of any reduction associated with cobalt support species. Consequently it is surprising to observe a hydrogen to cobalt molar ratio suggesting the presence of all cobalt in divalent form.

For the Co/MnO catalyst, the initial impregnation pH measured was 4.8. The pH increased to a value of 6.2 over two days of equilibration (Table 3.1). The zeta potential measurements indicated a point of zero charge at a pH of 4 for the MnO support. Above a pH of 4, the MnO surface carried a net negative charge (Figure 3.1). Thus the impregnation of cobalt onto MnO took place with MnO showing a net negative charge to the Co^{2+} ions in the impregnation solution. This does not imply that no positively charged groups exist, but that the ratio of negative to positive charge groups has increased. The result is an electronic attraction between the positively charged cobalt ions and the surface, creating a metal support interaction that decreases the ease of reducibility of the cobalt oxide on the MnO surface during TPR. This is indeed the case. Figure 3.5 illustrates a broad reduction peak between 450°C and 750°C indicating this interaction. For the MnO catalyst, the hydrogen to cobalt molar ratio is considerably higher than the theoretical value of 1.33 expected for Co_3O_4. The high hydrogen to cobalt molar ratio of 3.361 observed can be attributable to the ease with which the MnO support can shift between different oxidation states. This shift is probably induced during either impregnation or calcination as a result of the strong oxidising capabilities of NO_x gas released during the nitrate precursor decomposition. This oxidation would then be reversed during the temperature programmed reduction run, as the support shifts back to MnO, which represents the lowest oxidation state of Mn. This could account for the hydrogen to cobalt ratio well above the expected ratio of 1.33 associated with Co_3O_4 reduction. Below 400°C, 59% of the total hydrogen consumption had taken place.

3.2.1.1.1 Extent of Supported Cobalt Reduction

Figure 3.6 illustrates two TPR spectra for each base case catalyst. The first spectrum entitled 'calcined' corresponds to the pretreatment of the catalyst precursor which was applied. This pretreatment consisted of a calcination step of 1 hour in N_2 at 400°C to decompose the precursor.

The second spectrum entitled 'reduced' illustrates the TPR profile following activation of the catalyst by reduction in a 5% H_2 in N_2 gas mixture. The reduction pretreatment was the same applied to the catalyst as an activation procedure prior to loading into the reactor for Fischer-Tropsch synthesis. By comparison of the two spectra, information on the extent of reducibility of cobalt supported on SiO_2 (A), ZnO (B) and MnO (C) was obtained.

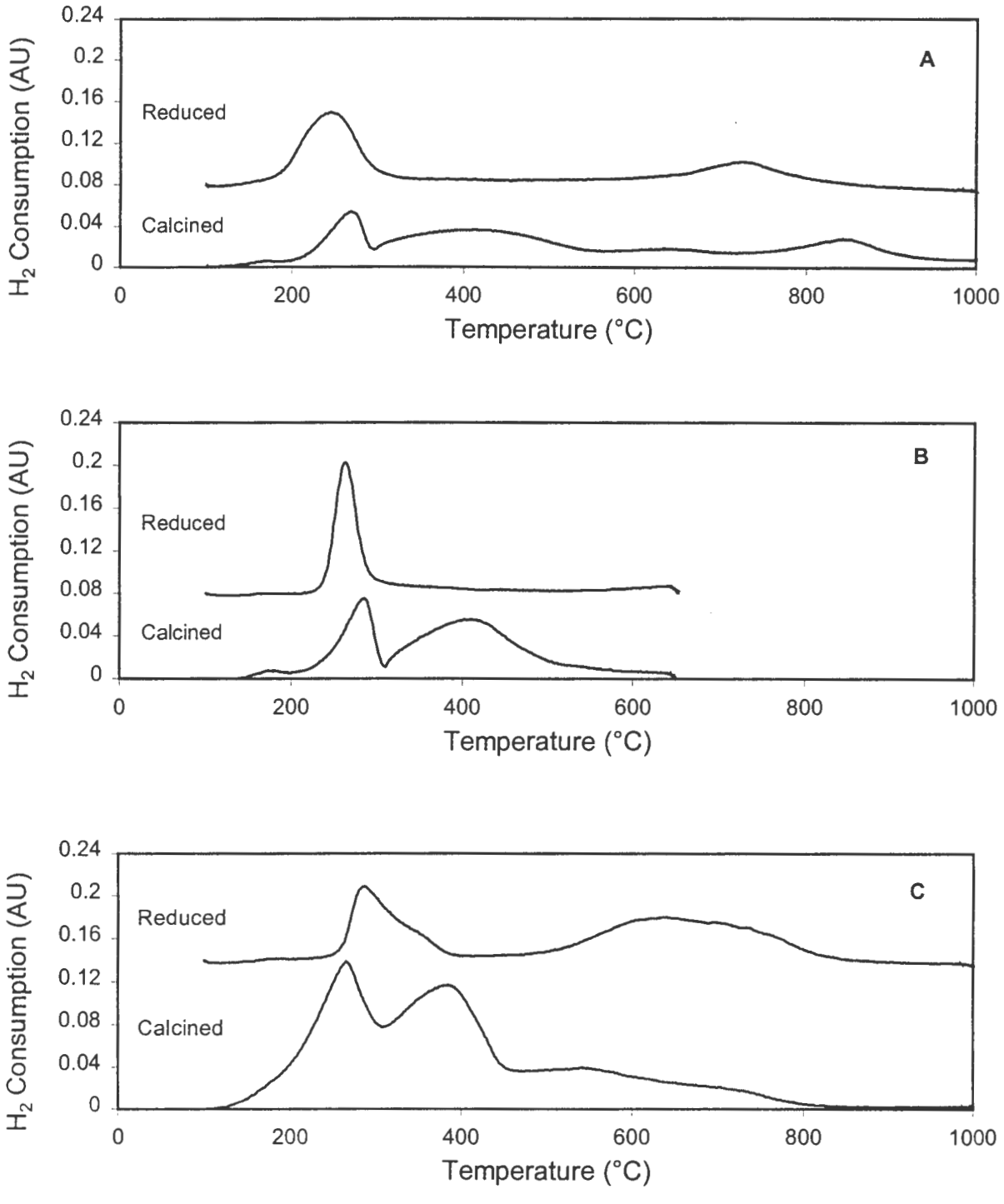

Figure 3.6. Evaluation of the extent of reduction of supported cobalt nitrate after reduction at 400°C for 16 hours. TPR spectra for (A) Co/SiO_2, (B) Co/ZnO and (C) Co/MnO.
($m_{cat} \sim 0.15g$, heating rate = 10°C/min, reducing gas = 60(NTP)ml/min 5% H_2 in N_2)

The extent of reducibility is defined as the fraction of the total cobalt present on the surface that is in the active zerovalent form, and was calculated using the 'reduced' spectrum for each catalyst. The assumption was made that all cobalt reduced above 400°C in the 'reduced' spectrum would be in divalent form. This assumption is very reasonable as Co_3O_4 reduction to CoO was seen to take place below 400°C for all catalysts where Co_3O_4 was present. The hydrogen to cobalt ratio associated with divalent cobalt reduction is 1. Consequently the extent of reduction was obtained by calculating the hydrogen to cobalt molar ratio above 400°C and subtracting this value from 1. The calculated extent of reductions for Co/SiO_2, Co/ZnO and Co/MnO can be seen in Table 3.4.

Table 3.4. TPR hydrogen consumption data for evaluation of the extent of reduction of supported cobalt for Co/SiO_2, Co/ZnO and Co/MnO.

Support	Pretreatment	H_2:Co Total	H_2:Co <400°C	Extent of Reduction (%)
SiO_2	Calcination	1.346	0.457	80.3
	Reduction	0.607	0.410	
ZnO	Calcination	1.040	0.607	91.4
	Reduction	0.398	0.312	
MnO	Calcination	3.361	1.968	28.7
	Reduction	1.130	0.417	

Reduction at 400°C for 16 hours significantly altered the reduction profile of the SiO_2 supported catalyst as compared to the calcined catalyst. The reduced sample underwent two reduction steps. The first step had a maximum at 230°C and resulted from surface reoxidation of zerovalent cobalt. The second reduction peak had a maximum at 730°C and was associated with cobalt silicate reduction. Consequently the cobalt present as cobalt silicate was not in the active form resulting in less than complete use of the supported cobalt. As a result, a significant fraction of the cobalt is unavailable for Fischer-Tropsch synthesis. The extent of reduction for the Co/SiO_2 catalyst was calculated to be 80.3%.

The ZnO supported cobalt catalyst showed a single peak in the 'reduced' TPR spectrum with

a maximum at 240°C. This peak was attributed to the reduction of cobalt oxide formed through surface reoxidation of zerovalent cobalt exposed to the atmosphere. As this peak accounted for most of the hydrogen consumed, it is safe to assume that almost complete reduction of cobalt to the zerovalent form has occurred. This indicates an extent of reduction close to 100% and confirms the expectation that the cobalt and ZnO support did not interact. The actual extent of reduction calculated for Co/ZnO was 91.4%.

The MnO supported cobalt catalyst shows considerable differences between the 'calcined' and 'reduced' samples. A broad high temperature peak is present following both calcination and reduction, however reduction in the 5% H_2 in N_2 mixture shifted the reduction region to a higher temperature . This peak derives from two factors. The first factor is the interaction between cobalt and support that is too strong to be reduced by 400°C, while the second contributing factor is the reduction of the support material itself.. The cobalt reduced at this temperature is lost in terms of catalyst activity in that this cobalt will not be present in the active zerovalent form. A low temperature peak during the 'reduced' run corresponds to reduction of surface oxidised cobalt species during exposure to the atmosphere. The extent of reduction obtained for Co/MnO was 28.7%. This value seems to contradict the total hydrogen to cobalt molar ratio of the calcined catalyst, however the bulk of the hydrogen consumption during that TPR run was a resulted from the reduction of the MnO support as explained in chapter 3.1.4.

3.2.1.2 Hydrogen Chemisorption

Table 3.5 shows the results obtained for the hydrogen chemisorption measurements taken on the SiO_2, ZnO and MnO catalysts prepared with the nitrate precursor.
The measured metal surface area decreased from 3.18 to 0.79 to 0.35 m^2/g as the support changed from SiO_2 to ZnO to MnO. This metal surface area is a function of both the extent of reduction of the cobalt on the surface as well as the degree of dispersion of the cobalt on the surface. A dispersion of 6.66% was obtained for Co/SiO_2, while a dispersion of 1.44% and 2.06% were obtained for Co/ZnO and Co/MnO respectively. The higher cobalt dispersion associated with Co/SiO_2 coincides with the formation of smaller cobalt crystallite sizes on the surface, resulting in a greater degree of cobalt metal exposure.

Table 3.5. Surface area, dispersion, particle diameter and hydrogen adsorption reversibility obtained for Co/SiO_2, Co/ZnO and Co/MnO.

Catalyst	Surface Area (m^2/g)	Dispersion (%)	Crystallite Size (nm)	Reversibility (%)
Co/SiO_2	3.18	6.66	14.5	65.8
Co/ZnO	0.79	1.44	66.6	39.1
Co/MnO	0.35	2.06	46.6	47.6

The hydrogen adsorption reversibility is a measure of the opportunity of readsorption of hydrogen on the cobalt following desorption and diffusion through the support pore structure. A high hydrogen adsorption reversibility indicates a high degree of readsorption. The reversibility increased in the order $Co/ZnO < Co/MnO < Co/SiO_2$. This finding reveals that the silica support shows the greatest dispersion of active sites through the support structure, while ZnO had less opportunity for readsorption due to a low dispersion and a low support surface area. Bartholomew and Reuel [1985] equated the degree of reversibility with the strength of metal support interaction. A higher reversibility was seen to be indicative of a stronger metal support interaction. The reason for this is that a high metal support interaction increases the dispersion of the cobalt through the support structure. In this way, desorbed species are more likely to come across cobalt sites during diffusion out of the catalyst particle. The hydrogen chemisorption and TPR results confirm this theory. TPR showed ZnO to give the minimal interaction with the cobalt [see Figure 3.6(B)] resulting in almost complete reducibility of the cobalt to zerovalent form below 400°C. However interaction was clearly visible with the MnO and SiO_2 supports, as evident from the high temperature reduction peaks in both spectra [Figure 3.6 (A) and (C)]. Even though the extent of reduction was significantly higher over Co/ZnO than both Co/SiO_2 and Co/MnO, the surface area was much lower for Co/ZnO than Co/SiO_2. The reason for this arises from cobalt particle agglomeration. Agglomeration refers to the formation of large groupings of cobalt metal. The effect arises as a result of the ease of mobility of cobalt on the ZnO support surface because of the minimal interaction between cobalt and support. Agglomeration thus reduces the exposed surface area in spite of the high extent of reduction. In fact, van't Blik et al., [1986] and Coenen, [1989] postulated that the presence of cobalt silicate species served as anchors

for the reduced metal clusters during activation by reduction. As no such species exist on ZnO, agglomeration becomes exaggerated. Cobalt crystallite sizes over the three supports increase from 14.5 nm to 46.6 nm to 66.6 nm as the support changed from SiO_2 to MnO to ZnO confirming that metal support interaction decreased in the same order.

3.2.1.3 Transmission Electron Microscopy

TEM photographs for Co/SiO_2, Co/ZnO and Co/MnO are illustrated in Figure 3.7. The Co/SiO_2 photograph (Figure 3.7 (A)) shows black spots, which represent the reduced cobalt crystallites, supported on the amorphous SiO_2 support. The amorphous nature of the SiO_2 support is revealed by the regular speckled nature of the material. No evidence of a distinct crystal structure can be seen. The cobalt clusters vary in size from 7 nm to 40 nm and are well dispersed through the support structure. This dispersion would be aided by the high interaction between support and cobalt, as well as by the large surface area of 300 m^2/g provided by the SiO_2 support.

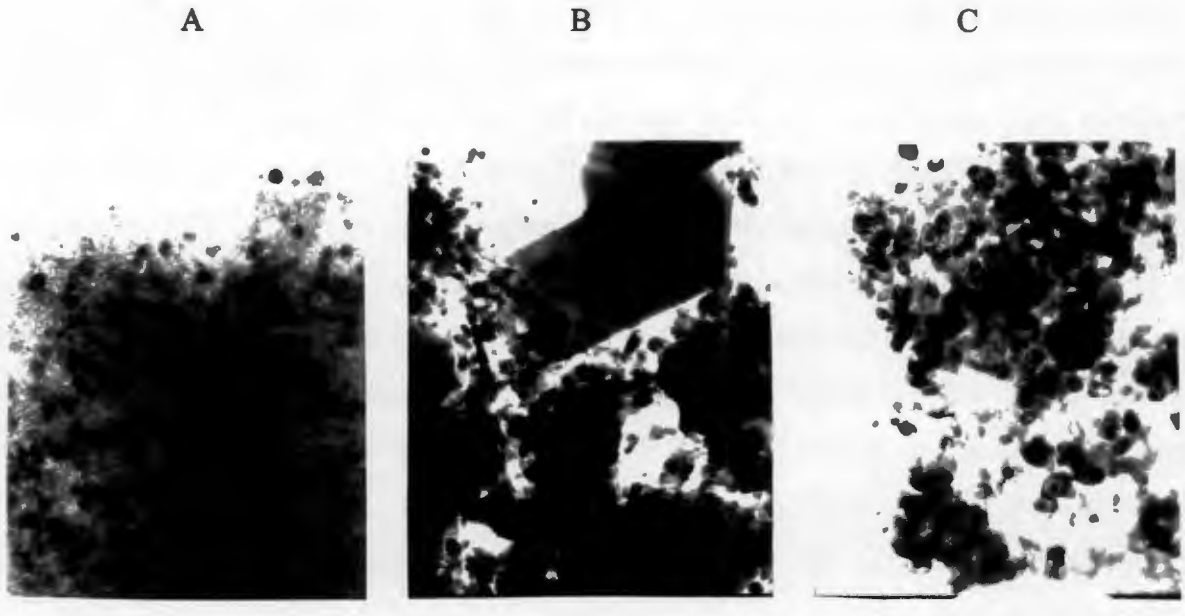

Figure 3.7. TEM photographs for (A) Co/SiO_2, (B) Co/ZnO and (C) Co/MnO

The Co/ZnO catalyst shows two distinct phases present in Figure 3.7 (B). The first phase consists of large rectangular ZnO crystals, while the second phase comprises the reduced cobalt as illustrated by the black phase. The large amount of reduced cobalt present results from the high extent of reducibility of cobalt obtained over the ZnO support. The ZnO support had a very low surface area of 3.1 m^2/g. Consequently the cobalt dispersion would have been lowered with most of the cobalt resting on the support surface. As interaction between cobalt and the ZnO support was minimal, cobalt may have become detached from the support surface resulting in the small black spots scattered around in Figure 3.7 (B).

The TEM photograph of Co/MnO is illustrated in Figure 3.7 (C). The photograph did not show clear distinction between reduced cobalt and support phases. This could be a result of their physical similarities such as electron density as they are situated near each other on the periodic table. The photograph illustrates that MnO shows a higher degree of crystallinity than SiO_2. Crystals of MnO are evident as square crystals. The darker spots may be the reduced cobalt. The amount of cobalt seems to be higher on MnO than on SiO_2 because more black spots are visible. These additional black areas may not be due to the presence of cobalt, but may in fact be a result of a different oxidation state of manganese oxide. It was shown in chapter 3.1.4 that presence of the nitrate resulted in oxidation of the MnO support. This manganese oxide phase may still be present following reduction at 400°C. An alternate explanation for the additional black areas may be is a result of the low surface area of the MnO support, which results in more cobalt per volume of MnO, however the low extent of reduction associated with the Co/MnO catalyst makes this unlikely.

3.2.1.4 Fischer Tropsch Synthesis

The base case catalysts were tested under Fischer Tropsch conditions in order to obtain activity and selectivity data necessary for performance characterisation.

The activity was measured in terms of the hydrocarbon yields obtained from the gas chromatograph analysis of the organic products, as conversion measurements were unreliable due to the low conversions obtained. The organic yield was calculated according to the procedure laid out in Appendix III. Table 3.6 shows that the activity, in terms of yield,

decreased from 5.67% to 1.39% to 0.18% as the support changed from SiO_2 to ZnO to MnO. This trend in activities paralleled the drop in metal surface area measured using hydrogen chemisorption, where the surface area of exposed cobalt metal atoms on SiO_2 was four times that on ZnO and ten times that on MnO. The dispersion of the cobalt on the surface determines the fraction of the active cobalt exposed for reaction. Co/SiO_2 showed a significantly higher dispersion than Co/ZnO and Co/MnO. Table 3.6 also shows the rate per square metre of exposed cobalt on the surface. The Co/SiO_2 catalyst gave the highest rate of 4.12×10^{-3} mmol/m^2_{Co}/min, followed by Co/ZnO with a rate of 3.82×10^{-3} mmol/m^2_{Co}/min and Co/MnO with a rate of 1.13×10^{-3} mmol/m^2_{Co}/min. These rates corresponded to dispersions of 6.66%, 1.44% and 2.06% for Co/SiO_2, Co/ZnO and Co/MnO respectively. Iglesia [1997] stated that the turnover rate was not a function of cobalt dispersion. This seems to be true for SiO_2 and MnO, however the Co/ZnO deviates significantly from this behaviour.

Table 3.6. Characteristic data obtained in the Fischer-Tropsch Synthesis for Co/SiO_2, Co/ZnO and Co/MnO respectively.
(T_{Rxn} = 200°C, P = 5 bar, $(H_2/CO)_{inlet}$ = 2, WHSV = 0.34 g_{CO}/g_{cat}.hr)

Catalyst	Co/SiO_2	Co/ZnO	Co/MnO
Reaction Time	14 hr 50	26 hr 00	22 hr 30
Yield of volatile organics (%)	5.67	1.39	0.18
S_{C1+C2} (carbon%)	14.97	20.65	27.52
$\alpha_{C4\text{-}C11}$	0.78	0.83	0.76
$r_{HC}.10^3$ (mmol/m^2_{Co}/min)	4.12	3.82	1.13
C_5 Composition (%)			
3-methyl-1-butene	0.60	0.29	0.80
2-methyl-butane	0.84	0.52	1.87
1-pentene	56.31	72.21	50.60
2-methyl-1-butene	0.00	0.00	0.00
n-pentane	28.26	22.13	30.09
trans-2-pentene	8.23	2.27	9.76
cis-2-pentene	5.61	1.79	6.21
2-methyl-2-butene	0.15	0.79	0.67

The selectivity to the C_{1+2} fraction, on a carbon % basis, increased from 14.97% to 20.65% to 27.52% as the support changed from SiO_2 to ZnO to MnO. This trend is probability associated with the availability of surrounding exposed cobalt metal sites that can enhance the probability of CH_x incorporation to form a growing chain. The presence of fewer active sites results in heightened termination as methane. This characteristic is observed here as the methane yield decreases from SiO_2 to ZnO to MnO.

Table 3.6 also gives information on the distribution of products within the C_5 fraction. The three major products formed on all three catalysts were α-olefins which are the primary products of the Fischer-Tropsch synthesis, and n-paraffins and β-olefins with small yields of branched olefins and paraffins, all of which are secondary products. The Co/ZnO catalyst gave the highest α-olefin content of 72.21% as compared to 56.31% for Co/SiO_2 and 50.60% for Co/MnO. As the formation of α-olefins is the primary reaction of the Fischer-Tropsch synthesis, the Co/ZnO catalyst suppresses the secondary hydrogenation reaction that would result in the n-paraffin, as well as the secondary isomerisation of the growing chain that leads to termination as a β-olefin. The Co/MnO catalyst showed the highest β-olefin selectivity of 16% of the organic yield as compared to 14% for Co/SiO_2 and 4% for the Co/ZnO catalyst. Secondary hydrogenation to the n-paraffin was greatest over the Co/MnO catalyst yielding an n-pentane selectivity of 30% compared to 28% for Co/SiO_2 and only 22% for Co/ZnO. consequently the different supports result in major changes in the product selectivity as well as catalyst activity. The activity was explainable in terms of exposed metal surface area as determined by the extent of reduction of the cobalt on each support. However, because the product spectrum is significantly altered, the physical characteristics of the support must play a role in the Fischer-Tropsch synthesis.

The chain growth probabilities for the three catalysts are given in Table 3.6. These values were calculated form the slope of the Anderson-Schulz-Flory distribution plots. The ASF plots are illustrated in Figure 3.8 for Co/SiO_2, Co/ZnO and Co/MnO. The probability, α, was calculated over the C_4 to C_{11} range, as the ASF plots generally deviated from straight line behaviour for higher carbon numbers. An increase in slope occurs at carbon number 15 for Co/SiO_2 and at carbon number 12 for Co/ZnO. These increases were attributed to bleeding of products from the wax trap. All the ASF plots give good straight line behaviour between C_4 and C_{11}. The C_1 point in all three ASF plots is an exaggerated value, as the C_1 and C_2 fractions were combined due to difficulties with separation using the gas chromatograph.

However the contribution of the C_2 fraction was minimal in relative terms for all runs performed. The C_3 fraction of the Co/MnO ASF plot was lower than the C_4 point. This was unexpected behaviour that was attributed to an error in the gas chromatograph settings.

The Co/ZnO catalyst gave the highest chain growth probability of 0.83. The chain growth probability for Co/SiO_2 and Co/MnO were found to be 0.78 and 0.76 respectively. The slightly higher chain growth probability observed over Co/ZnO may be attributable to the larger cobalt crystallites observed on the ZnO support from hydrogen chemisorption. The formation of these large cobalt crystallites stems from the weak interaction between cobalt and the ZnO support, and leads to the agglomeration of cobalt on the surface of the support. This agglomeration accounts for extensive reduction in the exposed metal surface area, however it may provide a benefit in that large clusters result in the continual presence of reactant in the vicinity of the growing chain. This could enhance growth by having adsorbed species continually available for incorporation into the growing chain.

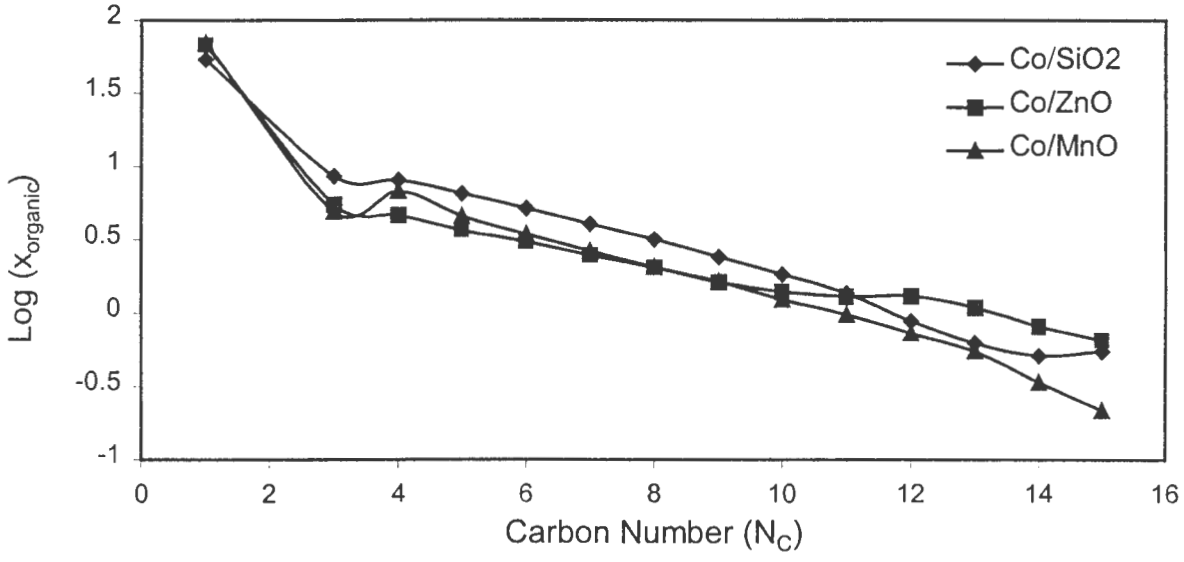

Figure 3.8. Anderson-Schulz-Flory distributions for the base case catalysts Co/SiO_2, Co/ZnO and Co/MnO. Cobalt nitrate loaded on SiO_2, ZnO and MnO.
(m_{cat} ~ 1g, T = 200°C, P = 5 bar, H_2 : CO = 2 : 1, WHSV = 0.34g_{CO}/g_{cat}.hr)

Figure 3.9 gives the rate of formation of the total organic products. The rate was calculated according to the procedure illustrated in Appendix III. The rates are measured per gram of catalyst, consequently they are comparable. The rate of formation is a measure of the activity of the catalyst. Thus the rate parallels the yield measurements from Table 3.6 for the three supported catalysts and decreasing from Co/SiO_2 to Co/ZnO to Co/MnO. Figure 3.9 illustrates the rate of formation as a function of carbon number. As the carbon number increases for each catalyst, the rate of formation decreases. The Fischer-Tropsch reaction follows a chain growth mechanism. A fraction of the growing alkyl chain at each carbon number terminates, decreasing the rate at which products with higher carbon numbers form. The surface area of exposed cobalt on the surface determines the availability of active sites on the support surface. Consequently, as the exposed cobalt surface area was highest on the SiO_2 support, it follows that the rate of formation of organic product should be significantly higher as well.

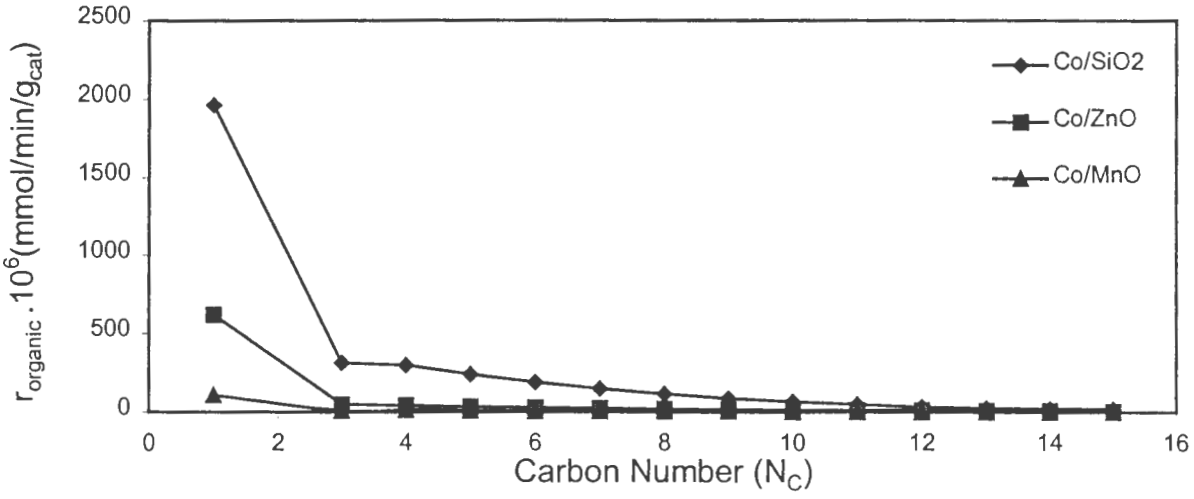

Figure 3.9. Total organic formation rates for the base case catalysts Co/SiO_2, Co/ZnO and Co/MnO. Cobalt nitrate loaded on SiO_2, ZnO and MnO.
(m_{cat} ~ 1g, T = 200°C, P = 5 bar, H_2 : CO = 2 : 1, WHSV = 0.34g_{CO}/g_{cat}.hr)

The olefinicity of the linear organic product is shown in Figure 3.10 for each of the base catalysts. In Table 3.6 the C_5 product breakdown was given for each catalyst. The Co/ZnO catalyst gave a linear olefin selectivity of 76%, compared to 70% for Co/SiO_2 and 67% for Co/MnO. Figure 3.10 indicates that the higher linear olefinicity of the Co/ZnO catalyst

continues over the analysed carbon number range. The Co/SiO_2 shows slightly higher olefinicity than the Co/MnO catalyst at lower carbon numbers, however the trend is reversed as the carbon number increases, with the changeover taking place at C_8. The olefinicity of Co/SiO_2 and Co/MnO drop off fairly quickly dropping below 60% by C_7. This is not the case with Co/ZnO which maintains a linear olefinicity of greater than 60% up to C_9.

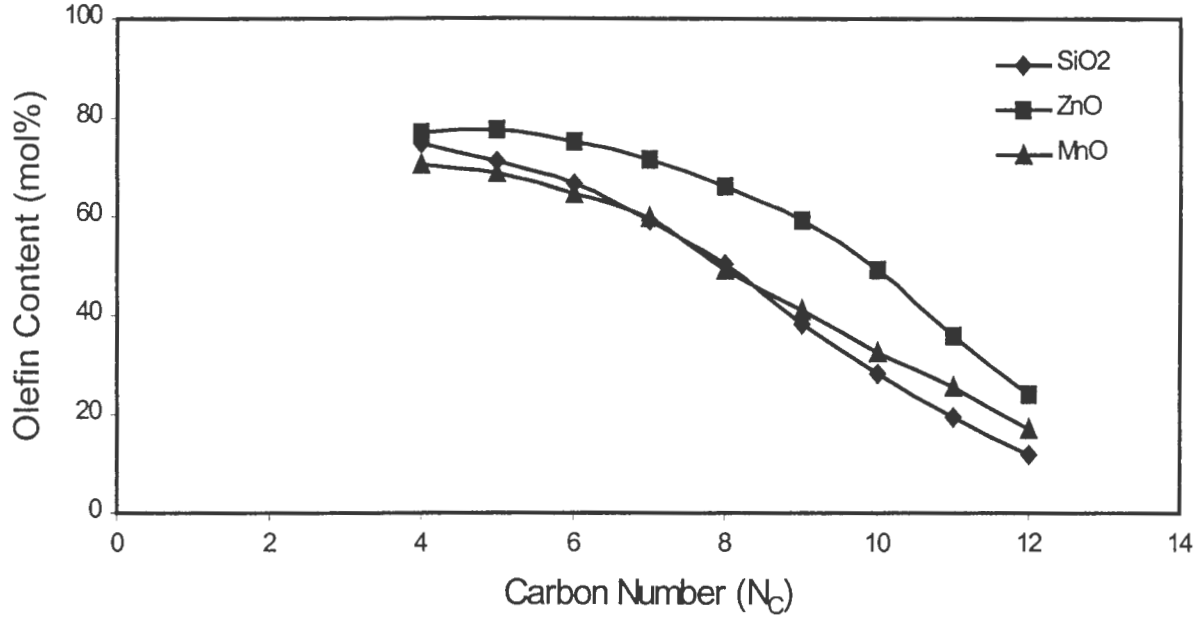

Figure 3.10. Olefin fraction of the linear organic product for the base case catalysts Co/SiO_2, Co/ZnO and Co/MnO. Cobalt nitrate loaded on SiO_2, ZnO and MnO. (m_{cat} ~ 1g, T = 200°C, P = 5 bar, H_2 : CO = 2 : 1, WHSV = 0.34g_{CO}/g_{cat}.hr)

The α-olefin fraction of the linear olefins is illustrated in Figure 3.11 for Co/SiO_2, Co/ZnO and Co/MnO. The most noticeable feature is the high α-olefinicity of the linear product formed over the Co/ZnO catalyst. Up to C_6, the α-olefin fraction accounts for over 90% of the linear olefin fraction over Co/ZnO. After C_6 the α-olefin fraction decreases more sharply, but remains significantly higher than the α-olefin fractions formed over Co/SiO_2 and Co/MnO. For Co/SiO_2 and Co/MnO, the α-olefin fraction of the linear olefin product are similar. As was the case in Figure 3.10, the Co/SiO_2 catalyst showed higher α-olefin selectivity relative to the Co/MnO catalyst up to the C_7 fraction, however this trend was

reversed as the carbon number increased above C_7. The high α-olefinicity observed over the Co/ZnO catalyst may be associated with the hydrogen adsorption reversibility measured during hydrogen chemisorption. A high adsorption reversibility indicates that the possibility of readsorption on the catalyst surface may be high due to high dispersion of the active phase and the resulting presence of numerous attachment sites on the surface. On the ZnO support, cobalt agglomeration is high and the support surface area is low. These two factors cause the primary α-olefin product to diffuse away from the catalyst surface with less chance of readsorption compared to Co/SiO_2 and Co/MnO. In conjunction with this, hydrogen may be less competitive for active sites lowering the tendency for termination of the growing chain as a hydrogenated paraffin. Thus the lower dispersion not only affects the activity but alters the selectivity by limiting both the secondary isomerisation and hydrogenation of the primary α-olefin.

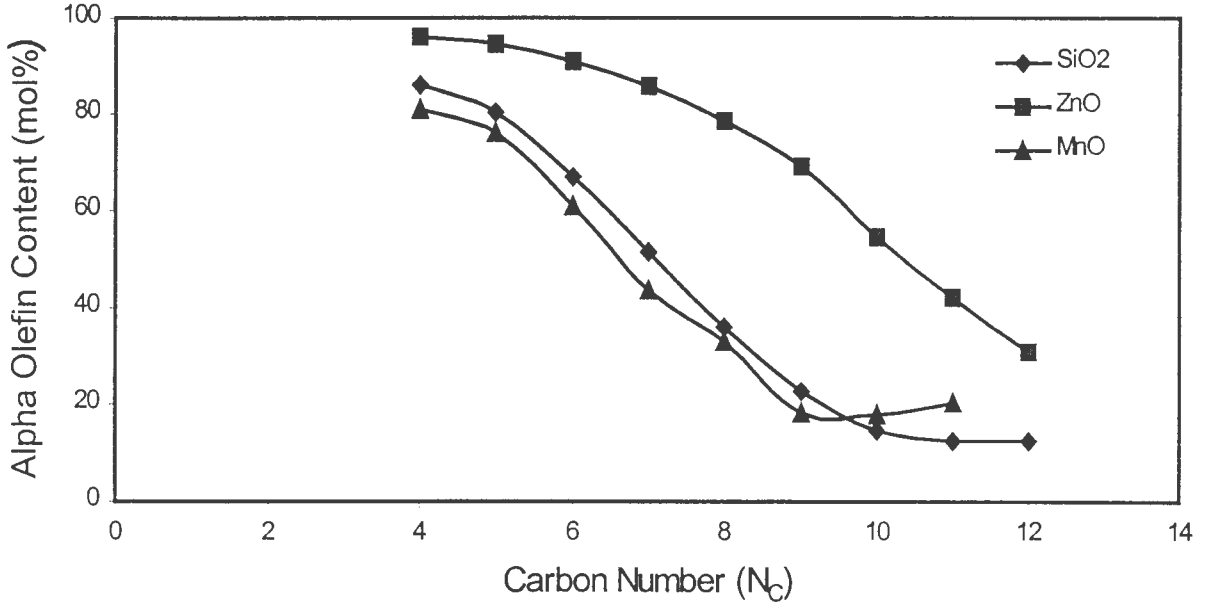

Figure 3.11. Alpha olefin fraction of the linear olefin product for the base case catalysts Co/SiO_2, Co/ZnO and Co/MnO. Cobalt nitrate loaded on SiO_2, ZnO and MnO. (m_{cat} ~ 1g, T = 200°C, P = 5 bar, H_2 : CO = 2 : 1, WHSV = 0.34g_{CO}/g_{cat}.hr)

3.2.2 Effect of the Type of Cobalt Precursor

The metal precursor plays a major role in determining the physical and performance characteristics of the catalyst. In terms of physical changes, the greatest change taking place is the strength with which the cobalt is bound to the support surface. The strength of this attachment affects the reducibility of the catalyst and ultimately alters the activity of the catalyst. SiO_2, ZnO and MnO supported cobalt catalysts were prepared using both a nitrate and acetate precursor. The reducibility of cobalt was evaluated using TPR, while the performance of the catalyst, in terms of activity and selectivity, was evaluated under Fischer Tropsch reaction conditions. Hydrogen chemisorption gave information on exposed cobalt surface area, cobalt crystallite size and dispersion, and the reversibility of the hydrogen adsorption.

3.2.2.1 Temperature Programmed Reduction

The TPR spectra obtained for cobalt nitrate and cobalt acetate loaded onto SiO_2, ZnO and MnO are shown in Figure 3.12 (A), (B) and (C) respectively. The choice of precursor significantly alters the TPR reduction profile for all three supports used. The temperature at which reduction takes place is a measure of the ease of metal reducibility. The effect of the precursor change from nitrate to acetate is to lower the ease with which the cobalt reduces to metal form.

For the SiO_2 support, the spectrum changed dramatically as the precursor was changed from nitrate to acetate. The TPR run for the Co(A)/SiO_2 catalyst was characterised by a dominant reduction peak from 650°C to 860°C as seen in Figure 3.12 (A). This peak accounted for 77% of the hydrogen consumed during the run. The remaining 23% of hydrogen was consumed in the peak with a maximum at 400°C. This reduction behaviour represents a major alteration from that observed for the nitrate precursor. In the case of the nitrate precursor, a fraction of 33% of the total hydrogen reduction took place before 400°C compared with a fraction of 11% for the acetate precursor. The precursor transforms the strength of interaction between the cobalt and the SiO_2 support. The change from nitrate to acetate precursor greatly enhances the interaction between cobalt and support.

This effect is explainable in terms of zeta potential. The zeta potential is a measure of the net charge of the support surface when suspended in solution. This charge is either a net positive or negative value, the specific polarity being dependent upon the pH of the solution and the nature of the support surface. For the case of SiO_2, the point of zero charge occurs over a pH range of approximately 2-5. As the pH increases above 5, the surface of the SiO_2 becomes progressively more negative in charge, making the surface susceptible to strong interaction with the positively charged cobalt ions. The nitrate precursor in 50ml deionised solution results in the SiO_2 experiencing an impregnation solution with an initial pH of 4.9. However, when the acetate precursor is used, the initial pH of the impregnation solution is 6.5. This higher pH promotes stronger interaction between the surface and cobalt via electronic attraction. The result is an increased formation of cobalt silicate species for the acetate precursor relative to the nitrate.

Table 3.7 shows that the overall hydrogen to cobalt molar ratio observed for the $Co(A)/SiO_2$ catalyst was 1.021. This value was lower than the 1.346 for Co/SiO_2 where the nitrate precursor was used. The reason for this is that cobalt is predominantly present as divalent cobalt, resulting in a hydrogen to cobalt molar ratio for complete reduction of approximately 1.

Table 3.7. Effect of the choice of precursor on hydrogen consumption during TPR. Cobalt nitrate and cobalt acetate impregnated onto SiO_2, ZnO and MnO.

Support	Precursor	$H_2:Co_{Total}$	$H_2:Co_{<400°C}$
SiO_2	Nitrate	1.346	0.457
	Acetate	1.021	0.109
ZnO	Nitrate	1.040	0.607
	Acetate	0.888	0.178
MnO	Nitrate	3.361	1.968
	Acetate	1.075	0.206

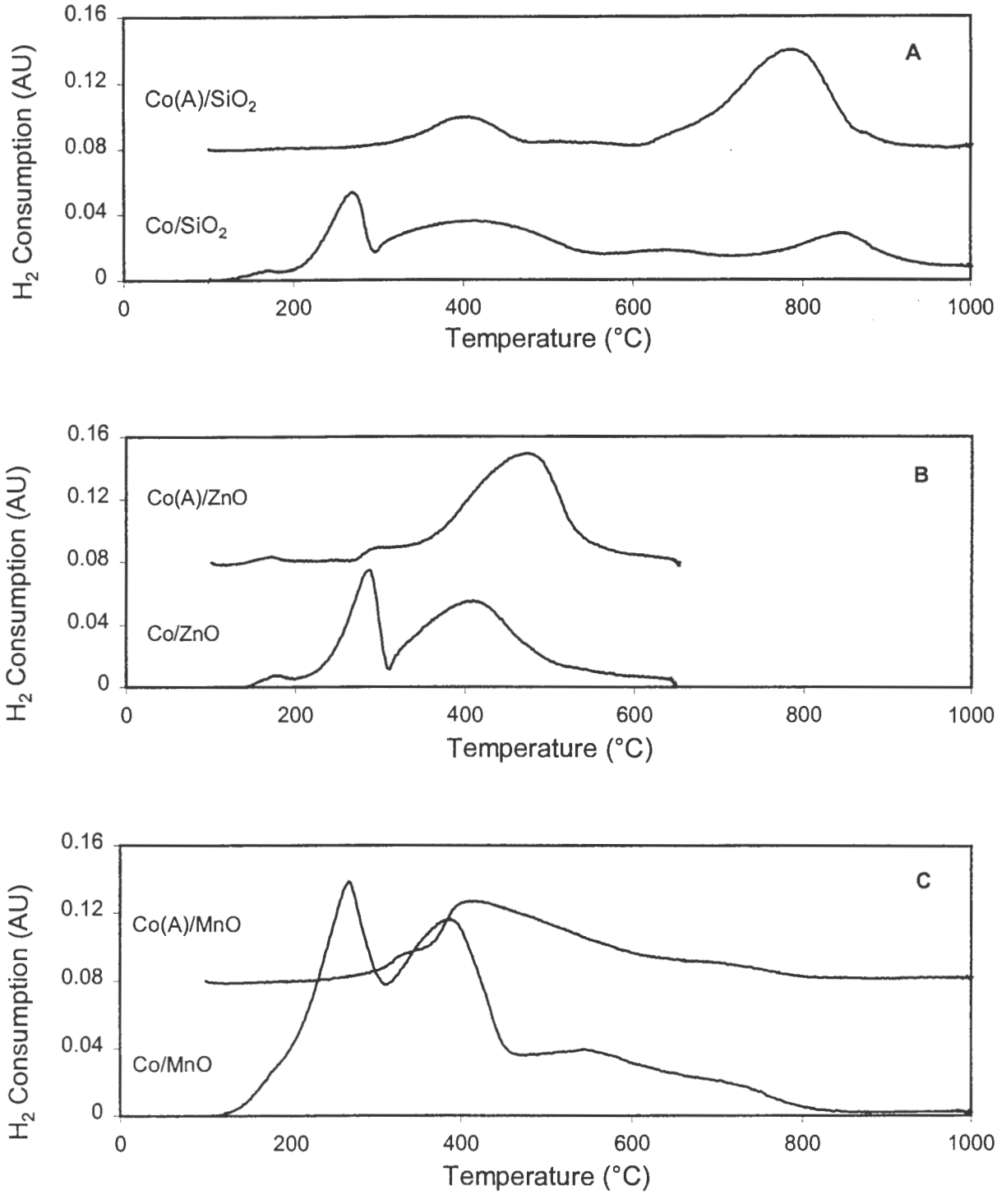

Figure 3.12. Effect of the choice of precursor on cobalt reducibility. TPR spectra for cobalt nitrate and cobalt acetate supported on (A) SiO_2, (B) ZnO and (C) MnO.
(m_{cat} ~ 0.15g, heating rate = 10°C/min, reducing gas = 60(NTP)ml/min 5% H_2 in N_2,)

With the ZnO support, the TPR spectrum was significantly different for the acetate prepared catalyst (Co(A)/ZnO) as illustrated in Figure 3.12 (B). The TPR spectrum for the acetate catalyst was characterised by a single broad reduction peak with a maximum at approximately 460°C. The peak begins at 280°C as a small flat shoulder. The nitrate spectrum consisted of two distinct reduction peaks attributable to the two-stage reduction of Co_3O_4 to zerovalent cobalt as described in chapter 3.1.4. The single peak reduction of the acetate catalyst indicates that cobalt is probably supported on the ZnO support in divalent cobalt oxide (CoO) form.

The Co(A)/ZnO catalyst was impregnated at an initial pH of 6.5, and remained at 6.5 for two days. In terms of zeta potential, the ZnO surface would still experience a net positive surface charge inhibiting interaction with the cobalt. However the higher pH experienced with the acetate precursor than with the nitrate precursor, would lower the extent of dissolution of ZnO consequently no cobalt would migrate into the ZnO structure.

The decomposition of the acetate precursor during calcination does not provide a strong enough oxidising environment to oxidise divalent cobalt to the trivalent form. Thus no Co_3O_4 is present on the support surface resulting in the absence of a second peak during hydrogen consumption. The shape of the divalent cobalt reduction peaks for the acetate and nitrate peaks have similar shapes, however the acetate peak takes place at a higher temperature. The reason for this shift arises from slightly increased interaction between cobalt and the ZnO support, or possibly that the reduction of Co_3O_4 initiates the reduction of divalent cobalt at a lower temperature. This temperature shift resulted in a hydrogen to cobalt molar ratio of 0.151 below 400°C for the acetate catalyst from Table 3.7. The overall hydrogen to cobalt molar ratio was calculated to be 0.888, lower than that experienced using the nitrate precursor. The ratio is also lower than the expected value for complete CoO reduction.

The TPR spectra for the nitrate and acetate precursors on MnO are illustrated in Figure 3.12(C). The TPR spectrum for the Co(A)/MnO catalyst was characterised low and high temperature reduction shoulder between 350°C and 385°C and 600°C and 800°C respectively, as well as a single reduction peak with a maximum at 405°C. The peak is associated with the reduction of divalent cobalt oxide (CoO). Minimal support reduction was noted using the acetate precursor indicating that the oxidising capability of the decomposing acetate is too weak to provide a significant shift in oxidation state of the MnO support that

was seen with the nitrate decomposition. The high temperature shoulder results from strong interaction due to the higher pH associated with the acetate precursor during impregnation. The pH of the impregnation solution was 7.0 as opposed to 4.8 during nitrate impregnation. This higher pH results in a MnO surface with a large net negative surface charge according to the zeta potential measurements of Figure 3.1. The hydrogen to cobalt molar ratio for the total acetate spectrum is given in Table 3.7 as 1.075, significantly lower than observed with the nitrate catalyst. The reduction of CoO results in a ratio of 1, while the remaining hydrogen is consumed during slight MnO support reduction.

The use or the acetate precursor induced cobalt to be supported in CoO form on all three supports used. This could be because the nitrate decomposition results in a stronger oxidising environment than the acetate decomposition. The oxidising environment associated with acetate decomposition is insufficient to induce the oxidation of Co^{2+} ions present in solution to the supported Co_3O_4 form where cobalt is a mixture of divalent and trivalent oxidation states. Consequently the hydrogen to cobalt molar ratios for complete reduction are significantly lower over the acetate catalysts than over the nitrate catalysts.

3.2.2.1.1 Extent of Supported Cobalt Reduction

Figure 3.13 illustrates two TPR spectra for each catalyst formed via cobalt acetate impregnation on SiO_2 (A), ZnO (B) and MnO (C). The first spectrum entitles 'calcined' corresponds to the standard pretreatment applied, while the second spectrum arose from the temperature programmed reduction of a mass of catalyst reduced at 400°C. By comparison of the two spectra, information on the extent of reducibility of cobalt acetate supported on SiO_2 (A), ZnO (B) and MnO (C) was obtained. The calculated extent of reductions for Co(A)/SiO_2, Co(A)/ZnO and Co(A)/MnO can be seen in Table 3.8.

Table 3.8. TPR hydrogen consumption data for evaluation of the extent of reduction of supported cobalt for Co(A)/SiO_2, Co(A)/ZnO and Co(A)/MnO.

Catalyst	Pretreatment	H_2:Co Total	H_2:Co <400°C	Extent of Reduction (%)
Co(A)/SiO_2	Calcination	1.021	0.109	26.8
	Reduction	0.798	0.066	
Co(A)/ZnO	Calcination	0.888	0.178	99.2
	Reduction	0.270	0.262	
Co(A)/MnO	Calcination	1.075	0.206	63.0
	Reduction	0.781	0.411	

Reduction at 400°C for 16 hours altered the reduction profile of the SiO_2 supported cobalt acetate impregnated catalyst as compared to the calcined catalyst. The reduced sample underwent a single reduction step at high temperature (peak maximum at 800°C). This step was associated with the reduction of cobalt present as cobalt silicate. Minimal low temperature reduction was noted indicating that surface reoxidation of zerovalent cobalt was insignificant. The cobalt present as cobalt silicate was not in the active form resulting in less than complete use of the supported cobalt. The extent of reduction for the Co/SiO_2 catalyst was calculated to be 26.8%.

The ZnO supported cobalt catalyst showed a single peak in the 'reduced' TPR spectrum with a maximum at 310°C. This peak was attributed to the reduction of cobalt oxide formed surface reoxidation of zerovalent cobalt exposed to the atmosphere. As this peak accounted for almost the entire amount of hydrogen consumed, it is safe to assume that almost complete reduction of cobalt to the zerovalent form has occurred. This indicates an extent of reduction close to 100%. The actual extent of reduction calculated for Co(A)/ZnO was 99.2%.

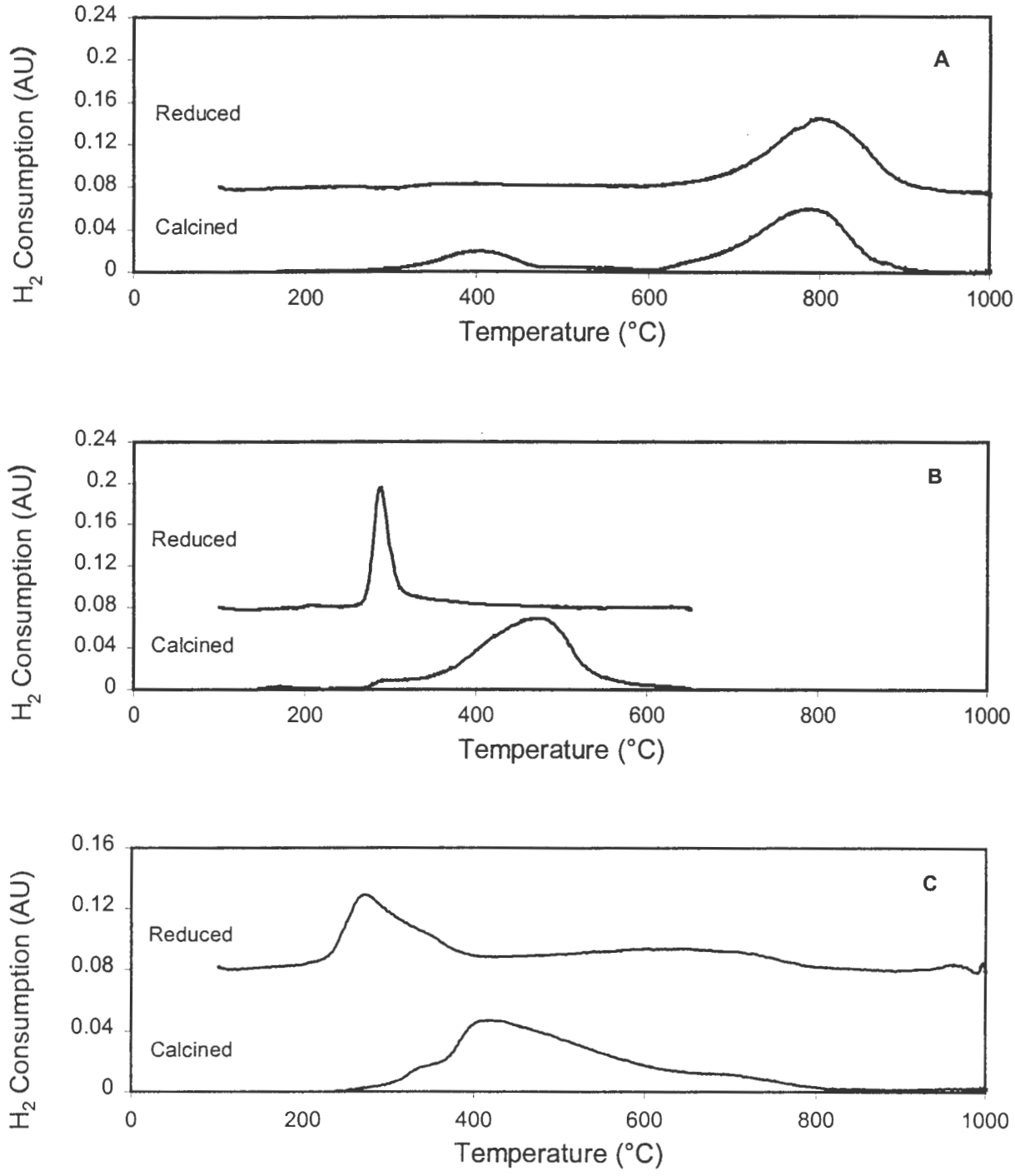

Figure 3.13. Evaluation of the extent of reduction of supported cobalt acetate after reduction at 400°C for 16 hours. TPR spectra for (A) Co(A)/SiO_2, (B) Co(A)/ZnO and (C) Co(A)/MnO.
(m_{cat} ~ 0.15g, heating rate = 10°C/min, reducing gas = 60(NTP)ml/min 5% H_2 in N_2,)

For Co(A)/MnO, the extent of reduction was calculated to be 63.0%. Figure 3.13 (C) shows the TPR spectra for the calcined and reduced catalysts. The calcined catalyst consisted of a broad band of reduction with a maximum consumption taking place at 410°C, with a low and high temperature shoulder on the main consumption peak. The reduced Co(A)/MnO catalyst had two regions of reduction. The first region with a maximum at 280°C showed evidence of surface reoxidation of exposed zerovalent cobalt. The second region was a broad flat reduction profile occurring above 450°C. The hydrogen consumption associated with this peak gave information on the fraction of cobalt present in inactive form following activation of the catalyst by reduction at 400°C. This information allowed calculation of the extent of reduction of the cobalt on the MnO support.

The extent of reduction was seen to decrease significantly over the SiO_2 supported catalyst as the cobalt precursor was changed from nitrate to acetate, decreasing from 80.3% to 26.8%. This major drop in reducibility stemmed from the increased strength of interaction arising during impregnation as a result of the higher impregnation pH associated with the acetate precursor.

For the ZnO supported catalyst, the opposite was true. The extent of reduction increased from 91.4% to 99.2%. It is thought that the strong acidity of the cobalt nitrate precursor during impregnation dissolves the ZnO support, lowering the surface area of the support and consequently decreasing the exposure of the reduced cobalt metal atoms on the surface. The acetate precursor does not have this effect as the pH during impregnation was sufficiently high.

The extent of reduction of the MnO supported catalyst increased from 28.7% to 63.0% when the precursor changed from cobalt nitrate to cobalt acetate. The nitrate decomposition was seen to oxidise the MnO support, but this oxidation wasn't noticed with the acetate precursor. The dramatic increase in the extent of reducibility was attributed to the decrease in oxidation of the support. The large degree of oxidation of MnO with the nitrate precursor may result in incorporation of cobalt into the MnO structure as the support takes up oxygen. This oxygen take up is not evident with the acetate precursor, resulting in less migration into the support structure and the consequent decrease in the hydrogen to cobalt molar ratio above 400°C for the Co(A)/MnO catalyst as compared to the Co/MnO catalyst.

3.2.2.2 Hydrogen Chemisorption

The influence of the precursor type on the surface area, dispersion, metal crystallite size and adsorption reversibility was measured using hydrogen chemisorption. The results are shown in Table 3.9. The use of the acetate precursor resulted in a lower exposed cobalt surface area over both the SiO_2 and ZnO supports. However Co(A)/MnO showed a significantly higher metal surface area than Co/MnO. The metal surface area is a function of both the extent of cobalt reduction and the dispersion of the cobalt on the surface. Thus the low surface area of the Co(A)/SiO_2 catalyst stems predominantly from the decrease in the extent of cobalt reduction from 80.3% to 26.8% as the precursor changed from the nitrate to the acetate.

Although the extent of reduction increased slightly from 91.4% for Co/ZnO to 99.2% for Co(A)/ZnO, the agglomeration of this zerovalent cobalt into large cobalt crystallites caused a drop in the exposed cobalt surface area. The hydrogen adsorption reversibility improved dramatically from 39.1% for Co/ZnO to 67.1% for Co(A)/ZnO. Higher adsorption reversibility is a result of increased metal support interaction. This is confirmed by the TPR findings where the acetate precursor resulted in an increased interaction between cobalt and support.

Table 3.9. Surface area, dispersion, particle diameter and hydrogen adsorption reversibility for Co(A)/SiO_2, Co(A)/ZnO and Co(A)/MnO.

Catalyst	Surface Area (m^2/g)	Dispersion (%)	Crystallite Size (nm)	Reversibility (%)
Co(A)/SiO_2	0.12	0.73	132.4	n.d. [1]
Co(A)/ZnO	0.31	0.53	181.8	67.1
Co(A)/MnO	0.90	2.40	40.1	55.8

[1] n.d. not determined

The extent of reduction increased from 28.7% to 63.0% as the precursor changed from nitrate to acetate. This coincided with an improvement in exposed metal surface area from 0.35 m^2/g

for Co/MnO to 0.90 m^2/g for Co(A)/MnO, while the cobalt dispersion increased from 2.06% to 2.40%. The adsorption reversibility also improved from 47.6% to 55.8% suggesting stronger interaction between the cobalt and the MnO support which in turn increases the cobalt dispersion and the chance for readsorption. This was indeed the case, as TPR showed that cobalt reduction took place at higher temperatures over the acetate prepared catalyst.

3.2.2.3 Transmission Electron Microscopy

Figure 3.14 shows the TEM photographs of Co(A)/SiO_2, Co(A)/ZnO and Co(A)/MnO. The Co(A)/SiO_2 photograph contains no black spots indicating clusters of reduced cobalt. This is in agreement with chemisorption data which showed minimal cobalt metal surface area.

The Co(A)/ZnO catalyst displays the same behaviour observed with Co/ZnO. Two phases are visible in Figure 3.14. The large crystallites are ZnO crystals, while black spots indicate the presence of cobalt in reduced form. Small amounts of the cobalt crystals are attached to the ZnO support, but the vast majority exist on their own. The small spots scattered around are probably cobalt oxide, as reoxidation of the reduced cobalt occurred on exposure to the atmosphere. The clear distinction between cobalt and the ZnO support results from the lack of interaction between them. The agglomeration that results may be so severe that cobalt is more comfortable separate from the ZnO support, especially following oxidation through exposure to the atmosphere. For this reason, the exposed metal surface area measured via hydrogen chemisorption measurements is low in spite of the high extent of reduction calculated through TPR.

The Co(A)/MnO catalyst showed similarities to the Co/MnO catalyst. The MnO support is evident as clear square crystals, while reduced cobalt shows itself as black spots. The Co(A)/MnO photograph contained less black than the Co/MnO, possibly a result of the absence of the nitrate and the lack of support oxidation as a result of this. The cobalt crystallite size is lower over Co(A)/MnO than over Co/MnO, dropping from approximately 60nm to 30nm. This contradicts chemisorption measurements. It is more likely that the acetate would cause a decrease in cobalt crystallite size according to the stronger interaction between cobalt and support observed over all three supports with the acetate precursor.

Increased interaction reduces agglomeration of the reduced cobalt on the surface, decreasing the metal crystallite size.

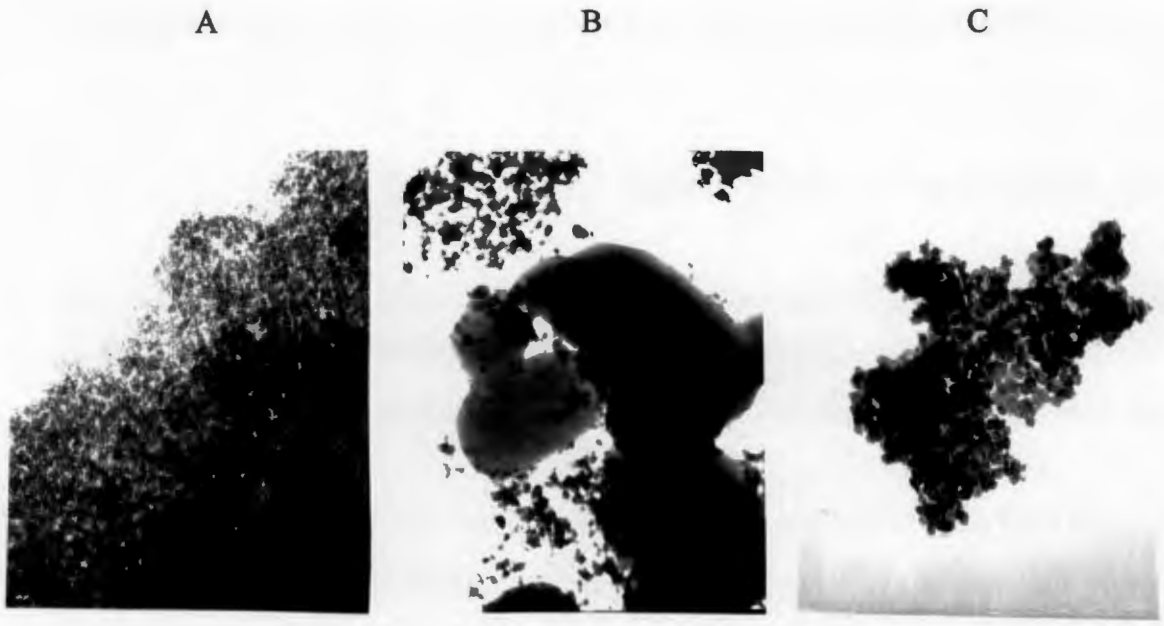

Figure 3.14. TEM photographs for (A) Co(A)/SiO_2, (B) Co(A)/ZnO and (C) Co(A)/MnO

3.2.2.4 Fischer Tropsch Synthesis

The effect of the precursor during preparation of the catalysts was tested under Fischer Tropsch conditions in order to obtain activity and selectivity data necessary for performance characterisation. The activity was measured in terms of the hydrocarbon yields obtained from the gas chromatograph analysis of the organic products and was calculated according to the procedure laid out in Appendix III.

3.2.2.4.1 SiO_2 as a Support

The change of precursor during impregnation had a major effect on performance of the SiO_2 supported catalyst under Fischer-Tropsch synthesis conditions. The results can be seen in Table 3.10. The yield of total organic product dropped from 5.67% to 0.24% when the metal precursor changed from nitrate to acetate. The Co/SiO_2 catalyst was more than 20 times as active as the $Co(A)/SiO_2$ catalyst. The turnover rate of carbon monoxide per square metre of exposed cobalt was 4.12×10^{-3} mmol/m^2_{Co}/min and 4.52×10^{-3} mmol/m^2_{Co}/min for Co/SiO_2 and $Co(A)/SiO_2$ respectively. Thus the activity per square metre of exposed cobalt increased slightly with the change in precursor. This result is in agreement with the TPR findings, where the $Co(A)/SiO_2$ catalyst showed minimal reduction below 400°C, resulting in a very small fraction of cobalt on the surface in the active zerovalent form. Hydrogen chemisorption data for $Co(A)/SiO_2$ indicated negligible exposed cobalt surface area providing further confirmation.

Table 3.10. Effect of the choice of precursor on the activity and selectivity of cobalt supported on SiO_2.
(m_{cat} ~ 1g, T = 200°C, P = 5 bar, H_2 : CO = 2 : 1, WHSV = 0.34g_{CO}/g_{cat}.hr)

Catalyst	Co/SiO_2	$Co(A)/SiO_2$
Reaction Time	14 hr 50	13 hr 31
Yield of volatile organics (%)	5.67	0.24
S_{C1+C2} (carbon%)	14.97	63.98
$\alpha_{C4\text{-}C11}$	0.78	0.75
r_{HC} .10^3 (mmol/m^2_{Co}/min)	4.12	4.52
C_5 Composition (%)		
3-methyl-1-butene	0.60	0.28
2-methyl-butane	0.84	0.40
1-pentene	56.31	36.19
2-methyl-1-butene	0.00	0.00
n-pentane	28.26	32.34
trans-2-pentene	8.23	16.88
cis-2-pentene	5.61	10.91
2-methyl-2-butene	0.15	3.00

The selectivity to the C_{1+2} fraction on a carbon percent basis was dramatically increased for $Co(A)/SiO_2$ compared to the Co/SiO_2 catalyst, rising from 14.97% to 63.98%, representing an increase of more than 400%. As the cobalt surface area decreases, the clusters become smaller and more widespread on the support surface. As the availability of adsorption sites becomes less, the growing chain becomes starved of reactant adsorbed in a close proximity. Furthermore, the low activity inhibits the formation of a liquid organic layer around the catalyst that would enhance readsorption. The result is that termination as methane increases, as this is the thermodynamically favoured product.

The C_5 compositions for the Co/SiO_2 and $Co(A)/SiO_2$ catalysts show considerable differences. The most notable feature of the $Co(A)/SiO_2$ catalyst is the large extent of secondary reactions taking place illustrated by the high selectivity to both β-olefin isomers which accounted for nearly 28% of the total C_5 fraction. This was approximately double the fraction produced over the nitrate impregnated SiO_2 catalyst. Part of the reason for this may be the slightly higher activity per square metre of exposed cobalt observed, as increased secondary activity generally results from a higher turnover rate. The α-olefin, the primary product of the Fischer-Tropsch synthesis, accounted for 36.19% of the C_5 fraction for $Co(A)/SiO_2$ as compared to 56.31% for the Co/SiO_2 catalyst, coinciding with the increase in the β-olefin selectivity from 13.84% to 27.79% as the precursor changed from nitrate to acetate. The linear alkane fractions were similar at 28.26% and 32.34% for the Co/SiO_2 and $Co(A)/SiO_2$ catalysts respectively, indicating similar hydrogenation activities.

The chain growth probabilities were calculated from the slope of the Anderson-Schulz-Flory (ASF) distribution illustrated in Figure 3.15 for both catalysts. The slopes were almost parallel, yielding chain growth probabilities, α, of 0.78 and 0.75 for Co/SiO_2 and $Co(A)/SiO_2$ catalysts respectively. Thus the change of precursor seemed to result in only a slight increase in the termination rate of the growing chain. The low yield for $Co(A)/SiO_2$ prevented accurate analysis of the organic product past the C_9 fraction resulting in a shorter ASF distribution.

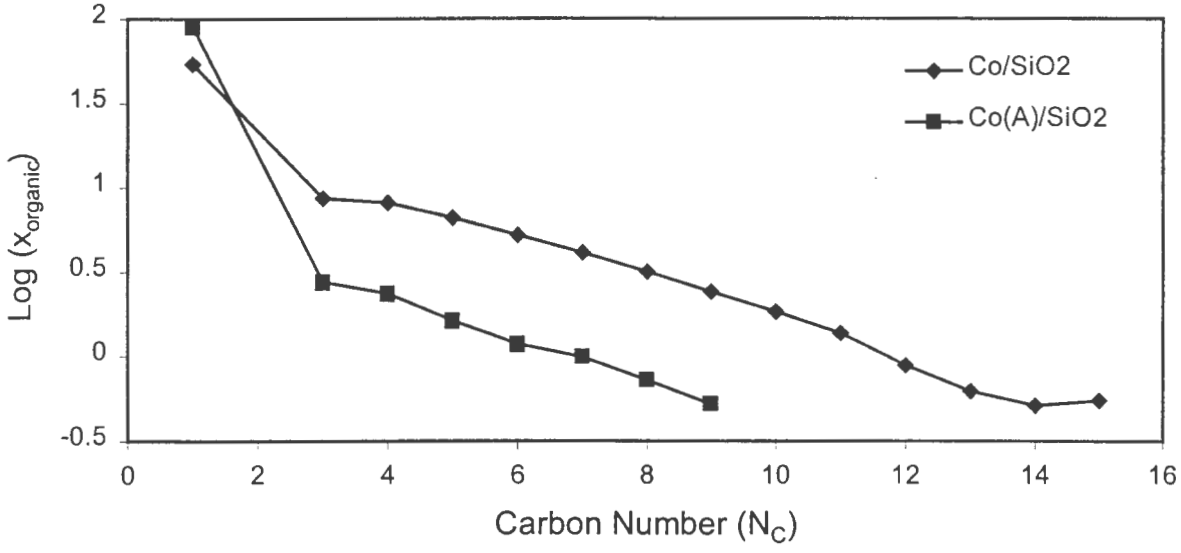

Figure 3.15. Effect of the choice of precursor on the Anderson-Schulz-Flory distribution with SiO_2 as support. Cobalt nitrate and cobalt acetate on SiO_2 support.
(m_{cat} ~ 1g, T = 200°C, P = 5 bar, H_2 : CO = 2 : 1, WHSV = 0.34g_{CO}/g_{cat}.hr)

Figure 3.16 shows the rate of formation of the total organic product for the Co/SiO_2 and $Co(A)/SiO_2$ catalysts.. The rate was calculated according to the procedure presented in Appendix III. The rates are given on a per gram of catalyst basis, allowing direct comparison. The rate of formation is a measure of the activity of the catalyst, thus the rate parallels the yield measurements from Table 3.10. Figure 3.16 illustrates the rate of formation as a function of carbon number. As the carbon number increases for each catalyst, the rate of formation decreases. The polymerisation behaviour of the Fischer-Tropsch reaction results in long hydrocarbon chains via a growing alkyl chain on the catalyst. At each carbon number a fraction of the growing chain terminates in one of several ways, decreasing the rate at which products with higher carbon numbers form. The rate at which this termination takes place is given by the change in rate between carbon numbers.

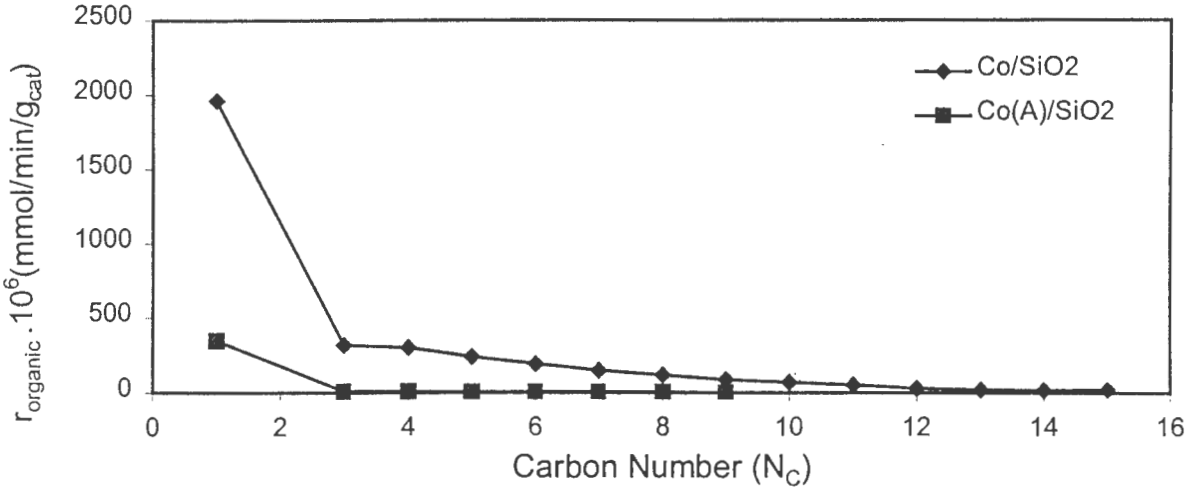

Figure 3.16. Effect of the choice of precursor on the total organic formation rate with SiO_2 as support. Cobalt nitrate and cobalt acetate on SiO_2 support.
(m_{cat} ~ 1g, T = 200°C, P = 5 bar, H_2 : CO = 2 : 1, WHSV = 0.34g_{CO}/g_{cat}.hr)

The olefinicity of the linear organic product is shown in Figure 3.17 for the Co/SiO_2 and $Co(A)/SiO_2$ catalysts. The selectivity to linear olefins of the two catalysts were similar for the full range of carbon numbers, indicating similar growth probabilities as the profiles in Figure 3.17 were approximately parallel. In Table 3.10 the C_5 product breakdown was given for each catalyst. The linear olefin fractions were 70.15% and 63.98% for the Co/SiO_2 and $Co(A)/SiO_2$ catalysts respectively. The linear olefin fraction was consistently higher for Co/SiO_2. The olefin fraction for the $Co(A)/SiO_2$ catalyst could only be analysed up to the C_9 fraction as the yield was too small to register as a peak in the gas chromatograph trace past this carbon number.

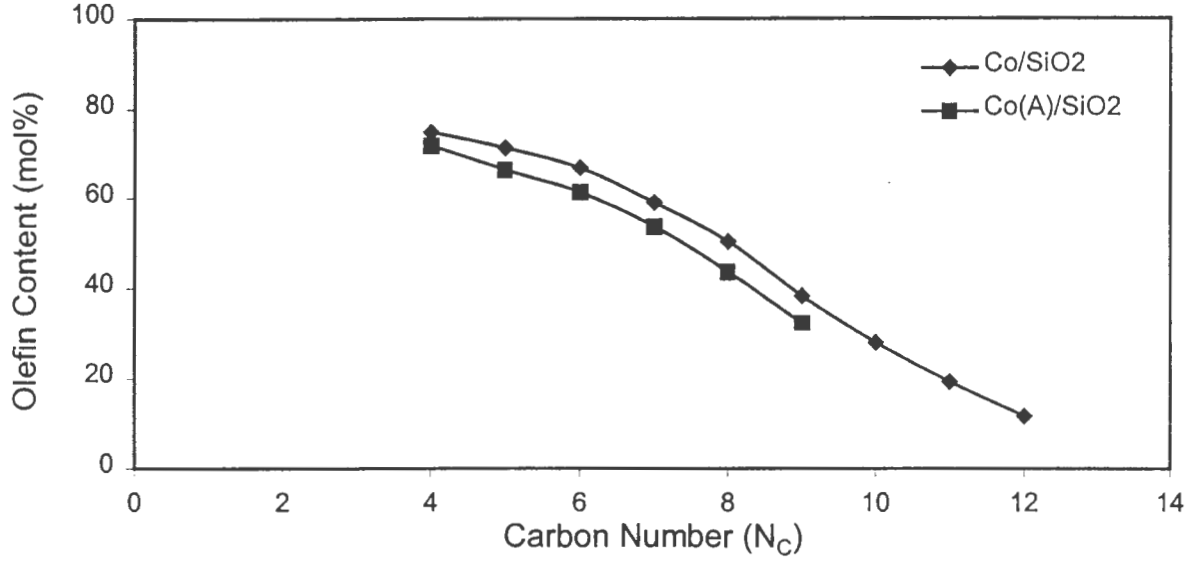

Figure 3.17. Effect of the choice of precursor on the olefin fraction of the linear organic product with SiO_2 as support. Cobalt nitrate and cobalt acetate on SiO_2 support.
(m_{cat} ~ 1g, T = 200°C, P = 5 bar, H_2 : CO = 2 : 1, WHSV = 0.34g_{CO}/g_{cat}.hr)

The α-olefin fraction of the linear olefins is illustrated in Figure 3.18 for Co/SiO_2 and $Co(A)/SiO_2$. The noticeable feature is the low α-olefinicity of the linear olefin product formed over the $Co(A)/SiO_2$ catalyst relative to the Co/SiO_2 catalyst. The difference in the α-olefin fractions was greatest for the C_6 fraction at 31%, but remained above 23% for higher carbon numbers. The difference in the overall linear olefin fraction of the linear organic product for the two catalysts was only 5.4% for the same carbon number. This indicates that the $Co(A)/SiO_2$ catalyst increases the rate of the secondary reaction resulting in termination as a β-olefin. A possible reason for the high selectivity to secondary olefins could be due to the size of the cobalt metal particles. The hydrogen chemisorption for the $Co(A)/SiO_2$ catalyst gave a very low cobalt metal surface area measurement resulting from low cobalt reducibility at 400°C. Because of the high surface area of the SiO_2 support, the exposed cobalt metal atoms would occur in very small groupings on the support surface. The smaller the cobalt metal clusters become, the larger is the presence or influence of the support in determining the product spectrum. In other words, if the support preferentially adsorbs some reactive species relative to others, and the cobalt clusters become small enough such that the support

becomes influential in providing growth or termination species, then the selectivity of the catalyst could be significantly altered. The low α-olefinicity of the Co(A)/SiO_2 catalyst may stem from the ability of the support to induce the double bond shift associated with β-olefin formation, as well as enhancing termination as the β-olefin.

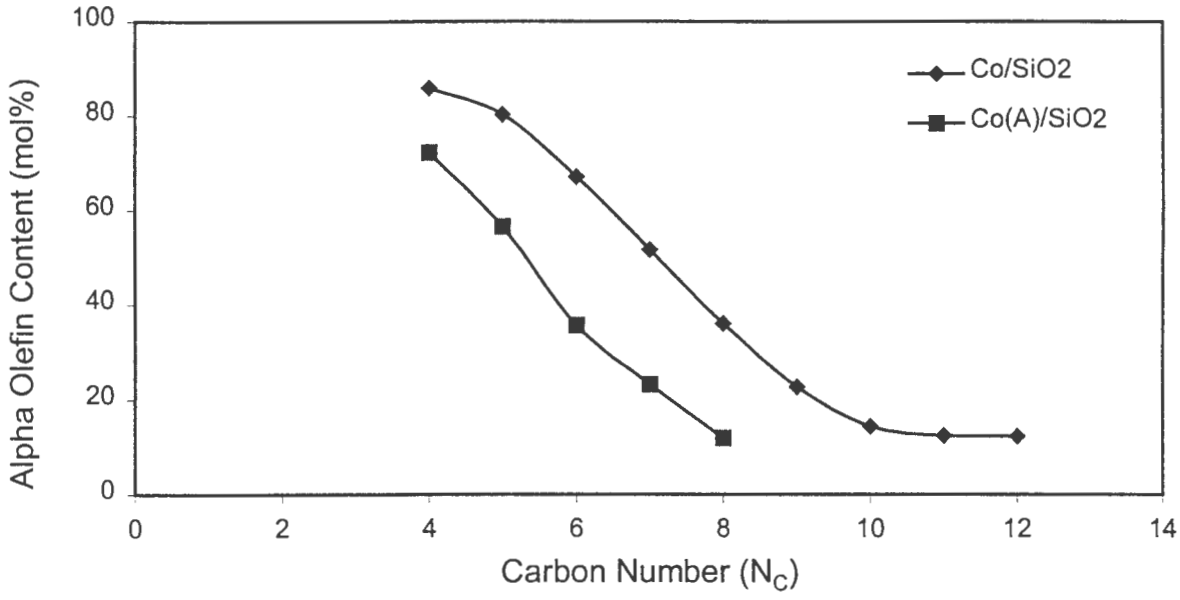

Figure 3.18. Effect of the choice of precursor on the α-olefin fraction of the linear olefins with SiO_2 as support. Cobalt nitrate and cobalt acetate on SiO_2 support.
(m_{cat} ~ 1g, T = 200°C, P = 5 bar, H_2 : CO = 2 : 1, WHSV = 0.34g_{CO}/g_{cat}.hr)

3.2.2.4.2 ZnO as a Support

The change of precursor during impregnation altered both the activity and selectivity of the ZnO supported catalyst under Fischer-Tropsch synthesis conditions. The results obtained are presented in Table 3.11. The Co(A)/ZnO catalyst, prepared with the acetate precursor, gave an organic product yield of 2.45% as opposed to 1.39% for the Co/ZnO catalyst prepared with the nitrate precursor. This result was unexpected as, even though the TPR spectra for the two catalysts revealed that the nitrate prepared catalyst had a lower extent of cobalt reduction, the exposed surface area of the acetate prepared Co(A)/ZnO catalyst was lower as measured by chemisorption. The turnover rate per square metre of exposed cobalt increased from

3.82×10^{-3} mmol/m^2_{Co}/min to 15.14×10^{-3} mmol/m^2_{Co}/min with the change in precursor. The rate of formation of product per square metre of exposed cobalt over Co(A)/ZnO was almost 4 times that of Co/ZnO. It is possible that cobalt rearranges itself on the surface when exposed to the Fischer-Tropsch environment leading to a exposed surface area different to that measured during chemisorption.

Table 3.11. Effect of the choice of precursor on the activity and selectivity of cobalt supported on ZnO.
(m_{cat} ~ 1g, T = 200°C, P = 5 bar, H_2 : CO = 2 : 1, WHSV = 0.34g_{CO}/g_{cat}.hr)

Catalyst	Co/ZnO	Co(A)/ZnO
Reaction Time	26 hr 00	15 hr 55
Yield of volatile organics (%)	1.39	2.45
S_{C1+C2} (carbon%)	20.65	22.33
α_{C4-C11}	0.81	0.79
$r_{HC}.10^3$ (mmol/m^2_{Co}/min)	3.82	15.14
C_5 Composition (%)		
3-methyl-1-butene	0.29	0.79
2-methyl-butane	0.52	1.05
1-pentene	72.21	56.81
2-methyl-1-butene	0.00	0.00
n-pentane	22.13	28.17
trans-2-pentene	2.27	7.58
cis-2-pentene	1.79	5.44
2-methyl-2-butene	0.79	0.15

The selectivity to the C_{1+2} fraction on a carbon percent basis were similar, with the selectivity for the Co(A)/ZnO catalyst not significantly higher at 22.33% as compared to 20.65% for the Co/ZnO catalyst. Paraffin formation was higher over Co(A)/ZnO making up 28.17% of the total organic C_5 product compared to 22.13% over Co/ZnO. β-linear olefins increased from 4.06% to 13.02% of the total organic product as the precursor changed from nitrate to acetate as expected on the basis of the higher activity of Co(A)/ZnO. Branched products made up 1.99% of the C_5 fraction over the Co(A)/ZnO catalyst, compared to 1.60% over the Co/ZnO

catalyst, once again indicating the enhanced formation of secondary reaction products over the acetate catalyst.

The chain growth probabilities for Co(A)/ZnO and Co/ZnO were calculated from the slope of the Anderson-Schulz-Flory distributions illustrated in Figure 3.19. The chain growth probabilities were similar for the two catalysts, giving α values of 0.81 and 0.79 for Co/ZnO and Co(A)/ZnO respectively. As was the case with the SiO_2 support, the change in precursor from nitrate to acetate seemed to increase the termination rate of the growing chain slightly. From C_1 to C_9, the ASF distributions matched each other closely, however above C_9 their behaviour deviated significantly, with the a value increasing for the Co/ZnO catalyst and decreasing for the Co(A)/ZnO catalyst. Other workers [Kuipers et al., 1995; Huff and Satterfield, 1984] have noted similar deviations from the expected straight line ASF behaviour. Wax trap bleeding may cause the increase in chain growth probability over Co/ZnO, while the drop in growth probability over the Co(A)/ZnO may result from the presence of different types of active sites as postulated by Satterfield and Huff [1984].

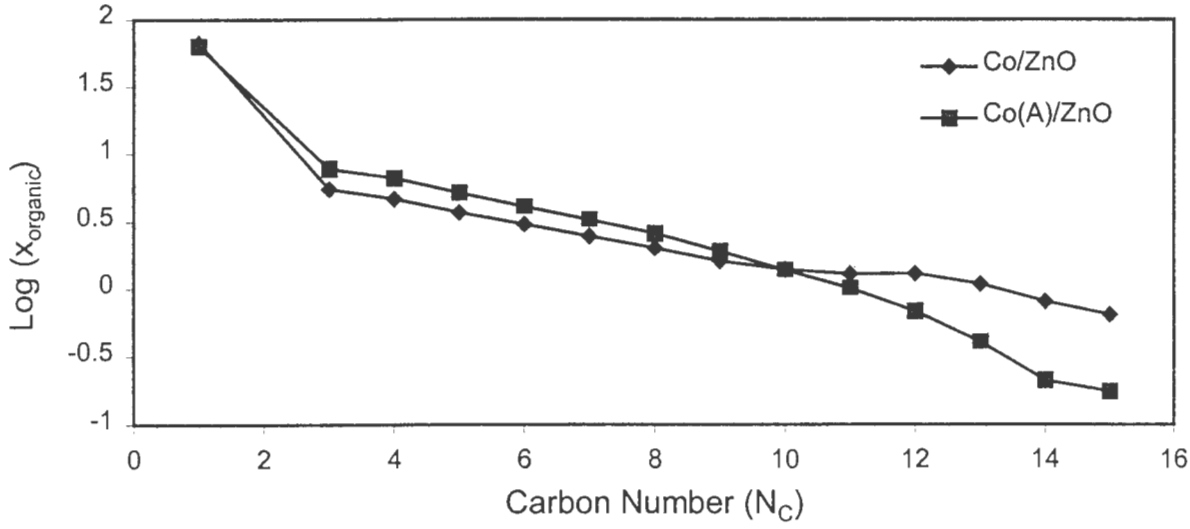

Figure 3.19. Effect of the choice of precursor on the Anderson-Schulz-Flory distribution with ZnO as support. Cobalt nitrate and cobalt acetate on ZnO support.
(m_{cat} ~ 1g, T = 200°C, P = 5 bar, H_2 : CO = 2 : 1, WHSV = 0.34g_{CO}/g_{cat}.hr)

Figure 3.20 shows the rate of formation of the total organic product for the Co/ZnO and Co(A)/ZnO catalysts as a function of carbon number. The rate was calculated according to

the procedure outlined in Appendix III. The rates are given on a per gram of catalyst basis, allowing direct comparison. The rate of formation is a measure of the activity of the catalyst. As the carbon number increases for each catalyst, the rate of formation decreases. This is a result of the polymerisation nature of the Fischer-Tropsch reaction, and the resulting termination of a fraction of each growing alkyl chain. The nature of the final product at termination is strongly dependent upon the molecular environment on the catalyst surface surrounding the growth point. This termination decreases the rate at which products with higher carbon numbers form. The rate at which this termination takes place is evident from the slope of the formation rate plots. The formation rate of Co(A)/ZnO is larger than that obtained for Co/ZnO, paralleling the yield measurements in Table 3.11.

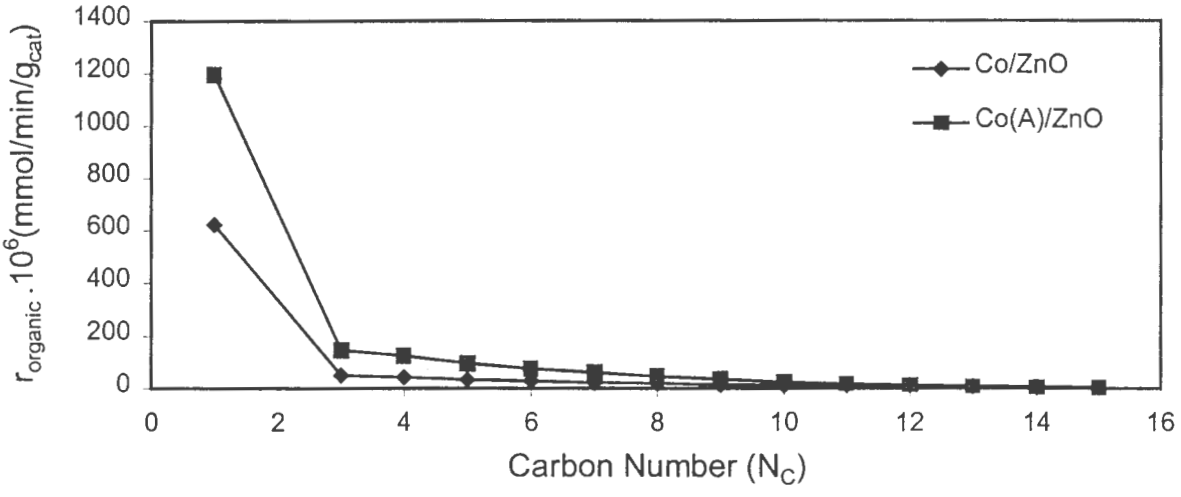

Figure 3.20. Effect of the choice of precursor on the total organic formation rate with ZnO as support. Cobalt nitrate and cobalt acetate on ZnO support.
(m_{cat} ~ 1g, T = 200°C, P = 5 bar, H_2 : CO = 2 : 1, WHSV = 0.34g_{CO}/g_{cat}.hr)

The olefinicities of the linear organic product for the Co/ZnO and Co(A)/ZnO catalysts are shown in Figure 3.21. This linear olefin fraction is a combination of the fractions of the linear α- and β-olefins. The overall olefinicities of the linear organic product for the two catalysts were similar in the C_4 fraction, but varied significantly from the C_5 fraction onwards. The Co/ZnO catalyst had a higher linear olefin growth probability than the Co(A)/ZnO catalyst. The use of the acetate precursor enhanced the rate of secondary reactions, increasing both the n-paraffin and the β-olefin fraction of the C_5 fraction. This heightened secondary product

selectivity associated with the acetate prepared catalyst was also seen on the SiO_2 supported cobalt acetate catalyst. The secondary reactions took place at the expense of the alpha olefin fraction which decreased from 72.21% of the total organic product in the C_5 fraction to 56.81% in the wake of increased hydrogenation and double bond shift activity. This is logical as increased secondary activity often coincides with increased activity.

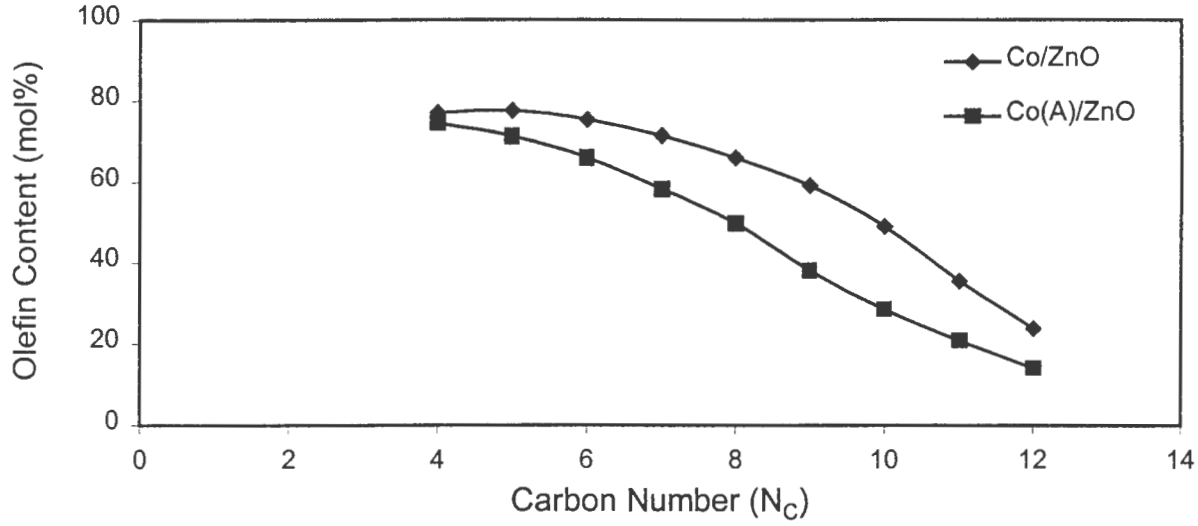

Figure 3.21. Effect of the choice of precursor on the olefin fraction of the linear organic product with ZnO as support. Cobalt nitrate and cobalt acetate on ZnO support.
(m_{cat} ~ 1g, T = 200°C, P = 5 bar, H_2 : CO = 2 : 1, WHSV = 0.34g_{CO}/g_{cat}.hr)

Figure 3.22 shows the behaviour of the α-olefin fraction of the linear olefins with increasing carbon number. The α-olefin was the major linear olefin formed over Co/ZnO, comprising 95% of the linear olefin product and 77% of the total organic product in the C_5 fraction. Over the Co(A)/ZnO catalyst, the α-olefin fraction dropped to 81% of the linear olefin product and 57% of the total organic product in the C_5 fraction. The acetate precursor resulted in a significant drop in the α-olefin selectivity of the catalyst as the selectivity to secondary reaction products rose. This drop may can be explained in terms of the strength with which reactant is adsorbed. The hydrogen adsorption reversibility gives an indication of the strength of the hydrogen adsorption during hydrogen chemisorption experiments. Increased reversibility indicates a higher strength of adsorption. The reversibility was seen to increase from 39.1% for Co/ZnO to 67.1% for Co(A)/ZnO. Consequently the acetate precursor

resulted in a greater distribution of cobalt enhancing readsorption forming more secondary product due to improved chance of primary product readsorption.

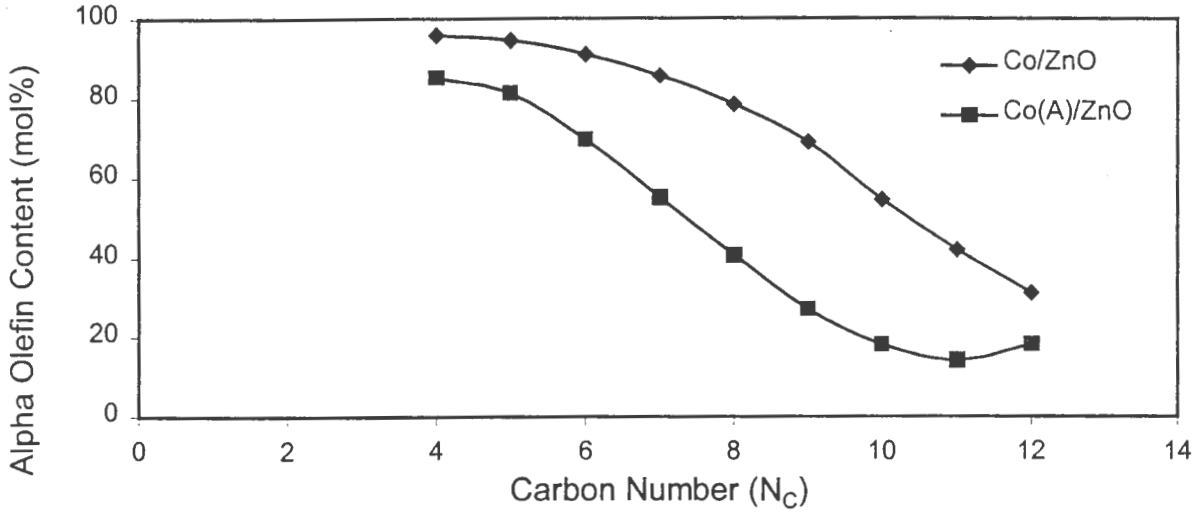

Figure 3.22. Effect of the choice of precursor on the α-olefin fraction of the linear olefins with ZnO as support. Cobalt nitrate and cobalt acetate on ZnO support.
(m_{cat} ~ 1g, T = 200°C, P = 5 bar, H_2 : CO = 2 : 1, WHSV = 0.34g_{CO}/g_{cat}.hr)

3.2.2.4.3 MnO as a Support

The change of precursor during impregnation had an unexpected effect on the activity and selectivity of the MnO supported cobalt catalyst under Fischer-Tropsch synthesis conditions. The results can be seen in Table 3.12. The Co(A)/MnO catalyst, prepared with the acetate precursor, gave an organic product yield of 0.28% as opposed to 0.18% for the Co/MnO catalyst prepared with the nitrate precursor. These activities were unexpectedly low. The TPR spectra for the two catalysts suggested that both catalysts would have a significant fraction of exposed metal atoms reaction due to the high reducibility of cobalt in both precursor cases. However MnO support studies indicated that this reducibility was largely a result of support reduction. In terms of zeta potential, both the Co/MnO and the Co(A)/MnO catalysts were prepared under pH conditions that resulted in a net negative charge on the MnO surface. The interaction between positive cobalt ions and the negative support surface may have resulted in strongly attached oxide species that were reducible at temperatures greater than 400°C.

Hydrogen chemisorption measurements however showed that the exposed surface area increased from 0.35 m^2/g to 0.90 m^2/g as the precursor was changed from nitrate to acetate. However the rate per square metre of exposed cobalt decreased from 1.13×10^{-3} $mmol/m^2_{Co}/min$ to 0.68×10^{-3} $mmol/m^2_{Co}/min$ following an increase in cobalt dispersion from 2.06% to 2.40%. The increased surface area was partly responsible for the higher activity noted over Co(A)/MnO, as the activity increased by a factor of 1.5 as the surface area almost tripled. It was also noted that the extent of reduction increased from 28.7% to 63.0% following the precursor change.

The selectivity to the C_{1+2} fraction on a carbon percent basis was 19.09% for the Co(A)/MnO catalyst, lower than the 27.52% obtained over the Co/MnO catalyst. This is expected, as the acetate prepared catalyst had the higher activity. Branched products made up 4.39% of the C_5 fraction over the Co(A)/MnO catalyst, compared to 3.34% over the Co/MnO catalyst, confirming the predisposition of the acetate prepared catalyst to secondary product formation as seen over the ZnO and SiO_2 supported catalysts.

Table 3.12. Effect of the choice of precursor on the activity and selectivity of cobalt supported on MnO.
(m_{cat} ~ 1g, T = 200°C, P = 5 bar, H_2 : CO = 2 : 1, WHSV = $0.34 g_{CO}/g_{cat}.hr$)

Catalyst	Co/MnO	Co(A)/MnO
Reaction Time	22 hr 30	22 hr 25
Yield of volatile organics (%)	0.18	0.28
S_{C1+C2} (carbon%)	27.52	19.09
α_{C4-C11}	0.76	0.70
$r_{HC}.10^3$ ($mmol/m^2_{Co}/min$)	1.13	0.68
C_5 Composition (%)		
3-methyl-1-butene	0.80	0.83
2-methyl-butane	1.87	3.06
1-pentene	50.60	42.81
2-methyl-1-butene	0.00	0.00
n-pentane	30.09	35.45
trans-2-pentene	9.76	10.71
cis-2-pentene	6.21	6.64
2-methyl-2-butene	0.67	0.50

The chain growth probabilities were calculated from the slope of the Anderson-Schulz-Flory (ASF) distribution illustrated in Figure 3.23 for both catalysts. The chain growth probabilities, α, were 0.76 and 0.70 for Co/MnO and Co(A)/MnO catalysts respectively. The acetate precursor resulted in a higher chain termination probability. The ASF distributions showed linear behaviour over the whole carbon number range analysed.

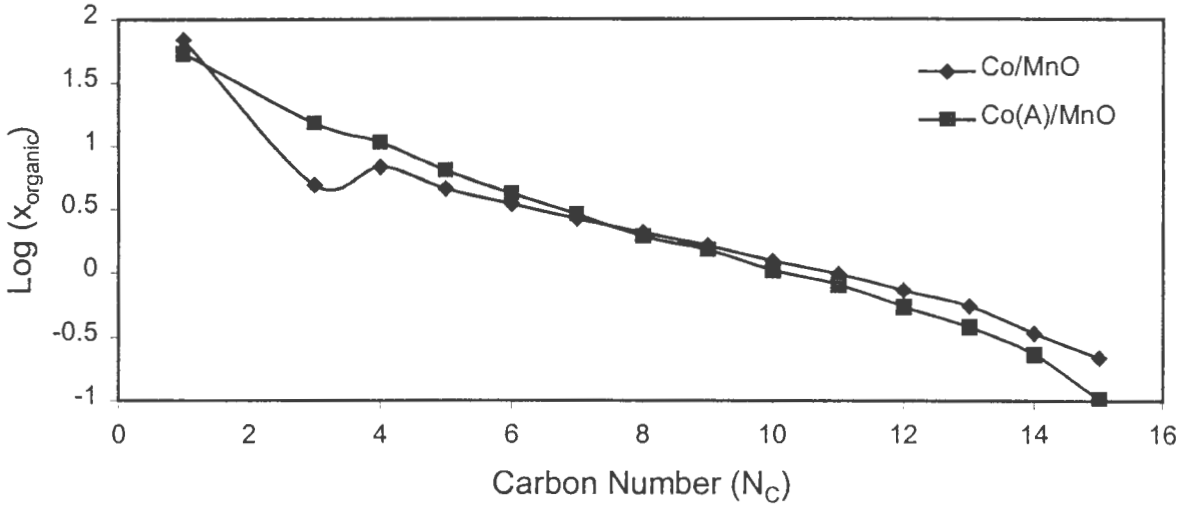

Figure 3.23. Effect of the choice of precursor on the Anderson-Schulz-Flory distribution with MnO as support. Cobalt nitrate and cobalt acetate on MnO support.
(m_{cat} ~ 1g, T = 200°C, P = 5 bar, H_2 : CO = 2 : 1, WHSV = 0.34g_{CO}/g_{cat}.hr)

Figure 3.24 shows the rate of formation of the total organic product for the Co/MnO and Co(A)/MnO catalysts as a function of carbon number. The rate was calculated according to the procedure outlined in Appendix III. The rates are given on a per gram of catalyst basis, allowing direct comparison. As the carbon number increases for each catalyst, the rate of formation is seen to decrease according to the probability of the growing alkyl chain adding another carbon containing group. The formation rate of Co(A)/MnO is significantly larger than that obtained for Co/MnO at low carbon numbers, but their behaviour overlaps at higher carbon numbers.

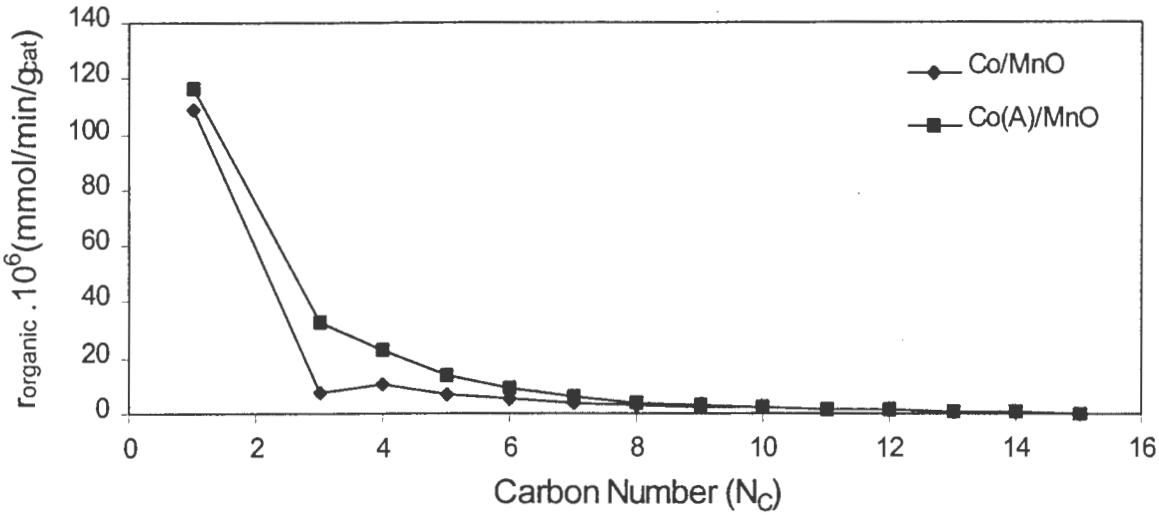

Figure 3.24. Effect of the choice of precursor on the total organic formation rate with MnO as support. Cobalt nitrate and cobalt acetate on MnO support.
(m_{cat} ~ 1g, T = 200°C, P = 5 bar, H_2 : CO = 2 : 1, WHSV = 0.34g_{CO}/g_{cat}.hr)

The olefinicity of the linear organic product is shown in Figure 3.25 for the Co/MnO and Co(A)/MnO catalysts. In Table 3.12 the C_5 product breakdown was given for each catalyst. The linear olefin fractions were 66.57% and 60.16% for the Co/MnO and Co(A)/MnO catalysts respectively. The selectivity to linear olefins was approximately 6% lower for the acetate prepared catalyst relative to the nitrate catalyst. This difference was maintained over the whole range of carbon numbers analysed. Once again the higher activity lead to an increase in the extent of secondary reaction.

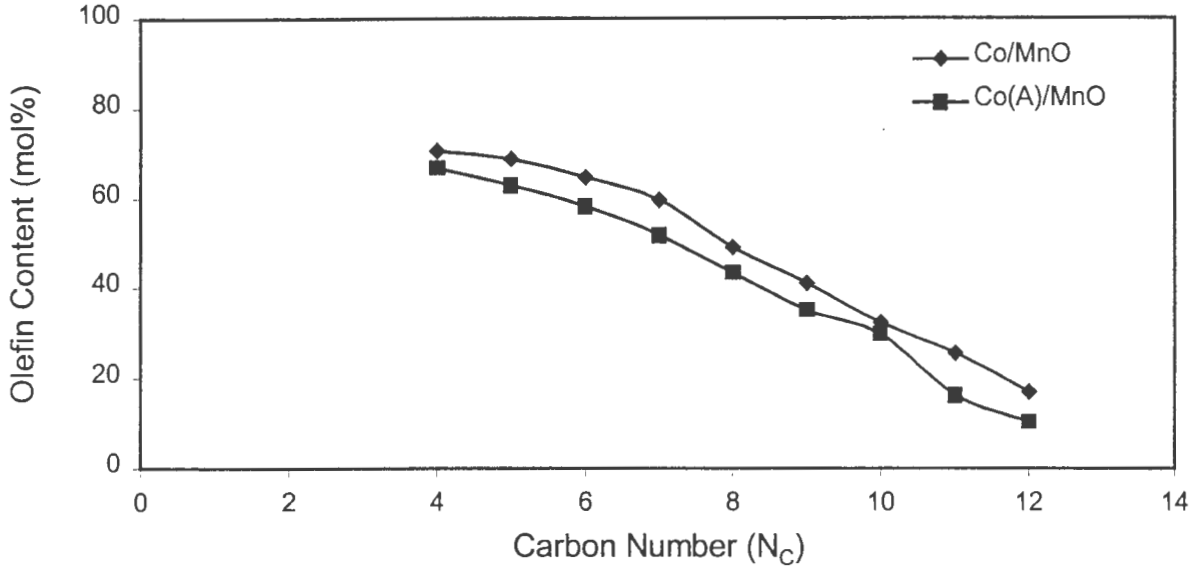

Figure 3.25. Effect of the choice of precursor on the olefin fraction of linear organic product with MnO as support. Cobalt nitrate and cobalt acetate on MnO support.
(m_{cat} ~ 1g, T = 200°C, P = 5 bar, H_2 : CO = 2 : 1, WHSV = 0.34g_{CO}/g_{cat}.hr)

Figure 3.26 shows the behaviour of the α-olefin fraction of the linear olefins with increasing carbon number for Co/MnO and Co(A)/MnO. The α-olefin selectivity comprised 50.60% of the overall C_5 product for Co/MnO as compared to 42.81% for the Co(A)/MnO catalyst. The α-olefin fraction of the linear olefin product was 76% and 71% for Co/MnO and Co(A)/MnO respectively. Thus the acetate precursor resulted in a drop in the α-olefin selectivity of the catalyst and increased the selectivity to secondary reaction products. The increase in secondary reactions was a result of the stronger interaction between the cobalt and the support. This increased interaction was observed through the hydrogen adsorption reversibility during hydrogen chemisorption. The reversibility increases with increasing interaction and is a measure of increasing probability of readsorption. Consequently readsorption of the terminated primary olefins will increase leading to further secondary reaction. This same effect could be responsible for the increase in the hydrogenated fraction of the C_5, as a fraction of the hydrogenated paraffin derives through secondary hydrogenation of a readsorbed α-olefin.

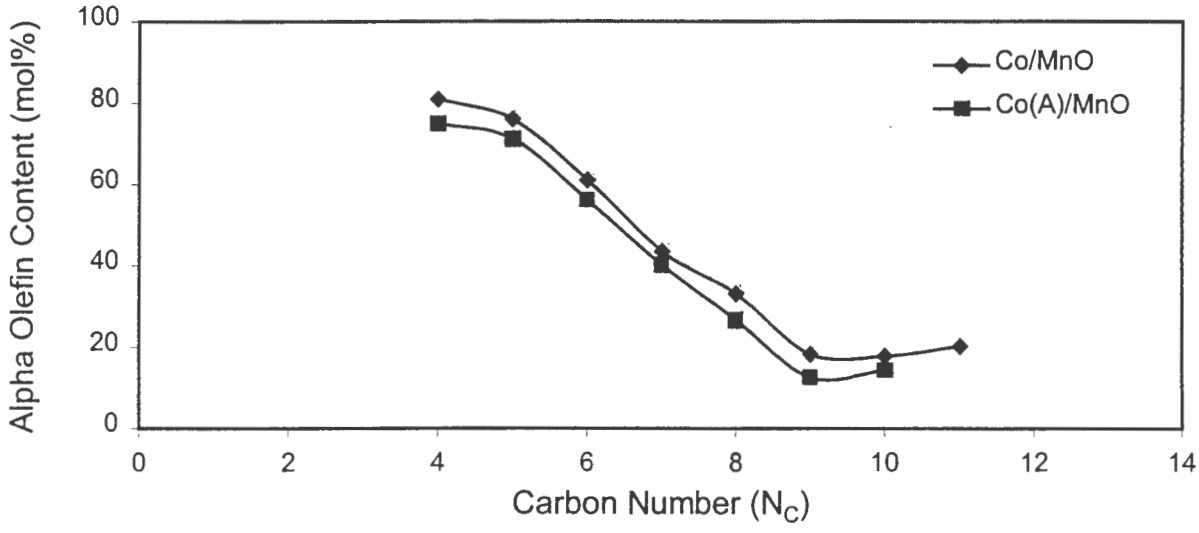

Figure 3.26. Effect of the choice of precursor on the α-olefin fraction of the linear olefins with MnO as support. Cobalt nitrate and cobalt acetate on MnO support. (m_{cat} ~ 1g, T = 200°C, P = 5 bar, H_2 : CO = 2 : 1, WHSV = 0.34g_{CO}/g_{cat}.hr)

3.2.3 Effect of the Type of Impregnation Solution

When the cobalt precursor is placed in solution, dissociation will take place and the cobalt ions present will become partially or totally solvated. The strength of this solvation and the extent to which it takes place determine the nature of the interaction between the cobalt ions and the associated anions in the solution. This interaction in turn will affect the attraction and the resulting strength of attachment to the support material used. Thus changes in impregnation solution are expected to affect the cobalt support interaction, resulting in alterations to cobalt reducibility, metal dispersion on the support surface, consequently influencing the activity and selectivity of the catalyst.

The effect of impregnation solution was investigated by comparing the effect of water and the effect of monoethylenediamine in aqueous solution on the prepared catalyst. Cobalt nitrate was chosen as the cobalt source for both impregnation solutions as the nitrate precursor was seen to yield significantly more active catalysts than the acetate precursor, as illustrated in

section 3.2.1.4. Monoethylenediamine will be abbreviated as MED for the remaining sections.

3.2.3.1 Temperature Programmed Reduction

The influence of the impregnation solvent on the reducibility of cobalt supported on SiO_2 (A), ZnO (B) and MnO (C) can be seen in Figure 3.27. The TPR spectra for catalysts prepared with MED added to the impregnation solution are distinctly different from those prepared without MED addition. This was true for all three supports.

The TPR spectrum of the SiO_2 prepared MED catalyst ($Co(MED)/SiO_2$) consisted of a single broad peak ranging from 430°C to 650°C with a maximum at 590°C. The spectrum was flat from the starting temperature of 100°C to the beginning of the single peak. This temperature range is usually characterised by the reduction peaks of Co_3O_4 and CoO indicating that the presence of MED has prevented the formation of trivalent cobalt oxide on the support surface. MED addition also eliminated cobalt silicate species that are frequently present following cobalt impregnation on SiO_2.

The reason for the absence of both the trivalent cobalt oxide and the cobalt silicates can be attributed to the strong chelating effect of MED. The MED ligands can complex with the cobalt ions, replacing the water ligands that initially surrounded them. This complexation induces a strong field that restricts access of support surface functional groups that might otherwise interact strongly with the cobalt ion. The hydrogen to cobalt molar ratio was 1.508, higher than for the water solvent catalyst. This was expected as it was thought that the MED complex would also reduce leading to a ratio greater than 1.33. No reduction was seen to take place below 400°C, indicating strong complexation between cobalt and MED, as well as interaction between cobalt and the support. This strong interaction may arise from the chelating effect of the silica surface, which acts as a driving force for the formation of a stable cis-octahedral complex [Che, 1993]

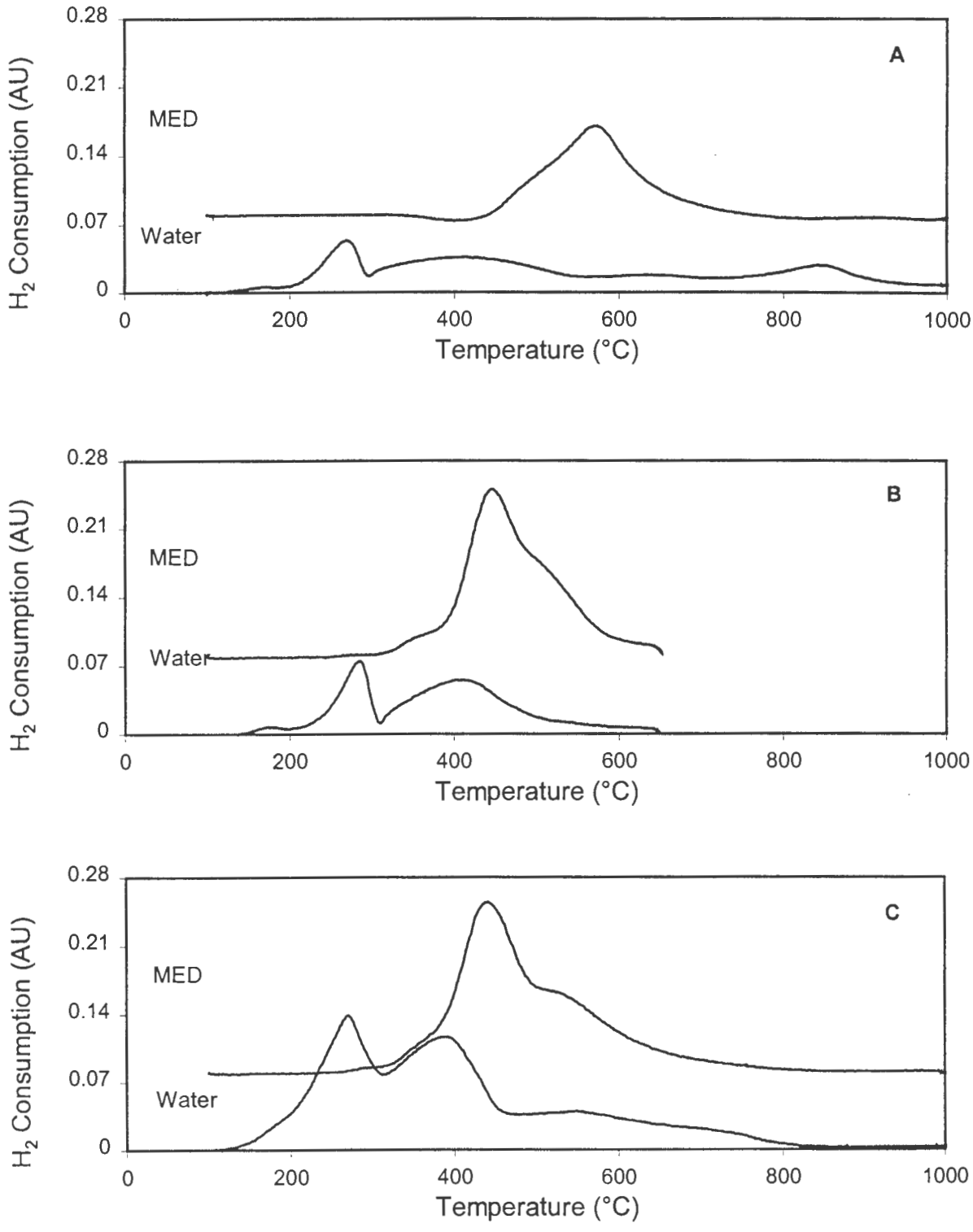

Figure 3.27. Effect of the addition of MED to the impregnation solution on supported cobalt reducibility. TPR spectra for cobalt nitrate supported on SiO_2 (A), ZnO (B) and MnO (C).
(m_{cat} ~ 0.15g, heating rate = 10°C/min, reducing gas = 60(NTP)ml/min 5% H_2 in N_2,)

The ZnO supported catalyst prepared with MED in solution gave a TPR spectrum with a single peak with maximum hydrogen consumption at 430°C. However, unlike the SiO_2 support, two shoulders were evident on the peak. These were a low temperature shoulder between 350°C and 400°C, and a larger shoulder at 580°C. The presence of these shoulders suggests that the cobalt is present in more than one form on the ZnO surface, or that irregularities on the ZnO surface result in varying strengths of interaction. The overall peak could be a combination of cobalt in both oxide and MED complexed form. The hydrogen to cobalt molar ratio for the ZnO supported catalyst was 2.361 for the total reduction spectrum, and 0.199 for reduction up to 400°C as shown in Table 3.13. The high ratio for the overall reduction is attributed to the reduction of both the cobalt oxide and the MED complex. The low ratio for reduction below 400°C may result from interaction between both the cobalt and the MED with the support, as the oxide support surface can also act as a monodentate ligand at the fluid-solid interface [Burwell et al., 1965].

Table 3.13. Effect of the addition of MED to the impregnation solution on hydrogen consumption during TPR for cobalt nitrate impregnated onto SiO_2, ZnO and MnO.

Support	Solvent Type	$H_2:Co_{Total}$	$H_2:Co_{<400°C}$
SiO_2	Water	1.346	0.457
	MED	1.508	0.0
ZnO	Water	1.040	0.607
	MED	2.361	0.199
MnO	Water	3.361	1.968
	MED	1.742	0.320

The effect of MED in the impregnation solution on the MnO support was similar to that seen for both the SiO_2 and ZnO supported cobalt catalysts. The notable feature once again was the single reduction peak with a maximum at a temperature of 440°C. For all three supports, the initial reduction began at a higher temperature, yielding a single broad peak. As for ZnO, the MnO catalyst reduction peak had a low and high temperature shoulder attributable to effects described above. It is possible that the shoulders may be associated with reduction of the

MnO support, as oxidation of the support is still likely due to the decomposition of the nitrate precursor. The hydrogen to cobalt molar ratio for the overall spectrum was 1.742, higher than the ratio of 1 associated with complete CoO reduction. Once again the MED complex may undergo reduction. The hydrogen to cobalt molar ratio for reduction below 400°C was 0.320 from Table 3.13. This low value stems from metal support interaction as discussed for the Co(MED)/ZnO catalyst.

3.2.3.1.1 Extent of Supported Cobalt Reduction

Figure 3.28 illustrates two TPR spectra for the catalyst formed through cobalt nitrate impregnation on SiO_2 (A), ZnO (B) and MnO (C) following the addition of MED to the impregnation solution. The first spectrum entitles 'calcined' corresponds to a pretreatment consisting of a calcination step of 1 hour in N_2 at 400°C to decompose the precursor. The second spectrum entitled 'reduced' illustrates the TPR profile following activation of the catalyst by reduction in a 5% H_2 in N_2 gas mixture. The reduction pretreatment was the same applied to the catalyst as an activation procedure prior to loading into the reactor for Fischer-Tropsch synthesis. By comparison of the two spectra, information on the extent of reducibility of cobalt acetate supported on SiO_2 (A), ZnO (B) and MnO (C) was obtained.

The extent of reduction calculations for the MED prepared catalysts were based on the assumption that, following reduction at 400°C for 16 hours, the unreduced cobalt was present on the catalyst as divalent cobalt. This assumption seems reasonable in light of the fact that MED is a strong field ligand that would prevent oxidation of the loaded divalent cobalt to the trivalent form.

Reduction at 400°C for 16 hours caused differences in the reduction profile of the Co(MED)/SiO_2 catalyst relative to the calcined catalyst as illustrated in Figure 3.28 (A). The 'reduced' sample showed three regions of reduction as opposed to the single reduction step over the 'calcined' catalyst. The low temperature region with maximum hydrogen consumption at 250°C is due to the reduction of reoxidised zerovalent cobalt following exposure to the atmosphere. The majority of hydrogen consumption took place in a broad peak with a maximum at 550°C. This reduction region corresponded to the single reduction peak present during the TPR spectrum of the 'calcined' catalyst, and was attributed to Co^{2+} strongly chelated by both the MED and the SiO_2 support.

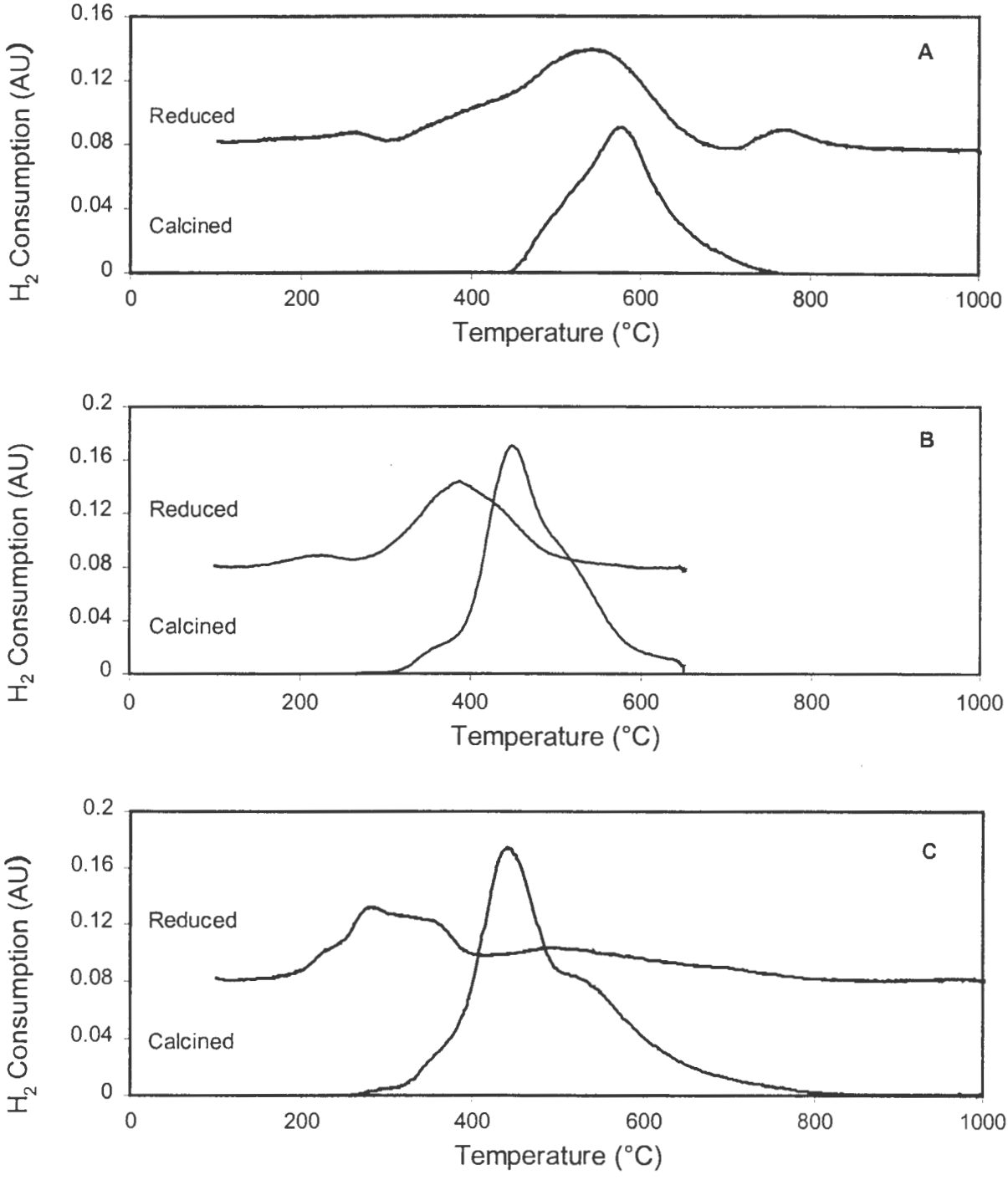

Figure 3.28. Evaluation of the extent of reduction of supported cobalt nitrate after reduction at 400°C for 16 hours for (A) Co(MED)/SiO_2, (B) Co(MED)/ZnO and (C) Co(MED)/MnO.
(m_{cat} ~ 0.15g, heating rate = 10°C/min, reducing gas = 60(NTP)ml/min 5% H_2 in N_2,)

The remaining reduction region was due to a small fraction of cobalt migrating into the bulk SiO_2 phase and transforming to cobalt silicates. The formation of this specie decreases the activity of the catalyst by lowering the extent of reduction of cobalt below 400°C.

Table 3.14 shows the extents of reduction for Co(MED)/SiO_2, Co(MED)/ZnO and Co(MED)/MnO, as well as the hydrogen to cobalt molar ratios obtained for each TPR spectrum. The extent of reduction calculated for the Co(MED)/SiO_2 catalyst was calculated to be 15.0%, as compared to 80.3% for the base case Co/SiO_2 catalyst. Consequently the presence of MED in the impregnation solution significantly lowered the extent of reduction of the cobalt loaded in nitrate form on SiO_2.

Table 3.14. TPR hydrogen consumption data for evaluation of the extent of reduction of supported cobalt for Co(MED)/SiO_2, Co(MED)/ZnO and Co(MED)/MnO.

Catalyst	Pretreatment	H_2:Co Total	H_2:Co <400°C	Extent of Reduction (%)
Co(MED)/SiO_2	Calcination	1.508	0	15.0
	Reduction	1.017	0.167	
Co(MED)/ZnO	Calcination	2.361	0.199	72.4
	Reduction	0.774	0.498	
Co(MED)/MnO	Calcination	1.742	0.320	46.7
	Reduction	1.169	0.636	

The 'reduced' Co(MED)/ZnO catalyst yielded a TPR spectrum illustrated in Figure 3.28 (B). The spectrum was characterised by a small reduction region between 180°C and 230°C associated with reduction of surface oxidised cobalt following exposure to the atmosphere. The most significant reduction region took place between 290°C and 450°C. This consumption was attributed to species that reverted to a stable Co^{2+} structure in association with the support following surface reoxidation. This would account for the large temperature range of the reduction region, and the fact that reduction took place both above and below 400°C. The extent of reduction calculated for the Co(MED)/ZnO catalyst was 72.4%, lower than 91.4% obtained over the base case Co/ZnO catalyst. As was the case with SiO_2, the

presence of MED has lowered the extent of reduction of the supported cobalt. The decrease results from the strong field ligand effect of MED on Co^{2+} ions that lowered the ease of reducibility of the Co^{2+}.

For Co(MED)/MnO, the extent of reduction was calculated to be 46.7% and is shown in Table 3.14. The extent of reduction increased from 28.7% to 46.7% with the addition of MED to the impregnation solution. Figure 3.28 (C) shows the TPR spectra for the 'calcined' and 'reduced' catalysts. The 'calcined' catalyst consisted of a single broad band of reduction with a maximum consumption taking place at 430°C, with a high temperature shoulder on the main consumption peak. The 'reduced' Co(MED)/MnO catalyst had two regions of reduction. The first region showed evidence of surface reoxidation of exposed zerovalent cobalt to Co_3O_4 as the reduction profile comprised two regions of reduction, a main section and a low temperature shoulder. Reoxidation to the Co_3O_4 form may occur as a result of the ease with which MnO can alter oxidation states. In this way, the support may be able to aid oxidation by supplying lattice oxygen while undergoing a change in oxidation state itself. The second region was a broad flat reduction profile occurring above 500°C. The hydrogen consumption associated with this peak gave information on the fraction of cobalt present in inactive form following activation of the catalyst by reduction at 400°C. This region may result from cobalt still bound to MED in the Co^{2+} form. This information allowed calculation of the extent of reduction of the cobalt on the MnO support. The increased extent of reduction obtained using MED was attributed to the strength with which the MED chelates with the Co^{2+} ions. In so doing, cobalt is restricted from interacting with the MnO support and support oxidation decreases as well. As MnO was seen to shift oxidation states easily, it is favourable to prevent this oxidation as the oxidised support may be able to supply lattice oxygen that results in oxidation of the supported cobalt which may enhance cobalt support interaction.

3.2.3.2 Hydrogen Chemisorption

Table 3.15 contains the results obtained from the hydrogen chemisorption measurements performed on the Co(MED)/SiO_2, Co(MED)/ZnO and Co(MED)/MnO cobalt nitrate loaded catalysts. The Co(MED)/MnO catalyst gave the highest surface area of 0.86 m^2/g compared to 0.44 m^2/g and 0.17 m^2/g for the ZnO and SiO_2 supported catalysts. Consequently the addition of MED to the impregnation solution caused large changes in the quantity of exposed metal on the support surface for all three support types.

The surface area of exposed metal atoms decreased from 3.18 m^2/g for Co/SiO_2 to 0.17 m^2/g for $Co(MED)/SiO_2$. The volume of adsorbed hydrogen dropped significantly from 0.865 cm^3 to 0.047 cm^3. This decrease is caused by the lower extent of reduction obtained with the addition of MED and the lower degree of dispersion of the cobalt on the support surface. The extent of reduction dropped from 80.3% to 15.0% while the dispersion decreased from 6.66% to 1.93% on addition of MED using SiO_2. The cobalt crystallite size increased from 14.5 nm to 49.9 nm. The reversibility of hydrogen adsorption decreased from 65.8% to 28.9% indicating that MED addition has decreased the concentration of strong hydrogen adsorption sites. Bartholomew and Reuel [1985] attributed an increased reversibility to a greater degree of interaction between metal and support. The strong chelating effect of the MED shields the cobalt ions during impregnation resulting in decreased interaction between cobalt and SiO_2. This accounts for the lower reversibility.

With the ZnO support, the metal surface area also decreased with MED addition from 0.79 m^2/g for the base catalyst to 0.44 m^2/g. This coincided with a lowering in the extent of reducibility from 91.4% to 72.4%. The dispersion decreased and the crystallite size increased upon MED addition. The reversibility increased significantly from 39.1% to 62.0%. This result confirms TPR findings. The Co/ZnO base catalyst showed minimal interaction between cobalt and support, however the addition of MED significantly increased the temperature at which cobalt reduction took place on the ZnO surface.

Table 3.15. Surface area, dispersion, particle diameter and hydrogen adsorption reversibility for $Co(MED)/SiO_2$, Co(MED)/ZnO and Co(MED)/MnO.

Catalyst	Surface Area (m^2/g)	Dispersion (%)	Crystallite Size (nm)	Reversibility (%)
$Co(MED)/SiO_2$	0.17	1.93	49.9	28.9
Co(MED)/ZnO	0.44	0.98	95.2	62.0
Co(MED)/MnO	0.86	3.07	31.3	57.6

The Co(MED)/MnO catalyst had an exposed cobalt metal surface area of 0.86 m^2/g. This was more than double that observed over Co/MnO. The reason for this behaviour is that the MED

is a strong field ligand that replaces the water ligands that surround the cobalt ions in aqueous impregnations. The MnO support was seen to oxidise readily due to the presence of the nitrate precursor, however the presence of MED protects the cobalt ions from the oxidising strength of the NO_2 gas released during nitrate decomposition. In this way, the cobalt ions interact to a lesser extent with the support resulting in a higher extent of reduction. The extent of reduction was seen to increase from 28.7% to 46.7% following MED addition. The reversibility of hydrogen adsorption increased from 47.6% to 57.6% through MED addition.

3.2.3.3 Transmission Electron Microscopy

The TEM photographs for Co(MED)/SiO_2, Co(MED)/ZnO and Co(MED)/MnO are shown in Figure 3.29 (A), (B) and (C) respectively. The photograph for Co(MED)/SiO_2 shows little evidence of reduced cobalt crystallites. The amorphous SiO_2 does show small areas that are darker, possibly a result of a small amount of reduced cobalt. The Co(MED)/SiO_2 catalyst was calculated to have a very low exposed metal surface area of 0.17 m^2/g as opposed to 3.18 m^2/g for Co/SiO_2. This drop in surface area means less cobalt present as reduced cobalt metal as observed.

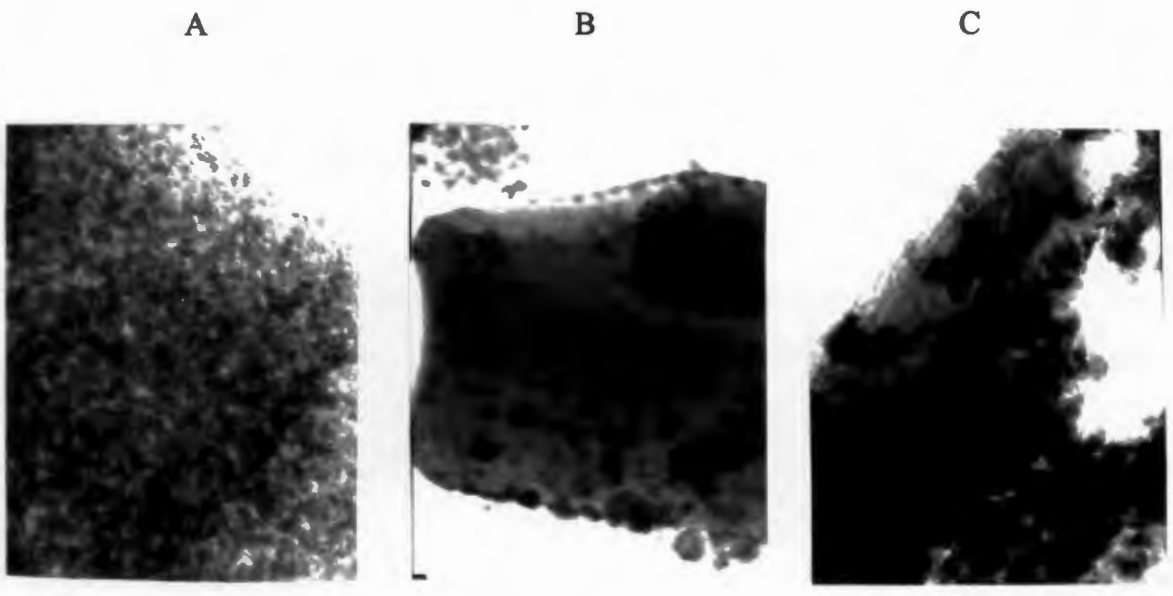

Figure 3.29. TEM photographs for (A) Co(MED)/SiO_2, (B) Co(MED)/ZnO and Co(MED)/MnO.

The Co(MED)/ZnO photograph is shown in Figure 3.29 (B). The notable feature is that a significantly larger fraction of the cobalt is supported on the ZnO support, in contrast with both Co/ZnO and Co(A).ZnO, where cobalt oxide particles existed independent of the support material. Consequently the MED has brought about an association between cobalt and the support material. This is beneficial as dispersion of the cobalt will be improved and the cobalt crystallites will be smaller.

The presence of MED in the impregnation solution resulted in the Co(MED)/MnO catalyst illustrated in Figure 3.29 (C). The photograph was inconclusive as to the nature of the cobalt crystallites or their association with the MnO support. However black spots are evident, possibly indicating the presence of the cobalt, as no support oxidation was noted during nitrate decomposition during TPR for this catalyst.

3.2.3.4 Fischer-Tropsch Synthesis

The effect of MED on the preparation of the catalysts was tested under Fischer-Tropsch conditions in order to obtain activity and selectivity data necessary for performance characterisation. The activity was measured in terms of the hydrocarbon yields obtained from the gas chromatograph analysis of the organic products. The organic yield was calculated according to the procedure laid out in Appendix III.

3.2.3.4.1 SiO_2 as a Support

Addition of MED to the impregnation solution resulted in a major change in both the activity and selectivity of the SiO_2 supported catalyst as illustrated in Table 3.16. The MED prepared catalyst, Co(MED)/SiO_2, was significantly less active than the water prepared catalyst, Co/SiO_2. The yield of organic product for the Co(MED)/SiO_2 catalyst was 1.20% as opposed to 5.67% for the Co/SiO_2 catalyst. This represented a drop in activity of nearly 500%. This lower yield is attributable to a decrease in exposed cobalt metal surface area from 3.18 m^2/g for Co/SiO_2 to 0.17 m^2/g for Co(MED)/SiO_2 measured by hydrogen chemisorption. It is interesting to note that the rate of consumption of carbon monoxide per square metre of exposed cobalt increased dramatically from 4.12×10^{-3} $mmol/m^2_{Co}/min$ to 15.33×10^{-3}

mmol/m^2_{Co}/min. Thus, although the surface area dropped by a factor of 19, the turnover rate at each site tripled as a result of MED addition.

The drop in the yield of volatile organic products coincided with an increase in the C_{1+2} fraction from 14.97% for the Co/SiO_2 catalyst to 32.84% for the MED prepared catalyst. The linear alkane fraction of $Co(MED)/SiO_2$ was 31.66%, slightly higher than the 28.26% formed over the Co/SiO_2 catalyst.

Table 3.16. Effect of the addition of MED to the impregnation solution on the activity and selectivity of cobalt nitrate on SiO_2.
(m_{cat} ~ 1g, T = 200°C, P = 5 bar, H_2 : CO = 2 : 1, WHSV = 0.34g_{CO}/g_{cat}.hr)

Catalyst	Co/SiO_2	$Co(MED)/SiO_2$
Reaction Time	14 hr 50	18 hr 53
Yield of volatile organics (%)	5.67	1.20
S_{C1+C2} (carbon%)	14.97	32.84
α_{C4-C11}	0.78	0.77
r_{HC} .10^3 (mmol/m^2_{Co}/min)	4.12	15.33
C_5 Composition (%)		
3-methyl-1-butene	0.60	0.19
2-methyl-butane	0.84	1.36
1-pentene	56.31	20.79
2-methyl-1-butene	0.00	0.00
n-pentane	28.26	31.66
trans-2-pentene	8.23	30.91
cis-2-pentene	5.61	14.12
2-methyl-2-butene	0.15	0.79

The chain growth probability, α, was calculated for each catalyst from the slope of the Anderson-Schulz-Flory distribution illustrated in Figure 3.30. The chain growth probability was 0.78 for Co/SiO_2, and 0.77 for $Co(MED)/SiO_2$. Thus the change in the nature of the impregnation solution had no effect on the chain growth probability for the SiO_2 supported cobalt catalyst.

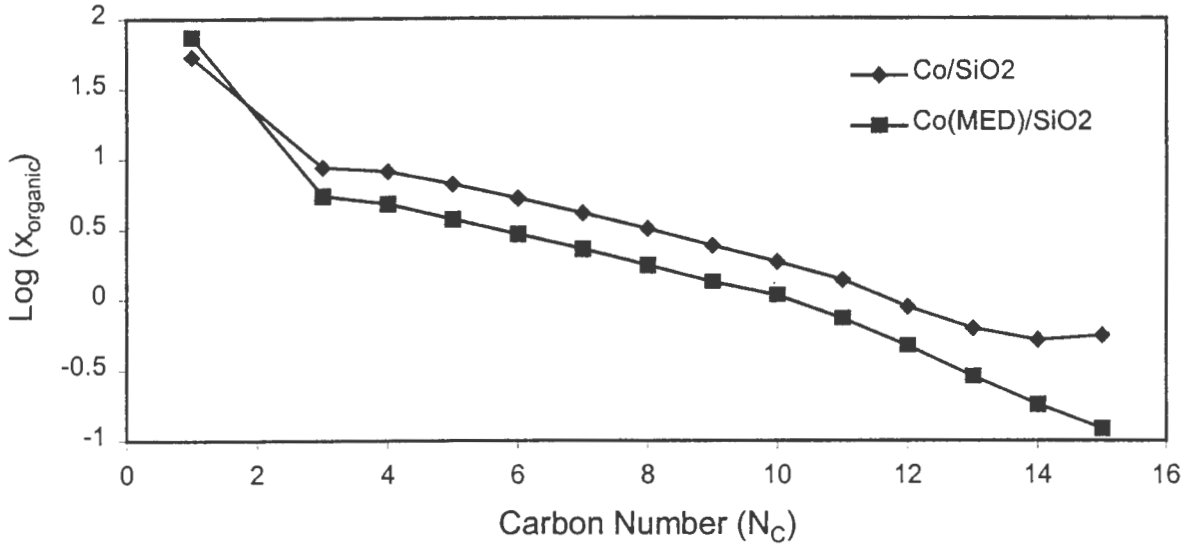

Figure 3.30. Effect of the type of impregnation solution on the Anderson-Schulz-Flory distribution for cobalt nitrate on SiO_2.
(m_{cat} ~ 1g, T = 200°C, P = 5 bar, H_2 : CO = 2 : 1, WHSV = 0.34g_{CO}/g_{cat}.hr)

The rate of formation of the total organic product is shown in Figure 3.31. As the rate of formation is a measure of the speed with which each carbon number product forms, the plots parallel the yield measurements for each catalyst. Consequently the rate of formation of the Co/SiO_2 water prepared catalyst was considerably higher than the formation rate plot of the $Co(MED)/SiO_2$ catalyst.

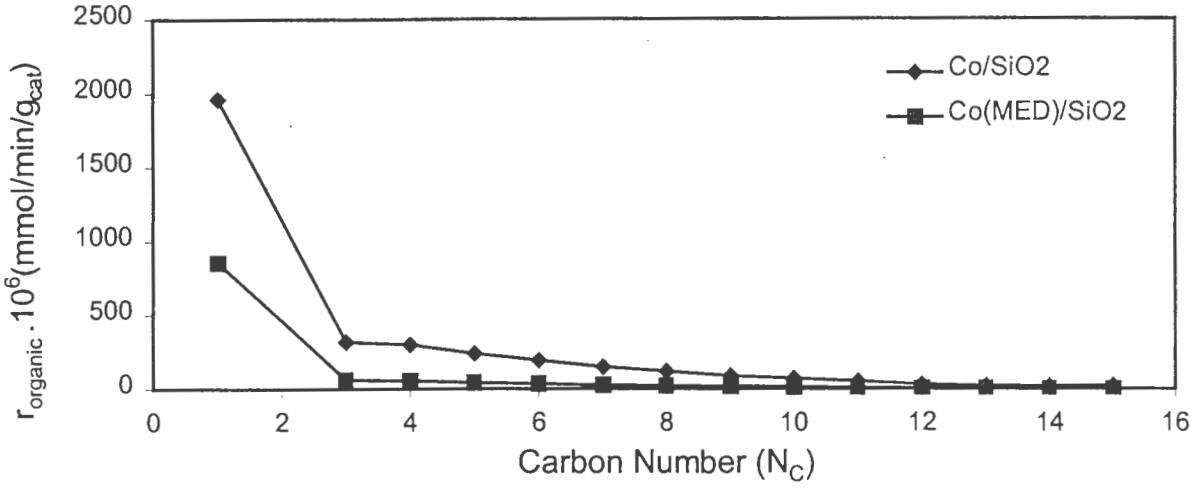

Figure 3.31. Effect of the type of impregnation solution on the total organic formation rate for cobalt nitrate on SiO_2.
(m_{cat} ~ 1g, T = 200°C, P = 5 bar, H_2 : CO = 2 : 1, WHSV = 0.34g_{CO}/g_{cat}.hr)

Figure 3.32 illustrates the linear olefin fraction of the total linear organic product at each carbon number. The linear olefin fraction of the two catalysts showed comparable values over the whole carbon number range. As the carbon number increased, the fraction of linear olefins in the linear organic product dropped from an initial fraction of between 60 and 80%, to a fraction of less than 20% in the C_{12} fraction for both catalysts. This decrease results from increased hydrogenation activity on larger growing chains causing termination as alkanes. The addition of MED had an small effect on the linear olefin content of the C_4 and C_5 fraction, which were slightly lower than for Co/SiO_2. From the C_6 fraction onwards, the trend was reversed with the $Co(MED)/SiO_2$ catalyst producing a higher fraction of linear olefins. The catalysts showed comparable values for the C_6 fraction and higher, with linear olefin fractions varying by less than 5%.

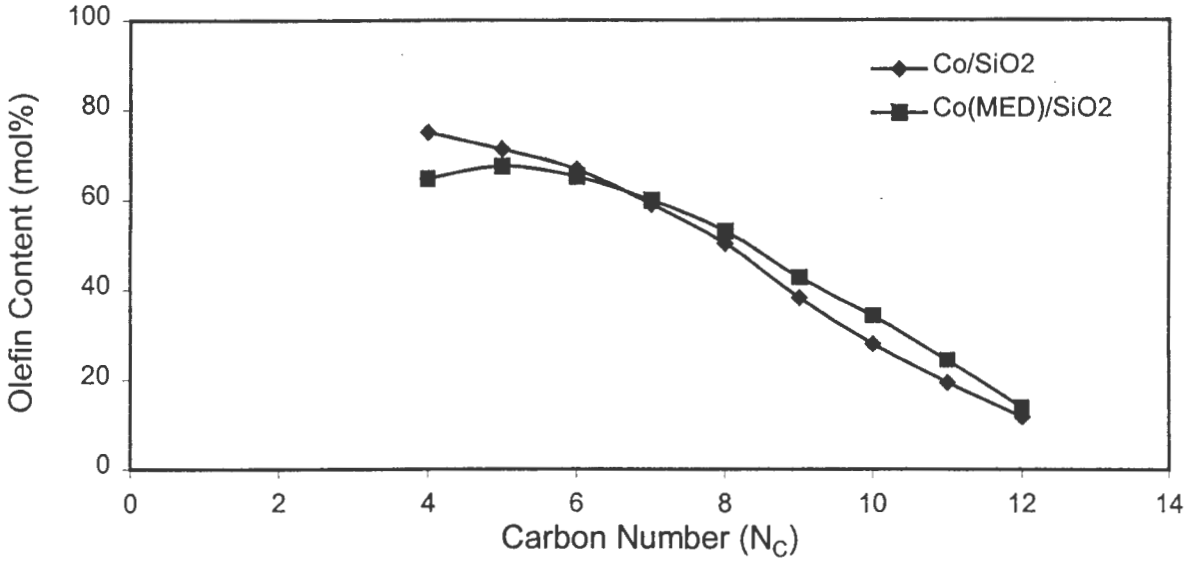

Figure 3.32. Effect of the type of impregnation solution on the olefin fraction of the linear organic product for cobalt nitrate on SiO_2.
(m_{cat} ~ 1g, T = 200°C, P = 5 bar, H_2 : CO = 2 : 1, WHSV = 0.34g_{CO}/g_{cat}.hr)

The α-olefin fraction of the total linear olefin fraction is shown in Figure 3.33. The addition of MED to the impregnation solution dramatically altered the α-olefin distribution of the silica supported catalyst. In the C_5 carbon number, the α-olefin fraction of the total linear olefin was 80.27%. This fraction dropped to 31.59% due to the effect of the MED during impregnation. The formation of α-olefins is the primary reaction during Fischer-Tropsch synthesis, consequently the Co(MED)/SiO_2 catalyst greatly enhances the formation of secondary reaction products. It is likely that the higher rate of carbon monoxide consumption per square metre of exposed cobalt observed over Co(MED)/SiO_2 is responsible for the higher secondary reaction activity, as higher secondary reaction activity generally coincides with higher overall activity. The α-olefin content of both catalysts was seen to decrease as the carbon number increased, indicating that the longer hydrocarbon chains are more susceptible to termination as hydrogenated products.

The higher secondary reaction activity over Co(MED)/SiO_2 may also be a result of the low surface area of active cobalt species increasing the influence of the SiO_2 support. As the cobalt surface area becomes smaller, active cobalt crystallites become smaller such that the

surface effect is more and more noticeable. This same effect was evident for the $Co(A)/SiO_2$ catalyst. It is thought that the SiO_2 surface promotes the double bond shift activity of the catalyst resulting in a higher proportion of secondary olefins in the product spectrum.

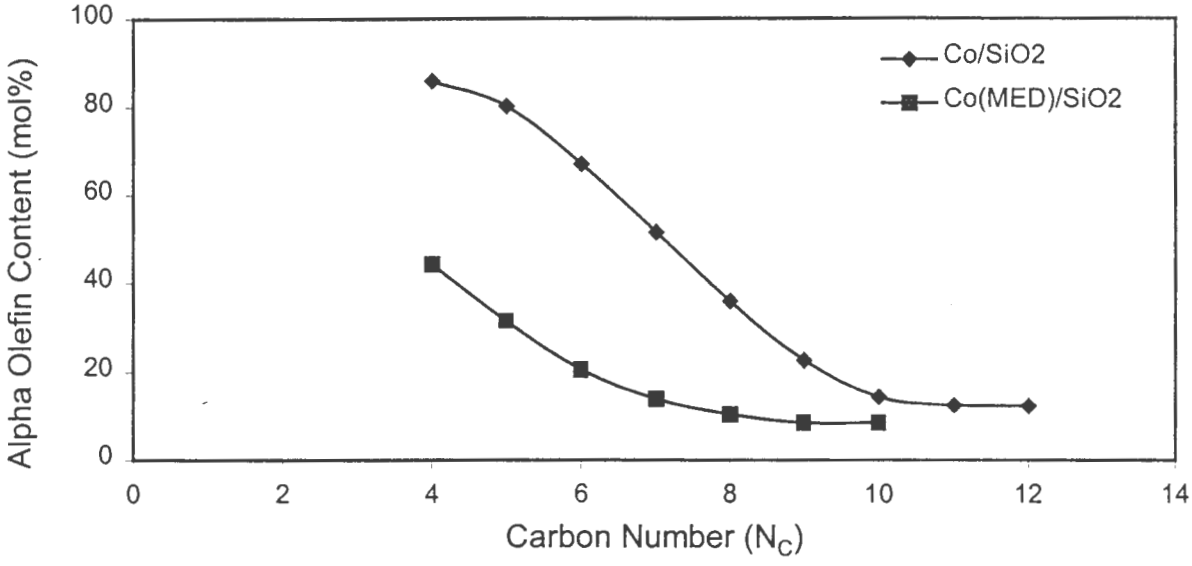

Figure 3.33. Effect of the type of impregnation solution on the α-olefin fraction of the linear olefins for cobalt nitrate on SiO_2.
(m_{cat} ~ 1g, T = 200°C, P = 5 bar, H_2 : CO = 2 : 1, WHSV = 0.34g_{CO}/g_{cat}.hr)

3.2.3.4.2 ZnO as a Support

The presence of MED in the impregnation solution significantly altered the performance of the ZnO supported cobalt catalysts under Fischer-Tropsch reaction conditions. The results can be seen in Table 3.17. The yield of total organic products formed over Co(MED)/ZnO was 0.93%, lower than the yield of 1.39% formed over the Co/ZnO catalyst. This findings correlates with the decrease in exposed cobalt surface area which dropped from 0.79m^2/g to 0.44 m^2/g following MED addition as well as a drop in cobalt dispersion from 1.44% to 0.98%. However the turnover rate per square metre of exposed cobalt on the surface increased from 3.82×10^{-3} mmol/m^2_{Co}/min to 4.57×10^{-3} mmol/m^2_{Co}/min. Consequently, even though the overall yield decreased, the activity per cobalt area increased. This increased activity per cobalt area may result in the higher secondary activity observed. Thus the

addition of MED to the impregnation solution lowered the observed activity of the ZnO supported catalyst, although not to a large extent.

Table 3.17. Effect of the addition of MED to the impregnation solution on the activity and selectivity of cobalt nitrate on ZnO.
(m_{cat} ~ 1g, T = 200°C, P = 5 bar, H_2 : CO = 2 : 1, WHSV = 0.34g_{CO}/g_{cat}.hr)

Catalyst	Co/ZnO	Co(MED)/ZnO
Reaction Time	26 hr 00	14 hr 50
Yield of volatile organics (%)	1.39	0.93
S_{C1+C2} (carbon%)	20.65	27.07
α_{C4-C11}	0.83	0.72
$r_{HC}.10^3$ (mmol/m^2_{Co}/min)	3.82	4.57
C_5 Composition (%)		
3-methyl-1-butene	0.29	0.53
2-methyl-butane	0.52	1.89
1-pentene	72.21	50.18
2-methyl-1-butene	0.00	0.00
n-pentane	22.13	32.06
trans-2-pentene	2.27	9.27
cis-2-pentene	1.79	6.06
2-methyl-2-butene	0.15	0.79

The C_{1+2} selectivity is given in Table 3.17. The Co(MED)/ZnO catalyst gave a selectivity to C_{1+2} of 27.07%, almost 7% higher than that produced by the Co/ZnO catalyst. This higher selectivity to the low molecular weight fraction is an unfavourable effect of MED addition. The addition of MED also enhanced the formation of secondary products on the ZnO supported cobalt catalyst. The linear alkane content of the C_5 fraction increased from 22.13% to 32.06% on addition of MED to the impregnation solution. This increased secondary hydrogenation coincided with an increase in the amount of branched product in the C_5 fraction from 0.96% to 3.21%, as well as increased alkene isomerisation as illustrated by the enhanced formation of secondary linear olefins from Table 3.17. Consequently the overall trend of MED addition to the ZnO catalyst was a decrease in activity accompanied by a propensity for secondary product formation.

Figure 3.34 shows the Anderson-Schulz-Flory distribution for both the Co/ZnO and Co(MED)/ZnO catalysts. From the slope of the straight line between the C_4 and C_{11} fractions, the chain growth probability , α, could be calculated. The values for α are given in Table 3.17. The chain growth probabilities were 0.83 and 0.72 for Co/ZnO and Co(MED)/ZnO respectively. Thus the presence of MED in the impregnation solution changed the chain growth probability of the ZnO supported catalyst significantly. The drop in growth probability coincided with a lower exposed metal surface area. At high carbon numbers, both ASF plots deviate from straight line behaviour. This deviation is due to the lower temperature of the wax trap resulting in capture and subsequent bleeding of a fraction of the higher molecular weight product.

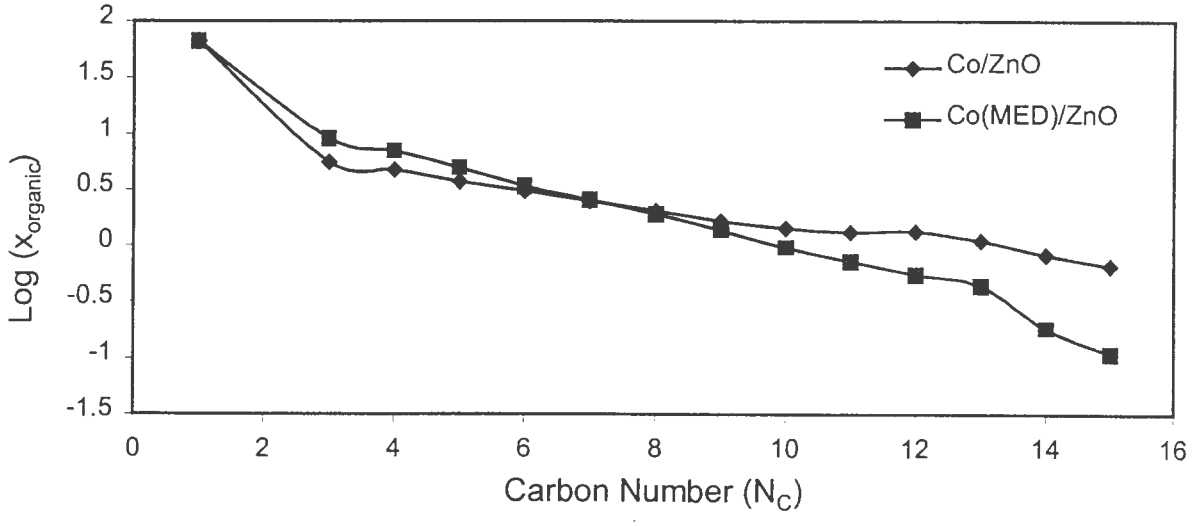

Figure 3.34. Effect of the type of impregnation solution on the Anderson-Schulz-Flory distribution for cobalt nitrate on ZnO.
(m_{cat} ~ 1g, T = 200°C, P = 5 bar, H_2 : CO = 2 : 1, WHSV = 0.34g_{CO}/g_{cat}.hr)

The rate of formation of total organic product at each successive carbon number is given by Figure 3.35. It can be seen that the rate of formation of each successive carbon number is lower than the previous one, due to the termination of a fraction of the growing chain in each carbon number. The rates of formation of the total organic product are very similar, coinciding with the comparative yield measurements obtained for each catalyst. The rate of formation of methane is higher over the Co(MED)/ZnO catalyst. The formation rate is

directly linked to the number of active sites available on the catalyst surface and the turnover rate per site. On this basis it is clear that either more active sites are present on the Co(MED)/ZnO catalyst than on the Co/ZnO, or the turnover rate on these sites is higher. As the exposed cobalt surface area on Co(MED)/ZnO was lower, the turnover rate per site must have been higher.

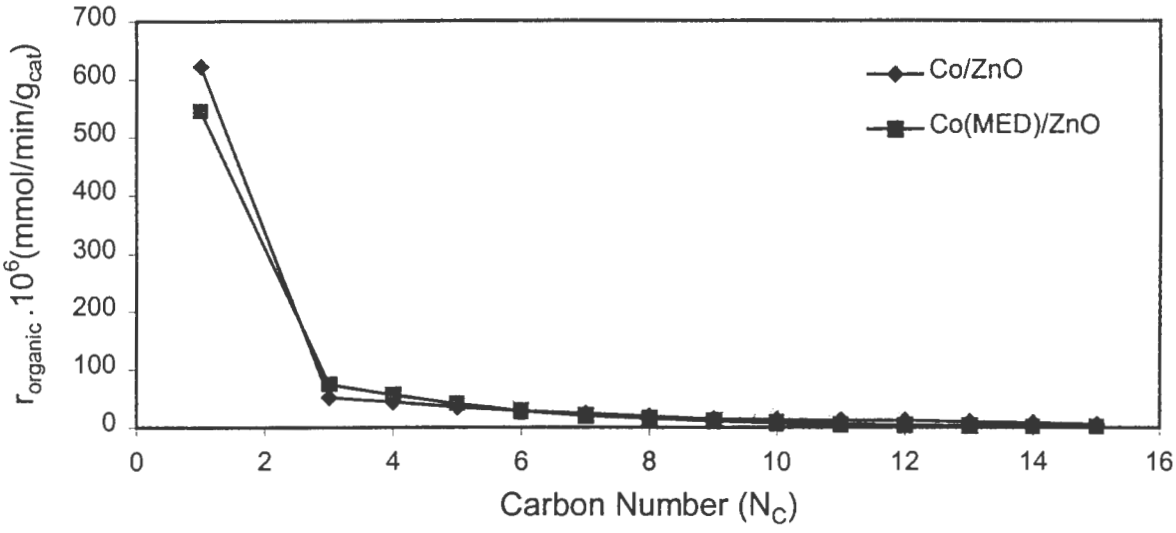

Figure 3.35. Effect of the type of impregnation solution on the total organic formation rate for cobalt nitrate on ZnO.
(m_{cat} ~ 1g, T = 200°C, P = 5 bar, H_2 : CO = 2 : 1, WHSV = 0.34g_{CO}/g_{cat}.hr)

The olefinicity of the linear organic product is shown in Figure 3.36 for the Co/ZnO and Co(MED)/ZnO catalysts. The total linear olefin fraction was made up from the α-olefin content and the β-olefin content of the C_5 fraction. The selectivity to linear olefins of the two catalysts differed by approximately 12% for the full range of carbon numbers, except for the C_{11} and C_{12} fractions where the linear olefinicities were the same. In Table 3.17 the C_5 product breakdown was given for each catalyst. The linear olefin fractions were 76.27% and 65.51% of the total organic product of the C_5 fraction for the Co/ZnO and Co(MED)/ZnO catalysts respectively.

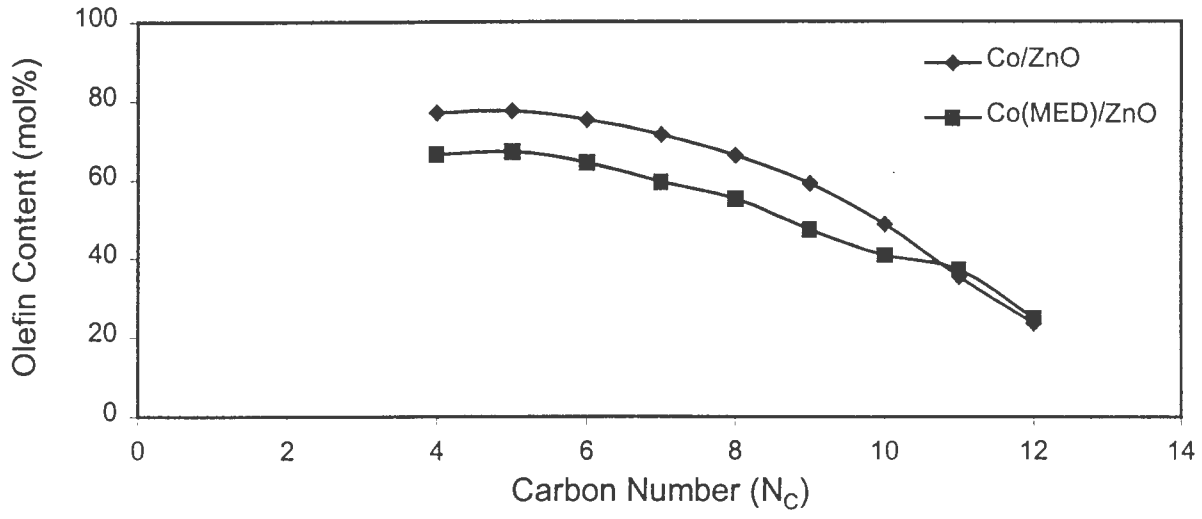

Figure 3.36. Effect of the type of impregnation solution on the olefin fraction of the linear organic product for cobalt nitrate on ZnO.
(m_{cat} ~ 1g, T = 200°C, P = 5 bar, H_2 : CO = 2 : 1, WHSV = 0.34g_{CO}/g_{cat}.hr)

Table 3.17 shows the breakdown of the total linear olefin content of the C_5 fraction for Co/ZnO and Co(MED/ZnO respectively. The total linear olefin content is split up between the α-olefin and the β-olefin content. The β-olefin fraction is made up of the cis and trans 2-pentene products. The α-olefin fraction of the linear olefins is illustrated in Figure 3.37 for Co/ZnO and Co(MED)/ZnO. The α-olefin fraction of the total organic product was 50.18% for the Co(MED)/ZnO catalyst, and 72.21% for the Co/ZnO catalyst. This meant that the α-olefin made up 76.60% and 94.68% of the linear olefin product over Co(MED)/ZnO and Co/ZnO respectively. The α-olefinicity of the linear olefin product formed over the Co/ZnO catalyst is consequently far higher than for the Co(MED)/ZnO catalyst for the complete carbon number range. The largest difference in the α-olefin fraction of the total linear olefin product occurs in the C_9 fraction where the difference is approximately 47%. The difference in the overall linear olefin fraction of the linear organic product for the two catalysts was only 12% for the same carbon number range. This indicates that the presence of MED in the impregnation solution alters the catalyst's behaviour resulting in an increased rate of secondary reaction resulting in product richer in branched and secondary olefin products and a lower yield of primary α-olefins. This result follows from the higher turnover rate per exposed cobalt surface area. The β-linear olefin content of the C_5 fraction increased from

4.06% for Co/ZnO to 15.33% for the Co(MED)/ZnO catalyst, an increase of nearly 4 times. The increase in secondary activity may also be a result of the higher hydrogen adsorption reversibility of the MED prepared catalyst. This result has significance in that the possibility of readsorption of terminated chains increases with increased reversibility. This adsorption strength may have increased the hydrogenation and secondary double bond shift activity of the catalyst.

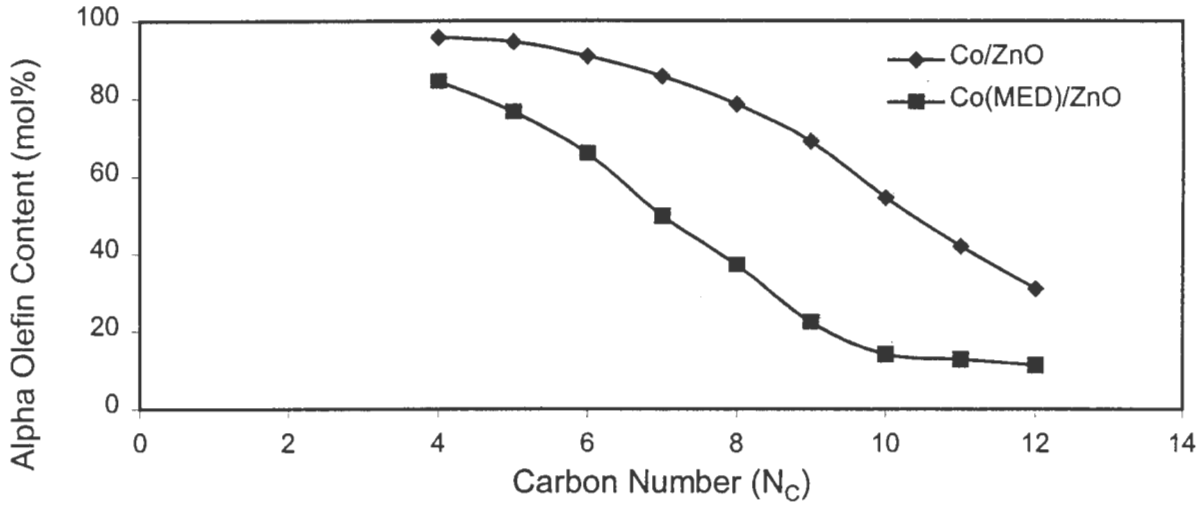

Figure 3.37. Effect of the type of impregnation solution on the α-olefin fraction of the linear olefins for cobalt nitrate on ZnO.
(m_{cat} ~ 1g, T = 200°C, P = 5 bar, H_2 : CO = 2 : 1, WHSV = 0.34g_{CO}/g_{cat}.hr)

3.2.3.4.3 MnO as a Support

The presence of MED in the impregnation solution significantly altered the performance of the MnO supported cobalt catalyst under Fischer-Tropsch reaction conditions. The yield of total organic products formed over Co(MED)/MnO was 1.23%, more than six times higher than the yield of 0.18% formed over the Co/MnO catalyst. Thus the addition of MED to the impregnation solution radically increased the activity of the MnO supported. The increased activity resulted from a larger exposed metal surface area observed through hydrogen chemisorption over Co(MED)/MnO than over Co/MnO. This increased activity was a result of the strong ligand presence of MED during impregnation and drying. The MED shielded

the cobalt during nitrate decomposition lowering the oxidising effect of the MnO support on the reduced cobalt. The C_{1+2} selectivity is given in Table 3.18. The Co(MED)/ZnO catalyst gave a selectivity to C_{1+2} of 25.13%, about 2% lower than that produced by the Co/ZnO catalyst. The addition of MED enhanced the formation of the α-olefin fraction from 50.60% of the total organic yield to 66.33%. This increase coincided with an increase in the rate of carbon monoxide consumption per exposed cobalt surface area from 1.13×10^{-3} $mmol/m^2_{Co}/min$ to 3.05×10^{-3} $mmol/m^2_{Co}/min$. This is surprising, as higher activity generally results in greater secondary reaction activity. The presence of MED decreased both the hydrogenation activity, as represented by the n-paraffin fraction, as well the secondary isomerisation of the α-olefin, as represented by the linear β-olefin fraction. The alkane content of the C_5 fraction decreased from 30.09% to 24.52% of the total organic product on addition of MED to the impregnation solution. The branched product content was unaffected by the presence of MED with Co/MnO containing 2.82% branched products and Co(MED)/MnO containing 2.99% branched products.

Table 3.18. Effect of the addition of MED to the impregnation solution on the activity and selectivity of cobalt nitrate on MnO.
(m_{cat} ~ 1g, T = 200°C, P = 5 bar, H_2 : CO = 2 : 1, WHSV = $0.34 g_{CO}/g_{cat}.hr$)

Catalyst	Co/MnO	Co(MED)/MnO
Reaction Time	22 hr 30	23 hr 46
Yield of volatile organics (%)	0.18	1.23
S_{C1+C2} (carbon%)	27.52	25.13
α_{C4-C11}	0.76	0.71
$r_{HC}.10^3$ ($mmol/m^2_{Co}/min$)	1.13	3.05
C_5 Composition (%)		
3-methyl-1-butene	0.80	1.48
2-methyl-butane	1.87	1.38
1-pentene	50.60	66.33
2-methyl-1-butene	0.00	0.00
n-pentane	30.09	24.52
trans-2-pentene	9.76	3.73
cis-2-pentene	6.21	2.43
2-methyl-2-butene	0.15	0.13

Figure 3.38 shows the Anderson-Schulz-Flory distribution for both the Co/MnO and Co(MED)/MnO catalysts. From the slope of the straight line between the C_4 and C_{11} for Co/MnO and C_4 and C_9 fractions for Co(MED)/MnO, the chain growth probability , α, could be calculated. The values for α are given in Table 3.18. The chain growth probabilities were 0.76 and 0.71 for Co/MnO and Co(MED)/MnO respectively. Thus the presence of MED in the impregnation solution decreased the chain growth probability of the MnO supported catalyst significantly. The ASF plot for the Co(MED)/MnO catalyst includes a hump ranging from C_{10} to C_{14}. This behaviour was attributed to the bleeding of product from the wax trap.

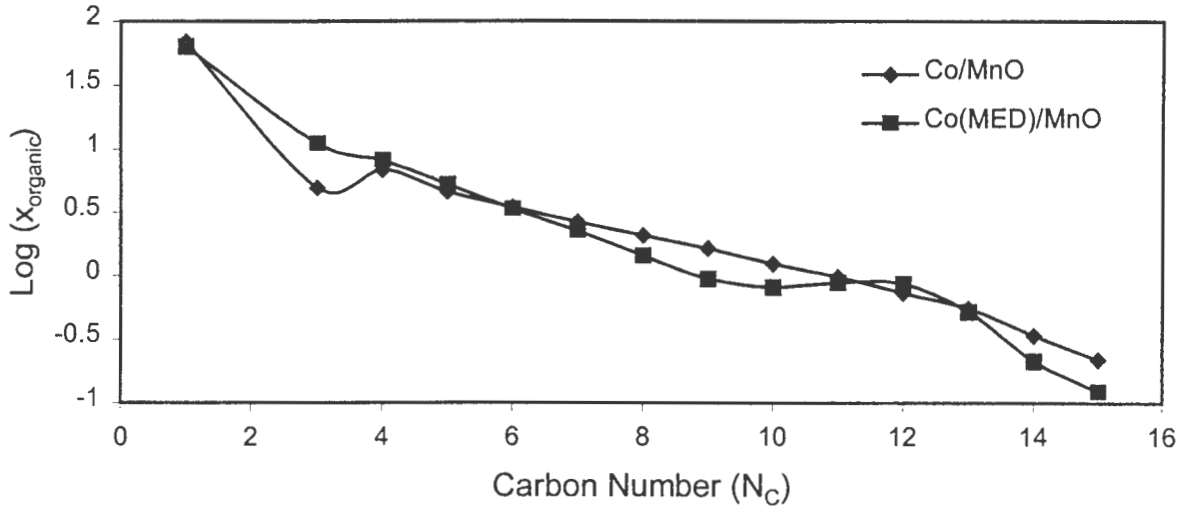

Figure 3.38. Effect of the type of impregnation solution on the Anderson-Schulz-Flory distribution for cobalt nitrate on MnO.
(m_{cat} ~ 1g, T = 200°C, P = 5 bar, H_2 : CO = 2 : 1, WHSV = 0.34g_{CO}/g_{cat}.hr)

The rate of formation of total organic product at each successive carbon number is given by Figure 3.39. It can be seen that the rate of formation of each successive carbon number is lower than the previous one, due to the termination of a fraction of the growing chain in each carbon number. The rates of formation of the total organic product are very different, coinciding with the comparative yield measurements obtained for each catalyst. The rate of formation of product was significantly higher over the Co(MED)/MnO catalyst than the Co/MnO catalyst paralleling the exposed metal surface area measurements obtained from hydrogen chemisorption experiments.

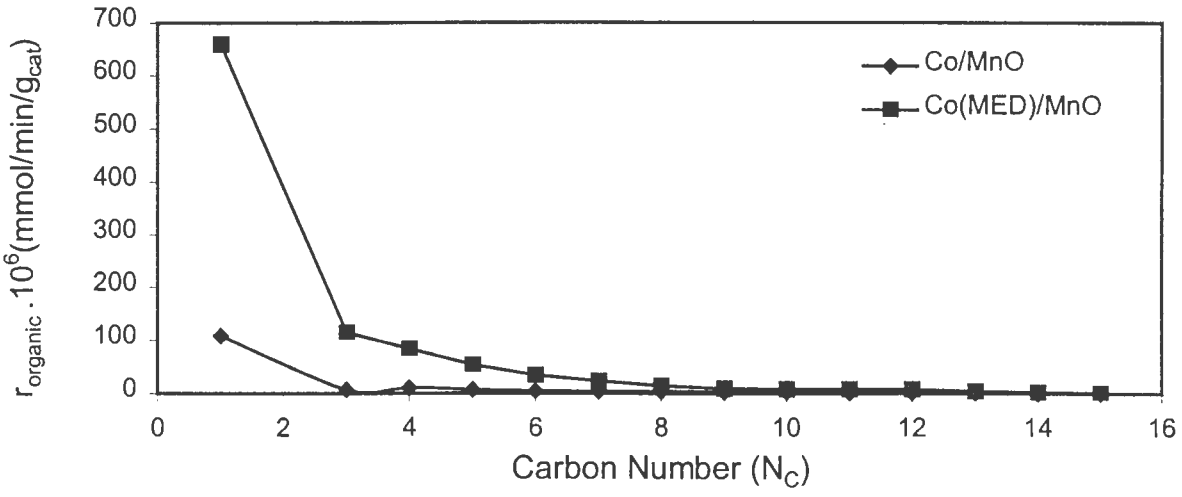

Figure 3.39. Effect of the type of impregnation solution on the total organic formation rate for cobalt nitrate on MnO.
(m_{cat} ~ 1g, T = 200°C, P = 5 bar, H_2 : CO = 2 : 1, WHSV = 0.34g_{CO}/g_{cat}.hr)

The olefinicity of the linear organic product is shown in Figure 3.40 for the Co/MnO and Co(MED)/MnO catalysts. The total linear olefin fraction was made up from the α-olefin content and the β-olefin content of the C_5 fraction. The selectivity of linear olefins in the total linear product for the two catalysts differed by varying degrees over the range of carbon numbers. The olefinicity of the Co(MED)/MnO catalyst was continually higher than that of the Co/MnO catalyst. At low carbon numbers (C_4 and C_5) and high carbon numbers (C_{11} and C_{12}), the difference in olefinicity of the linear product was within 6% for the two catalysts. However in the middle carbon number range, the olefinicities of the two catalysts showed a sizeable difference. The greatest difference of 18% occurred in the C_8 fraction. In Table 3.18 the C_5 product breakdown was given for each catalyst. The linear olefin fractions were 66.57% and 72.49% for the Co/MnO and Co(MED)/MnO catalysts respectively.

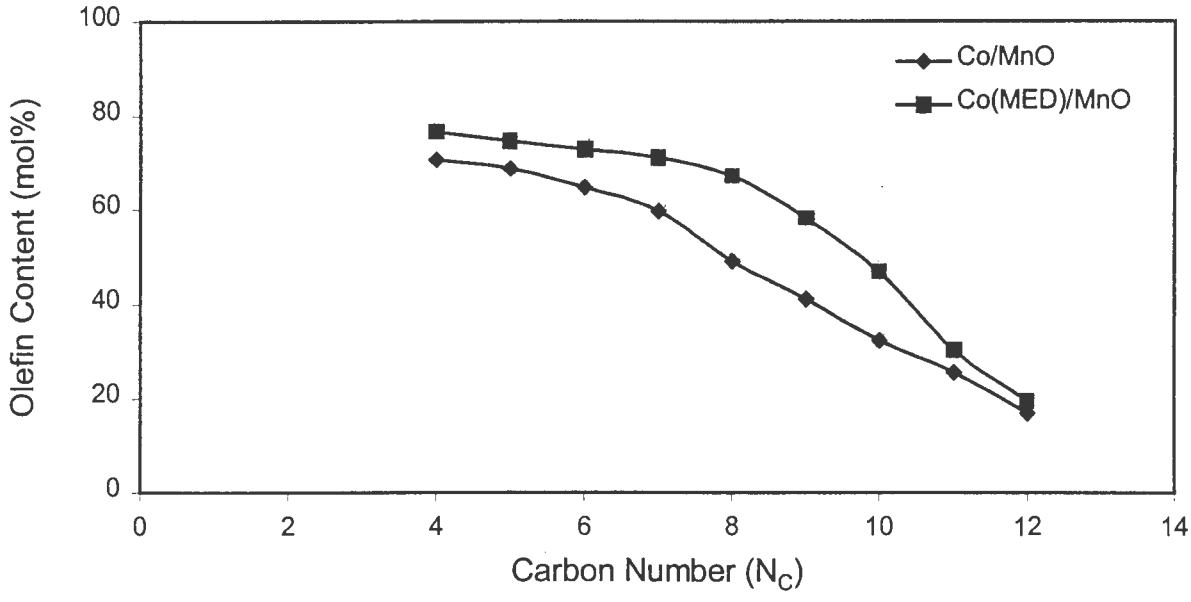

Figure 3.40. Effect of the type of impregnation solution on the olefin fraction of the linear organic product for cobalt nitrate on MnO.
(m_{cat} ~ 1g, T = 200°C, P = 5 bar, H_2 : CO = 2 : 1, WHSV = 0.34g_{CO}/g_{cat}.hr)

Table 3.18 shows the breakdown of the total linear olefin content of the C_5 fraction for Co/MnO and Co(MED/MnO respectively. The total linear olefin content is split up between the α-olefin content and the β-olefin content. The β-olefin fraction is made up of the cis and trans 2-pentene products. The α-olefin fraction of the linear olefins is illustrated in Figure 3.41 for Co/MnO and Co(MED)/MnO. The α-olefin fraction of the total organic product was 66.33% for the Co(MED)/MnO catalyst, and 50.60% for the Co/MnO catalyst. This meant that the α-olefin made up 91.49% and 76.01% of the linear olefin product over Co(MED)/MnO and Co/MnO respectively. The α-olefinicity of the linear olefin product formed over the Co(MED)/MnO catalyst is consequently far higher than for the Co/MnO catalyst for the complete carbon number range. The largest difference in the α-olefin fraction of the total linear olefin product occurs in the C_9 fraction where the difference is approximately 41%. The difference in the overall linear olefin fraction of the linear organic product for the two catalysts was only 17% for the same carbon number. This indicates that the presence of MED in the impregnation solution alters the catalyst's behaviour resulting in a decreased rate of secondary reaction forming a product richer in α-olefins while

suppressing secondary isomerisation and hydrogenation reactions. The β-linear olefin content of the C_5 fraction decreased from 15.97% for Co/MnO to 6.16% for the Co(MED)/MnO catalyst.

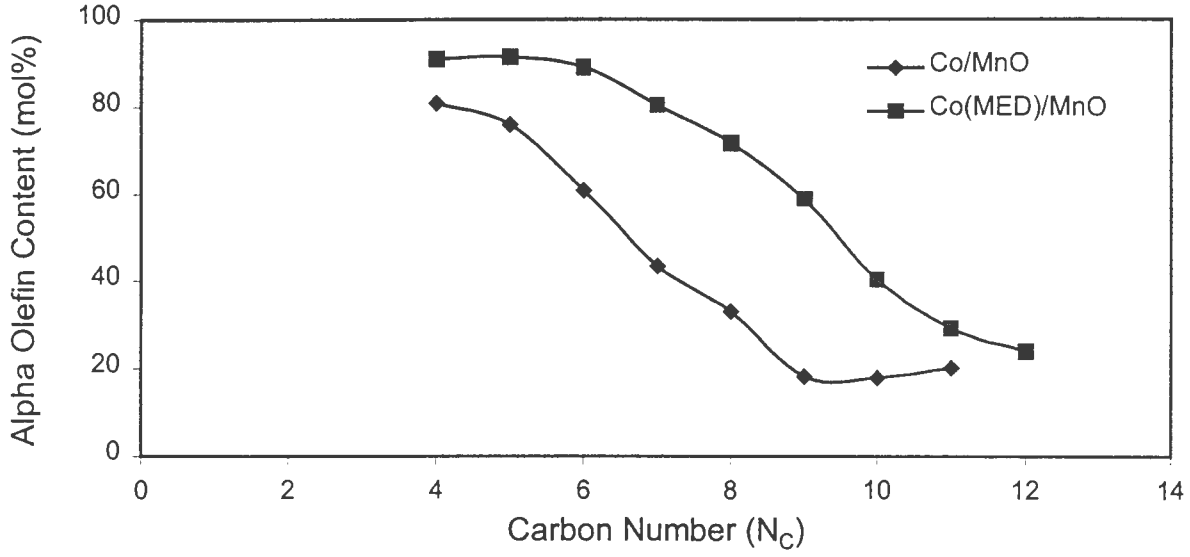

Figure 3.41. Effect of the type of impregnation solution on the α-olefin fraction of the linear olefins for cobalt nitrate on MnO.
(m_{cat} ~ 1g, T = 200°C, P = 5 bar, H_2 : CO = 2 : 1, WHSV = 0.34g_{CO}/g_{cat}.hr)

3.2.4 Effect of the pH of Impregnation Solution

The pH of the impregnation solution is known to influence the net surface charge of inorganic oxides. By altering the pH of the solution, the surface charge can be adjusted to a net positive, neutral or negative value. It is important to stress that a positive net surface charge results from a surplus of positive charge, and not an absence of negative charge. Figure 3.1 shows a plot of surface charge measured in millivolts as a function of pH. As the charge on the support surface changes, the electronic interaction with the positively charged cobalt ions in the impregnation solution changes. The more positive the surface charge, the stronger is the repulsion expected between surface and metal, and the more negative the surface the greater the attraction will be. At low pH's when the solution is strongly acidic, the surface charge is positive. At a certain point or pH range for each support, the surface

experiences a net surface charge of zero. This is called the point of zero charge, or isoelectric point. At pH's above this point the surface bears a net negative charge.

In order to obtain a catalyst that is easily reducible, it is necessary to inhibit attraction between the support and the cobalt ions. On the contrary however, the stronger the metal support interaction, the lower the cobalt agglomeration will be yielding a more dispersed active metal which is also highly favourable. Thus a trade-off exists. Improved reducibility can be achieved by lowering the pH to promote an electronic repulsion between support and the cobalt ions. Thus the effect of the pH of the impregnation solution was investigated by adding the appropriate acid so as not in introduce extra ionic species. The pH of the cobalt nitrate impregnation solution was adjusted with concentrated nitric acid, while the pH of the cobalt acetate impregnation solution was altered with glacial acetic acid.

3.2.4.1 Temperature Programmed Reduction

The reduction behaviour of the catalysts was determined using a 5% H_2 in N_2 gas stream as a reducing agent. The influence of the pH of the impregnation solution on the TPR spectra of the catalysts was investigated. The solution pH for cobalt nitrate prepared catalysts was adjusted using nitric acid, while the pH of the cobalt acetate prepared catalysts was adjusted using glacial acetic acid. The TPR spectra for cobalt nitrate on SiO_2 and MnO following pH adjustment are shown in Figure 3.42, and the TPR spectrum following acetic acid addition to the SiO_2 supported cobalt acetate catalyst can be seen in Figure 3.43. No ZnO supported catalyst was prepared at a lower pH for either metal precursor due to the fact that even small amounts of acid were seen to dissolve the ZnO support making preparation unfeasible. No MnO catalyst was prepared using cobalt acetate as the presence of glacial acetic acid was seen to change the nature of the MnO support material.

The pH of the SiO_2 supported cobalt nitrate catalyst was adjusted to a pH of 1 using nitric acid. Figure 3.42 (A) shows the effect of acid addition on the TPR spectrum of cobalt nitrate on SiO_2. The addition of nitric acid to the impregnation solution had a small effect on the TPR spectrum of cobalt nitrate on SiO_2. The spectrum for Co/1/SiO_2 had a similar profile as the spectrum for Co/SiO_2, with four bands of reduction between 100°C and 1000°C. The first

peak between 200°C and 300°C is attributed to the reduction of Co_3O_4 to CoO. The second broad band is a result of CoO reduction to zerovalent cobalt. The two high temperature reduction regions are due to the reduction of hydrosilicate and cobalt silicate species respectively. The addition of nitric acid flattened the second peak associated with CoO reduction. Another effect associated with the acid addition was the enhancement of the cobalt silicate peak with a peak maximum at 860°C. Thus the addition of acid increased the formation of cobalt silicates slightly at the expense of supported Co_3O_4. In terms of the surface charge, acid addition should induce a net positive charge on the surface, lessening the interaction between the support surface and the positively charged cobalt ions in the impregnation solution, however the opposite was observed. A possible reason for this is that the SiO_2 support may become slightly soluble in the acidic solution. In the strong acidic medium, the surface becomes less well defined allowing incorporation of cobalt ions deep into the SiO_2 support structure. This incorporation would account for the increased cobalt silicate formation. Table 3.19 shows the hydrogen to cobalt molar ratios obtained during the TPR runs. The total ratio was far higher for Co/SiO_2 at 1.346 than for the nitric acid catalyst $Co/1/SiO_2$, which gave a total ratio of 1.280. The smaller ratio indicates that more cobalt is supported as divalent cobalt at the lower pH of impregnation.

The influence of nitric acid addition on the MnO supported cobalt nitrate prepared catalyst can be seen in Figure 3.42 (B). The lower pH is expected to increase the ease of reducibility of the cobalt on the support by decreasing the interaction between support and cobalt ions during impregnation. This decreased interaction is expected due to the net positive charge of the support at lower pH's resulting in repulsion between surface and Co^{2+} ions. The Co(4)/MnO catalyst was impregnated at a pH of 4 following nitric acid addition to the impregnation solution. The TPR spectra for Co/MnO and Co/4/MnO showed reduction profiles. The reduction spectrum for Co/MnO consisted of two large peaks between 150°C and 450°C, as well as a broad shoulder from 450°C to 820°C. Table 3.19 showed that the total hydrogen to cobalt molar ratio increased from 3.361 to 3.684. This increase was not isolated to one peak, but was seen to occur at every reduction step. Consequently the hydrogen to cobalt molar ratio below 400°C increased from 1.968 to 2.226. The hydrogen consumption during this reduction was too high to have resulted from cobalt reduction alone, but was due in part to the reduction of the oxidised support material. The two peaks were attributed to either the two step reduction pathway of Co_3O_4 to metallic cobalt, or to the

reduction of divalent cobalt as well as reduction of the MnO support. The only way the two peaks could result from Co_3O_4 reduction would be if this reduction was superimposed over reduction of the oxidised MnO support. It is more likely that the first peak results from the reduction of cobalt oxide, with the second peak attributable to the reduction of the MnO support. The broad shoulder resulted from the interaction between cobalt and support, as well as the reduction of the oxidised MnO support material.

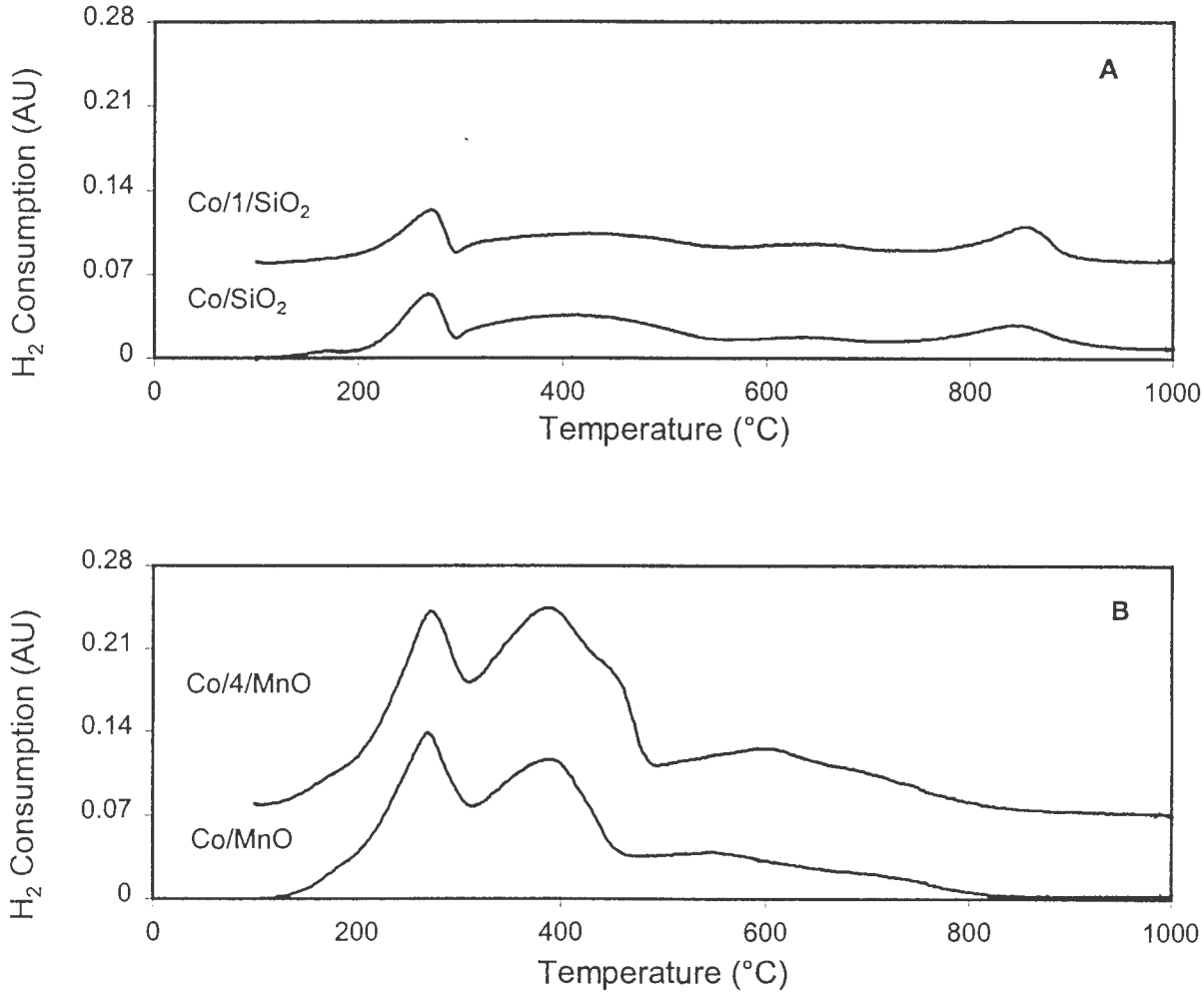

Figure 3.42. Effect of the pH of the impregnation solution on supported cobalt nitrate reducibility for (A) $Co/1/SiO_2$ and (B) Co/4/MnO.
(m_{cat} ~ 0.15g, heating rate = 10°C/min, reducing gas = 60(NTP)ml/min 5% H_2 in N_2,)

The second peak shows a high temperature shoulder. The numerous stages of reduction observed may result from oxidation of MnO to several oxidation states during preparation and calcination. During preparation, the nitric acid is known to oxidise the support resulting in a reduction peak as illustrated in Figure 3.4. As no nitric acid was added to the Co/MnO catalyst and enhanced hydrogen consumption was observed, the decomposition of the precursor must oxidise the MnO support as well. These two factors may oxidise the MnO to different extents, resulting in at least two higher oxidation states of MnO, possibly Mn_2O_3 and MnO_2. As a result the TPR spectrum for Co/4/MnO shows hydrogen consumption associated with this oxidation as the manganese shifts back to its oxidation state.

Table 3.19. Effect of the addition of acid to the impregnation solution on hydrogen consumption during TPR for Co/1/SiO_2, Co/4/MnO and Co(A)/4/SiO_2.

Support	Precursor	pH	H_2:Co_{Total}	H_2:$Co_{<400°C}$
SiO_2	Nitrate	5.8	1.346	0.457
	Nitrate	1	1.280	0.435
SiO_2	Acetate	6.5	1.021	0.109
	Acetate	4	1.141	0.232
MnO	Nitrate	6.2	3.361	1.968
	Nitrate	4	3.684	2.226

The effect of acetic acid addition to the impregnation solution was investigated on the SiO_2 supported cobalt acetate catalyst, Co(A)/SiO_2. Glacial acetic acid was added adjusting the pH to 4. The aim of the acid addition was to reduce the strong electronic interaction between the negatively charge support and the Co^{2+} ions in solution. Figure 3.1 indicated that the net surface charge on the SiO_2 support was approximately zero at a pH of 4 as opposed to strongly negative at a pH of 6.5. Figure 3.43 shows the effect of acetic acid addition to the impregnation solution on the reducibility of cobalt acetate supported on SiO_2. The TPR spectrum for Co(A)/SiO_2 was characterised by the presence of a low temperature peak with a maximum at 400°C, and a high temperature cobalt silicate peak with a maximum at a temperature of 790°C. The addition of acid resulted in the spectrum for Co(A)/4/SiO_2.

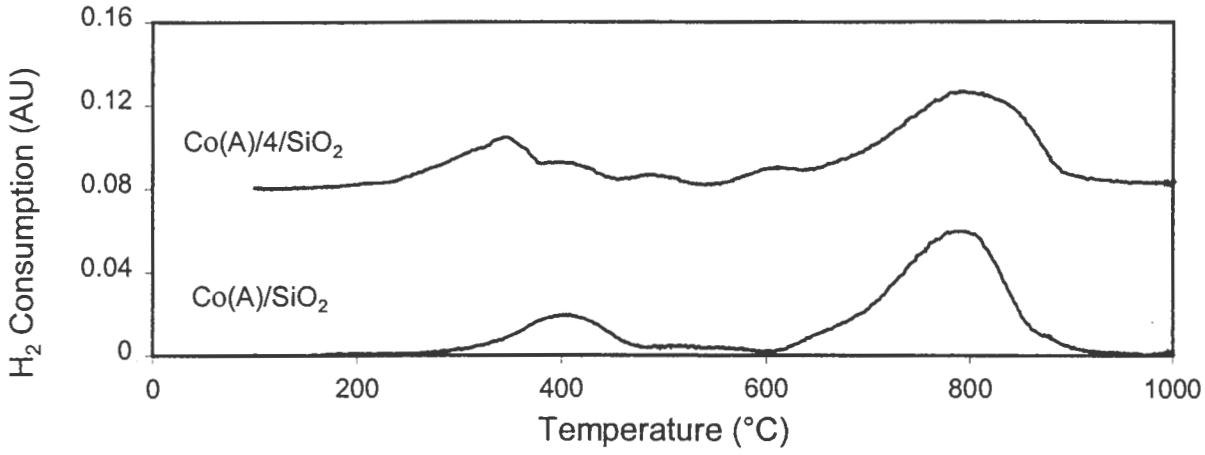

Figure 3.43. Effect of the pH of the impregnation solution on supported cobalt acetate reducibility for Co(A)/4/SiO_2.
(m_{cat} ~ 0.15g, heating rate = 10°C/min, reducing gas = 60(NTP)ml/min 5% H_2 in N_2,)

3.2.4.1.1 Extent of Supported Cobalt Reduction

Figure 3.44 illustrates two TPR spectra for the catalyst formed through acid addition to the impregnation solution. Figure 3.44 (A) and (B) correspond to acid addition for cobalt nitrate and cobalt acetate impregnation on SiO_2 respectively, while (C) refers to nitric acid addition during cobalt acetate impregnation on MnO. The first spectrum entitles 'calcined' corresponds to the pretreatment consisting of a calcination step of 1 hour in N_2 at 400°C to decompose the precursor. The second spectrum entitled 'reduced' illustrates the TPR profile following activation of the catalyst by reduction in a 5% H_2 in N_2 gas mixture. The reduction pretreatment was the same applied to the catalyst as an activation procedure prior to loading into the reactor for Fischer-Tropsch synthesis. By comparison of the two spectra, information on the extent of reducibility of cobalt supported on SiO_2 (A), ZnO (B) and MnO (C) was obtained after lowering the pH of impregnation solution. The presence of acetic acid caused the low temperature peak to shift to a lower temperature with a maximum at 370°C. The formation of reducible species between 450°C and 600°C resulted from the addition of acetic acid. The increased ease of reducibility experienced for the Co(A)/4/SiO_2 catalyst was expected due to the decreased interaction between the SiO_2 surface and cobalt ions as a result of a net neutral charge on the support surface.

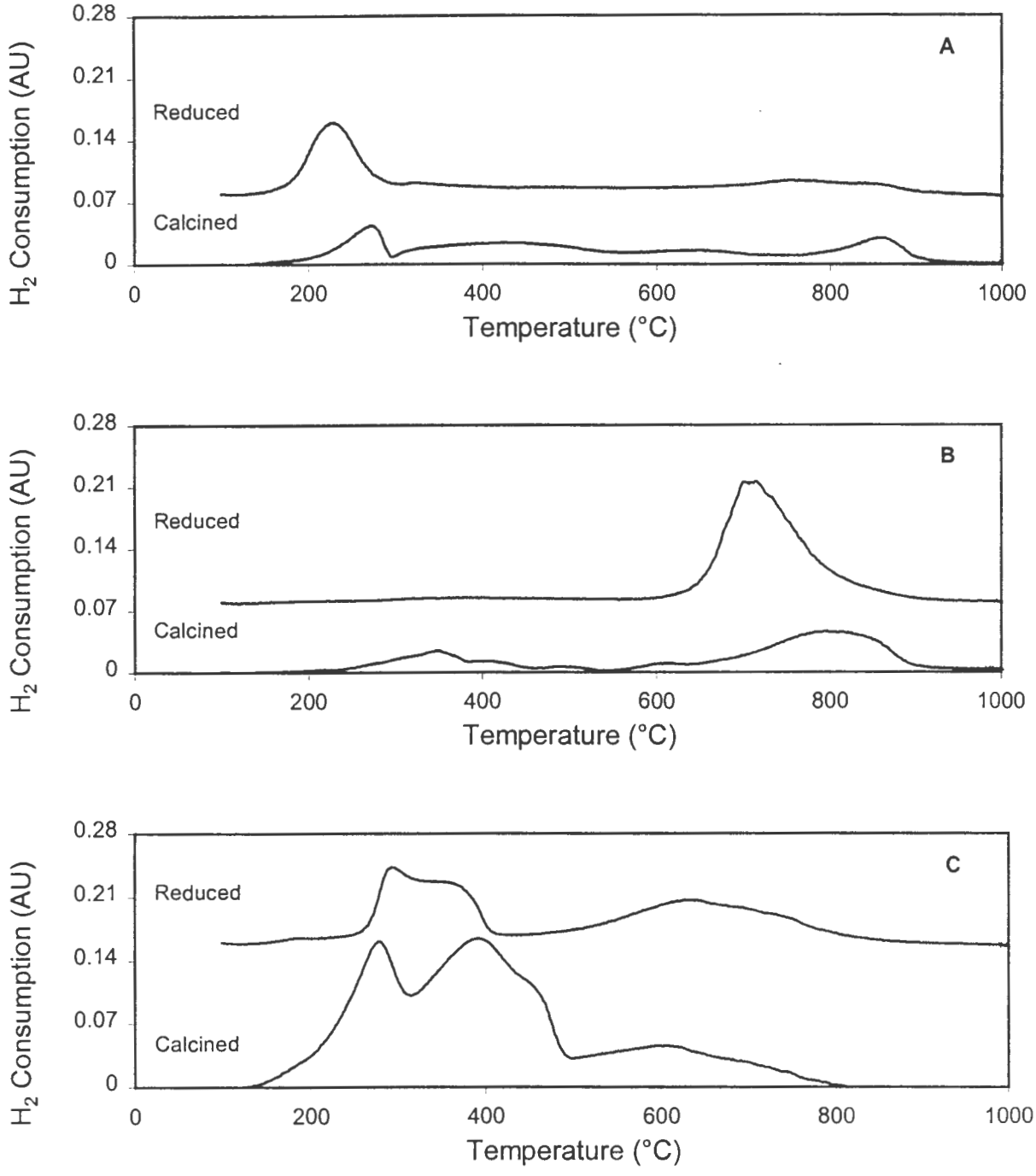

Figure 3.44. Evaluation of the extent of reduction of supported cobalt after reduction at 400°C for 16 hours for (A) Co/1/SiO_2, (B) Co(A)/4/SiO_2 and (C) Co/4/MnO. (m_{cat} ~ 0.15g, heating rate = 10°C/min, reducing gas = 60(NTP)ml/min 5% H_2 in N_2,)

The acid addition was accompanied by an increased total hydrogen to cobalt molar ratio as seen in Table 3.20. The total ratio increased from 1.021 for $Co(A)/SiO_2$ to 1.141 for $Co(A)/4/SiO_2$, while the ratio for reduction below 400°C increased from 0.109 for $Co(A)/SiO_2$ to 0.232 for $Co(A)/4/SiO_2$. Consequently the presence of acetic acid lowered the pH of the impregnation solution resulting in a small decrease in interaction between support and cobalt. The net result was an increased formation of Co_3O_4 on the support, as the overall hydrogen to cobalt molar ratio increased. Reduction at 400°C had a marked effect upon the TPR spectrum obtained for all three catalysts. The hydrogen consumption for the reduced $Co/1/SiO_2$ catalyst resulted predominantly from surface reoxidation of the exposed cobalt metal atoms on the support. The remaining consumption took place in a broad high temperature peak (>600°C). The cobalt responsible for this reduction region was present on the SiO_2 support as cobalt silicate, a specie whose formation dramatically inhibits the extent of reduction obtained for cobalt supported on SiO_2. The calculated extent of reduction for the $Co/1/SiO_2$ catalyst was 58.8%.

Table 3.20. TPR hydrogen consumption data for evaluation of the extent of reduction of supported cobalt for $Co/1/SiO_2$, $Co(A)/4/SiO_2$ and Co/4/MnO.
(mass cat ~ 0.15g, heating rate = 10°C/min, Reducing gas = 60ml(STP)/min 5% H_2 in N_2)

Catalyst	Pretreatment	H_2:Co Total	H_2:Co <400°C	Extent of Reduction (%)
$Co/1/SiO_2$	Calcination	1.280	0.435	58.8
	Reduction	1.001	0.588	
$Co(A)/4/SiO_2$	Calcination	1.141	0.232	1.6
	Reduction	1.129	0.018	
Co/4/MnO	Calcination	3.684	2.226	21.1
	Reduction	1.696	0.789	

Figure 3.44 (B) indicates that reduction of the $Co(A)/4/SiO_2$ for 16 hours at 400°C has resulted in the elimination of all cobalt species reducible below 400°C. The reduced TPR run contained a single high temperature peak characteristic of extensive cobalt silicate formation. Consequently very little of the cobalt was present on the surface as zerovalent metal, yielding

an extent of reducibility of 1.6%.

Reduction of Co/4/MnO at 400°C resulted in a TPR spectrum with a double humped low temperature peak complete by 400°C, as well as a broad hydrogen consumption band present in the calcined TPR spectrum as well from 430°C to 800°C. The high temperature region was attributed to the reduction of cobalt interacting with the MnO support, as well as reduction of the support. The low temperature reduction results from surface reoxidation of cobalt. The extent of reduction was calculated to be 21.1%.

3.2.4.2 Hydrogen Chemisorption

Table 3.21 shows the results obtained from the hydrogen chemisorption measurements performed on the Co/1/SiO_2, Co(A)4/SiO_2 and Co/4/MnO catalysts prepared by nitric or acetic acid addition.. The Co/1/SiO_2 catalyst had a exposed metal surface area of 2.50 m^2/g compared to 3.18 m^2/g obtained for the base case Co/SiO_2 catalyst. Thus the addition of acid decreased the metal surface area of the catalyst. The addition of acid lowered the extent of reduction of supported cobalt from 80.3% for Co/SiO_2 to 58.8% for Co/1/SiO_2. The combination of surface area and extent of reduction resulted in a slightly higher dispersion and smaller cobalt crystallite sizes following preparation in nitric acid. The reversibility dropped from 65.8% to 56.1% with nitric acid addition to the impregnation solution.

No meaningful results were obtained for the Co(A)/4/SiO_2 catalyst prepared by acetic acid addition during cobalt acetate impregnation on SiO_2.

Nitric acid addition during cobalt nitrate impregnation on MnO yielded the Co/4/MnO catalyst. The acid addition improved the extent of reduction of the supported cobalt, leading to an improved metal surface area. The lower acid addition also increased the cobalt dispersion from 2.06% to 5.60%, while decreasing the cobalt crystallite size from 46.6 nm to 17.2 nm.

Table 3.21. Surface area, dispersion, particle diameter and hydrogen adsorption reversibility for Co/1/SiO_2, Co(A)/4/SiO_2 and Co/4/MnO.

Catalyst	Surface Area (m^2/g)	Dispersion (%)	Crystallite Size (nm)	Reversibility (%)
Co/1/SiO_2	2.50	7.15	13.5	56.1
Co(A)/4/SiO_2	-	-	-	-
Co/4/MnO	0.70	5.60	17.2	47.3

3.2.4.3 Transmission Electron Microscopy

The pH of the solution did not have any noticeable effect on the physical properties of the three catalysts prepared. For this reason, these photographs have been placed in Appendix IV for perusal.

3.2.4.4 Fischer Tropsch Synthesis

The effect of the change in pH through acid addition during preparation of the catalysts was tested under Fischer Tropsch conditions in order to obtain activity and selectivity data necessary for performance characterisation. The synthesis was carried out at a temperature of 200°C and a pressure of 5 bar. The activity was measured in terms of the hydrocarbon yields obtained from the gas chromatograph analysis of the organic products.

3.2.4.4.1 SiO_2 as a Support

The effect of the pH of the impregnation solution was studied by lowering the impregnation pH of the cobalt nitrate and cobalt acetate prepared SiO_2 catalysts with nitric acid and acetic acid respectively.

3.2.4.4.1.1 The Effect of Nitric Acid Addition

The change of pH during impregnation had a minor effect on the performance of the SiO_2 supported catalyst under Fischer-Tropsch synthesis conditions. The yield of total organic product dropped from 5.67% to 5.41% when the pH of the final impregnation solution was changed from 5.8 to 1. Table 3.22 also shows the rate per square metre of exposed cobalt on the surface. The Co/1/SiO_2 catalyst gave a higher rate of 4.65×10^{-3} mmol/m^2_{Co}/min compared to a rate of 4.12×10^{-3} mmol/m^2_{Co}/min over Co/SiO_2. These rates corresponded to dispersions of 7.15% and 6.66%. Iglesia [1997] stated that the turnover rate was not a function of cobalt dispersion. This seems to hold true on SiO_2 following nitric acid addition as the dispersion increased in proportion to the increase in rate per exposed cobalt area. In terms of yield, the Co/SiO_2 catalyst was only slightly more active than the Co/1/SiO_2 catalyst. This result corresponds to the amount of exposed cobalt on each catalyst as well as the hydrogen adsorption reversibility.

Table 3.22. Effect of the pH of impregnation solution on the activity and selectivity of cobalt nitrate on SiO_2.
(m_{cat} ~ 1g, T = 200°C, P = 5 bar, H_2 : CO = 2 : 1, WHSV = 0.34g_{CO}/g_{cat}.hr)

Catalyst	Co/SiO_2	Co/1/SiO_2
Reaction Time	14 hr 50	16 hr 34
Yield of volatile organics (%)	5.67	5.41
S_{C1+C2} (carbon%)	14.97	18.87
α_{C4-C11}	0.78	0.78
r_{HC} .10^3 (mmol/m^2_{Co}/min)	4.12	4.65
C_5 Composition (%)		
3-methyl-1-butene	0.60	0.42
2-methyl-butane	0.84	0.66
1-pentene	56.31	60.45
2-methyl-1-butene	0.00	0.07
n-pentane	28.26	28.87
trans-2-pentene	8.23	5.26
cis-2-pentene	5.61	4.09
2-methyl-2-butene	0.15	0.18

The selectivity to the C_{1+2} fraction on a carbon percent basis was higher for $Co/1/SiO_2$ compared to the Co/SiO_2 catalyst, rising from 14.97% to 18.87%.

The C_5 compositions for the Co/SiO_2 and $Co/1/SiO_2$ catalysts show small differences. The branched fraction were similar at 1.59% for Co/SiO_2 and 1.24% for $Co/1/SiO_2$. The most notable feature of the $Co/1/SiO_2$ catalyst is the marginally higher fraction of the primary reaction product, the α-olefin, formed. For the acid prepared catalyst, the α-olefin comprised 60.45% of the C_5 fraction as opposed to 56.31% for the Co/SiO_2 catalyst. The lower α-olefin percent over Co/SiO_2 resulted from increased secondary reaction to linear β-olefins and branched paraffins and olefins. The n-paraffin content of both catalysts were the same.

The chain growth probabilities were calculated from the slope of the Anderson-Schulz-Flory (ASF) distribution illustrated in Figure 3.45 for both catalysts. The slopes were parallel, yielding chain growth probabilities, α, of 0.78 for both Co/SiO_2 and $Co/1/SiO_2$ respectively. Thus the change in pH seemed to have no effect on the termination rate of the growing chain. Deviation in the ASF plots occurred for products larger than the C_{11} fraction. The growth probability of the $Co/1/SiO_2$ catalyst dropped off dramatically from the C_{12} fraction onwards. The chain growth probability for Co/SiO_2 rose slightly above one at C_{15} due to wax trap bleeding.

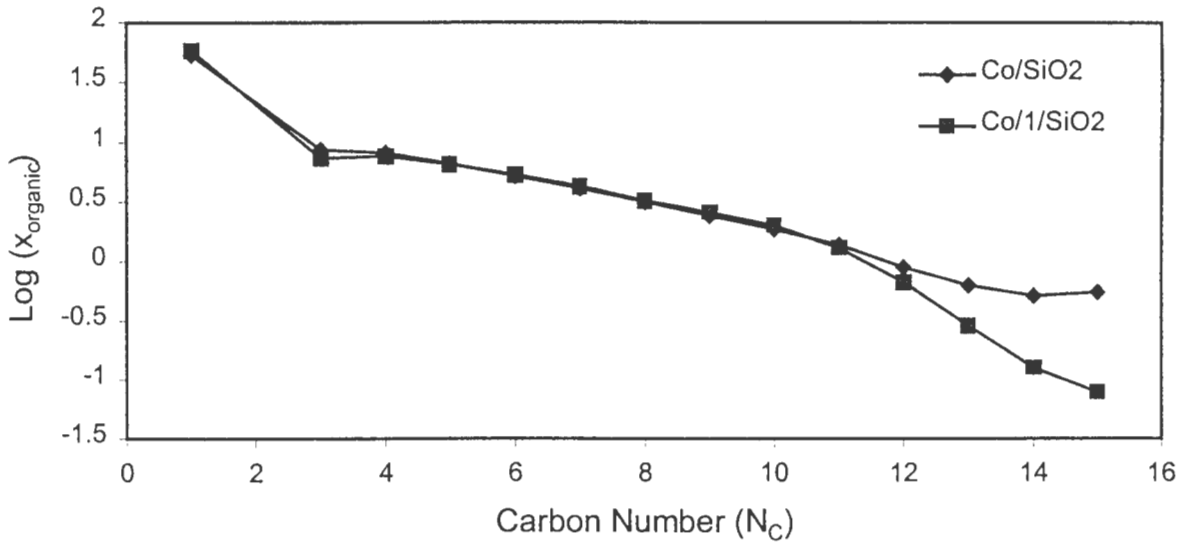

Figure 3.45. Effect of the pH of impregnation solution on the Anderson-Schulz-Flory distribution for cobalt nitrate on SiO_2.
(m_{cat} ~ 1g, T = 200°C, P = 5 bar, H_2 : CO = 2 : 1, WHSV = 0.34g_{CO}/g_{cat}.hr)

Figure 3.46 shows the rate of formation of the total organic product for the Co/SiO_2 and $Co/1/SiO_2$ catalysts. The rate was calculated according to the procedure presented in Appendix III. The rates are given on a per gram of catalyst basis, allowing direct comparison. The rate of formation is a measure of the activity of the catalyst, thus the rate parallels the yield measurements from Table 3.22. Figure 3.46 shows that as the carbon number increases for each catalyst, the rate of formation decreases. The polymerisation behaviour of the Fischer-Tropsch reaction results in long hydrocarbon chains via a growing alkyl chain on the catalyst. Consequently as the carbon number increases the rate of formation of each successively higher carbon number fraction decreases as illustrated. The only difference in the rate of formation between the catalysts was seen in the C_1 and C_2 fraction which were grouped as C_1, where the Co/SiO_2 catalyst showed a higher formation rate.

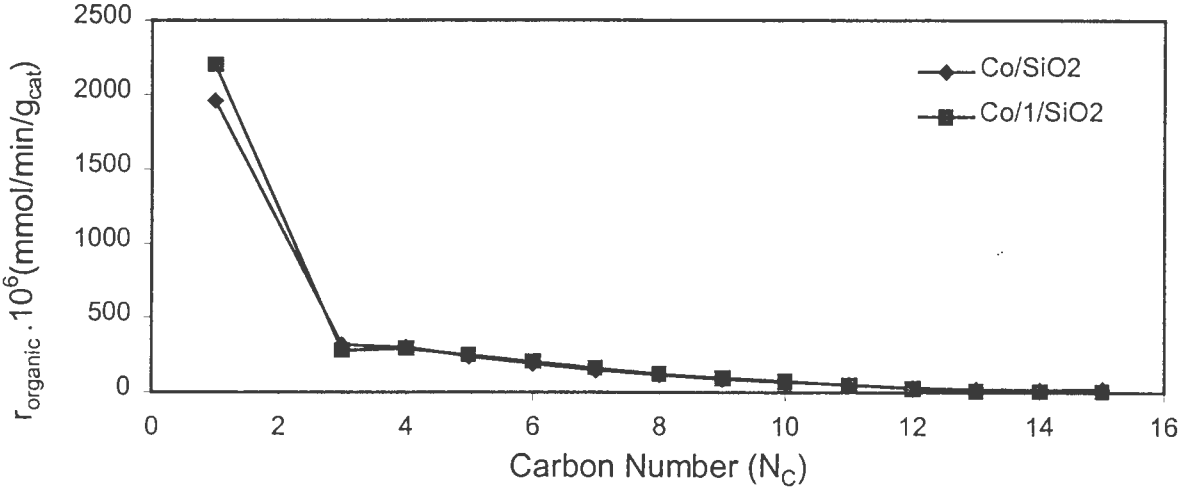

Figure 3.46. Effect of the pH of impregnation on the total organic formation rate for cobalt nitrate on SiO_2.
(m_{cat} ~ 1g, T = 200°C, P = 5 bar, H_2 : CO = 2 : 1, WHSV = 0.34g_{CO}/g_{cat}.hr)

The olefinicity of the linear organic product is shown in Figure 3.47 for the Co/SiO_2 and $Co/1/SiO_2$ catalysts. The total linear olefin fraction was made up from the α-olefin content and the β-olefin content of the C_5 fraction. The selectivity to linear olefins of the two catalysts were similar for the full range of carbon numbers, indicating similar growth probabilities as the profiles in Figure 3.47 were approximately parallel. In Table 3.22 the C_5 product breakdown was given for each catalyst. The linear olefin fractions were 70.15% and

69.80% for the Co/SiO_2 and $Co/1/SiO_2$ catalysts respectively. The linear olefin fraction was consistently higher for Co/SiO_2 up to the C_{10} fraction, above which, the linear olefin fraction of the $Co/1/SiO_2$ catalyst was higher but only marginally so.

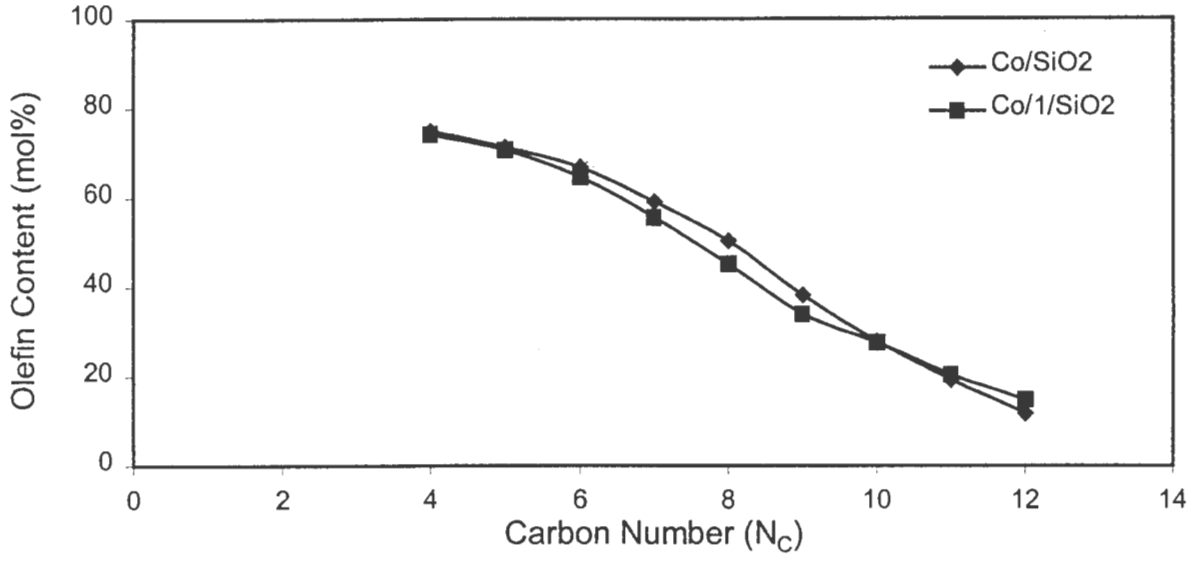

Figure 3.47. Effect of the pH of impregnation solution on the olefin fraction of the linear organic product for cobalt nitrate on SiO_2.
(m_{cat} ~ 1g, T = 200°C, P = 5 bar, H_2 : CO = 2 : 1, WHSV = 0.34g_{CO}/g_{cat}.hr)

Table 3.22 shows the breakdown of the total linear olefin content of the C_5 fraction for Co/SiO_2 and $Co/1/SiO_2$ respectively. The total linear olefin content is split up between the α-olefin content and the β-olefin content. The β-olefin fraction is made up of the cis and trans 2-pentene products. The α-olefin fraction of the linear olefins is illustrated in Figure 3.48 for Co/SiO_2 and $Co/1/SiO_2$. The α-olefin fraction of the total organic product was 60.45% for the $Co/1/SiO_2$ catalyst, and 56.31% for the Co/SiO_2 catalyst. This meant that the α-olefin made up 86.60% and 80.27% of the linear olefin product over $Co/1/SiO_2$ and Co/SiO_2 respectively. The α-olefinicity of the linear olefin product formed over the $Co/1/SiO_2$ catalyst is higher than the Co/SiO_2 catalyst for the complete carbon number range. The largest difference occurs from the C_7 to C_9 fractions where the difference is approximately 16%. The difference in the overall linear olefin fraction of the linear organic product for the two catalysts was only 4% for the same carbon number range. This indicates that the acid addition during

impregnation alters the catalyst surface resulting in a decreased rate of secondary reaction resulting in less branched product and less secondary linear olefins. The β-olefin content of the C_5 fraction dropped from 13.84% for Co/SiO_2 to 9.35% for the $Co/1/SiO_2$ catalyst.

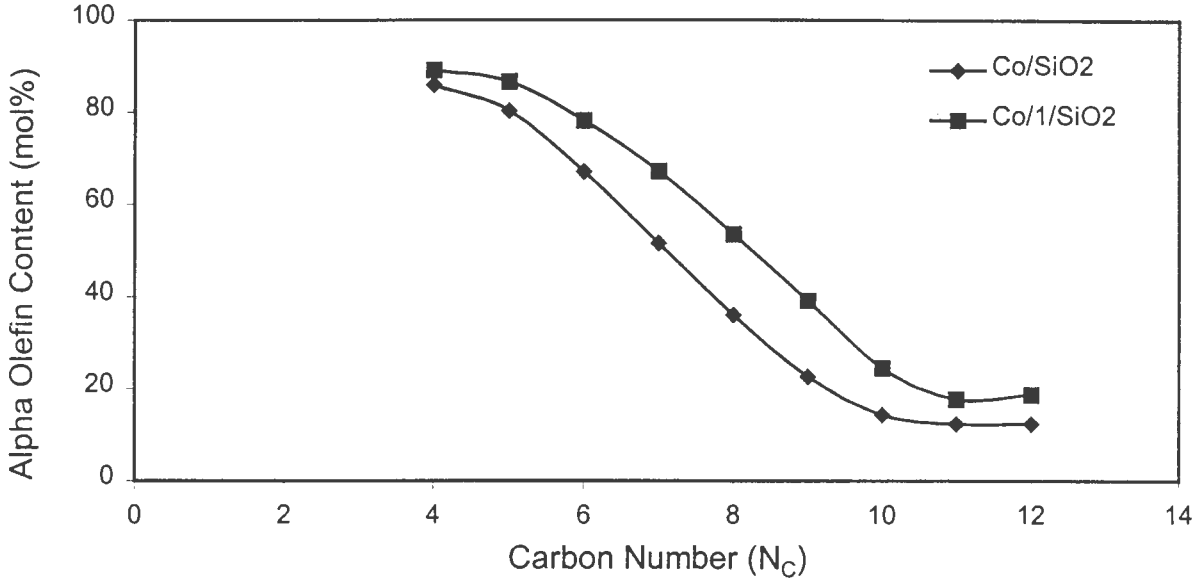

Figure 3.48. Effect of the pH of impregnation solution on the α-olefin fraction of the linear olefins for cobalt nitrate on SiO_2.
(m_{cat} ~ 1g, T = 200°C, P = 5 bar, H_2 : CO = 2 : 1, WHSV = 0.34g_{CO}/g_{cat}.hr)

3.2.4.4.1.2 The Effect of Acetic Acid Addition

Glacial acetic acid was used to lower the pH of the impregnation solution for the preparation of cobalt acetate on SiO_2. As acetic acid is a weak acid, the lowest achievable pH was 4. The catalyst prepared in the presence of acetic acid was named $Co(A)/4/SiO_2$.

The change of pH during impregnation had a major effect on the performance of the SiO_2 supported catalyst under Fischer-Tropsch synthesis conditions. Table 3.23 gives information on the yield, C_{1+2} selectivity, the chain growth probability and the product breakdown of the C_5 fraction for the $Co(A)/SiO_2$ and $Co(A)/4/SiO_2$ catalysts. The yield of total organic product increased from 0.24% to 0.46% when the pH of the final impregnation solution was changed from 6.5 to 4. Thus the $Co(A)/4/SiO_2$ catalyst was more than twice as active as the

$Co(A)/SiO_2$ catalyst. This result is in agreement with the TPR findings, where the $Co(A)/4/SiO_2$ catalyst had a higher hydrogen to cobalt molar ratios for reduction below 400°C than the $Co(A)/SiO_2$, resulting in a larger fraction of cobalt on the surface in the active zerovalent form. As no chemisorption data was obtained for $Co(A)/4/SiO_2$, no comparisons between metal surface area, dispersion or rate per exposed cobalt area could be made.

Table 3.23. Effect of the pH of impregnation solution on the activity and selectivity of cobalt acetate on SiO_2.
(m_{cat} ~ 1g, T = 200°C, P = 5 bar, H_2 : CO = 2 : 1, WHSV = 0.34g_{CO}/g_{cat}.hr)

Catalyst	$Co(A)/SiO_2$	$Co(A)/4/SiO_2$
Reaction Time	13 hr 31	23 hr 40
Yield of volatile organics (%)	0.24	0.46
S_{C1+C2} (carbon%)	63.98	35.70
α_{C4-C11}	0.75	0.84
$r_{HC} .10^3$ (mmol/m^2_{Co}/min)	4.52	-
C_5 Composition (%)		
3-methyl-1-butene	0.28	0.26
2-methyl-butane	0.40	0.45
1-pentene	36.19	41.27
2-methyl-1-butene	0.00	0.00
n-pentane	32.34	32.36
trans-2-pentene	16.88	14.87
cis-2-pentene	10.91	9.28
2-methyl-2-butene	3.00	1.51

The C_{1+2} selectivity on a carbon percent basis dropped dramatically from 63.98% to 35.70% as a result of the lower impregnation pH. The C_5 compositions for the $Co(A)/SiO_2$ and $Co(A)/4/SiO_2$ catalysts show small differences. The branched fraction were decreased upon acid addition from 3.68% for $Co(A)/SiO_2$ to 2.22% for $Co(A)/4/SiO_2$. The C_5 α-olefin content of $Co(A)/4/SiO_2$ was marginally higher at 41.27% as opposed to 36.19% for the $Co(A)/SiO_2$ catalyst. The higher α-olefin percent over $Co(A)/4/SiO_2$ coincided with a decrease in secondary reactions to linear β-olefins and branched paraffins and olefins. The n-

paraffin content of both catalysts were the same, indicating comparative hydrogenation activities.

The chain growth probabilities were calculated from the slope of the Anderson-Schulz-Flory (ASF) distribution illustrated in Figure 3.49 for both catalysts. The product spectrum of the Co(A)/4/SiO_2 catalyst gave a product with a higher largest carbon number. The Co(A)/SiO_2 catalyst showed such poor activity that the product spectrum could only be analysed up to the C_9 fraction. The slopes of the ASF plots differed considerably yielding chain growth probabilities, α, of 0.75 and 0.84 for Co(A)/SiO_2 and Co(A)/4/SiO_2 respectively. Thus the change in pH seemed to have a dramatic effect on the termination rate of the growing chain. This was probably more a result of the poor activity of the Co(A)/SiO_2 catalyst than a defining characteristic of acid addition.

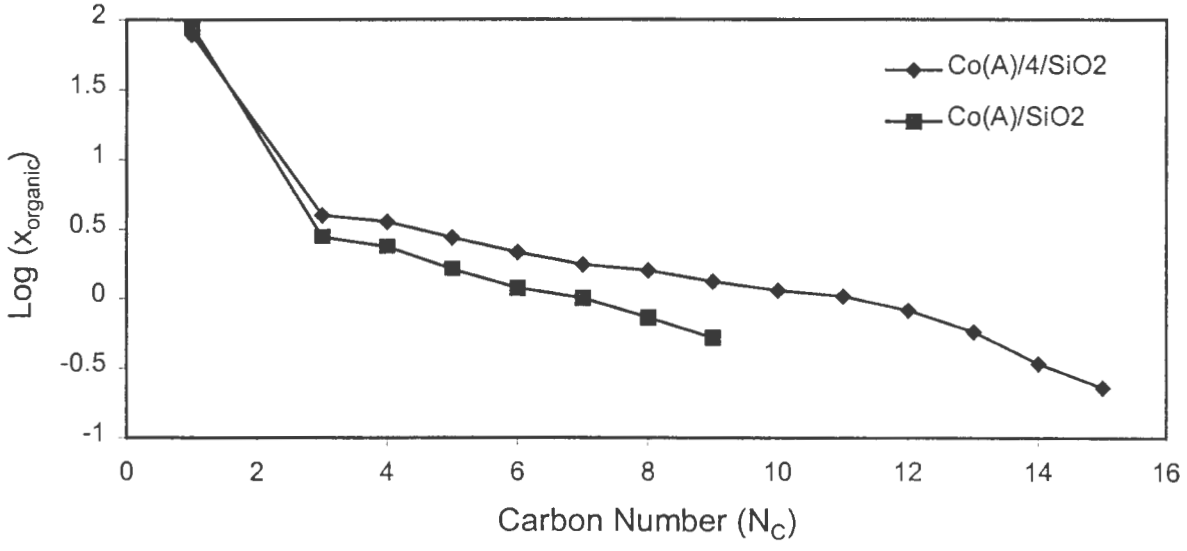

Figure 3.49. Effect of the pH of impregnation solution on the Anderson-Schulz-Flory distribution for cobalt acetate on SiO_2.
(m_{cat} ~ 1g, T = 200°C, P = 5 bar, H_2 : CO = 2 : 1, WHSV = 0.34g_{CO}/g_{cat}.hr)

Figure 3.50 shows the rate of formation of the total organic product for the Co/SiO_2 and Co/1/SiO_2 catalysts.. The rate was calculated according to the procedure presented in Appendix III. The rates are given on a per gram of catalyst basis, allowing direct comparison. The rate of formation is a measure of the activity of the catalyst, thus the rate parallels the

yield measurements from Table 3.23. Figure 3.50 illustrates the rate of formation as a function of carbon number. The diagram is deceiving as the formation rate of $Co(A)/4/SiO_2$ is almost double that of $Co(A)/SiO_2$, however as organic yields are so small over both catalysts, little definition is visible in Figure 3.50.

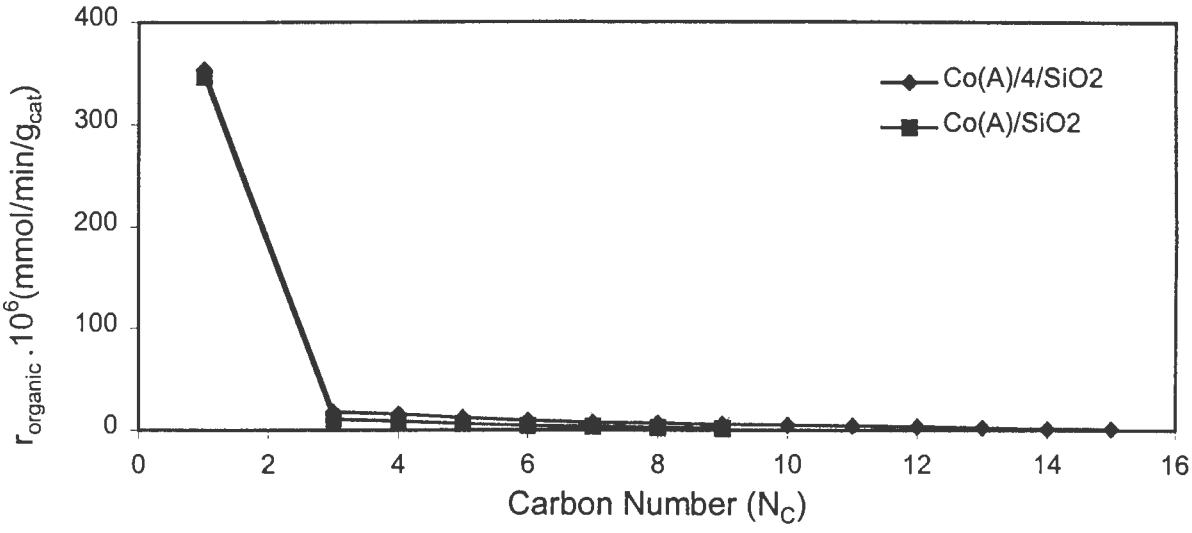

Figure 3.50. Effect of the pH of impregnation solution on the total organic formation rate for cobalt acetate on SiO_2.
(m_{cat} ~ 1g, T = 200°C, P = 5 bar, H_2 : CO = 2 : 1, WHSV = 0.34g_{CO}/g_{cat}.hr)

The olefinicity of the linear organic product is shown in Figure 3.51 for the $Co(A)/SiO_2$ and $Co(A)/4/SiO_2$ catalysts. The total linear olefin fraction was made up from the α-olefin content and the β-olefin content of the C_5 fraction. The selectivity to linear olefins of the two catalysts differed by about 5% with the acid catalyst showing higher olefinicity except in the C_4 and C_5 fractions where they were equal. In Table 3.23 the C_5 product breakdown was given for each catalyst. In the C_5 fraction, the linear olefin fractions comprised 65.42% and 63.98% of the total organic product for the $Co(A)/SiO_2$ and $Co(A)/4/SiO_2$ catalysts respectively.

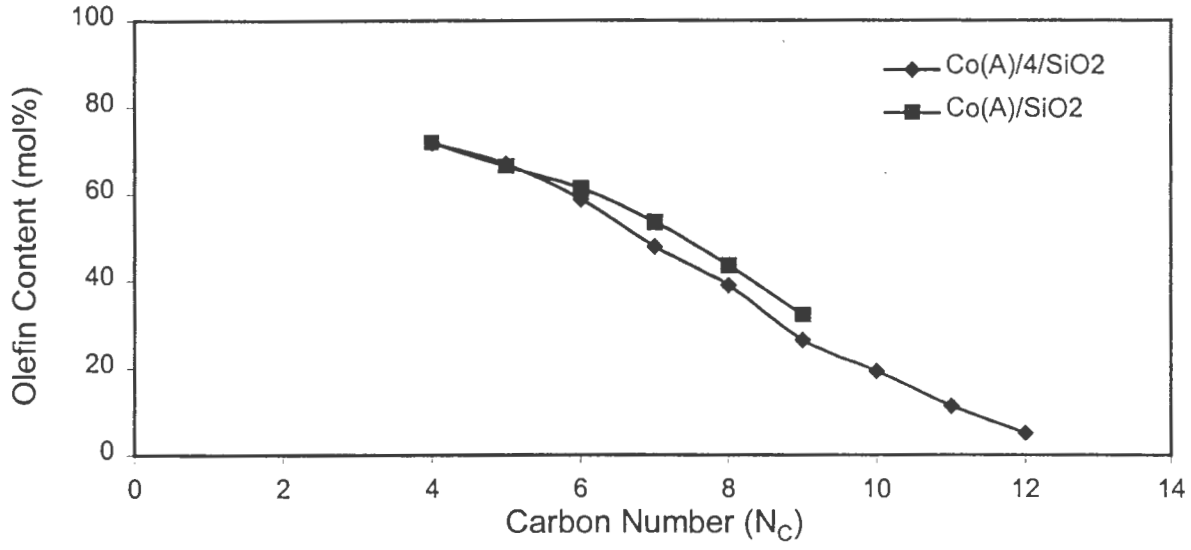

Figure 3.51. Effect of the pH of impregnation solution on the olefin fraction of the linear organic product for cobalt acetate on SiO_2.
(m_{cat} ~ 1g, T = 200°C, P = 5 bar, H_2 : CO = 2 : 1, WHSV = 0.34g_{CO}/g_{cat}.hr)

Table 3.23 shows the breakdown of the total linear olefin content of the C_5 fraction for Co(A)/SiO_2 and Co(A)/4/SiO_2 respectively. The total linear olefin is made up from the α-olefin content and the β-olefin content of the C_5 fraction. The β-olefin fraction is made up of the cis and trans 2-pentene products. The α-olefin fraction of the linear olefins is illustrated in Figure 3.52 for Co(A)/SiO_2 and Co(A)/4/SiO_2. The α-olefin fraction of the total organic product was 41.27% for the Co(A)/4/SiO_2 catalyst, and 36.19% for the Co(A)/SiO_2 catalyst. These percentages translated into 63.08% and 56.56% of the linear olefin product respectively. The α-olefinicity of the linear olefin product formed over the Co(A)/4/SiO_2 catalyst was higher than for the Co(A)/SiO_2 catalyst for the complete carbon number range. However the overall linear olefin content was higher for the Co(A)/SiO_2 catalyst than for the Co(A)/4/SiO_2 catalyst. This indicates that the acid addition during impregnation alters the catalyst surface resulting in a decreased rate of secondary reaction. This results in the formation of less branched products and less secondary linear olefins over the acid prepared catalyst. To illustrate this, the β-olefin content of the C_6 fraction dropped from 39.44% for Co(A)/SiO_2 to 33.03% for the Co(A)/4/SiO_2 catalyst. Lower secondary reaction activity coincided with increased activity. It is possible that the SiO_2 surface promotes secondary

activity, and as the cobalt crystallites become more substantial, the support plays less of a role.

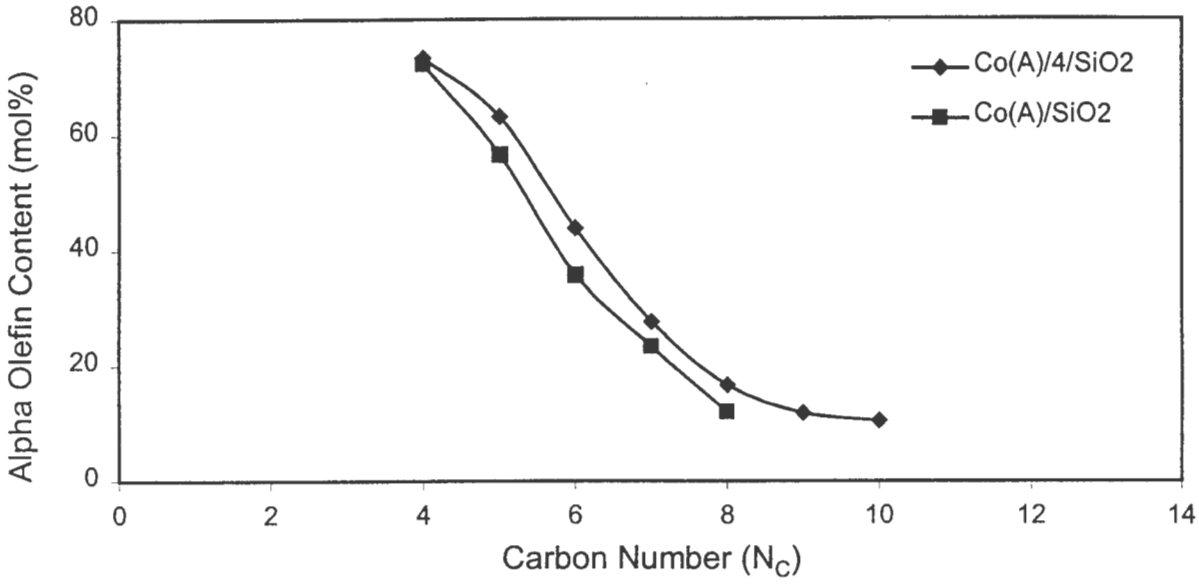

Figure 3.52. Effect of the pH of impregnation on the α-olefin fraction of the linear olefins for cobalt acetate on SiO_2.
(m_{cat} ~ 1g, T = 200°C, P = 5 bar, H_2 : CO = 2 : 1, WHSV = 0.34g_{CO}/g_{cat}.hr)

3.2.4.4.2 MnO as a Support

The change of pH during impregnation had a minor effect on the selectivity of the MnO supported catalyst under Fischer-Tropsch synthesis conditions, but had a marked effect upon the catalyst activity. The catalyst prepared in nitric acid was called Co/4/MnO as the final pH of the impregnation solution was 4. Table 3.24 shows the FT reaction results for Co/4/MnO and Co/MnO. The yield of total organic product increased from 0.18% to 0.46% when the pH of the final impregnation solution was lowered from 7.1 to 4. Thus the Co/4/MnO catalyst was 2.5 times more active than the Co/MnO catalyst. This result is in agreement with the hydrogen chemisorption findings, where the exposed cobalt metal surface area was seen to double from 0.35 m^2/g for Co/MnO to 0.70 m^2/g for Co/4/MnO. The dispersion also increased from 2.06% to 5.60%. These two factors together combine to give a larger fraction

of cobalt on the surface in the active zerovalent form. Although the overall yield increased with acid addition, the rate of carbon monoxide consumption per square metre of exposed cobalt was similar at 1.13×10^{-3} mmol/m^2_{Co}/min and 1.44×10^{-3} mmol/m^2_{Co}/min for Co/MnO and Co/4/MnO respectively. This indicates that the acid has enhanced the amount of exposed cobalt without significantly altering the activity per site, as observed following nitric addition during cobalt nitrate impregnation on SiO_2.

The C_{1+2} selectivity on a carbon percent basis was increased for Co/4/MnO compared to the Co/MnO catalyst, rising from 27.52% to 33.53%.

Table 3.24. Effect of the pH of impregnation solution on the activity and selectivity of cobalt nitrate on MnO.
(m_{cat} ~ 1g, T = 200°C, P = 5 bar, H_2 : CO = 2 : 1, WHSV = 0.34g_{CO}/g_{cat}.hr)

Catalyst	Co/MnO	Co/4/MnO
Reaction Time	22 hr 30	22 hr 25
Yield of volatile organics (%)	0.18	0.46
S_{C1+C2} (carbon%)	27.52	33.53
α_{C4-C11}	0.76	0.76
r_{HC} .10^3 (mmol/m^2_{Co}/min)	1.13	1.44
C_5 Composition (%)		
3-methyl-1-butene	0.80	0.72
2-methyl-butane	1.87	2.36
1-pentene	50.60	52.90
2-methyl-1-butene	0.00	0.00
n-pentane	30.09	32.18
trans-2-pentene	9.76	7.23
cis-2-pentene	6.21	4.33
2-methyl-2-butene	0.67	0.29

The C_5 compositions for the Co/MnO and Co/4/MnO catalysts show small differences. The branched fraction were similar at 3.34% for Co/MnO and 3.37% for Co/4/MnO. The Co/4/MnO catalyst showed increased hydrogenation activity, resulting in a n-paraffin fraction of 32.18%, an increase from the 30.09% of the Co/MnO catalyst. This increased hydrogenation activity was accompanied by slightly increased α-olefin formation and

decreased secondary isomerization of the growing chain to cis and trans 2-pentene. For the acid prepared catalyst, the α-olefin comprised 52.90% of the C_5 fraction as opposed to 50.60% for the Co/MnO catalyst. This difference is negligible.

The chain growth probabilities were calculated from the slope of the Anderson-Schulz-Flory (ASF) distribution illustrated in Figure 3.53 for both the Co/MnO and Co/4/MnO catalysts. The slopes were parallel, yielding chain growth probabilities, α, of 0.76 for both Co/MnO and Co/4/MnO catalysts respectively. Thus the change in pH seemed to have no effect on the termination rate of the growing chain. This was observed over SiO_2 as well. The C_3 fraction for the Co/MnO catalyst was unexpectedly low, a result of an error in gas chromatograph sensitivity.

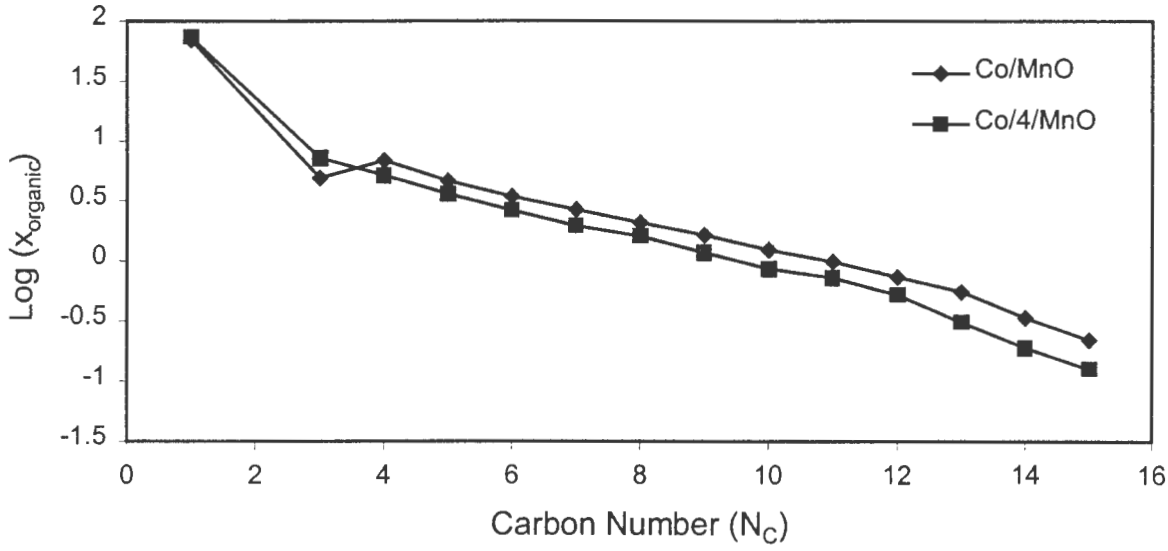

Figure 3.53. Effect of the pH of impregnation solution on the Anderson-Schulz-Flory distribution for cobalt nitrate on MnO.
(m_{cat} ~ 1g, T = 200°C, P = 5 bar, H_2 : CO = 2 : 1, WHSV = 0.34g_{CO}/g_{cat}.hr)

Figure 3.54 shows the rate of formation of the total organic product for the Co/MnO and Co/4/MnO catalysts. The rate was calculated according to the procedure presented in Appendix III. The rates are given on a per gram of catalyst basis, allowing direct comparison. The rate of formation is a measure of the activity of the catalyst, thus the rate parallels the yield measurements from Table 3.24. Figure 3.54 indicates that the lower pH resulted in an

increased formation rate, particularly for the C_{1+2} fraction. This result parallels the exposed metal surface area measurement from hydrogen chemisorption, with increased activity deriving from a greater number of exposed active sites.

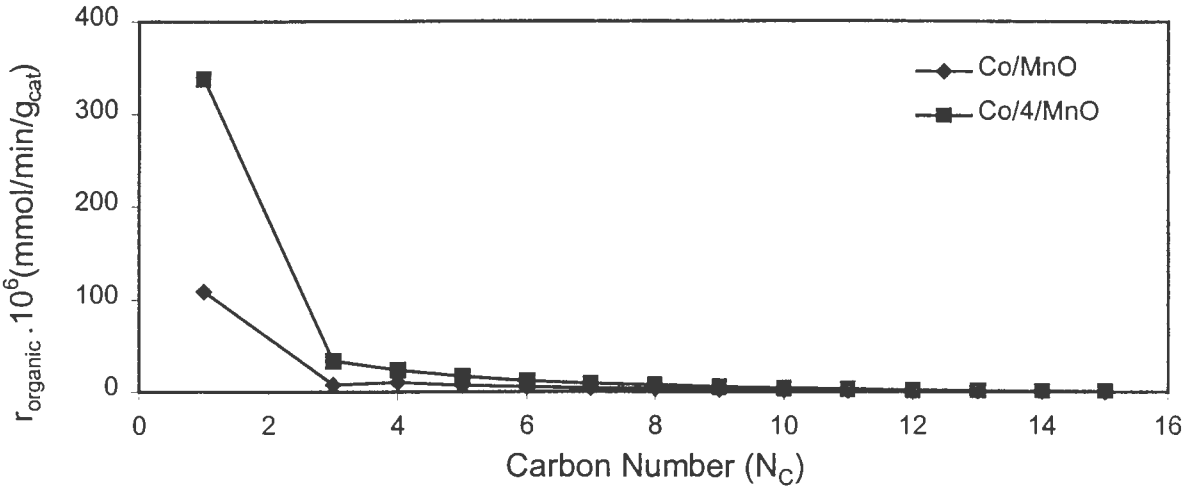

Figure 3.54. Effect of the pH of impregnation solution on the total organic formation rate for cobalt nitrate on MnO.
(m_{cat} ~ 1g, T = 200°C, P = 5 bar, H_2 : CO = 2 : 1, WHSV = 0.34g_{CO}/g_{cat}.hr)

The olefinicity of the linear organic product is shown in Figure 3.55 for the Co/MnO and Co/4/MnO catalysts. The linear olefin product comprised the α– and β–olefin fractions. The selectivity to linear olefins for the two catalysts were similar for the full range of carbon numbers, except for the C_8 fraction, where the linear olefin content was higher. In Table 3.24 the C_5 product breakdown was given for each catalyst. The linear olefin fractions made up 66.57% and 64.46% of the total organic product in the C_5 fraction for the Co/MnO and Co/4/MnO catalysts respectively.

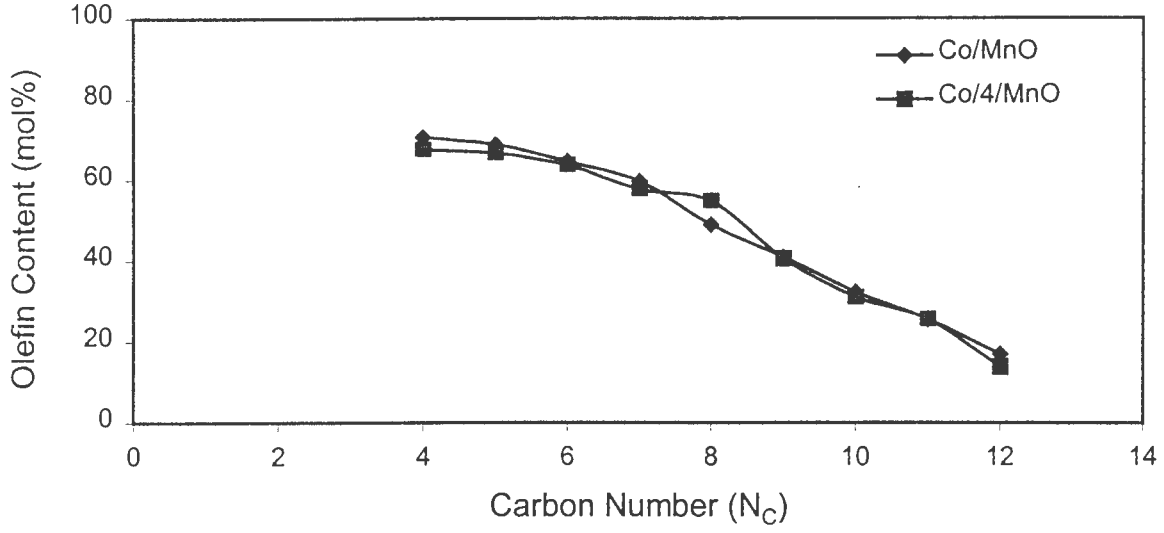

Figure 3.55. Effect of the pH of impregnation solution on the olefin fraction of the linear organic product for cobalt nitrate on MnO.
(m_{cat} ~ 1g, T = 200°C, P = 5 bar, H_2 : CO = 2 : 1, WHSV = 0.34g_{CO}/g_{cat}.hr)

Table 3.24 shows the breakdown of the total linear olefin content of the C_5 fraction for Co/MnO and Co/4/MnO respectively. The total linear olefin content is split up between the α-olefin content and the β-olefin content. The β-olefin fraction is made up of the cis and trans 2-pentene products. The α-olefin fraction of the linear olefins is illustrated in Figure 3.56 for Co/MnO and Co/4/MnO. The α-olefin fraction of the total organic product was 52.90% for the Co/4/MnO catalyst, and 50.60% for the Co/MnO catalyst. The α-olefin fraction made up 82.07% and 76.01% of the linear olefin product formed over the Co/4/MnO and Co/MnO catalysts respectively. The α-olefinicity of the linear olefin product formed over the Co/4/MnO catalyst was higher than that of the Co/MnO catalyst for the complete carbon number range, except for the C_{11} fraction where a switch occurred. The fact that the α-olefin content was higher for the acid treated catalyst while the linear olefin content of the catalyst remained the same for the two catalysts indicates that the addition of acid to the impregnation solution slightly suppressed the secondary isomerization of α-olefins to β-olefins.

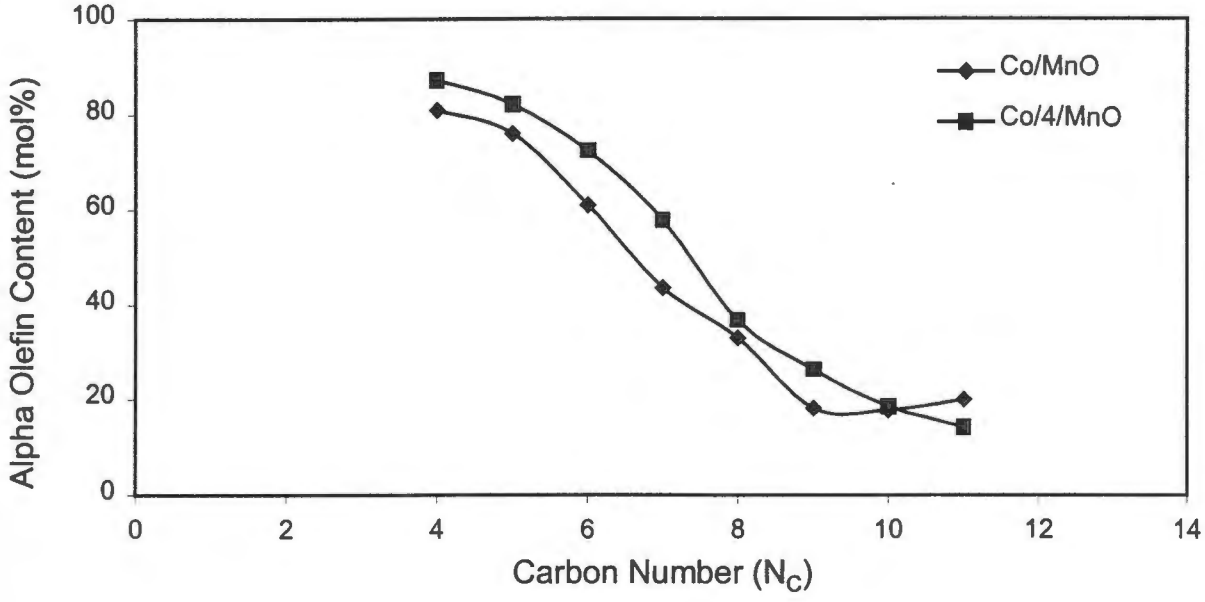

Figure 3.56. Effect of the pH of impregnation solution on the α-olefin fraction of the linear olefins for cobalt nitrate on MnO.
(m_{cat} ~ 1g, T = 200°C, P = 5 bar, H_2 : CO = 2 : 1, WHSV = 0.34g_{CO}/g_{cat}.hr)

3.2.5 Effect of the Contact Time between Solution and Support

Inorganic oxides are known to take a long time to reach charge equilibrium when placed in solution. The presence of functional groups on the support surface leads to charge imbalances between the support and the solution. These imbalances are rectified by the adsorption of either positive or negative ions from the solution onto the support. Consequently the pH of the impregnation solution varies as contact time between the support and the solution is increased. This trend is illustrated in Table 3.1, where the pH of the impregnation solution was seen to vary significantly from the initial impregnation to two days later when drying was done. This change in pH coincides with an alteration in the net charge on the support surface as the support takes up Co^{2+} ions and nitrate/acetate ions from solution. The net surface charge plays an important role in determining the strength of interaction between the support and cobalt ions. Table 3.1 showed that the initial pH of the impregnation solution to be lower than the final pH of impregnation indicating that the solution is becoming increasingly basic. As the solution becomes more basic, the net surface charge on the support

surface sees increasingly more negative charge. The effect of solution contact time with the support was studied by comparing cobalt nitrate on SiO_2 that was dried immediately following impregnation with the base SiO_2 catalyst contacted for two days.

3.2.5.1 Temperature Programmed Reduction

The influence of the impregnation contact time with the support on the TPR spectra of the catalysts was investigated. The catalysts were named Co/SiO_2 and $Co/0/SiO_2$ for the 2 day and 0 day impregnation contact times respectively. The final pH of the impregnation solution was 5.8 for the Co/SiO_2 catalyst and 4.8 for $Co/0/SiO_2$. The TPR spectra obtained for the two catalysts are illustrated in Figure 3.25. The profile for $Co/0/SiO_2$ indicated lower hydrogen consumption. This was a result of a smaller mass of catalyst loaded into the quartz TPR cell.

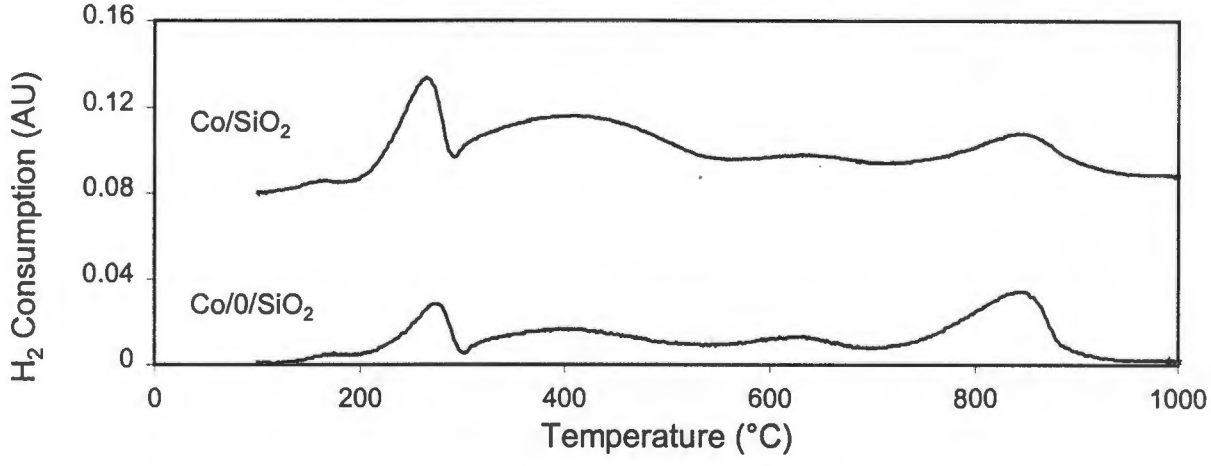

Figure 3.57. Effect of the contact time between impregnation solution and support on the reducibility of cobalt nitrate on SiO_2.
(m_{cat} ~ 0.15g, heating rate = 10°C/min, reducing gas = 60(NTP)ml/min 5% H_2 in N_2,)

The hydrogen to cobalt molar ratios achieved during reduction are given in Table 3.25. The $Co/0/SiO_2$ catalyst shows four regions of cobalt reduction. This parallels the behaviour of the Co/SiO_2. Consequently the TPR profiles look similar, but a closer inspections reveals differences. The $Co/0/SiO_2$ catalyst has increased formation of cobalt silicates. These form at the expense of the more easily reducible cobalt supported species. The effect is to lower the hydrogen to cobalt molar ratio below 400°C from 0.457 to 0.298 as the contact time

decreased from 2 to 0 days. At the same time the overall hydrogen to cobalt molar ratio decreased from 1.346 to 1.124. This change indicates that a greater proportion of cobalt is present on $Co/0/SiO_2$ in divalent form compared to the trivalent form predominant on the Co/SiO_2 catalyst.

Table 3.25. Effect of the impregnation solution contact time on hydrogen consumption during TPR for cobalt nitrate impregnated onto SiO_2.

Support	Precursor	pH	$H_2:Co_{Total}$	$H_2:Co_{<400°C}$
SiO_2	Nitrate	5.8	1.346	0.457
	Nitrate	4.8	1.124	0.298

3.2.5.1.1 Extent of Supported Cobalt Reduction

Figure 3.26 illustrates two TPR spectra for the catalyst formed through impregnation of cobalt nitrate on SiO_2 without any equilibration time. The first spectrum entitles 'calcined' corresponds to a pretreatment consisting of a calcination step of 1 hour in N_2 at 400°C to decompose the precursor. The second spectrum entitled 'reduced' illustrates the TPR profile following activation of the catalyst by reduction in a 5% H_2 in N_2 gas mixture. The reduction pretreatment was the same applied to the catalyst as an activation procedure prior to loading into the reactor for Fischer-Tropsch synthesis. By comparison of the two spectra, information on the extent of reducibility of $Co/0/SiO_2$ was obtained.

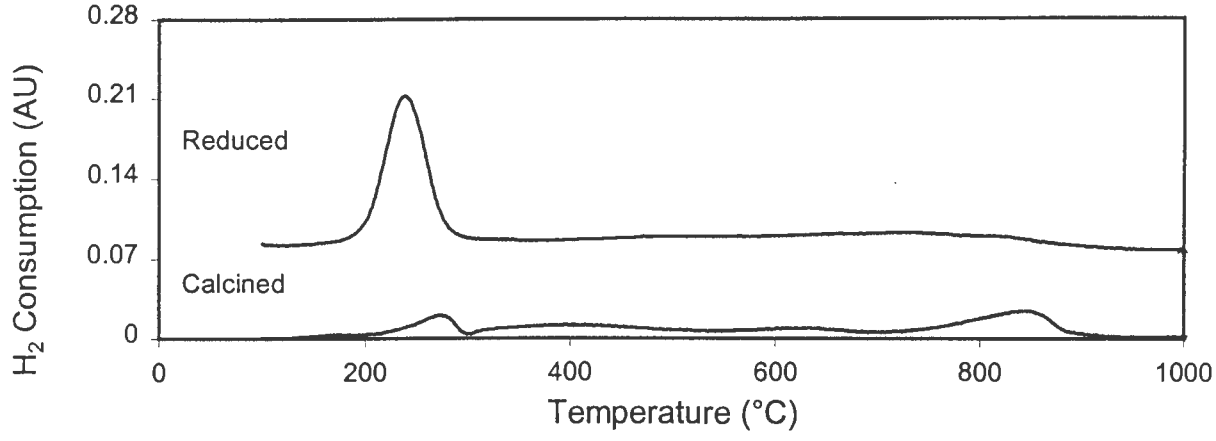

Figure 3.58. Evaluation of the extent of reduction of $Co/0/SiO_2$ after reduction at 400°C for 16 hours.
(m_{cat} ~ 0.15g, heating rate = 10°C/min, reducing gas = 60(NTP)ml/min 5% H_2 in N_2,)

Table 3.26 shows hydrogen consumption data associated with the TPR runs illustrated in Figure 3.58. The 'reduced' TPR spectrum consisted of a major low temperature peak (maximum at 220°C) and a broad high temperature region of reduction between 600°C and 900°C. The low temperature peak arose from surface reoxidation of zerovalent cobalt exposed to the atmosphere, while the high temperature reduction region was attributed to the presence of cobalt silicates that resulted in the loss of active phase (zerovalent) cobalt. The extent of reduction calculated for $Co/0/SiO_2$ was 62.7%, lower than the 80.3% obtained with Co/SiO_2.

Table 3.26. TPR hydrogen consumption data for evaluation of the extent of reduction of supported cobalt for $Co/0/SiO_2$.
(mass cat ~ 0.15g, heating rate = 10°C/min, Reducing gas = 60ml(STP)/min 5% H_2 in N_2)

Catalyst	Pretreatment	H_2:Co Total	H_2:Co <400°C	Extent of Reduction (%)
$Co/0/SiO_2$	Calcination	1.124	0.298	62.7
	Reduction	1.035	0.662	

3.2.5.2 Hydrogen Chemisorption

Table 3.27 gives the hydrogen chemisorption measurements for the $Co/0/SiO_2$ catalyst prepared through cobalt nitrate impregnation onto SiO_2, followed by immediate drying. As minimal contact time was allowed between support and cobalt ions, no charge equilibration of the impregnation solution took place. This lead to slight alterations in the nature of the cobalt interaction with the SiO_2 as observed through TPR. These alterations were also seen by means of hydrogen chemisorption. The smaller impregnation solution contact time lowered the surface area of exposed cobalt metal on the support surface from 3.18 m^2/g to 2.91m^2/g. This decrease in metal surface area coincided with a slight decrease in the extent of reducibility calculated using TPR from 80.3% to 62.7%. The reversibility increased from 65.8% to 70.2% indicating marginally higher interaction between support and cobalt. The cobalt particle size was higher and the cobalt dispersion was lower for the smaller contact time. The cobalt dispersion improved from 6.66% to 7.79%.

Table 3.27. Surface area, dispersion, particle diameter and hydrogen adsorption reversibility for $Co/0/SiO_2$.

Catalyst	Surface Area (m^2/g)	Dispersion (%)	Crystallite Size (nm)	Reversibility (%)
$Co/0/SiO_2$	2.91	7.79	12.4	70.2

3.2.5.3 Transmission Electron Microscopy

No noticeable change in the TEM photograph was noticed, and consequently the TEM photograph for $Co(0)/SiO_2$ can be viewed in Appendix IV.

3.2.5.4 Fischer Tropsch Synthesis

The influence of the length of contact time between impregnation solution and support was tested under Fischer Tropsch conditions in order to obtain activity and selectivity data. The

activity was measured in terms of the hydrocarbon yields obtained from the gas chromatograph analysis of the organic products, as conversion measurements were unreliable. The organic yield was calculated according to the procedure laid out in Appendix III.

Table 3.28 shows the effect that the length of contact time had on the performance of the SiO_2 catalyst. The yield of organic product dropped was 4.65% for small contact time ($Co/0/SiO_2$), and 5.67% for a contact time of 2 days (CO/SiO_2). The shorter contact time has lowered the activity of the catalyst. This result is in agreement with the TPR results. The $Co/0/SiO_2$ catalyst gave a lower hydrogen to cobalt molar ratio below 400°C than the Co/SiO_2 catalyst, as well as an increased formation of cobalt silicates that confines cobalt to an inactive form. This indicated that less cobalt was in the zerovalent form for the $Co/0/SiO_2$ catalyst than for the Co/SiO_2 catalyst, resulting in lower activity.

Table 3.28. Effect of the contact time between support and impregnation solution on the activity and selectivity of cobalt nitrate on SiO_2.
(m_{cat} ~ 1g, T = 200°C, P = 5 bar, H_2 : CO = 2 : 1, WHSV = 0.34g_{CO}/g_{cat}.hr)

Catalyst	Co/SiO_2	$Co/0/SiO_2$
Reaction Time	14 hr 50	19 hr 52
Yield of volatile organics (%)	5.67	4.65
S_{C1+C2} (carbon%)	14.97	15.28
α_{C4-C11}	0.78	0.86
r_{HC} .10^3 (mmol/m^2_{Co}/min)	4.12	3.38
C_5 Composition (%)		
3-methyl-1-butene	0.60	0.50
2-methyl-butane	0.84	1.01
1-pentene	56.31	56.00
2-methyl-1-butene	0.00	0.00
n-pentane	28.26	29.01
trans-2-pentene	8.23	8.07
cis-2-pentene	5.61	5.33
2-methyl-2-butene	0.15	0.07

Hydrogen chemisorption and TPR data showed that the metal surface area and extent of reduction were higher for Co/SiO_2 than for $Co/0/SiO_2$. This increased exposure of zerovalent cobalt resulted in the higher activity of the Co/SiO_2 catalyst. The activity per exposed cobalt surface area decreased from 4.12×10^{-3} $mmol/m^2_{Co}/min$ to 3.38×10^{-3} $mmol/m^2_{Co}/min$ with the shorter contact time even though the dispersion improved.

The selectivity to the C_{1+2} fraction on a carbon percent basis was higher for $Co/0/SiO_2$ compared to the Co/SiO_2 catalyst, rising from 14.97% to 15.28%. This increase is marginal.

The C_5 compositions for the Co/SiO_2 and $Co/0/SiO_2$ catalysts are almost identical. The branched fraction were similar at 1.59% for Co/SiO_2 and 1.58% for $Co/1/SiO_2$. The n-paraffin, α-olefin and β-olefin contents of both catalysts were also very similar with $Co/0/SiO_2$ giving a slightly more hydrogenated product.

The chain growth probabilities were calculated from the slope of the Anderson-Schulz-Flory (ASF) distribution illustrated in Figure 3.59 for both catalysts. The chain growth probabilities, α, were 0.78 and 0.86 for the Co/SiO_2 and $Co/0/SiO_2$ catalysts respectively. Thus the change in impregnation solution contact time had a marked effect on the growth probability of the growing chain with the shorter contact time resulting in an increase in the growth probability. It is interesting that the increased growth probability did not coincide with a change in product spectrum. It is logical to think that increased secondary reaction would involve readsorption of a terminated chain prolonging the growth period and increasing the α value. However this is not the case. One possible cause could be that catalyst from a previous run had ended up in the wax trap. The temperature and liquid wax environment would further the reaction of product formed over the catalyst bed increasing the apparent growth probability.

A distinct change in the growth probability can be seen from C_{12} onwards for the $Co/0/SiO_2$ catalyst. Huff and Satterfield [1984] noted a similar shift in growth probability, explaining it in terms of the superimposition of two separate growth probabilities. They explained this in terms of two types of sites available for CO hydrogenation on the SiO_2 surface, yielding differing growth rates. This distinction in sites is unlikely though. An alternate explanation

could be that the presence of a liquid film around the catalyst may inhibit diffusion of higher molecular weight hydrocarbons, or that C_{12} or higher fractions are trapped in the wax trap.

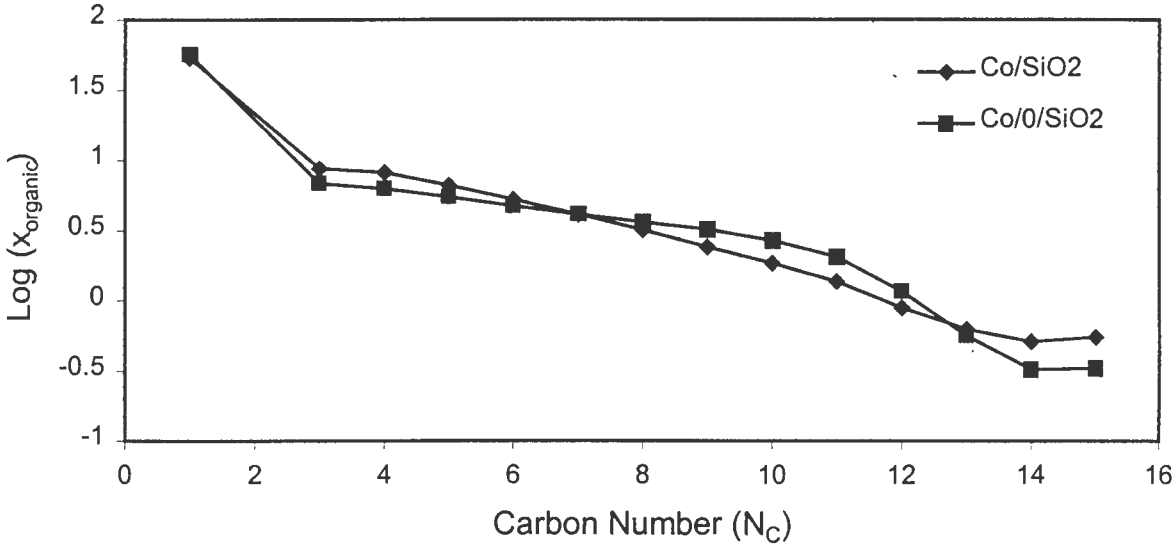

Figure 3.59. Effect of the contact time between impregnation solution and support on the Anderson-Schulz-Flory distribution for cobalt nitrate on SiO_2.
(m_{cat} ~ 1g, T = 200°C, P = 5 bar, H_2 : CO = 2 : 1, WHSV = 0.34g_{CO}/g_{cat}.hr)

Figure 3.60 shows the rate of formation of the total organic product for the Co/SiO_2 and $Co/0/SiO_2$ catalysts. The rate was calculated according to the procedure presented in Appendix III. The rates are given on a per gram of catalyst basis, allowing direct comparison. The rate of formation is a measure of the activity of the catalyst, thus the rate parallels the yield measurements from Table 3.28. Figure 3.60 illustrates the rate of formation as a function of carbon number. As the carbon number increases for each catalyst, the rate of formation decreases. The rate of formation was higher over the Co/SiO_2 catalyst relative to the $Co/0/SiO_2$ catalyst coinciding with chemisorption measurements.

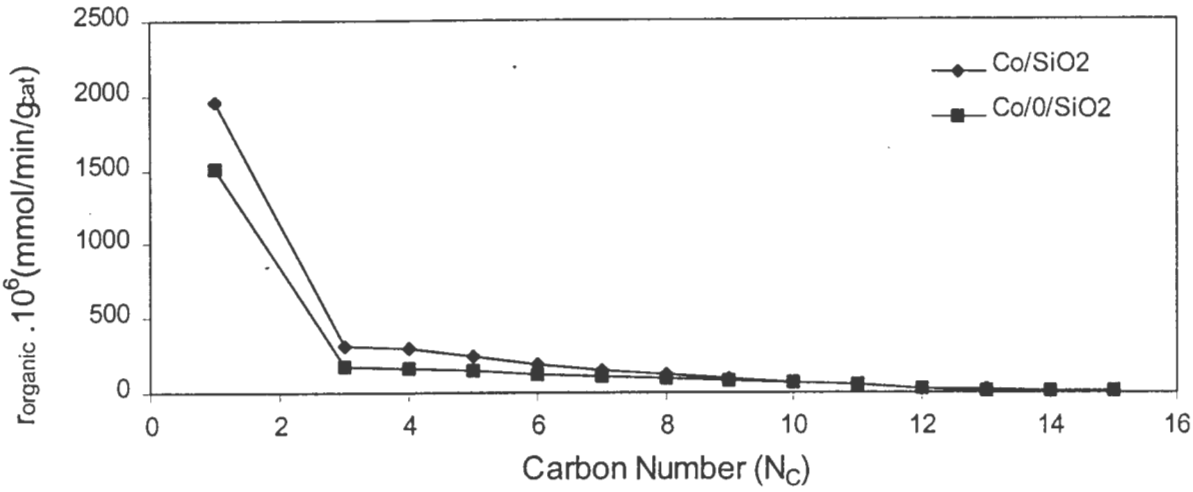

Figure 3.60. Effect of the contact time between impregnation solution and support on the total organic formation rate for cobalt nitrate on SiO_2.
(m_{cat} ~ 1g, T = 200°C, P = 5 bar, H_2 : CO = 2 : 1, WHSV = 0.34g_{CO}/g_{cat}.hr)

The olefinicity of the linear organic product is shown in Figure 3.61 for the Co/SiO_2 and $Co/0/SiO_2$ catalysts. The selectivity to linear olefins of the two catalysts were almost exactly the same for the full range of carbon numbers, indicating similar growth probabilities as the profiles in Figure 3.61 were approximately parallel. In Table 3.28 the C_5 product breakdown was given for each catalyst. The linear olefin fractions of the total organic product were 70.15% and 69.40% for the Co/SiO_2 and $Co/0/SiO_2$ catalysts respectively. Consequently the length of contact time had no effect on the linear olefinicity of the organic product.

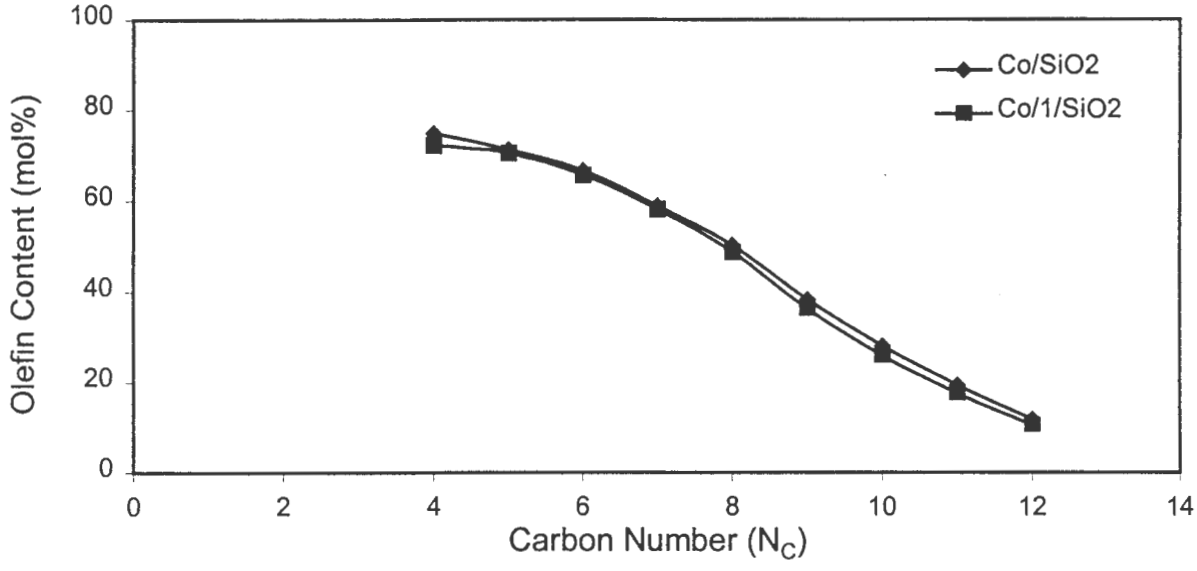

Figure 3.61. Effect of the contact time between impregnation solution and support on the olefin fraction of the linear organic product for cobalt nitrate on SiO_2.
(m_{cat} ~ 1g, T = 200°C, P = 5 bar, H_2 : CO = 2 : 1, WHSV = 0.34g_{CO}/g_{cat}.hr)

Table 3.28 shows the breakdown of the total linear olefin content of the C_5 fraction for Co/SiO_2 and $Co/1/SiO_2$ respectively. The total linear olefin content is split up between the α-olefin content and the β-olefin content. The β-olefin fraction is made up of the cis and trans 2-pentene products. The α-olefin fraction of the linear olefins is illustrated in Figure 3.62 for Co/SiO_2 and $Co/0/SiO_2$. The α-olefin fraction of the total organic product was 56.00% for the $Co/1/SiO_2$ catalyst, and 56.31% for the Co/SiO_2 catalyst. This meant that the α-olefin fraction of the linear olefin product over $Co/0/SiO_2$ and Co/SiO_2 were the same. Thus the product spectrum remains unaltered as a result of a shorter contact time. This indicates that the catalyst surfaces are identical in structure, and only differ in the availability of active sites that affects the activity.

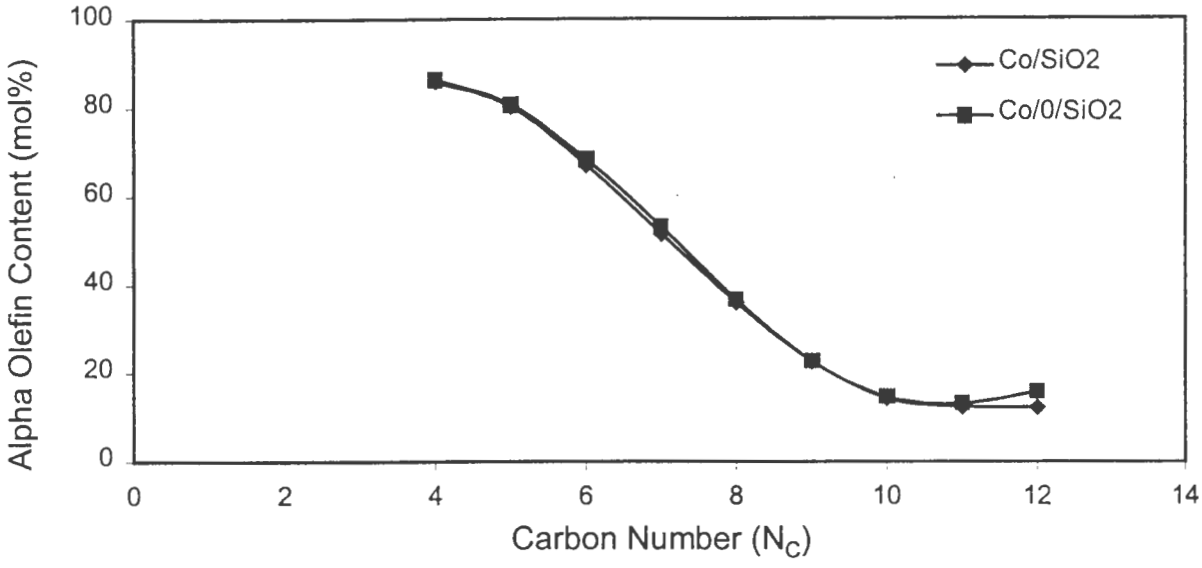

Figure 3.62. Effect of the contact time between impregnation solution and support on the α-olefin fraction of the linear olefins for cobalt nitrate on SiO_2.
(m_{cat} ~ 1g, T = 200°C, P = 5 bar, H_2 : CO = 2 : 1, WHSV = 0.34g_{CO}/g_{cat}.hr)

3.3 Time on Stream Behaviour

The time on stream behaviour of the Co/SiO_2, Co(A)/ZnO and Co(MED)/MnO were evaluated by analysing the product at a short and long time on stream. The three catalysts chosen included all three supports, each having different preparation conditions.

3.3.1 SiO_2 as a Support

The conversion was measured for the Co/SiO_2 catalyst using a Varian TCD gas chromatograph. The exact values obtained in Figure 3.63 are not to be taken as absolute as variations and irregularities were noted with the TCD gas chromatograph. However Figure 3.63 does illustrate the trends observed during Fischer-Tropsch synthesis over Co/SiO_2. Of most significance is the initial uptake of reactant at the beginning of the reaction. Reactant uptake lasted approximately 55 minutes after which the catalyst reached a pseudo steady

state. This steady state refers only to the activity, as the selectivity was still changing dramatically. The activity of the catalyst dropped from a hydrocarbon yield of 7.37% at 51 minutes to 5.67% at 14hr50. This deactivation resulted from a combination of factors. The first cause could be that the full product range was not completely established at 51 minutes. Accordingly the fraction of higher molecular weight hydrocarbons at 51 minutes was smaller, resulting in less product being trapped in the wax trap due to the lower boiling point of the organic fraction. Thus at the 51 minutes, the yield measurement is probably a truer reflection of the activity of the catalyst than at 14hr50 when more product would be trapped. The second cause may be true deactivation resulting from the build up of heavier molecular weight hydrocarbons in the pore structure. This would lead to diffusional constraints as well as decreasing the accessibility of reactant to the active sites. A small amount of deactivation may result from the presence of water reoxidizing active sites, however this is unlikely due to the strong reducing capability of both hydrogen and carbon monoxide.

Figure 3.63 gives both the hydrogen and carbon monoxide conversions. The Fischer-Tropsch mechanism requires that hydrogen consumption is either equal or greater than carbon monoxide consumption. During the initial reactant uptake, carbon monoxide uptake may be higher as the catalyst surface is already predominantly covered with hydrogen following the activation in hydrogen prior to reaction.

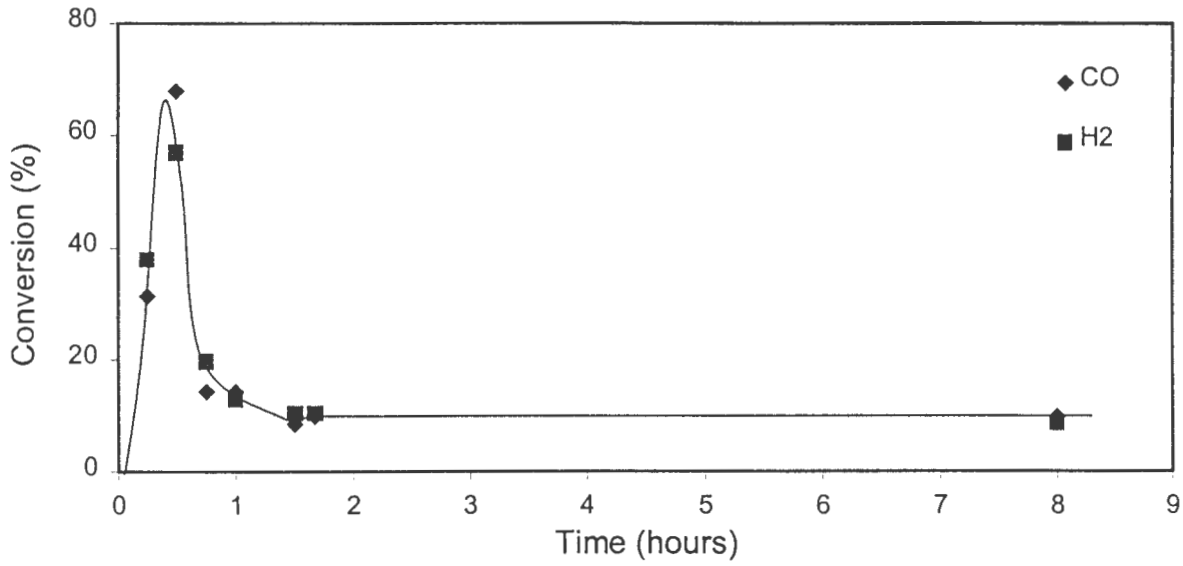

Figure 3.63. Time on stream activity for Co/SiO_2. Cobalt nitrate supported on SiO_2. (m_{cat} ~ 1g, T = 200°C, P = 5 bar, H_2 : CO = 2 : 1, WHSV = 0.34g_{CO}/g_{cat}.hr)

Figure 3.64 shows the variation in chain growth with time on stream. The chain growth probability was largely unaffected, except at higher molecular weight hydrocarbons where the chain growth probability was not maintained at small times on stream. Increased reaction time allows an equilibrium to be formed for the product diffusion from the catalyst surface through the liquid film surrounding the catalyst into the gaseous phase to be carried out in the product line. The saturation of the catalyst with hydrocarbon is at this stage not fully realised. As a result the rate of readsorption of product has not been fully established yielding a drop in the ASF plot at high carbon numbers. After 51 minutes on stream, the product termination probability was stable up to the C_{11} fraction indicating that this equilibrium was still developing for higher molecular weight hydrocarbons.

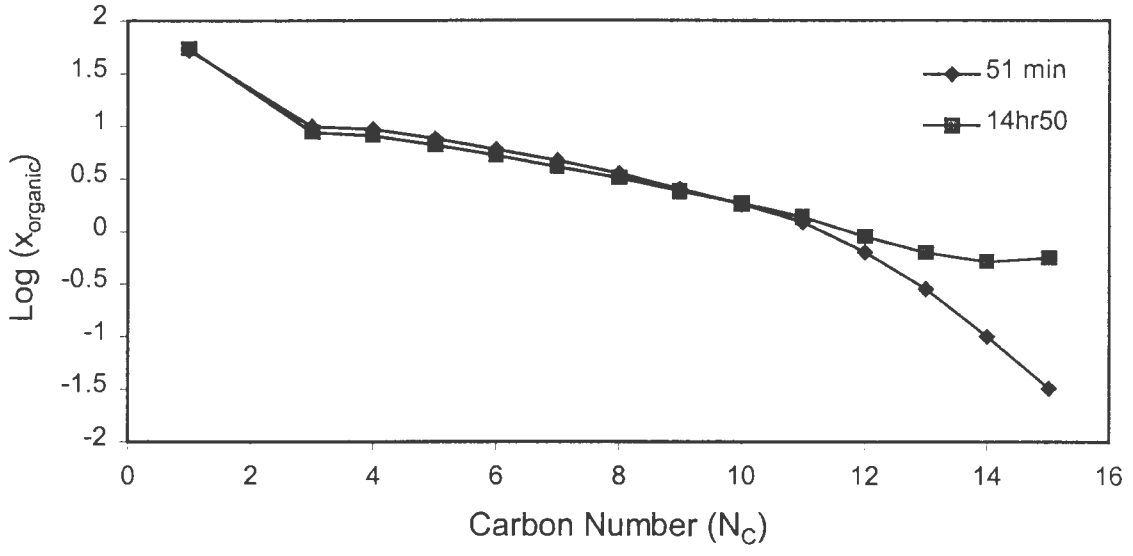

Figure 3.64. Time on stream behaviour of the Anderson-Schulz-Flory distribution for Co/SiO_2.
(m_{cat} ~ 1g, T = 200°C, P = 5 bar, H_2 : CO = 2 : 1, WHSV = 0.34g_{CO}/g_{cat}.hr)

The time on stream behaviour of the olefin fraction of the total organic product is illustrated in Figure 3.65. The olefin fraction consists of both the linear and branched olefin product. The overall olefin selectivity was lower over the complete carbon number range for the shorter time on stream. Figure 3.66 illustrates the ratio of the α-olefin to the n-paraffin at each carbon number for the two times on stream. The longer time on stream of 14hr50 yielded a product richer in α-olefin relative to the hydrogenated product. The difference

between the α-olefin and the n-paraffin arises in the termination step. The α-olefin forms through hydrogen abstraction, while the n-paraffin results from the addition of hydrogen. Figure 3.65 shows that at 51 minutes on stream, the hydrogenation reaction is more dominant than after 14hr 50 resulting in the lower olefinicity of the organic product. Thus initially hydrogen is more readily accessible than at later stages. This finding is explainable in terms of the reduction prior to reaction. The catalyst was reduced at 400°C in a hydrogen atmosphere. Hydrogen chemisorption indicated that the reversibility of hydrogen adsorption was high over Co/SiO_2.

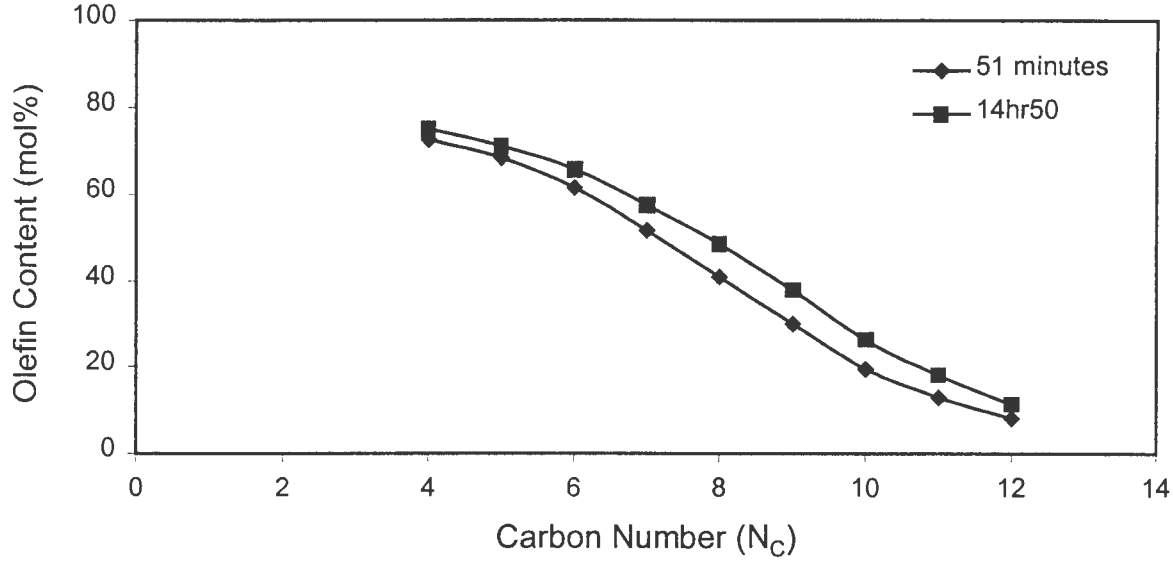

Figure 3.65. Time on stream behaviour of the total olefin fraction of the organic product for Co/SiO_2. Olefin fraction includes linear and branched olefins.
(m_{cat} ~ 1g, T = 200°C, P = 5 bar, H_2 : CO = 2 : 1, WHSV = 0.34g_{CO}/g_{cat}.hr)

This would suggest that hydrogen remains on the active sites during transfer to the reactor, as well as during the initial phase of reaction. Carbon monoxide and hydrogen compete for active sites. If the active sites are predominantly covered with hydrogen at the start, then it seems logical that carbon monoxide will begin to replace hydrogen due to the fact that CO adsorbs more strongly on cobalt. With time on stream the catalyst begins to favour the α-olefin primary product due to the enhanced presence of CO on the active sites. The high activity of the Co/SiO_2 catalyst results in this replacement taking place at a rapid rate. As this

takes place, the catalyst becomes saturated with liquid product. This increases the diffusion restrictions lowering the ease with which reactant reaches and product leaves the active sites. The high activity allows this condition to take place quickly, and consequently will bring about fast equilibration of reactant and product concentrations. For this reason, the product spectrums and chain growth probabilities at 51 minutes and 14hr50 are quite similar already.

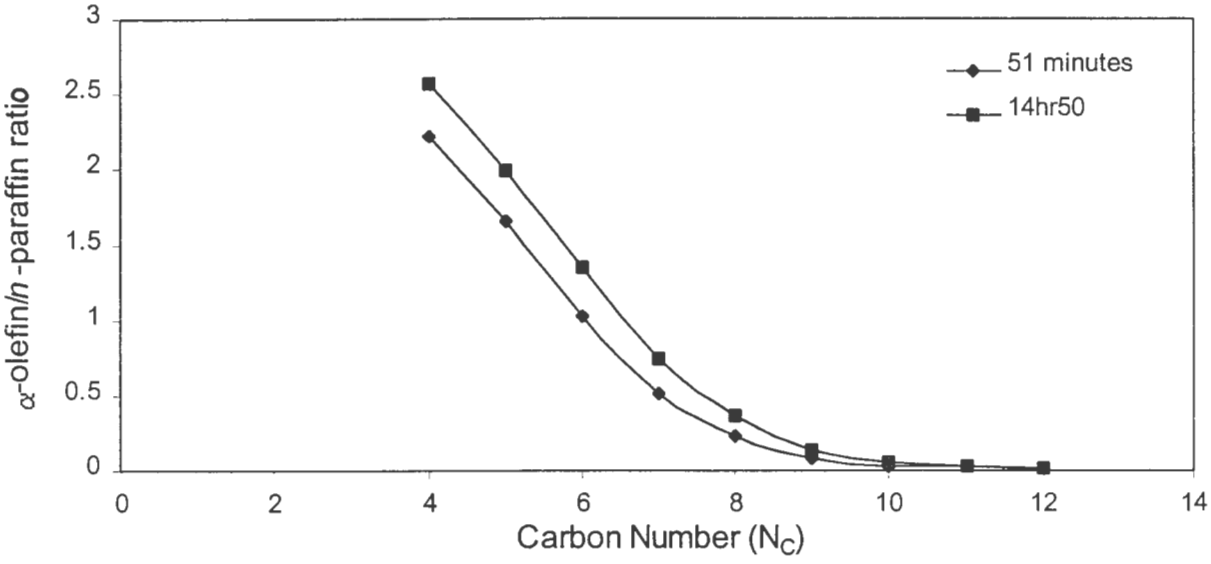

Figure 3.66. Time on stream behaviour of the α-olefin to n-paraffin ratio of the organic product formed over Co/SiO_2.
(m_{cat} ~ 1g, T = 200°C, P = 5 bar, H_2 : CO = 2 : 1, WHSV = 0.34g_{CO}/g_{cat}.hr)

3.3.2 ZnO as a Support

The carbon monoxide and hydrogen conversions were measured for the Co(A)/ZnO catalyst and are illustrated in Figure 3.67. The most noticeable feature is the initial uptake of reactant at the beginning of the reaction. Reactant uptake lasted approximately 1 hour after which the catalyst reached a pseudo steady state. The activity of the catalyst dropped from a hydrocarbon yield of 2.60% at 2hr31 to 2.45% at 15hr55. As was observed over Co/SiO_2, activity dropped with time on stream. After two and a half hours the yields were almost the same. The deactivation observed resulted from a combination of factors as described for the Co/SiO_2 catalyst. Figure 3.67 gives both the hydrogen and carbon monoxide conversions.

The Fischer-Tropsch mechanism requires that hydrogen consumption is either equal or greater than carbon monoxide consumption. During the initial reactant uptake, carbon monoxide uptake was observed to be higher at certain stages as the catalyst surface is already predominantly covered with hydrogen following the activation in hydrogen prior to reaction.

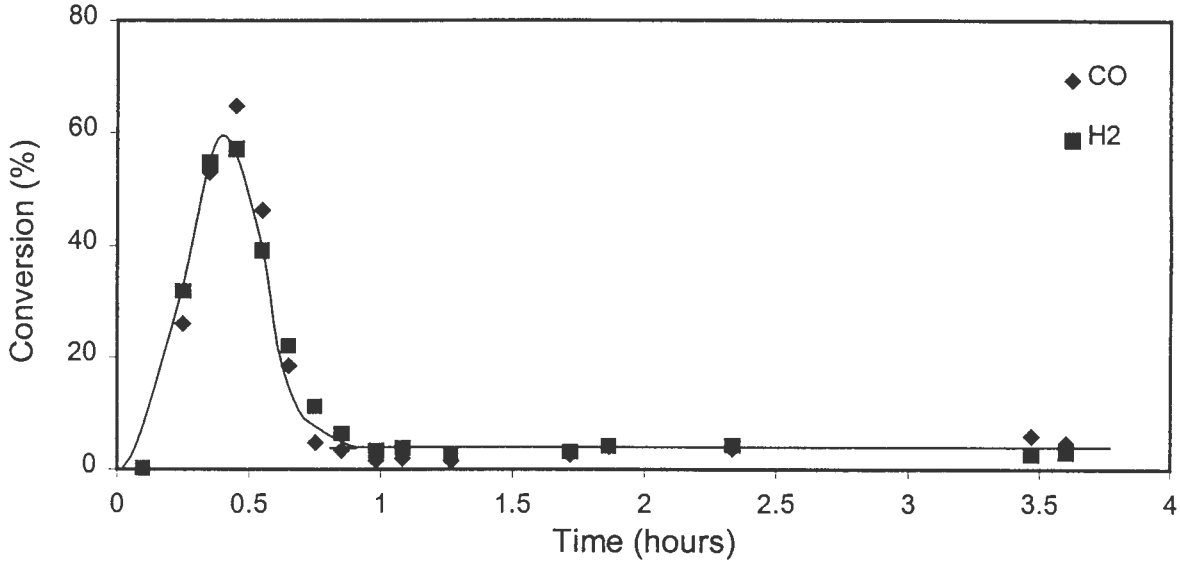

Figure 3.67. Time on stream activity for Co(A)/ZnO.
(m_{cat} ~ 1g, T = 200°C, P = 5 bar, H_2 : CO = 2 : 1, WHSV = 0.34g_{CO}/g_{cat}.hr)

The chain growth probability can be seen in the Anderson-Schulz-Flory plots in Figure 3.68. After 2hr31 of reaction, the ASF plots are almost an exact match. This indicates that the diffusion pathway of product away from the catalyst surface has fully established itself for the hydrocarbon range up to at least C_{15}. In other words, the liquid organic film around the catalyst particles is formed, and product and reactant diffusion rates have stabilised, and settled at steady state values. As the concentration of products leaving is still changing with time on stream due to alterations observed in the product selectivity, however these differences would not upset the density of the surrounding mixture as the changes taking place are specific to each carbon number, due to variations in the final termination product with time on stream.

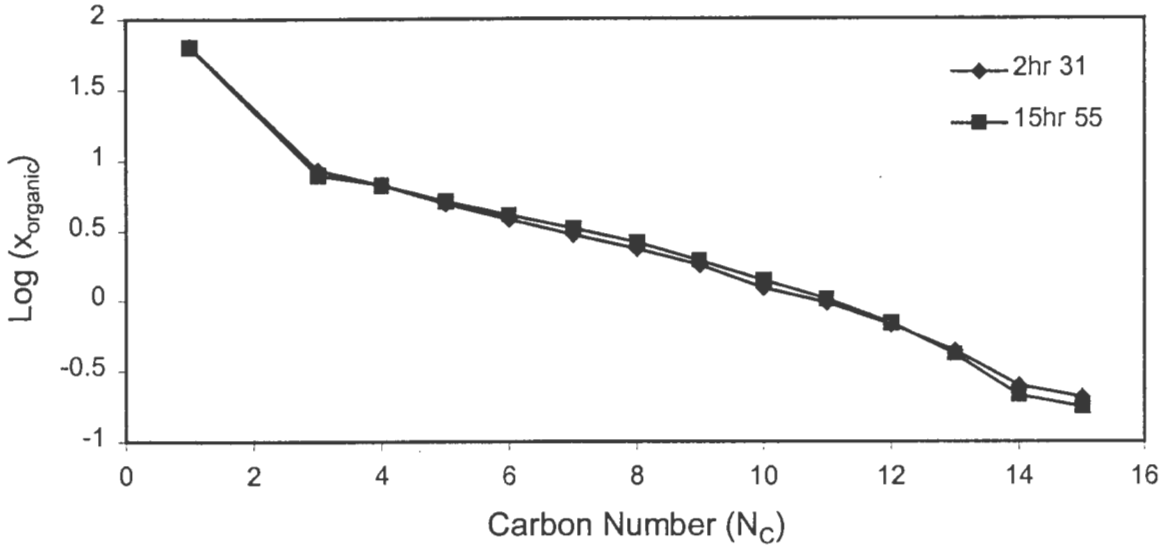

Figure 3.68. Time on stream behaviour of the Anderson-Schulz-Flory distribution for Co(A)/ZnO.
(m_{cat} ~ 1g, T = 200°C, P = 5 bar, H_2 : CO = 2 : 1, WHSV = 0.34g_{CO}/g_{cat}.hr)

Figure 3.69 illustrates the behaviour of the total olefin fraction of the organic product with time on stream. For the shorter time on stream of 2hr31, the total olefin fraction is significantly lower than after reaction for 15hr55. Consequently the catalyst produces a more hydrogenated product during the earlier stages of reaction. The secondary olefinicity as well as the α-olefin selectivity increase with time on stream causing a lowering in hydrogenation activity with longer times on stream.

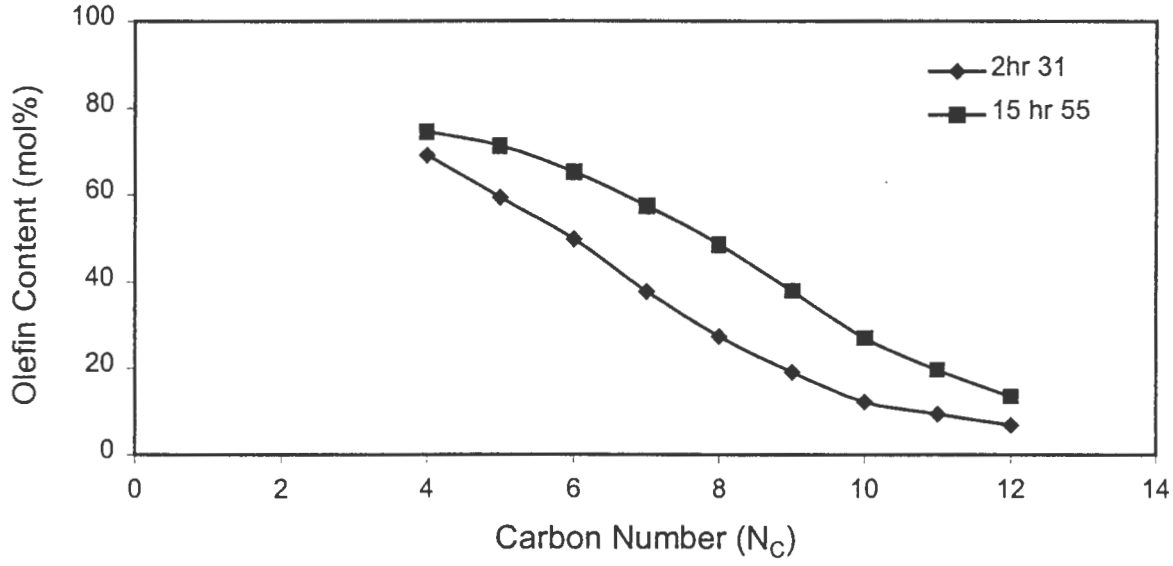

Figure 3.69. Time on stream behaviour of the total olefin fraction of the organic product for Co(A)/ZnO. Olefin fraction includes linear and branched olefins.
(m_{cat} ~ 1g, T = 200°C, P = 5 bar, H_2 : CO = 2 : 1, WHSV = 0.34g_{CO}/g_{cat}.hr)

Figure 3.70 shows the behaviour of the ratio of α-olefin to n-paraffin with variation in time on stream. At 2hr31, the low time on stream, the ratio of α-olefin to n-paraffin is significantly lower than at 15hr55. This behaviour is attributed the still strong presence of hydrogen adsorbed on the catalyst surface. As the catalyst activity is lower than that observed over Co/SiO_2, the transition from a predominantly hydrogen covered surface following reduction to a carbon monoxide dominated surface will take place more slowly. During the first few hours of reaction, the reactant exchange, as well as the reduction of oxidised cobalt surface species may enhance the hydrogenation activity.

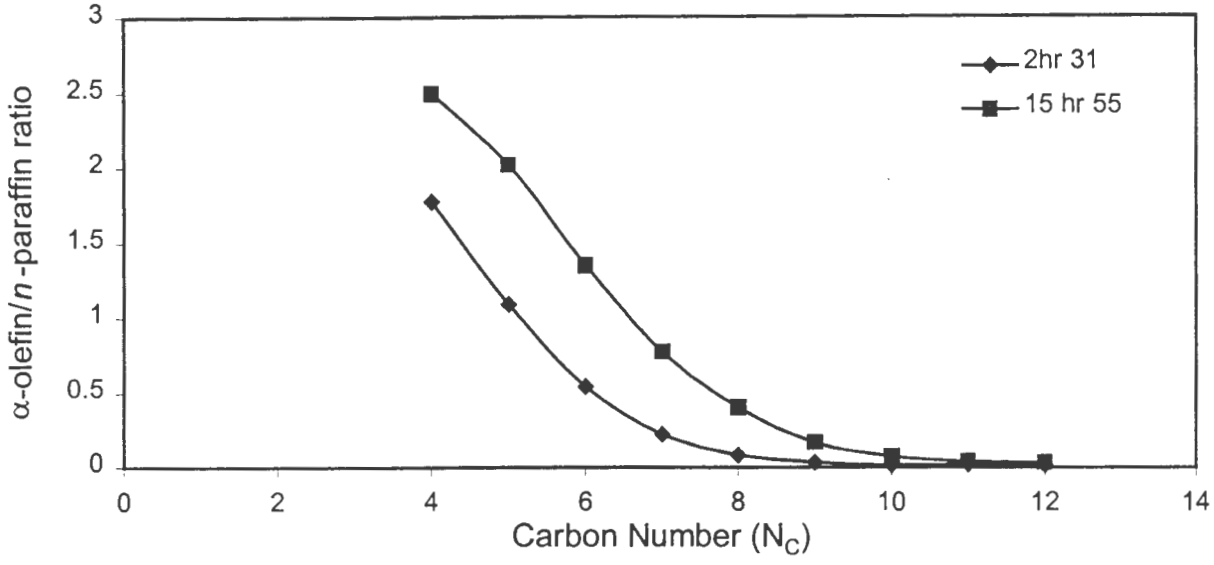

Figure 3.70. Time on stream behaviour of the α-olefin to n-paraffin ratio of the organic product formed over Co(A)/ZnO.
(m_{cat} ~ 1g, T = 200°C, P = 5 bar, H_2 : CO = 2 : 1, WHSV = 0.34g_{CO}/g_{cat}.hr)

3.3.3 MnO as a Support

The carbon monoxide and hydrogen conversions observed over the Co(MED)/MnO catalyst can be seen in Figure 3.71. Once again the most noticeable feature is the initial uptake of reactant at the beginning of the reaction. Reactant uptake lasted approximately 1 hour after which the catalyst reached a pseudo steady state. The yield of organic product increased from 1.05% after 21 minutes to 1.23% after 23hr46. According to Figure 3.71, after 21 minutes reactant is being taken up through adsorption onto available surface sites. Consequently a fraction of the active sites will not be completely covered, hence the catalyst is still not making full use of the exposed active area.

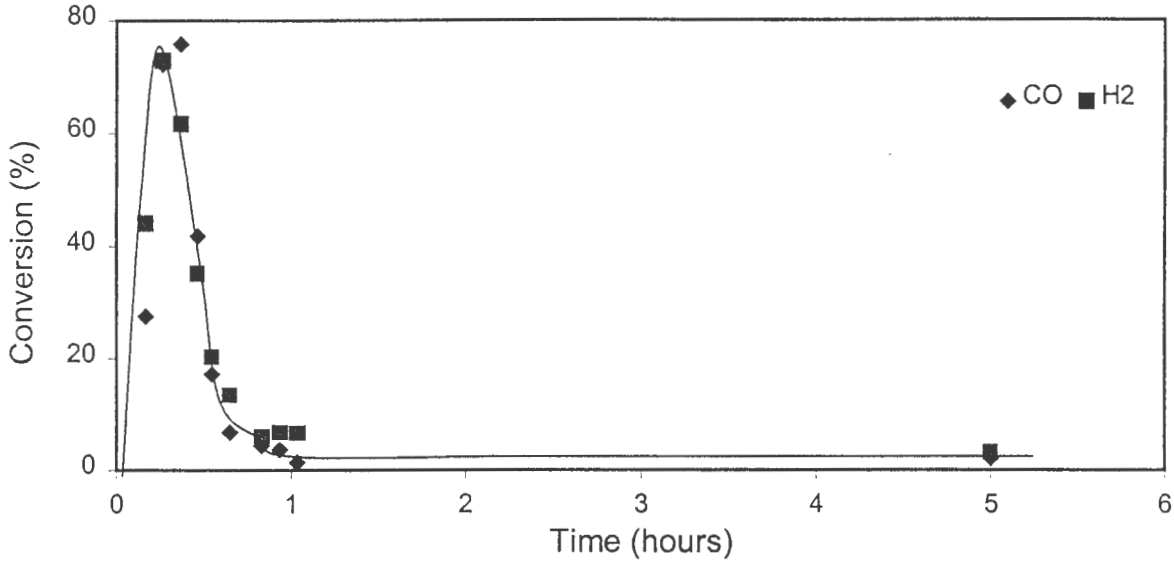

Figure 3.71. Time on stream activity for Co(MED)/MnO. Cobalt nitrate supported on MnO with MED added to the impregnation solution.
(m_{cat} ~ 1g, T = 200°C, P = 5 bar, H_2 : CO = 2 : 1, WHSV = 0.34g_{CO}/g_{cat}.hr)

The ASF plots at the different times on stream are illustrated in Figure 3.72. The chain growth behaviour is only meaningful up to the C_9 fraction. For higher molecular weight hydrocarbons, a hump can be observed that is possibly associated with wax trap bleeding. The fact that both ASF plots show this hump is indicative of bleeding. It is interesting to note that the hump is more pronounced after 23hr46 on stream. The reason for this is that higher molecular weight hydrocarbons are being formed as well as seeping from the wax trap as opposed to the reaction behaviour after 21 minutes where no high molecular fraction has been formed.

The absence of the heavier organic product after 21 minutes is understandable as the product spectrum is still developing, as the FT reaction follows polymerisation behaviour. The higher chain growth probability for the C_3 to C_9 fraction results from the lower extent of readsorption during the early reaction stage prior to the formation of a liquid film around the catalyst particles. The liquid film decreases the rate of diffusion of product away from the catalyst enhancing readsorption and further chain growth. No liquid film limits readsorption

resulting in a larger formation of lower molecular weight products and consequently increases the chain growth probability over this range.

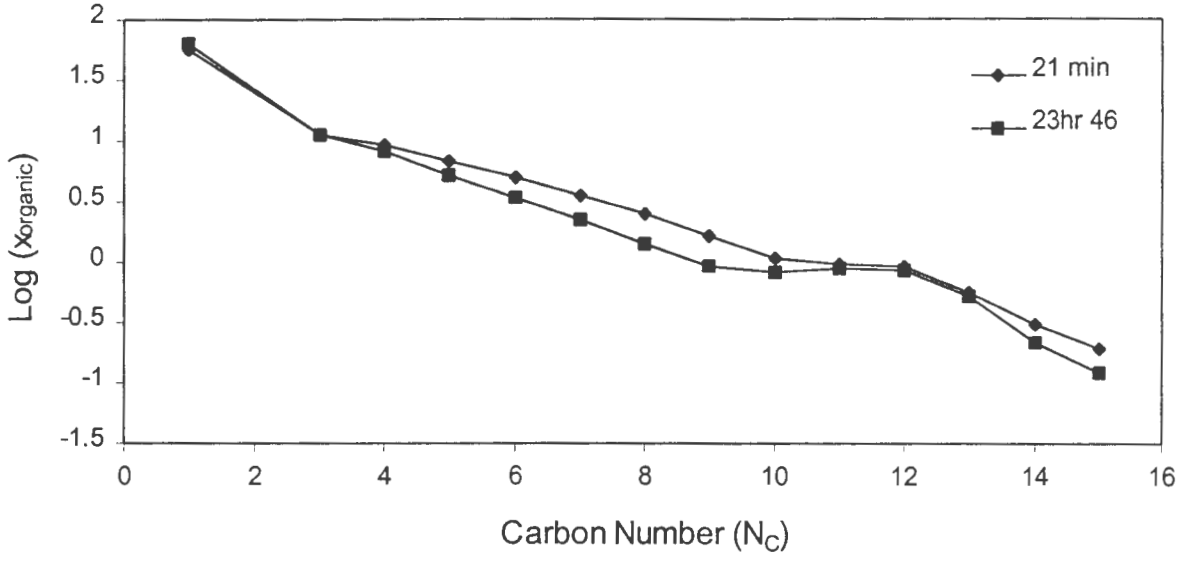

Figure 3.72. Time on stream behaviour of the Anderson-Schulz-Flory distribution for Co(MED)/MnO.
(m_{cat} ~ 1g, T = 200°C, P = 5 bar, H_2 : CO = 2 : 1, WHSV = 0.34g_{CO}/g_{cat}.hr)

The time on stream behaviour of the total olefin fraction of the organic product observed over Co(MED)/MnO is illustrated in Figure 3.73. At the shorter time on stream, less olefin is formed. The reason for this was attributed to the strong presence of hydrogen on the surface during the initial reaction stage. This promotes the termination of a hydrogenated product instead of the expected α-olefin.

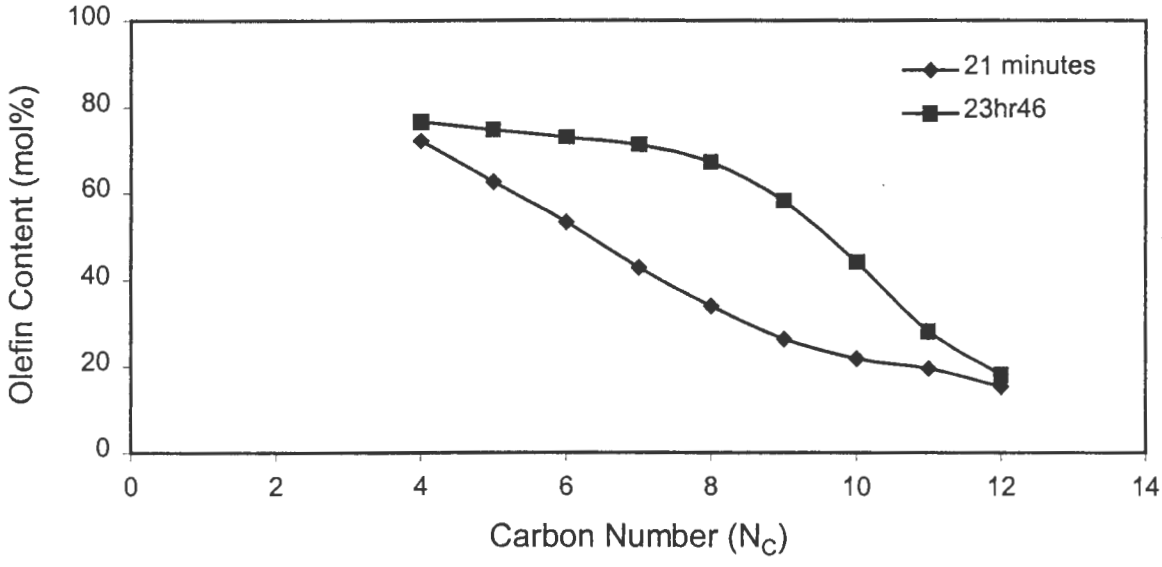

Figure 3.73. Time on stream behaviour of the primary product fraction of the total organic product for Co(MED)/MnO. Primary product consists of the α-olefin and the n-paraffin.
(m_{cat} ~ 1g, T = 200°C, P = 5 bar, H_2 : CO = 2 : 1, WHSV = 0.34g_{CO}/g_{cat}.hr)

Figure 3.74 shows that the α-olefin to n-paraffin ratio at 21 minutes is significantly lower than at 23hr46. This confirms the heightened hydrogenation activity discussed earlier. With time on stream, hydrogen becomes replaced by carbon monoxide through competitive adsorption. As this happens, the hydrogenation activity decreases and the α-olefin selectivity improves. It is interesting to note that all three support types showed the same trends with respect to product variations with time on stream.

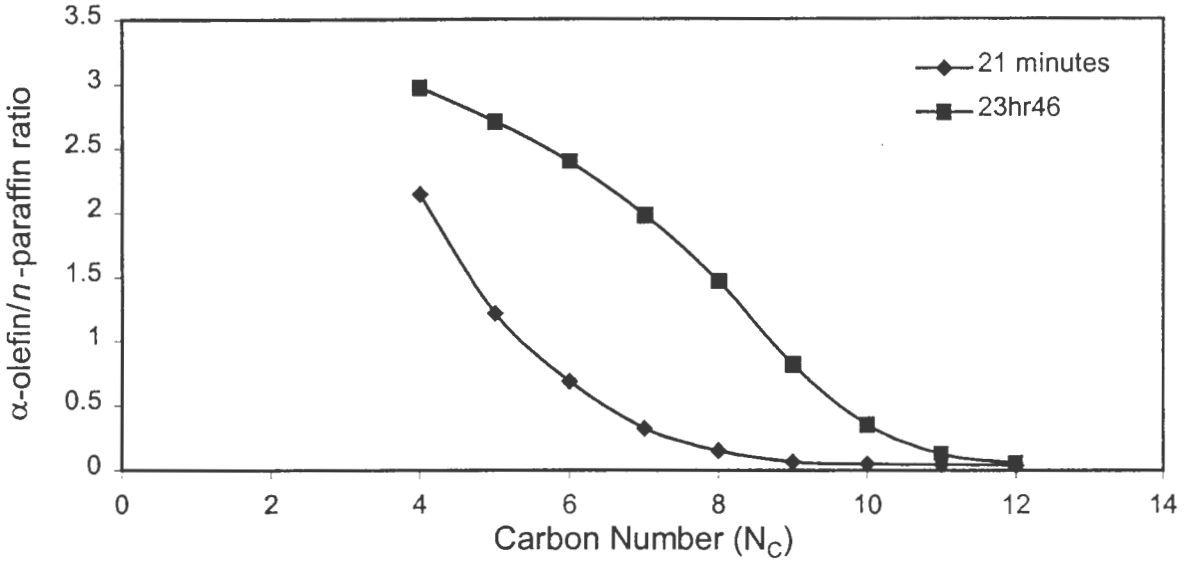

Figure 3.74. Time on stream behaviour of the α-olefin to n-paraffin ratio of the organic product formed over Co(MED)/MnO.
(m_{cat} ~ 1g, T = 200°C, P = 5 bar, H_2 : CO = 2 : 1, WHSV = 0.34g_{CO}/g_{cat}.hr)

CHAPTER 4

DISCUSSION

4. Comparison of SiO_2, ZnO and MnO Supports

Studies documented in literature with respect to support type for cobalt supported Fischer-Tropsch catalysts indicate that the majority of work is carried out on silica (SiO_2) [e.g. Kuipers et al., 1996; Kogelbauer et al., 1995; Coulter and Sault, 1995] and alumina (Al_2O_3) [e.g. Ragaini et al., 1996; Zsoldos et al., 1995]. SiO_2 has the benefit of a high surface area for dispersion of the active component, but often a significant fraction of the loaded cobalt deposits in inactive form as cobalt silicates arising through interaction with the support. Using the cobalt supported on SiO_2 as a base case catalyst, ZnO and MnO were looked to as alternative supports for cobalt supported Fischer-Tropsch catalysts. The effect of support can be evaluated by comparing their physical characteristics and understanding how these physical characteristics determine the performance characteristics under Fischer-Tropsch conditions.

4.1 Physical Characterisation of SiO_2, ZnO and MnO Catalysts

The zeta potential measurements for the catalyst indicated that the point of zero charge (PZC) was different for the three supports SiO_2, ZnO and MnO. The PZC for the SiO_2 support occurred at the lowest pH of 2 , followed by MnO at a pH of 4 and finally ZnO at a pH of 8. The plot of zeta potential versus pH gives an indication of the balance between positive and negative charge on the support surface. At a pH below the PZC, each support bears a net positive charge, and visa versa.

The zeta potential itself is not sufficient to characterise the interaction between cobalt and support at any given pH. The zeta potential will indicate whether the cobalt is attracted to or repelled by the majority of the support surface, however it can not show the magnitude of this interaction. Consequently, when loading cobalt onto SiO_2 in a strong acidic medium, it seems immediately apparent that strong repulsion should take place between support and cobalt. However TPR showed that cobalt loaded at a pH of 1 showed minimal difference to the same loading at a pH of 5.8. Consequently other effects are key to the level of interaction between cobalt and support.

Probably the most important effect must be the nature of the support surface. The support nature refers to the various types of groups present, and both the charge on these groups and the frequency with which they occur. These factors are determined by the degree of crystallinity of the support material. A high crystallinity intimates a rigid repetitive structure with few defects, and visa versa. Defects refer to the terminal groupings such as oxygen atoms, hydroxyl groups and silanol groups that provide points of attachment for the charged cobalt ions. It is these defects that are so important as attachment sites for the cobalt ions.

It was shown through XRD that ZnO had by far the highest degree of crystallinity, while SiO_2 was completely amorphous. This difference has a significant effect on the physical characteristics of the support material. SiO_2, being an amorphous material, is physically defective in terms of the surface structure. The result is the availability of a wide range of attachment points, especially groups bearing a negative charge, such as SiO^-, which would seek to interact with the Co^{2+} ions. These same groups are not available on the crystalline ZnO support. The high crystallinity results in structured planes with minimal defective groups for cobalt attachment. The frequency of surface defects on SiO_2 suggests that the surface atoms, such as hydrogen, may be more mobile due to the apparent lack of repetitive structure. This mobility may aid charge redistribution following cobalt impregnation increasing the ease with which Co^{2+} ions are incorporated or attached. The formation of cobalt silicates over SiO_2 may be accompanied by a lowering in the Gibbs free energy at the surface through formation of more stable terminal species. This would not be the case on ZnO, which would seek to maintain the crystal structure already in place. The MnO support shows a degree of crystallinity between SiO_2 and ZnO, however a somewhat different effect may be at play during cobalt impregnation on MnO, specifically with respect to the ease with which manganese changes oxidation states.
Consequently both the crystallinity of the support material and the zeta potential of the support in solution contribute to the strength of interaction arising during impregnation, however the degree of crystallinity plays by far the greater role.

The extent of reduction and the exposed metal surface area were measured by TPR and hydrogen chemisorption for the three support types. From these measurements, information was obtained on the interaction between cobalt, loaded in both nitrate and acetate form, and the support.

The extent of reduction measured the fraction of the cobalt supported as the active zerovalent form following reduction at 400°C for 16 hours in 5% H_2 in N_2 gas. On this basis, the ZnO supported catalyst showed the highest extent of reduction, followed by SiO_2 and then MnO. The extent of reduction of cobalt supported on MnO proved to be a problematic calculation as the greater fraction of hydrogen consumption during TPR occurred through reduction of the support material. Accordingly, no exact value could be attributed to the extent of reduction of the cobalt, as no specific reduction step could be assigned to each reduction peak due to offset hydrogen to cobalt molar ratios. It was assumed that the high temperature peak of the Co/MnO reduction spectrum was due to supported cobalt oxide reduction arising from interaction between cobalt and the MnO support. If this peak was a result of support reduction alone, the extent of reduction would change significantly from 28.7% to approximately 100%, unlikely considering the low activity obtained over the Co/MnO catalyst under Fischer-Tropsch conditions. The differing extents of reduction for the three supports derived from the type of interaction arising between cobalt and support for each case or from interaction between cobalt as well as between cobalt and MED where used.

The ZnO supported catalysts maintained an extent of reduction consistently higher than the other two supports irrespective of preparation conditions due to the low interaction between support and cobalt. In fact, the support may even have repelled the positively charged cobalt ions. Repulsion would arise due to electronic interactions as observed using zeta potential measurements. A strongly positive support surface resulting from the acidic impregnation medium used would attempt to counter the presence of positively charged Co^{2+} ions. This positive surface, combined with the fact that ZnO shows a highly ordered crystal framework yielding few surface defects, would mean few terminal surface sites attractive to cobalt ions. Thus the ZnO surface behaves as little more than a physical resting point for cobalt following evaporation of the impregnation solution. In fact, as the impregnation solution equilibrated over two days, no solution colour change was observed intimating that cobalt remained preferentially in solution as opposed to being adsorbed on the support. This has great significance in terms of the final physical characteristics of the activated catalyst. Hydrogen chemisorption revealed a lower exposed metal surface area than expected for cobalt loaded on ZnO in both acetate and nitrate form. The reason for this is that zerovalent cobalt on the surface groups together as large clusters. In so doing active cobalt particles are buried under subsequent cobalt layers and are no longer available as active sites. This grouping or

agglomeration of cobalt on the surface is a direct response to the absence of metal support interaction. The result is that cobalt mobility across the surface of the support becomes greatly enhanced, and cobalt finds stability among its own kind on the surface. The above described effects are specific to the ZnO support. Far greater metal support interaction was noted over both SiO_2 and MnO, but the interactions differed in that they were resulted from different effects.

The SiO_2 support has long been known to interact with cobalt following aqueous impregnation. The metal support interaction has been seen to vary significantly with changes in precursor, calcination temperature and activation temperature indicating that the physical nature of the SiO_2 surface is readily alterable [Sewell, 1996]. The reason for this stems from the amorphous nature of the SiO_2 material. Amorphous refers to a structure that is not rigidly repetitive as is the case with a strong crystal lattice. The result is that the surface is more defective and provides a number of different options for attachment which would not be available under more structured conditions. With this in mind, it seems logical that temperature would enhance the ease with which the surface could rearrange itself into a structure favourable for cobalt incorporation. This is exactly what is observed following calcination. Sewell [1996] showed that higher calcination temperatures lead to significantly higher cobalt silicate formation. The surface defects are present as positive and negative groupings, the negative groups showing an electronic attraction to Co^{2+} ions. The strength of the interaction serves to prevent significant relocation of the adsorbed cobalt during activation, as was evident with the ZnO support. This inhibition prompted higher cobalt dispersions and lower cobalt crystallite sizes. The exposed metal surface area on SiO_2 was seen to be a function of the propensity for cobalt to migrate into the SiO_2 network resulting in cobalt silicates. The more silicates present the lower the metal surface area. The performance of the Fischer-Tropsch catalyst is largely determined by the cobalt dispersion and the extent of reduction of the cobalt. These effects are counterproductive, with high dispersion generally coinciding with low extents of reduction and visa versa. The Co/SiO_2 catalyst harnesses these two features the best out of the catalysts studied, yielding a high dispersion with a moderate metal support interaction which in turn did not suppress the extent of reduction to a great degree. Figure 4.1 illustrates the relationship between the exposed surface area of metallic cobalt and the extent of reduction of the total cobalt on the support for each catalyst prepared. In all cases, irrespective of the preparation procedure, the catalyst with the extent of reduction in between the other two catalysts prepared with the same method always had the highest

exposed cobalt surface area. For example, of the catalysts prepared through MED addition to the impregnation solution Co(MED)/MnO showed the highest exposed cobalt surface area but had the second highest extent of reduction. For every preparation procedure, the same trend occurred, with the middle extent of reduction resulting in a catalyst with the highest exposed cobalt surface area for that preparation procedure. This phenomenon explains the apparent lack of activity of the ZnO supported catalysts. Prior to reaction work, it was thought that ZnO supported catalysts would yield high FT activities due to the ease with which cobalt reduction took place. The conclusion to be drawn from this is that metal support interaction, a phenomenon with a predominantly negative connotation, is as imperative to the catalyst functioning as a high degree of reducibility is. On their own, neither characteristic is sufficient to achieve the much sought after activity.

Thus ZnO alone is inadequate as a Fischer-Tropsch support. The low surface area of 3.1 m^2/g is insufficient as cobalt agglomeration becomes increasingly more probable. This, together with it's high crystallinity that suppresses metal support interaction, results in a catalyst ill equipped for Fischer-Tropsch synthesis in terms of activity.

Much the same conclusion can be drawn for MnO supported catalysts, however for different reasons than those associated with ZnO. MnO is problematic as a support material due to it's innate ability to alter oxidation states. This characteristic is influential in terms of activity, as the shift of oxidation state of the manganese support enhances the formation of spinel structures at the expense of the zerovalent active cobalt.

Thus SiO_2, chosen as a base case on which to evaluate the ZnO and MnO performance, remains the superior choice of support due to the materials amorphous nature and it's ability to use metal support interaction to promote cobalt dispersion leading to significantly improved activity.

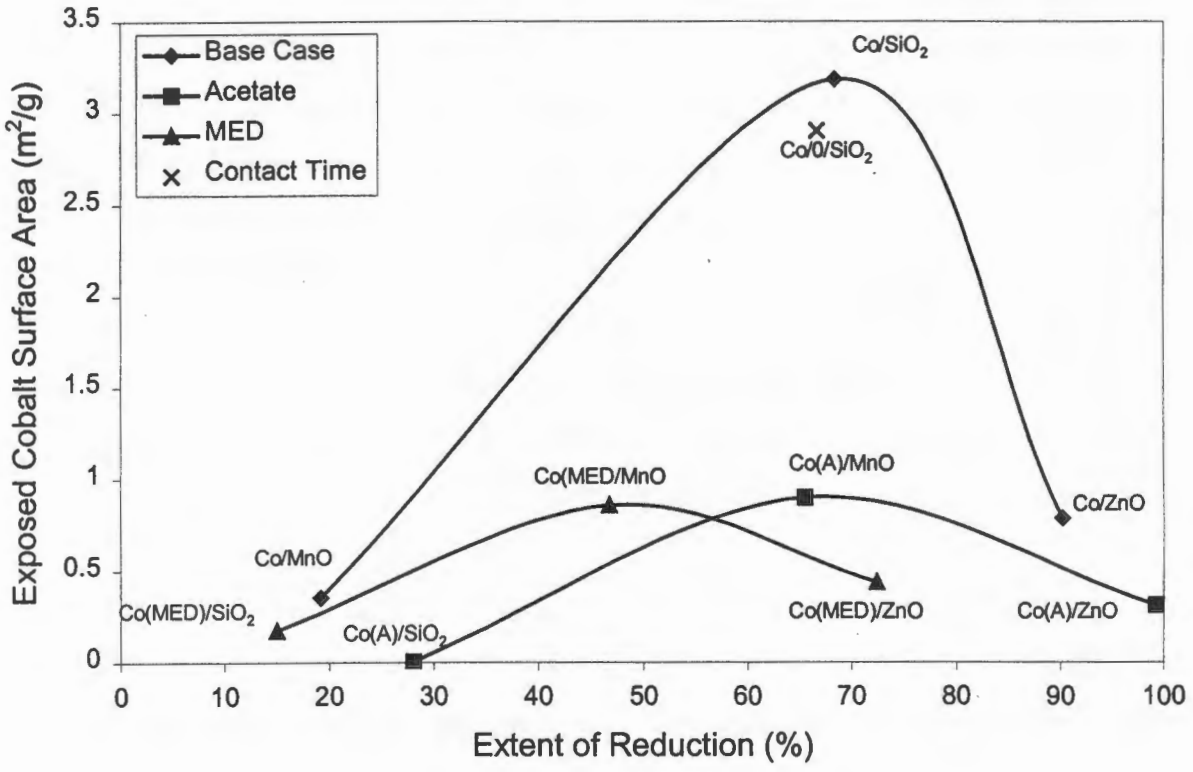

Figure 4.1. Exposed cobalt surface area as a function of the extent of reduction of cobalt obtained during TPR.

4.2 Performance of Supported Cobalt Catalysts

The activity of the catalysts studied varied dramatically with the type of support employed, the choice of cobalt precursor, and the nature of the impregnation solution. For example, changing the cobalt source from cobalt nitrate to cobalt acetate lowered the activity of the SiO_2 supported catalyst by more than 20 times, but almost doubled the activity of the ZnO supported catalyst. The activity of the Fischer-Tropsch catalyst is determined by the number of accessible active sites on the surface. The rate of reaction on each catalytic site is determined by the accessibility of that site, or if easily accessible, then upon the controlling step of the Fischer-Tropsch reaction. This controlling step is thought to be the desorption of the product from the catalytic site. Figure 4.2 shows the relationship between the organic yield obtained through FT reaction and the exposed cobalt surface area for each catalyst measured through hydrogen chemisorption. Clearly low exposed cobalt surface areas result in

inactive catalysts that give low organic yields and visa versa. Consequently as the exposed cobalt surface area increases, the yield of product should also increase. It is logical that this relationship is linear, as more available active sites should coincide with a comparative increase in yield of product. The scatter of points at low yields may arise from the inaccuracy of the hydrogen chemisorption measurements. The three points at high exposed cobalt surface area are from cobalt nitrate supported on SiO_2. From Figure 4.2 it is clear that there exists a significant difference in catalytic activity between the cobalt nitrate on SiO_2 catalysts and the other catalysts prepared. The MnO support resulted in a consistently low activity irrespective of preparation procedure, while the changes in the preparation procedure resulted in significant variances when using the ZnO support.

Changes in the support type resulted in significant variations in the selectivity of each catalyst. These differences stemmed from the interaction between cobalt and the support used. This interaction could be altered by changing the preparation conditions through adjustment of different variables.

The selectivity of each catalyst was strongly dependent upon the interaction between cobalt and support. Hydrogen chemisorption gave information on the reversibility of adsorption of hydrogen on the active sites. Hydrogen adsorption reversibility was calculated as the fraction of hydrogen not removed from the catalyst following 15 minutes of evacuation. Bartholomew and Reuel [1985] equated the degree of reversibility with the strength of metal support interaction. A higher reversibility was seen to be indicative of a stronger metal support interaction. The hydrogen adsorption reversibility is also described as a measure of the strength with which the hydrogen is adsorbed on the cobalt. It is unlikely that different sites offer differing strengths of adsorption. Thus a high hydrogen adsorption reversibility indicates a high degree of readsorption of hydrogen during diffusion out of the catalyst pore structure and is related to the strength of metal support interaction in that strong interaction favours higher cobalt dispersion. The higher dispersion results in a greater availability of zerovalent cobalt attachment points as the hydrogen moves through the pore structure.

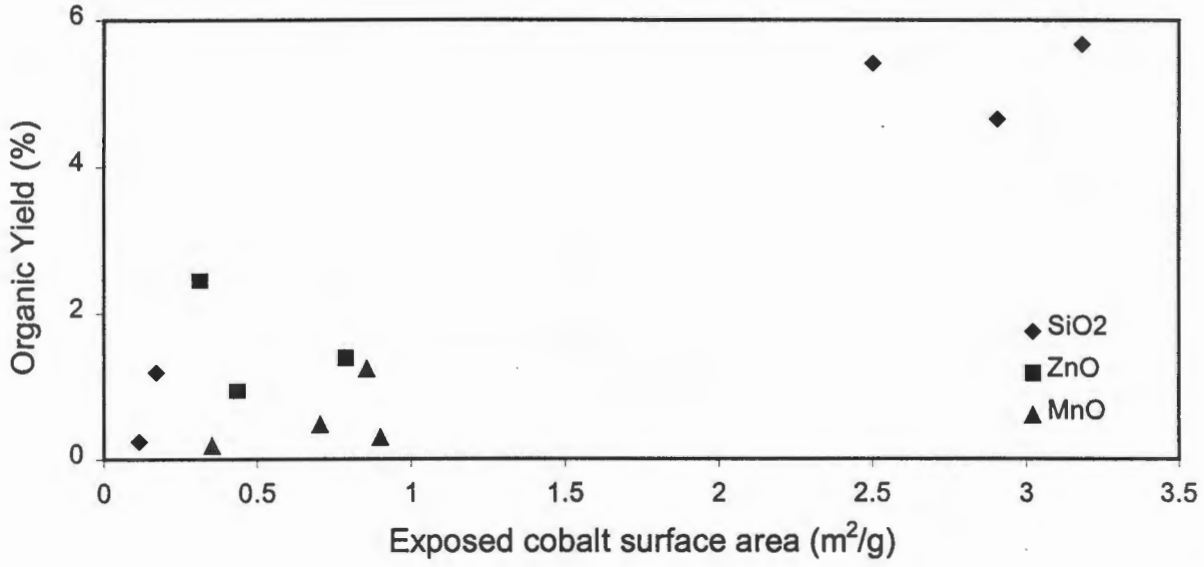

Figure 4.2. Organic yield at steady state as a function of the exposed cobalt surface area obtained from hydrogen chemisorption measurements.

To explain this further, it is necessary to discuss the desorption of hydrogen from active sites. The reversibility of adsorption is an equilibrium process which takes place at a rate that is determined by the temperature and by the concentration of hydrogen on the catalyst surface and in the surrounding atmosphere. The temperature of desorption during chemisorption was fixed at 100°C. The rate of desorption was determined as a function of the reversibility of the catalyst as follows:

Consider hydrogen atoms dissociated on zerovalent cobalt sites on the catalyst surface. Then the following equilibrium would be established between the surface and the gas phase in terms of hydrogen desorption:

$$\theta_H + \theta_H \leftrightarrow H_2 + 2\theta \qquad ...(1)$$

where θ refers to the fraction of the surface that does not have adsorbed hydrogen, θ_H corresponds to the fraction of vacant sites covered with dissociated hydrogen atoms, and H_2

is gas phase hydrogen. It is assumed that each site can only occupy a single hydrogen atom. It follows that the rate at which desorption takes place can be described as follows:

$$-\delta \theta_H / \delta t = k_d \theta_H^2 \quad \ldots(2)$$

where k_d is the intrinsic rate constant of desorption in units of time^{-1}. Rearranging and integrating this expression yields the following time dependence of the hydrogen coverage of the surface:

$$1/\theta_{H,t} - 1 = k_d t \quad \ldots(3)$$

The reversibility is defined as the amount of hydrogen not removed by evacuation relative to the total hydrogen uptake of the catalyst and can be written as follows:

$$\text{Reversibility} = \frac{V_{H2,irr}}{V_{H2,\,total}} \quad \ldots(4)$$

where $V_{H2,irr}$ denotes the volume of hydrogen not removed at time t, while $V_{H2,total}$ refers to the total hydrogen uptake of the catalyst. $V_{H2,irr}$ is not an absolute reversibility. It refers only to the fraction of sites still covered after time t of desorption. It is possible to remove all hydrogen atoms under vacuum if the surrounding atmosphere is free of diatomic hydrogen, as the desorption is time dependent. However during chemisorption, desorbed hydrogen passes through the pore system to the surrounding atmosphere. As this happens, the desorbed hydrogen has further opportunity to readsorb on other sites within the pore structure. Consequently each site experiences an intrinsic desorption constant, k_d, but the catalyst sees an overall desorption constant, $k_{d,observed}$, which includes the readsorption rate constant.

θ_H also describes the fraction of surface sites occupied by hydrogen atoms at time t such that the following expression arises:

$$\theta_H = \frac{V_{H2,irr}}{V_{H2,\,total}} = \text{Reversibility} \quad \ldots(5)$$

Combining equations (3) and (5), the following expression for the rate of desorption ($k_{d,observed}$) as a function of reversibility and time is attained:

$$k_{d,observed}\ [\text{units} : \text{time}^{-1}] = \frac{1 - \text{Reversibility}}{t \,.\, \text{Reversibility}} \quad \ldots(6)$$

Thus the reversibility can be seen to be a function of time and the overall rate at which hydrogen desorbs during this time. Consequently, the higher the rate of readsorption of hydrogen, the lower the observed rate constant will be, resulting in a higher reversibility of adsorption. As reversibility was measure after 15 minutes, the t term was constant for all reversibility calculations. Thus the reversibility was only a measure of the observed rate constant of desorption for each catalyst. The above discussion gives physical meaning to the term reversibility. It remains to describe the implications of this reversibility of hydrogen adsorption on the performance of the catalyst under FT conditions.

The Fischer-Tropsch synthesis reaction consists of a polymerisation reaction that combines a complex system of primary and secondary reaction steps to attain a product rich in a wide variety of organic species. It is this broad spectrum of products that necessitates an understanding of the principle factors governing specific products within this spectrum so as to create an environment conducive to increasing their selectivity. Earlier, the metal surface area was discussed, and it was shown that generally the higher the exposed cobalt surface area, the higher the activity of the catalyst would be. However the availability of cobalt sites is not enough to explain the acquired product spectrums achieved. It is here that the reversibility of hydrogen adsorption may play a significant role. As a high reversibility of hydrogen adsorption was shown to denote a higher degree of readsorption of hydrogen atoms to the surface, it would seem logical that the following changes would result in the product spectrum. The increased opportunity for readsorption on the surface through greater distribution of active phase through the support pore structure would increase secondary reaction activity. Consequently the hydrogenation activity and secondary isomerisation activity would increase. From the FT product spectrums obtained, it was noted that the changes in these selectivity parameters following alterations to the preparation procedure

paralleled the change in reversibility for a given support. This was true for all catalysts prepared with the exception of Co(MED)/SiO_2 and Co(MED)/MnO where the opposite occurred.

The reversibility effect was especially prevalent over the ZnO supported catalysts. The hydrogen adsorption reversibility over Co/ZnO was the lowest of all catalysts prepared at 39.1%. Following impregnation of cobalt acetate on ZnO to yield the Co(A)/ZnO catalyst, the reversibility increased from 39.1% to 67.1%. This corresponded to a decrease in the α-olefin percent of the C_5 fraction from 77.21% to 56.81%, while the n-paraffin fraction increased from 22.13% to 28.17%. The double bond shift activity increased resulting in an increase in secondary linear olefins from 4.06% to 13.02% of the C_5 fraction. The chain growth probability dropped from 0.81 to 0.79. Exactly the same trends were observed following addition of MED to the impregnation solution.

Bartholomew and Reuel [1985] equated the degree of reversibility with the strength of metal support interaction. On this basis, the SiO_2 supported catalysts should show the highest hydrogen adsorption reversibilities. This was observed for the base case catalysts prepared. Thus the reversibility of adsorption may in turn be partly determined by the crystallinity of the support material, with a more amorphous structure enhancing the metal support interaction and consequent reversibility.

CHAPTER 5

CONCLUSIONS

5. Conclusions

SiO_2, ZnO and MnO were investigated as supports for cobalt Fischer-Tropsch catalysts. SiO_2 is well established as a support, but little work has taken place with respect to the other two support types. Cobalt nitrate impregnated on each of the three supports in aqueous medium served as a base case with which to compare variations in the catalyst precursor, type of impregnation solution, pH of impregnation solution and the contact time between the impregnation solution and the support. It was shown that cobalt nitrate on SiO_2 impregnated in a water medium gave the best activity under Fischer-Tropsch conditions, a result of the factors discussed below.

The physical characteristics of the three supports were seen to vary significantly. The crystallinity of the supports, obtained through X-ray diffractometry, differed greatly. The degree of crystallinity was lowest for the amorphous SiO_2 support, increasing for MnO, with ZnO showing the by far the highest degree of crystallinity. The degree of crystallinity has an important role to play in determining the strength of interaction between cobalt and support. The higher degree of crystallinity of ZnO resulted in a catalyst with weak and possibly non-existent metal support interaction. The net effect was to heighten the degree of reducibility of the supported cobalt precursor, a favourable result of the low interaction. The opposite effect was noted over SiO_2 and MnO. Both SiO_2 and MnO showed a more amorphous structure, leading to stronger metal support interaction. This interaction decreased the degree of reduction of the supported cobalt. In the case of SiO_2, the formation of cobalt silicate species was largely responsible for the lower reducibility. With the MnO support, the presence of either nitric acid or the decomposition of the nitrate precursor created a strong oxidising environment that lead to the oxidation of the MnO to a higher oxidation state. Where this oxidation was noted, the formation of spinel structures between the Co^{2+} and Mn^{3+} species resulted lowering the degree of reducibility of the supported cobalt.

It was seen that the presence of a degree of metal support interaction was a key factor in determining the activity of the catalyst. Metal support interaction results in the binding of the cobalt to the support surface and lowers the cobalt mobility during drying and activation. In so doing cobalt dispersion is maintained increasing the exposure of the active cobalt phase to

reactant under Fischer-Tropsch conditions. Over ZnO, the absence of metal support interaction resulted in agglomeration of the cobalt lowering the exposed cobalt surface area available for reaction. On this basis, it is clear that catalyst activity is optimised through achieving a high degree of cobalt reduction while maintaining dispersion through the presence of metal support interaction. Of the catalysts prepared, cobalt nitrate impregnated on SiO_2 (Co/SiO_2) combined these two factors to give the highest activity.

A second physical characteristic important in determining the strength of interaction between the cobalt precursor and the support is the zeta potential of the support at the pH of impregnation, where the zeta potential is a measure of the net surface charge on the support. It was found that the point of zero charge (PZC) of the three supports took place at significantly different pH's. The PZC of SiO_2 occurred between a pH of 2 and 5, while for ZnO and MnO, the PZC was at a pH of 8 and 4 respectively. The net surface charge at a pH below the PZC was positive for each support, and vice versa.

For the base catalysts, the activity decreased from Co/SiO_2 to Co/ZnO to Co/MnO coinciding with the exposed metal surface area calculated through hydrogen chemisorption. Co/ZnO showed significantly less secondary product formation under Fischer-Tropsch synthesis conditions, a consequence of the lower reversibility of adsorption indicating less opportunity for readsorption of terminated primary product during diffusion out of the catalyst pore structure.

The effect of precursor was studied by changing from cobalt nitrate to cobalt acetate. The use of the acetate precursor resulted in the presence of Co^{2+} on the support surface following drying and calcination as the oxidizing environment created through acetate decomposition was too weak to shift divalent cobalt to the trivalent form. The extent of reduction increased for the ZnO and MnO supported catalysts, and decreased dramatically for the SiO_2 catalyst as a result of increased cobalt silicate formation. Activities improved for the ZnO and MnO supported catalysts, coinciding with higher secondary hydrogenation and isomerisation activity as a result of higher reversibilities of adsorption for both catalysts.

MED addition to the impregnation solution resulted in the complexation of Co^{2+} ions in solution with the strong field MED ligands, replacing water ligands initially surrounding the

cobalt in solution. As MED is a strong field ligand, interaction between cobalt and the support was decreased lowering the ease of attachment of cobalt to the support surface. In so doing, the influence of the support was lowered, with reduction taking place as a single peak. The extent of reduction was lower over SiO_2 and ZnO, but increased over MnO following the addition of MED. The dispersion and exposed metal surface area followed the same trend, both decreasing over SiO_2 and ZnO, but increasing over MnO. MED addition enhanced the secondary hydrogenation and isomerisation activity over SiO_2 and ZnO, but lowered the same activity over MnO.

The pH, adjusted with nitric acid for cobalt nitrate impregnation and with acetic acid for cobalt acetate impregnation, altered the net surface charge of the support surface bringing about the following changes in physical and performance characteristics. The extent of reduction of cobalt nitrate on SiO_2 dropped with nitric acid addition, while the cobalt dispersion improved. Performance under Fischer-Tropsch conditions showed minor differences in terms of activity and selectivity, with acid addition showing less secondary reaction activity. The addition of acetic acid to cobalt acetate on SiO_2 lowered the impregnation pH from 6.5 to 4 resulting in an organic yield twice that prior to acid addition, a lower selectivity to the C_{1+2} fraction, and slightly lower secondary activity. The addition of nitric acid to cobalt nitrate impregnated on MnO resulted in the further oxidation of the MnO support already observed without acid addition. It was found that both the decomposition of the nitrate precursor as well as the presence of nitric acid in the impregnation solution resulted in the oxidation of the MnO support. As a result, the addition of nitric acid had little effect on the extent of reduction of the cobalt, but dramatically improved the exposed cobalt surface area which lead to increased activity. The selectivity remained largely unaffected by nitric acid addition.

It was found that the pH of the impregnation solution changed with the length of contact time between support and the impregnation solution, especially for cobalt nitrate impregnation. The increased pH was a result of charge equilibration between the support and the cobalt nitrate. The contact time between support and impregnation solution had little effect upon the physical and performance characteristics of cobalt nitrate impregnated on SiO_2. The extent of reduction was lower for the shorter contact time, while the cobalt dispersion improved. The hydrogen adsorption reversibility also improved coinciding with a higher chain growth

probability. The overall activity was lower for the shorter contact time, while the selectivity of the C_5 fraction was generally unaffected.

Investigation of the time on stream behaviour showed that hydrogenation activity was higher during the early reaction stages as a result of the hydrogen coverage of the catalyst following reduction. With increasing time on stream, the α-olefin fraction increases as carbon monoxide competes for adsorption sites.

REFERENCES

References

Adesina, A. A., *Appl. Catal.*, **138** (1996) 345-367.

Ali, S., Chen, B. and Goodwin, J. G., Jr., *J. Catal.*, **157** (1995) 35.

Amelse, J. A., Butt, J. B. and Schwartz, L. J., *J. Phys. Chem.*, **82** (1978) 558.

Anderson, R. B., in "Catalysis IV", P. H. Emmett (Editor), Reinhold, New York, 1956.

Anderson, R. B., Seligman, B., Schulz, J. F., Kelly, R. and Elliott, M. A., *Ind. Eng. Chem.*, **44** (1952) 391.

Anderson, R. B., The Fischer-Tropsch Synthesis, Academic Press, New York, (1984).

Antoniu, A. A., *J. Phys. Chem.*, **68** (1964) 2754.

Arnouldy, P. and Moulijn, J. A., *J. Catal.*, **93** (1985) 38.

Badische Analin Soda Fabriek, *German Patent 293*, (1913) 787.

Bartholomew, C. H. and Reuel, R. C., *Appl. Catal.*, **73** (1991) 65.

Brötz, W., *Z. Elektrochemie*, **5** (1949) 301.

Brunelle, J. P., *Pure Appl. Chem.*, **50** (1978) 1211.

Bukur, B. B., Nowicki, L., Manne, R. K., and Lang, X., *J. Catal*, **155** (1995) 366.

Burwell, R. L., Jr., Pearson, R. G., Haller, G. L., Tjok, P. B. and Chock, S. P., *Inorg. Chem.*, **4** (1965) 1123.

Che, M. and Bonneviot, L., *Pure and Appl. Chem.*, **60** (1988) 1369.

Che, M. and Bonneviot, L., Successful Design of Catalysts. Future Requirements and Development, T. Inui (ed.), Elsevier, Amsterdam, (1988) 147.

Che, M., in Proc. 10^{th} Int. Congr. on Catalysis, Budapest, 1992, Guzci, L., Solymosi, F., and Tetteny, P., eds., Elsevier, Amsterdam, (1993) 31.

Chin, R. L. and Hercules, D. M., *J. Phys. Chem.*, **86** (1982) 3079.

Chin, R. L. and Hercules, D. M., *J. Phys. Chem.*, **86** (1982) 360.

Claeys, M., Schulz, H. and Harms, S., Studies in Surface Science and Catalysis, Elsevier, **107** (1997) 193.

Coenen, J. W. E., *Appl. Catal.*, **54** (1989) 65

Coulter, K. E. and Sault, A. G., *J. Catal.*, **154** (1995) 56.

Deo, G., Wachs, I. E., *J. Phys. Chem.*, **95** (1991) 5889.

Dictor, R. A. and Bell, A. T., *J. Catal.*, **97** (1986) 121.

Donnelly, T. J. and Satterfield, C. N., *Appl. Catal.*, **52** (1989) 93.

Dry, M. E., in "Catalysis Science and Technology", Anderson, J. R. and Boudart, M. (eds.), New York, **1** (1981) 159.

Dry, M. E., in "Catalysis Science and Technology", Anderson, J. R. and Boudart, M. (eds.), New York, **1** (1981) 160.

Dry, M. E., in "The Fischer-Tropsch Synthesis", Research Division, Sasol, (1981).

Egiebor, N. O. and Cooper, W. C., *Appl. Catal.*, **14** (1985) 323.

Ekerdt, J. G. and Bell, A. T., *J. Catal.*, **58** (1979) 170.

Fenelov, V. B., Neimark, A., Kheifets, L. A. and Samakhov, A. A., in "Preparations of Catalysts II", Delmon, B., Grange, P., Jacobs, P. A. and Poncelet, G. (eds.), Amsterdam, Elsevier, (1979) 223.

Fischer, F. and Tropsch, H., *Brennst. Chem.*, **4** (1923) 276.

Foger, K., in "Catalysis Science and Technology", Anderson, J. R. and Boudart, M., **6** (1985) 228.

Friedman, S. and Schlesinger, M. D., *US Bur. Mines Bull.*, (1964) 614.

Frohning, C. D., Kolbel, H., Ralek, M., Rottig, W., Schur, F. and Schulz, H., Fischer-Tropsch-Synthese, Chemierohstoffe aus Kohle, Falbe J. (ed.), Thieme Verlag, Stuttgart, (1997).

Gall, D., Gibson, E. J. and Hall, C. C., *J. Appl. Chem.*, **2** (1952) 371.

Gaube, J. and Hochstadt, G., *Chem. Ing. Tech.*, **50** (1978) 627.

Goodwin, J. G., Jr., *Prep. ACS Div. Petr. Chem.*, **36** (1991) 156.

Hilmen, A. M., Schanke, D. and Holmen, A., *Catal. Lett.*, **38** (1996) 143.

Hilmen, A. M., Schanke, D. and Holmen, A., in "Natural gas Conversion IV", Studies in Surface Science and Catalysis, **107** (1997) 237.

Huff, G. A. and Satterfield, C. N., *J. Catal.*, **85** (1984) 370.

Huffman G. P., Shah, N., Zhao, J., Huggins, F. E., Hoost, T. E., Halvorsen, S. and Goodwin J. G. Jr., *J. Catal.*, **151** (1995) 17.

Iglesia, E., *Appl. Catal.*, **161**, (1997) 59.

Iglesia, E., in "Natural Gas Conversion IV", Studies in Surface Science and Catalysis, Amsterdam, Elsevier, **107** (1997) 153.

Iglesia, E., Reyes, S. C. and Madon, R. J., *J. Catal.*, **129** (1991) 238.

Iglesia, E., Reyes, S. C., Madon, R. A. and Soled, S. L., *Adv. Catal.*, **39** (1993).

Iglesia, E., Soled, S. L., and Fiato, R. A., *J. Catal.*, **137** (1992) 212.

Iglesia, E., Soled, S. L., Rocco, A. F. and Via, G. H., *J. Catal.*, **143** (1993) 345.

Jordan, D. S. and Bell, A. T., *J. Catal.*, **107** (1987) 338.

Jordan, D. S. and Bell, A. T., *J. Catal.*, **108** (1987) 63.

Jung, H. and Thomson, W. J., *J. Catal.*, **134** (1992) 654.

Kogelbauer, A., Goodwin, J. G. Jr., and Oukaci, R., *J. Catal.*, **160** (1996) 125.

Kogelbauer, A., Weber, J. C. and Goodwin, J. G. Jr., *Catal. Lett.*, **34** (1995) 259.

Komaya, T. and Bell, A. T., *J. Catal.*, **146** (1994) 237.

Konig, L. and Gaube, J., *Chem. Ing. Tech.*, **55** (1983) 14.

Kotter, M. and Riekert, L., in "Preparations of Catalysts II", Delmon, B., Grange, P., Jacobs, P. A. and Poncelet, G. (eds.), Amsterdam, Elsevier, (1979) 51.

Kuipers, E. W., Scheper, C., Wilson, J. H., Vinkenburg, I. H. and Oosterbeek, H., *J. Catal.*, **158** (1996) 288.

Kuipers, E. W., Vinkenburg, I. H. and Oosterbeek, H., *J. Catal.*, **152** (1995) 137.

Luyten, L. and Jurgens, J. C., *Bull. Soc. Chim. Belg.*, **54** (1945) 303.

Madon, R. J., Reyes, S. C. and Iglesia, E., *J. Phys. Chem.*, **95** (1991) 7795.

Martin, F., *Chem Fabriek*, **12** (1939) 233.

Mehanjiev, D. and Dimitrova, P., *Commun. Dep. Chem. Bulg. Acad. Sci.*, **14** (1981) 330.

Mehanjiev, D., Dimitrova, P. and Dyakova, B., *Commun. Dep. Chem. Bulg. Acad. Sci.*, **17** (1984) 204.

Ming, H. and Baker, B. G., *Appl. Catal.*, **123** (1995) 23.

Newsome, D. S., *Catal. Rev.-Sci. Eng.*, **21** (1980) 275.

Parks, G. A. and DeBruyn, P. L., *J. Phys. Chem.*, **66** (1962) 967.

Pichler, H., *Advances in Catalysis*, Vol. 4, Frankenburg, Komarewsky and Rideal (eds.), New York, Academic Press Inc., (1952).

Pichler, H., Schulz, H. and Elstner, M., *Brennst. Chem.*, **48** (1967) 78.

Puskas, I., Fleisch, T. H., Hall, J. B., Meyers, B. L. and Roginski, R. T., *J. Catal.*, **134** (1992) 615.

Raupp, G. B. and Delgass, W. N., *J. Catal.*, **58** (1979) 348.

Regaini, V., Carli, R., Bianchi, C. L., Lorenzetti, D., Predieri, G. and Moggi, P., *Appl. Catal.*, **139** (1996) 31.

Reuel, R. C. and Bartholomew, C. H., *J. Catal.*, **85** (1984) 63.

Rosch, S., Dissertation, University of Karlsruhe, (1980).

Royo, C., Percides, J. M., Monzon, A. and Santamaria, J., *Ind. Eng. Chem. Res.*, **35** (1996) 1813.

Sabatier, P. and Senderens, J. B., *Compte Rendus Hebd.*, **134** (1902) 514.

Schulz, H., Beck, K. and Erich, E., *Methane Conversion*, Elsevier, (1988) 457.

Sewell, G. S., O'Connor, C. T. and van Steen, E., Appl. Catal., **125** (1995) 99.

Sewell, G. S., Ph. D. Thesis, University of Cape Town, (1996).

Smith, G. W. and Jacobson, H. W., *J. Phys. Chem.*, **60** (1956) 1008.

Vada, S., Chen, B. and Goodwin, J. G., Jr., *J. Catal.*, **153** (1995) 224.

Van Berge, P. J. and Everson, R. C., in "Natural Gas Conversion IV", Studies in Surface Science and Catalysis, **107** (1997) 207.

Van Schalkwyk, E., M. Sc. Thesis, University of Cape Town, (1998).

Vannice, M. A. and Garten, R. L., *J. Catal.*, **86** (1980) 242.

Vannice, M. A., *J. Catal.*, **37** (1975) 449.

Vannice, M. A., *J. Catal.*, **50** (1977) 228.

van't Blik, H. F. J., Koningsberger, D. C. and Prins, R. J., *J. Catal.*, **97** (1986) 210.

Wojchiechowski, B. W, *Cat. Rev. Sci. Eng.*, **30**(4) (1988) 629.

Wojchiechowski, B. W. and Sarup, B., *Can. J. Chem. Eng.*, **66** (1988) 831.

Zsoldos, Z., Garin, F., Hiliare, L. and Guzci, L., *Cat. Lett.*, **33** (1995) 39.

APPENDICES

Appendix I

TPR calibration and Sample Calculation

The hydrogen concentration of the H_2 in N_2 gas mixture was calculated using a known mass of CuO, according to the following reaction stoichiometry:

$$CuO + H_2 \rightarrow Cu + H_2O$$

The CuO was placed in a quartz reactor described previously, and secured in the furnace. The thermal conductivity of 60ml/min N_2 and 60 ml/min H_2 in N_2 were measured consecutively relative to a reference nitrogen gas stream flowing at 60 ml/min. The difference in the TCD measurement between the N_2 and the H_2 in N_2 gas streams yielded the thermal conductivity of the hydrogen present in the H_2 in N_2 gas mixture. During the TPR run, the thermal conductivity of the exit stream is recorded. As hydrogen was consumed during copper reduction, the thermal conductivity of the exit gas changed reflecting the hydrogen consumption.

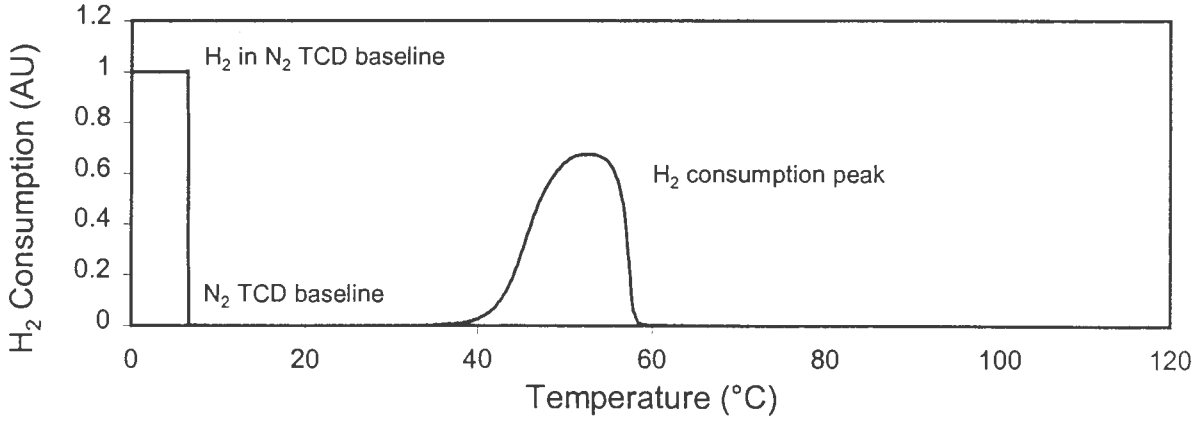

The hydrogen consumed in terms of the logged thermal conductivity acquired data was calculated using the trapezoidal rule given by the following expression:

$$H_2 \text{ consumption} = \Sigma_n (s_{n+1} + s_n) \times (t_{n+1} + t_n) \times 0.5$$

where s is the value logged for a given TCD reading and t is the time elapsed in minutes. The above expression was converted into mmols of hydrogen consumed on the assumption that the hydrogen concentration was 5%. On this basis, 1.020 mmols of hydrogen were consumed. However, the mass of CuO used was 0.107g, giving 1.340 mmols of Cu. As the stoichiometry of complete CuO reduction requires a 1:1 ratio of hydrogen to copper, the first guess of 5% for the hydrogen concentration was seen to be inaccurate. The correct hydrogen concentration was calculated from the following expression:

$$H_2 \text{ concentration} = 1.340 \times 5\% = 6.6 \text{ vol\% } H_2 \text{ in } N_2.$$

All TPR runs used a similar procedure to obtain the hydrogen consumption, however for all other runs a hydrogen concentration of 6.6% was used.

Appendix II

Hydrogen Chemisorption Sample Calculation

Hydrogen chemisorption was used to measure the number of exposed cobalt atoms of the reduced catalyst. As the cobalt content of the catalyst was known, the metallic dispersion and the average particle diameter could be calculated. Chemisorption was carried out twice at 100°C. The first chemisorption measurement was followed by a 15 minute evacuation period during which time weakly adsorbed hydrogen desorbed. After this the hydrogen uptake of the catalyst was remeasured. From these two chemisorption measurements, the amount of strongly bound hydrogen was calculated.

The hydrogen chemisorption data obtained for the Co/SiO_2 catalyst will be used below to show the calculation procedure.

The total hydrogen uptake was 0.865 cm^3/g_{cat}, while the amount of hydrogen not removed through evacuation was 0.570 cm^3/g_{cat}. According to Bartholomew et al. [1980], hydrogen desorption is dissociative on cobalt. Accordingly the total number of exposed cobalt atoms can be obtained from the following calculation:

$$N_{cobalt} = (0.865\ cm^3H_2/g_{cat})/(22414\ cm^3H_2/mol\ H_2) \cdot (2\ mol\ Co/mol\ H_2) \cdot N_{Av}$$
$$= 4.648 \times 10^{19}\ atoms\ Co/g_{cat}$$

where N_{Av} is Avogadro's number. Using a site density for fcc cobalt of 14.6 $atoms/nm^2$ [Bartholomew et al., 1980], the metallic surface area can be calculated using the following relationship:

$$Surface\ Area = (4.648 \times 10^{19}\ atoms)/(14.6\ atoms/nm^2) \cdot 10^{-18}\ m^2/nm^2$$
$$= 3.18\ m^2/g_{cat}$$

The reversibility of hydrogen adsorption was is calculated as a percentage of the total hydrogen uptake that is strongly adsorbed, according to the following calculation:

Reversibility of adsorption = $(0.570\ cm^3/g_{cat}) / (0.865\ cm^3/g_{cat})$. 100%

= 65.8%

The metallic dispersion is defined as the number of exposed cobalt atoms relative to the total number of cobalt atoms present in the catalyst sample. As the extent of reduction was less than 100% for all catalyst prepared in this study, the dispersion calculations were based on the amount of reduced cobalt and not on the total amount of cobalt in the sample. The number of reduced atoms in the sample were obtained from extent of reduction calculations obtained from TPR work. The dispersion obtained for Co/SiO_2 was calculated as follows:

Dispersion = $(4.648 \times 10^{19}$ exposed Co atoms) / $(6.976 \times 10^{20}$ reduced Co atoms) . 100%

= 6.66 %

The average crystallite size (or average diameter) of the cobalt particles was calculated assuming spherical clusters. The volume of reduced cobalt present was obtained as follows using a density of 8.9 g/cm^3 [Perry and Green, 1984]:

Volume = $(6.976 \times 10^{20}$ atoms / $N_{Av})$. (58.9 g/mol / 8.9 g/cm^3) . $10^{-6}\ m^3 / cm^3$

= $7.665 \times 10^{-9}\ m^3$

From the volume to surface area relationship, the average crystallite size was calculated as follows:

Average particle diameter = $6 . (6.533 \times 10^{-9}\ m^3/g_{cat}) / (3.183\ m^2/g_{cat}) . 10^9$ nm / m

= 14.45 nm

Appendix III

Sample calculation of conversion, yield and selectivity of the Fischer-Tropsch Synthesis reaction

The syngas feed of CO and H_2 were flowed over the catalyst in a 1 : 2 ratio. Downstream of the reactor a stream of 0.121% of toluene in nitrogen was flowed as an inert internal standard for both the conversion and organic yield calculations. The conversion of carbon monoxide and hydrogen was calculated using a TCD gas chromatograph following calibration. The calibration was done by injecting known percentages of a H_2, CO and N_2 gas mixture and noting the TCD response of for each gas. The relative response factor for CO and H_2 were obtained by dividing the response factor of the gas by the response factor of the nitrogen mixture.

Using the relative response factors, the areas obtained upon integration of the TCD signal following injection of gas from the product stream could be converted to molar ratios. As the molar fraction of the bypass was measured in the same way prior to the start of reaction, comparison of the bypass and reaction streams allowed calculation of the carbon monoxide and hydrogen conversions as illustrated in the following table for the Co/SiO_2 catalyst after 1.5 hours of reaction:

Component	Standard		Bypass Flow	Product Stream	Conversion
	Area (a.u.)	Rel. Response	Molar ratio	Molar ratio	(%)
H_2	375268	11.890	1.026	10.928	10.43
N_2	31561	1	1	1	
CO	31915	1.011	0.539	0.498	8.51

The yield of total organic product and the selectivity of the product were determined using an FID gas chromatograph. The fraction of each organic product could be evaluated because the molar fraction of toluene in the product stream was known. As the relative response factors for all products formed were the same, easy evaluation of the relative amounts of each

product was possible. The yield of organic product was obtained from the following expressions:

$$\text{Yield} = [(\text{Area}_{HC} / \text{Area}_{Tol}).(n_{c,tol} / n_{N2})] / [n_{CO} / n_{N2}] \cdot 100\%$$

where Area_{HC} : Area of hydrocarbon product in the FID GC trace

Area_{Tol} : Area of toluene in the FID GC trace

$n_{c,tol}$: molar flow of carbon in standard toluene in N_2 gas mixture

n_{N2} : Molar flow of N_2 in standard toluene in N_2 gas mixture

n_{CO} : Molar flow of carbon monoxide in syngas feed stream

n_{N2} : Molar flow of standard N_2 gas mixture.

The yield calculated for Co/SiO_2 was as follows:

$$\text{Yield} = [(3.559).(0.008576)] / [0.537] \cdot 100\%$$
$$= 5.67\%$$

Selectivity calculations were performed on a molar basis from the gas chromatograph traces. The area of each peak was on a carbon basis. To obtain the number of moles, the peak was divided by the carbon number associated with that particular product to obtain an area per molecule measurement. From this the selectivity of that particular specie could be obtained as follows:

$$\text{Selectivity} = [\text{Area}_{I,Nc} / N_C] / [\text{Area}_{Total,Nc} / N_C] \cdot 100\%$$

where N_C : Carbon number

$\text{Area}_{I,Nc}$: Area of specie i in the carbon number fraction N_C

$\text{Area}_{Total,Nc}$: Area of total organic product of carbon number N_C

The rate of formation of organic product in each carbon number was calculated as follows:

$$\text{Formation Rate} = [(\text{Area}_{HC,Nc} / N_C) \cdot F_{Tol}] \cdot [\text{Area}_{Tol} / N_C]$$

where N_C : Carbon number

$Area_{HC,Nc}$: Area of total hydrocarbons of carbon number N_C

F_{Tol} : Molar flow of toluene

$Area_{Tol}$: Area of toluene

Appendix IV

TEM Photographs for $Co/1/SiO_2$, $Co(A)/4/SiO_2$, $Co/4/MnO$ and $Co/0/SiO_2$

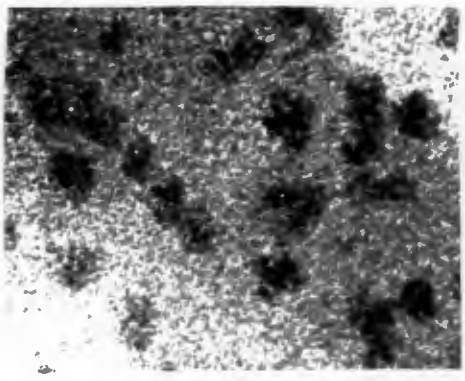

$Co/1/SiO_2$

$Co(A)/4/SiO_2$

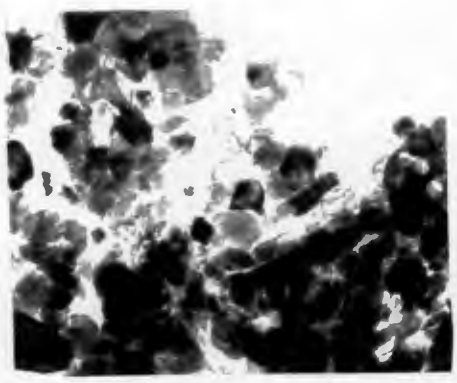

$Co/4/MnO$

$Co/0/SiO_2$

Appendix V

Reaction Data for Fischer-Tropsch Synthesis

Base Case Catalysts

Co/SiO_2	Reaction Time: 14hr50min										
Carbon Number Cn	A_Paraffin	A_par/Cn	A_Olefin	A_ole/Cn	Log(X_{Cn}) mol%	Total Area	A_α-olefin	$X_{\alpha\text{-olefin}}$ mol%	X_{olefin} mol%	X_{Cn_total} carbon%	Rate.10^5 (mmol/min)
1	876267	876267			1.73	876267				15.0	1952.3
3	424046	141349			0.94	424046				7.2	316.5
4	133361	33340	399033	99758	0.91	532394	343015	86.0	75.0	9.1	298.1
5	154186	30837	382730	76712	0.82	537745	307226	80.1	71.3	9.2	240.8
6	167398	27900	335934	57210	0.72	510656	225261	65.6	67.2	8.7	190.6
7	186493	26642	268660	40185	0.61	467785	136607	49.3	60.1	8.0	149.6
8	199088	24886	201822	27049	0.50	415478	72690	33.6	52.1	7.1	116.3
9	216416	24046	134100	15496	0.38	355877	30348	21.8	39.2	6.1	88.5
10	202482	20248	78929	9931	0.27	301793	11373	11.5	32.9	5.2	67.6
11	184920	16811	44366	5529	0.14	246836	5522	8.9	25.1	4.2	50.2
12	146149	12179	19402	2268	-0.05	173368	2397	8.8	15.7	3.0	32.4
13	115521	8894	8165	1313	-0.20	132685	1191	7.0	12.9	2.3	22.9
14	110399	7886	3642	505	-0.29	117475	568	8.0	6.0	2.0	18.8
15	133036	8869	1556	159	-0.26	135423			1.8	2.3	20.2

Co/ZnO	Time: 26hr00min										
Carbon Number Cn	A_Paraffin	A_par/Cn	A_Olefin	A_ole/Cn	Log(X_{Cn}) mol%	Total Area	A_α-olefin	$X_{\alpha\text{-olefin}}$ mol%	X_{olefin} mol%	X_{Cn_total} carbon%	Rate.10^5 (mmol/min)
1	273425	273425			1.83					20.6	622.5
3	67725	22575			0.74	67725				5.1	51.4
4	17499	4375	58694	14674	0.67	76193	55293	95.9	77.0	5.8	43.4
5	16915	3383	55290	11668	0.57	75205	55184	94.7	77.5	5.7	34.2
6	18444	3074	55157	9360	0.49	74601	51106	91.0	75.3	5.6	28.3
7	20257	2894	50637	7234	0.40	70894	43425	85.8	71.4	5.4	23.1
8	22570	2821	43998	5500	0.31	66568	34568	78.6	66.1	5.0	18.9
9	24469	2719	35377	3931	0.21	59846	24469	69.2	59.1	4.5	15.1
10	28942	2894	27774	2843	0.15	55716	15179	54.7	49.0	4.3	13.1
11	36177	3289	20019	2015	0.12	55196	8421	42.1	35.6	4.4	12.1
12	45291	3774	14184	1597	0.12	59475	4401	31.0	23.8	4.9	12.2
13	45549	3504	9375	992	0.04	54924	2531	27.0	17.1	4.4	10.2
14	36789	2771	5524	553	-0.09	44413	1088	19.3	12.7	3.5	7.6
15	34764	2318	3993	359	-0.18	38757	877	22.0	10.3	3.0	6.1

Co/MnO			Reaction Time : 22h30min								
Carbon Number Cn	A_Paraffin	A_par/Cn	A_Olefin	A_ole/Cn	Log(X_{Cn}) mol%	Total Area	A_α-olefin	$X_{\alpha\text{-olefin}}$ mol%	X_{olefin} mol%	X_{Cn_total} carbon%	Rate.10^5 (mmol/min)
1	66660	66660			1.84	66660				27.5	108.8
3	14000	4667			0.70	14000				5.9	7.7
4	7581	1895	18271	4568	0.84	25852	14772	80.8	70.7	10.9	10.7
5	6772	1354	14984	2997	0.66	21756	11390	76.0	68.9	9.1	7.2
6	6894	1149	12629	2105	0.54	19523	7694	60.9	64.7	8.2	5.4
7	6848	978	10147	1522	0.42	16995	4413	43.5	59.7	7.3	4.2
8	7289	911	7010	1039	0.32	14299	2310	33.0	49.0	6.5	3.2
9	7877	875	5478	678	0.22	13355	1623	29.6	41.0	5.9	2.6
10	7057	706	3365	460	0.09	10422	601	17.9	32.3	4.9	1.9
11	6621	602	2272	322	-0.01	8893	459	20.2	25.5	4.3	1.5
12	6434	536	1312	155	-0.13	7746			16.9	3.5	1.1
13	5742	442	1000	77	-0.26	6742			14.8	2.8	0.9
14	4455	318			-0.47	4455				1.9	0.5
15	3100	207			-0.66	3100				1.3	0.3

Effect of Cobalt Acetate

Co(Ac)/SiO_2			Reaction Time : 13h31min								
Carbon Number Cn	A_Paraffin	A_par/Cn	A_Olefin	A_ole/Cn	Log(X_{Cn}) mol%	Total Area	A_α-olefin	$X_{\alpha\text{-olefin}}$ mol%	X_{olefin} mol%	X_{Cn_total} carbon%	Rate.10^5 (mmol/min)
1	194129	194129			1.95	194129				64.0	346.9
3	18000	6000			0.44	18000				5.9	10.7
4	5768	1442	14706	3677	0.37	20474	10630	72.3	71.8	6.7	9.1
5	5716	1143	11310	2368	0.21	17026	6397	56.6	66.4	5.8	6.3
6	5963	994	9463	1577	0.08	15426	3378	35.7	61.3	5.1	4.6
7	6267	895	7252	1264	0.00	13519	1689	23.3	53.6	5.0	3.9
8	6282	785	4853	782	-0.14	11135	579	11.9	43.6	4.1	2.8
9	5900	656	2800	478	-0.28	8700			32.2	3.4	2.0

Co(A)ZrO	Time: 15h55min										
Carbon Number Cn	A_Paraffin	A_par/Cn	A_Olefin	A_ole/Cn	$Log(X_{Cn})$ mol%	Total Area	A_α-olefin	$X_{\alpha\text{-olefin}}$ mol%	X_{olefin} mol%	X_{Cn_total} carbon%	Rate.10^5 (mmol/min)
1	62907	62907			1.80	62907				22.3	1195.6
3	23632	7877			0.90	23632				8.3	148.1
4	67755	16939	19255	4564	0.83	266011	168900	85.2	74.5	9.4	126.4
5	73418	14684	18203	3640.1	0.71	255421	146054	81.3	71.3	9.1	97.1
6	82191	13699	15980	2704	0.61	241871	111185	69.6	66.0	8.7	76.6
7	93601	13372	13132	1902	0.52	224733	72286	55.1	58.4	8.1	61.0
8	100989	12624	10063	1310	0.42	201152	40845	40.8	49.8	7.3	47.8
9	105845	11761	6628	739	0.29	171143	17640	27.0	38.2	6.1	36.2
10	93345	9335	3765	427	0.14	130510	6705	18.0	28.5	4.9	24.8
11	83105	7555	2189	252	0.01	104864	3086	14.1	20.8	3.9	18.1
12	67151	5596	1105	124	-0.16	78236	2000	18.0	14.2	2.9	12.4
13	45836	3526	508	58	-0.38	50924	1300	25.6	10.0	1.9	7.4
14	29357	2098	229	16.4	-0.64	31660	700	30.5	7.2	1.1	4.3
15	26059	1737			-0.76	26059			0.0	0.9	3.3

Co(A)MnO	Reaction Time: 22h25min										
Carbon Number Cn	A_Paraffin	A_par/Cn	A_Olefin	A_ole/Cn	$Log(X_{Cn})$ mol%	Total Area	A_a-olefin	$X_{a\text{-olefin}}$ mol%	X_{olefin} mol%	X_{Cn_total} carbon%	Rate.10^5 (mmol/min)
1	98256	98256			1.73	98256				19.1	116.4
3	28311	9437	53883	17961	1.18	82194	53883			16.0	32.4
4	25602	6401	51555	12889	1.03	77157	38557	74.8	66.8	15.0	22.8
5	21368	4272	35246	7249	0.80	57604	25793	71.2	62.9	11.2	13.6
6	18612	3102	26037	4448	0.62	44649	14580	56.0	58.3	8.8	8.9
7	17183	2455	18493	2779	0.46	35676	7407	40.1	51.8	7.1	6.2
8	15961	1995	12232	1529	0.29	28193	3261	26.7	43.4	5.5	4.2
9	16026	1781	8650	961	0.18	24676	1088	12.6	35.1	4.8	3.2
10	12678	1268	5344	640	0.02	18022	760	14.2	29.7	3.7	2.3
11	11506	1046	2237	421	-0.09	13743			16.3	3.1	1.7
12	10072	839	1146	146	-0.26	11218			10.2	2.3	1.2
13	8258	635	700	54	-0.42	8958			7.8	1.7	0.8
14	5861	419			-0.64	5861				1.1	0.5
15	2800	187			-0.99	2800				0.5	0.2

Effect of MED Addition

Co(MED)/SiO_2	Time: 18h53min										
Carbon Number Cn	A_Paraffin	A_par/Cn	A_Olefin	A_ole/Cn	Log(X_{Cn}) mol%	Total Area	A_α-olefin	$X_{\alpha\text{-olefin}}$ mol%	X_{olefin} mol%	$X_{Cn\ total}$ Carbon%	Rate.10^5 (mmol/min)
1	627844	627844			1.87					32.8	855.1
3	114022	38007	23805	7935	0.74	137828			17.3	7.2	62.6
4	57055	14264	104888	26225	0.68	161953	46471	44.3	64.8	8.5	55.1
5	50713	10143	105438	21399	0.57	156151	33304	31.6	67.5	8.2	43.0
6	46380	7730	86524	16980	0.47	133004	17819	20.6	65.1	7.8	33.7
7	43210	6173	64347	13128	0.36	107557	9000	14.0	59.8	7.1	26.3
8	40246	5031	45427	9785	0.25	85673	4724	10.4	53.0	6.2	20.2
9	39762	4418	29690	6797	0.12	69452	2541	8.6	42.7	5.3	15.3
10	38219	3822	19846	5153	0.03	58065	1686	8.5	34.2	4.7	12.2
11	32604	2964	10453	3219	-0.13	43057			24.3	3.6	8.4
12	27278	2273	4362	1659	-0.33	31640			13.8	2.5	5.4
13	21344	1642	2325	755	-0.55	23669			9.8	1.6	3.3
14	17292	1235		286	-0.74	17292			0.0	1.1	2.1
15	15431	1029			-0.91	15431				0.8	1.4

Co(MED)/ZnO	Time: 6h08min										
Carbon Number Cn	A_Paraffin	A_par/Cn	A_Olefin	A_ole/Cn	Log(X_{Cn}) mol%	Total Area	A_α-olefin	$X_{\alpha\text{-olefin}}$ mol%	X_{olefin} mol%	$X_{Cn\ total}$ carbon%	Rate.10^5 (mmol/min)
1	249459	249459			1.83	249459				27.1	544.7
3	101607	33869			0.96	101607				11.0	74.0
4	34677	8669	68764	17191	0.84	103441	58126	84.5	66.5	11.2	55.5
5	29981	5996	61257	12251	0.69	91238	46925	76.6	67.1	9.9	39.8
6	27098	4516	48794	8132	0.53	75892	32197	66.0	64.3	8.2	27.6
7	26888	3841	39390	5627	0.40	66278	19630	49.8	59.4	7.2	20.7
8	25389	3174	31150	3894	0.28	56539	11585	37.2	55.1	6.1	15.4
9	23892	2655	21543	2394	0.13	45435	4805	22.3	47.4	4.9	11.0
10	21000	2100	14647	1465	-0.02	35647	2080	14.2	41.1	3.9	7.8
11	17062	1551	10183	1122	-0.14	27245	1313	12.9	37.4	3.2	5.8
12	15880	1323	5322	739	-0.26	21202		6.8	25.1	2.7	4.5
13	13316	1024	2520	604	-0.36	15836			15.9	2.3	3.6
14	9533	681			-0.74	9533				1.0	1.5
15	6099	407			-0.95	6099				0.7	0.9

Co(MED)/MnO			Time: 23h46min								
Carbon Number Cn	A_Paraffin	A_par/Cn	A_Olefin	A_ole/Cn	Log(X_{Cn}) mol%	Total Area	A_a-olefin	$X_{a\text{-}olefin}$ mol%	X_{olefin} mol%	X_{Cn_total} carbon%	Rate.10^5 (mmol/min)
1	275945	275945			1.81	275945				25.1	659.9
3	37657	12552	106380	35460	1.05	144037	106380		73.9	13.1	114.8
4	33146	8287	108394	27099	0.91	141540	98650	91.0	76.6	12.9	84.6
5	28396	5679	83955	16791	0.72	112351	76817	91.5	74.7	10.2	53.7
6	23698	3953	63468	10578	0.53	87066	56526	89.1	72.9	7.9	34.7
7	19529	2790	48149	6878	0.35	67678	38668	80.3	71.1	6.2	23.1
8	16306	2038	33259	4157	0.16	49565	23855	71.7	67.1	4.5	14.8
9	15340	1704	21310	2368	-0.03	36650	12536	58.8	58.1	3.3	9.7
10	17678	1768	15439	1745	-0.09	33117	6217	40.3	46.6	3.2	8.4
11	27164	2469	11797	1335	-0.05	38961	3437	29.1	30.3	3.8	9.1
12	33382	2782	8062	932	-0.07	41444	1933	24.0	19.5	4.1	8.9
13	23810	1832	3806	423	-0.28	27616	917	24.1	13.8	2.7	5.4
14	12267	876	658	47	-0.67	12925			5.1	1.2	2.2
15	7949	530			-0.91	7949			0.0	0.7	1.3

Effect of the pH of Impregnation

Co/$TiSiO_2$			Reaction Time: 16h34min								
Carbon Number Cn	A_Paraffin	A_par/Cn	A_Olefin	A_ole/Cn	Log(X_{Cn}) mol%	Total Area	A_α-olefin	$X_{\alpha\text{-}olefin}$ mol%	X_{olefin} mol%	X_{Cn_total} carbon%	Rate.10^5 (mmol/min)
1	124199	124199			1.77	124199				18.9	218.9
3	47647.5	15882.5		0	0.87	47647.5	38865			7.2	27.96
4	171029	42757	49246.9	12311.7	0.89	66348.8	43882.8	89.1	74.2	10.1	29.20
5	204146	40829	49347.5	9948.8	0.82	69762.1	42737.5	86.6	70.7	10.6	24.70
6	243872	40645	44492.5	7474.2	0.73	68879.7	34770.9	78.2	64.6	10.5	20.31
7	279938	39991	35036.6	5165.5	0.63	63029.4	23636.9	67.2	55.6	9.7	16.13
8	298610	37326	24698.4	3217.9	0.51	54659.4	13248.5	53.6	45.3	8.4	12.23
9	314664	34963	16325.8	2013.3	0.41	47792.2	6388.8	39.1	34.2	7.5	9.70
10	291200	29120	11135.2	1387.8	0.30	40255.2	2732.0	24.5	27.7	6.5	7.57
11	224124	20375	5755.4	734.0	0.11	28167.8	1016.3	17.7	20.4	4.6	4.88
12	130176	10848	2260.9	345.3	-0.18	15276.5	424.3	18.8	14.8	2.6	2.52
13	61885	4760	824.7	136.5	-0.54	7013.2	193.2	23.4	11.8	1.2	1.08
14	31838	2274	304.1	38.0	-0.91	3467.9		0.0	8.7	0.6	0.47
15	2508.4	167.2			-1.11	2508.4				0.4	0.29

Co/Al$_2$O$_3$-SiO$_2$	Reaction Time: 23h40min										
Carbon Number Cn	A_Paraffin	A_par/Cn	A_Olefin	A_ole/Cn	Log(X_{Cn}) mol%	Total Area	A_α-olefin	$X_{\alpha\text{-olefin}}$ mol%	X_{olefin} mol%	X_{Cn_total} carbon%	Rate.10^5 (mmol/min)
1	149861	149861			1.90	149861				35.7	354.2
3	22858	7619			0.60	22858				5.4	18.0
4	7710	1928	19718	4930	0.55	27428	14463	73.3	71.9	6.5	16.2
5	8699	1720	17388	3478	0.44	25987	10989	63.1	66.9	6.2	12.3
6	10151	1692	14479	2413	0.33	24630	6344	43.8	58.8	5.9	9.7
7	11702	1672	10739	1649	0.24	22441	2965	27.6	47.9	5.5	7.8
8	13299	1662	8510	1366	0.20	21809	1420	16.7	39.0	5.8	7.2
9	16126	1792	5794	726	0.12	21920	686	11.8	26.4	5.4	6.0
10	15597	1560	3754	610	0.06	19351	391	10.4	19.4	5.2	5.1
11	16575	1507	2115	466	0.01	18690			11.3	5.2	4.7
12	16252	1354	861	207	-0.09	17113			5.0	4.5	3.7
13	13290	1022		77	-0.24	13290			0.0	3.4	2.6
14	9168	655			-0.46	9168				2.2	1.5
15	6603	440			-0.64	6603				1.6	1.0

Co4MnO	Time: 22h25min										
Carbon Number Cn	A_Paraffin	A_par/Cn	A_Olefin	A_ole/Cn	Log(X_{Cn}) mol%	Total Area	A_α-olefin	$X_{\alpha\text{-olefin}}$ mol%	X_{olefin} mol%	X_{Cn_total} carbon%	Rate (mmol/min)
1	272924	272924			1.87	272924				33.5	337.8
3	24643	8214	55103	18701	0.85	80746				9.9	33.3
4	24885	6221	51980	12995	0.72	76865	45329	87.2	67.6	9.4	23.8
5	22308	4462	44680	8936	0.55	66988	36571	82.1	66.7	8.2	16.6
6	21025	3504	36972	6162	0.42	57997	26732	72.3	63.7	7.1	12.0
7	21261	3037	29144	4163	0.29	50405	16806	57.7	57.8	6.2	8.9
8	21419	2677	26018	3252	0.20	47437	9542	36.7	54.8	5.8	7.3
9	23148	2572	15879	1764	0.07	39027	4184	26.3	40.7	4.8	5.4
10	20940	2094	9868	1111	-0.05	30808	1747	18.6	30.9	3.9	4.0
11	19270	1752	6608	922	-0.14	25878	944	14.3	25.5	3.6	3.3
12	17116	1426	2746	504	-0.28	19862			13.8	2.8	2.4
13	13000	1000	1800	138	-0.51	14800			12.2	1.8	1.4
14	8699	614	1289	91	-0.72	9988			12.9	1.2	0.9
15	7000	467			-0.90	7000				0.9	0.6

Effect of Contact Time

Co_3O_4/SiO_2	Reaction Time: 19h52min										
Carbon Number Cn	A_Paraffin	A_par/Cn	A_Olefin	A_ole/Cn	Log(X_{Cn}) mol%	Total Area	A_α-olefin	$X_{\alpha\text{-olefin}}$ mol%	X_{olefin} mol%	X_{Cn_total} carbon%	Rate.10^3 (mmol/min)
1	114857	114857			1.75	114857				15.3	150.7
3	416153	138718		0	0.83	416153				5.5	181.3
4	142239	35560	37043.9	9261.0	0.80	512678	31994.0	86.4	72.3	6.8	167.5
5	165194	33038	39528.0	7905.6	0.74	560474	31885.0	80.7	70.5	7.5	146.5
6	198952	32659	37449.9	6336.4	0.67	570451	25633.3	68.4	65.6	7.7	125.5
7	238806	34115	33304.4	4972.7	0.61	571850	17724.9	53.2	58.2	7.8	109.6
8	288907	36113	27726.6	3746.8	0.55	566173	10156.1	36.6	49.0	7.8	96.2
9	338736	40971	21060.5	2461.2	0.51	579941	4768.7	22.6	36.4	7.8	85.7
10	377789	37779	13150.7	1731.1	0.43	509296	1934.9	14.7	25.8	7.3	72.0
11	351228	31930	7429.8	1024.1	0.31	425526	982.6	13.2	17.5	6.2	55.1
12	239131	19928	2539.8	388.1	0.07	264529	400.0	15.7	9.6	3.8	31.1
13	130692	10053	756.2	152.2	-0.25	136254	229.5	30.3	5.5	2.0	15.1
14	87778	6270	347.1	36.6	-0.49	91249	112.5	32.4	3.8	1.2	8.7
15	100934	6729	105.4	7.0	-0.48	101938			1.0	1.4	8.9